

Segmented hydrogels: Process development of a  
reproducible 3D tissue engineered interface system  
and its use as a muscle-tendon model

By

Kyle Efendi

A Doctoral Thesis

Submitted in partial fulfilment of requirements

for the award of

Doctor of Philosophy of Loughborough University

October 2018

© Kyle Efendi 2018

# Table of Contents

List of figures	1
List of tables	3
List of abbreviations	4
Abstract	6
Acknowledgements	8
1 Literature Review	9
1.1 Embryonic development of the musculoskeletal system	9
1.2 Skeletal muscle	9
1.2.1 Structure of skeletal muscle	9
1.2.2 Formation of skeletal muscle	10
1.2.3 Function of skeletal muscle	11
1.3 Tendon	12
1.3.1 Structure and function of tendon tissue	12
1.3.2 Development of tissue tendon	13
1.4 Bone	15
1.5 Connective tissues	15
1.5.1 Myotendinous junction	15
1.5.2 Osteotendinous Junction (Enthesis)	16
1.6 Co-culture models	19
1.6.1 Types of models	19
1.6.2 Current skeletal muscle hydrogel designs	22
1.6.3 Types of Monolayer Co-cultures	25
1.6.4 Musculoskeletal co-cultures	28
1.7 Rationale for developing high-throughput, 3D tissue engineered systems for tissue interfaces	30
1.8 Conclusions	31
1.9 Thesis Aims	32
2 General materials and methods	33
2.1 Mammalian cell culture	33
2.2 C <sub>2</sub> C <sub>12</sub> skeletal muscle cell line	33
2.3 hDF human dermal fibroblasts cells	33
2.4 Cell passage	33
2.5 Centrifuging	34
2.6 Cell counting	34

2.7	Cryopreservation	34
2.8	Tissue engineering of cell seeded 3D constructs	35
2.8.1	Preparation of reagents and equipment	35
2.8.2	Fabrication of PDMS	35
2.8.3	Fabrication of constructs	35
2.9	Construct culture	35
2.9.1	Calculation of gel success rates	36
2.9.2	Calculation of gel survival rates	36
2.10	Macroscopic imaging during culture	36
2.11	Immunocytochemistry and microscopy	36
2.11.1	Fixation, permeabilization and blocking	36
2.11.2	Immunostaining	36
2.12	Image analysis	37
2.13	Gene expression	37
2.13.1	RNA extraction	37
2.13.2	RT-PCR	38
2.13.3	Primers	40
2.13.4	Analysis	40
2.14	Statistical methods	40
3	Developing the gel-making process to allow for higher throughput and co-culture of multiple gel regions	41
3.1	Specific Chapter aims	41
3.2	Introduction	42
3.2.1	Process development methodology	42
3.2.2	Components and setup	44
3.2.3	Fabrication method breakdown	47
3.2.4	Key points moving forward	49
3.3	Materials and methods	50
3.3.1	Cell culture and gel fabrication	50
3.3.2	Initial fabrication method – Single glass bath	50
3.3.3	Gel success and survival rates	51
3.3.4	Angle of components measurements	52
3.4	Results	53
3.4.1	Single bespoke chamber method – segmentation trial	53
3.4.2	8-well plate method	55
3.4.3	PDMS mould from 3D printed negative with steel dividers	59

3.4.4	3D printed moulds	62
3.4.5	Evaluation of design specifications met	66
3.4.6	Insertable moulds method	67
3.4.7	Comparison of models' success and survival rates	70
3.4.8	Gel neutralisation and associated polymerisation times	70
3.4.9	Use of ice to slow polymerisation	71
3.4.10	Insertable moulds with ice compared to the standard methods	72
3.5	Discussion	80
3.5.1	Sharing of knowledge for model development	81
3.5.2	Gel fabrication parameters	82
3.5.3	Development process of the design of the model	83
3.5.4	Collagen gel polymerisation times	84
3.5.5	Comparison of 3D-printed inserts to the 8-well plate model	86
3.5.6	Segmentation of the model to create co-culture gels	87
3.6	Conclusions	87
4	Evaluating the new segmented hydrogel system by incorporating a skeletal muscle model between two unseeded regions	88
4.1	Introduction	88
4.1.1	Chapter aims	90
4.2	Materials and Methods	90
4.2.1	Cell culture	90
4.2.2	Tissue engineering of 3D constructs	90
4.2.3	Macroscopic imaging	91
4.2.4	Macroscopic image analysis	92
4.2.5	Immunofluorescence imaging	92
4.2.6	Image stitching	92
4.2.7	Microscopic analysis of myotube measurements	92
4.2.8	RT-PCR measurements	94
4.2.9	Gel success and survival rates	94
4.3	Results	94
4.3.1	Gel contraction	94
4.3.2	Microscopic analysis of cellular regions in segmented gels and controls	97
4.3.3	Peripheral region observations	105
4.4	Discussion	112
4.4.1	Gel comparisons	112
4.4.2	Gene expression	117

4.4.3	Evaluation of current measuring techniques _____	117
4.5	Conclusions _____	119
5	Developing the segmented system by incorporating a “tendon” region to create a tendon-muscle-tendon construct _____	121
5.1	Introduction _____	121
5.2	Materials and methods _____	123
5.2.1	Cell culture _____	123
5.2.2	Gel fabrication _____	123
5.2.3	Gel survival rate _____	124
5.2.4	Immunostaining of gels and microscopy _____	124
5.3	Results _____	124
5.3.1	Gel survival rate _____	124
5.3.2	Gel contraction _____	125
5.3.3	Microscopic analysis of cellular regions _____	129
5.3.4	Myotube comparisons in central regions _____	134
5.3.5	Gene expression _____	139
5.4	Discussion _____	139
5.4.1	Comparison of macroscopic behaviour _____	140
5.4.2	Comparisons of cellular properties _____	141
5.4.3	Cellular interaction observations _____	141
5.4.4	Comparison of cellular architecture _____	143
5.5	Conclusions _____	144
5.6	Key findings _____	145
6	Future work _____	149
6.1	Future work on previous Chapter outcomes _____	149
6.1.1	Segmentation improvements _____	149
6.1.2	Versatility in geometry of 3D printed moulds _____	150
6.1.3	“Skinny” gels _____	151
6.2	Miniature Joint models _____	153
7	References _____	154

## List of figures

Figure 1.1: Schematic of the structure of skeletal muscle.	10
Figure 1.2: Embryonic development of skeletal muscle.	11
Figure 2.1: Schematic of quantitative polymerase chain reaction.	39
Figure 3.1: Glass chamber setup	50
Figure 3.2: Schematic of how anchor points were fabricated.	50
Figure 3.3: Diagram of the steps involved in creating a segmented gel using blockers.	52
Figure 3.4: Measurement of angles in gel models.	53
Figure 3.5: Macroscopic scans of bespoke chamber method for segmenting gels.	54
Figure 3.7: The miniature (one-third, 500ul) gels with smaller A-frames.	55
Figure 3.8: Image of the adapted 8-well plate and PDMS setup to attempt segmented gels.	56
Figure 3.9: Scanned macroscopic examples of the 8-well segmented method.	56
Figure 3.10: Images illustrating issues with the method which included separated gels	58
Figure 3.11: Image of premade PDMS blockers which were paired together to provide a more precise seal between segments.	58
Figure 3.12: Image showing the development of the PDMS mould system.	59
Figure 3.13: Image showing the process cycle for creating segmented gels using the PDMS mould.	60
Figure 3.14: Image showing PDMS mould method with segmented gels.	61
Figure 3.15 : Images showing the long 3D printed model.	63
Figure 3.16: Images after 24 hr of culture of the 3D printed long mould method.	63
Figure 3.17: Images showing design and finished product of the elevated reservoir model.	65
Figure 3.18: Image of six well-plate with all 3D printed moulds adhered using silicon.	68
Figure 3.19: (A) The original PEEK mould, image taken from Jones et al. (B) 3D printed PLA mould adapted for segmented gels.	69
Figure 3.20: The percentage of total gels made using each method that survive to 24hr and then to 14 days without becoming void.	70
Figure 3.21: Times required for a neutralised collagen gel to set on five different occasions.	71
Figure 3.22: Flowchart of the standard for fabricating a gel.	72
Figure 3.23: The times required to make constructs vs. number of constructs made after cell count stage.	73
Figure 3.24: A breakdown of the times to prepare and neutralise collagen and seed it with cells and the time to pipette the suspension.	74
Figure 3.25: Width reduction comparison between 8-well plate method and insertable 3D printed moulds.	75
Figure 3.26 : Comparison of angle created by the two anchor points and the wall of the chamber compared in both systems.	76
Figure 3.27: Angle created between the two anchor points at both ends between insertable moulds and 8-well plate method.	77
Figure 3.28: Comparison of how anchor points moved throughout the culture period between the 8-well plate method and the insertable moulds.	78
Figure 3.29: Comparison of the imprecision in both methods for creating a mould.	79
Figure 3.30: Comparisons of stained micrographs of the 3D printed inserts to the 8-well model	80
Figure 4.1: Schematic for the fabrication and layout of the segmented gels and controls.	91
Figure 4.2: Example of how the stitch function was used on ImageJ to combine microscopic images.	92
Figure 4.3: Example of how myotube lengths and widths were measured and how myotube angles were measured).	93
Figure 4.4: Contraction of control gels and segmented gels at key time points over the 14-day culture period.	95
Figure 4.5: Contraction of the segmented gels compared to the contraction of skeletal muscle contracts based on width of central region and total surface area of gel measured using imageJ.	96
Figure 4.6: Comparison of the percentage of the original surface area in the peripheral regions of both the control and segmented gels.	97

Figure 4.7: Image demonstrating how the central (cell-seeded for seg) regions were analysed and compared between the two gel types initially for microscopic and macroscopic measurements. _____	98
Figure 4.8: Immunostained images for C <sub>2</sub> C <sub>12</sub> control gels and segmented gels. _____	99
Figure 4.9: Comparison of data gathered from immunostained images between C <sub>2</sub> C <sub>12</sub> control gels and segmented gels for myotubes per microscope frame visible and length of myotubes in each frame. _____	101
Figure 4.10: Comparison of data gathered from immunostained images between C <sub>2</sub> C <sub>12</sub> control gels and segmented gels for myotubes width and number of nuclei per myotube. _____	102
Figure 4.11: The difference between the measured myotube angles and the average for the frame it is in for the control gels and the segmented gels. _____	103
Figure 4.12: Difference in the deviation from alignment between the segmented gels and the controls. _____	104
Figure 4.13: Genetic markers for muscle maturity comparisons between the control and segmented gels. _____	105
Figure 4.14: Schematic demonstrating the regions that were analysed in this Section. _____	105
Figure 4.15: Immunostained images of the acellular (unseeded) regions in segmented gels. _____	106
Figure 4.16: Comparison of segmented gels with C <sub>2</sub> C <sub>12</sub> gels and how the interfaces look at different time points. _____	107
Figure 4.17: Stitched images of the length of the centre of the gel displaying the nuclei distribution at three points in the culture period and the control at 14 days. _____	108
Figure 4.18: Comparison of the acellular region to the cell seeded region in segmented gels. _____	110
Figure 4.19: Myotube deviation from average frame alignment in the acellular regions of the segmented gels and the comparison of the average deviation in absolute terms to the cellular regions. _____	111
Figure 4.20: Comparison of the standard frame-by-frame analysis of stained images to the tile scan analysis. _____	112
Figure 4.21: Example of measuring different orientations of myotubes in a limited frame size. _____	118
Figure 4.22: Comparison of the standard measurement in a single frame and the measurement of a fused myotube in a tile scan. _____	119
Figure 5.1: Schematics of all the experimental models that were tested in this Chapter in regards to the seeding of each region of the gel. _____	124
Figure 5.2: Comparison of the number of the percentage of gels attempted that make it through the entire culture period. _____	125
Figure 5.3: Images of gel types at each macroscopic measurement time point. _____	126
Figure 5.4: Comparisons of contraction in peripheral regions and central regions of the gels. _____	127
Figure 5.5 Comparisons of total gel surface area reduction. _____	128
Figure 5.6: Examples of control gels for C <sub>2</sub> C <sub>12</sub> cells and hDF. _____	129
Figure 5.7: Example of hDF-only control demonstrating desmin positivity in some regions. _____	130
Figure 5.8: Examples of central regions in the Muscle-Tendon model and the peripheral region. _____	131
Figure 5.9: Examples of images of cellular interfaces in muscle-tendon gels. _____	132
Figure 5.10: Example of how many gels showed no clear difference between two cell regions throughout the entirety of the gel. _____	133
Figure 5.11: Comparison of myotube length and width between the muscle-tendon, C <sub>2</sub> C <sub>12</sub> controls and segmented controls. _____	135
Figure 5.12: Comparison of microscopic parameters between the muscle-tendon, C <sub>2</sub> C <sub>12</sub> controls and segmented controls. _____	136
Figure 5.13: The difference between the measured myotube angles and the average for the containing frame in the muscle-tendon gels and the muscle control gels. _____	137
Figure 5.14: How far each individual myotube in the segmented control gel was from the average for the containing frame the absolute differences in average alignment for all gel _____	138
Figure 5.15: RT-qPCR results for the two myosin heavy chain isoforms MYH1 (adult) and MYH3 (embryonic) in segmented and muscle-tendon gels. _____	139
Figure 7.1: "Skinny" gel geometry, macroscopic images and day 0 and day 14. _____	152
Figure 7.2: How the mini-joint model could use two constructs in a single mould. _____	153

## List of tables

<i>Table 1.1: Table of systems currently used to 3D tissue engineered skeletal muscle</i>	23
<i>Table 1.2: Summary of types of co-culture in monolayer systems adapted from Bogdanowicz et al.<sup>130</sup></i>	26
<hr/>	
<i>Table 3.1: Comparison of fabrication methods of Smith et al. and Wragg et al., benefits in line with the aim of this Chapter are highlighted in green and undesirable properties in red.</i>	46
<i>Table 3.2: Table evaluating the design specifications for the new system.</i>	47
<i>Table 3.3: Breakdown of the method for fabricating a gel, the number of * represents the increase in time requirement of the stage when making multiple gels based on preliminary experiments</i>	48
<i>Table 3.4: Summary table for the original attempt at segmented gels in a glass chamber</i>	54
<i>Table 3.5: Summary table for miniature (500 <math>\mu</math>l) gels arranged across the glass chambers</i>	55
<i>Table 3.6: Summary table for outcomes of segmented gels in the 8-well plate</i>	57
<i>Table 3.7: Summary table for outcomes of segmented gels in the PDMS mould method</i>	62
<i>Table 3.8: Summary table for outcomes making segmented gels in the long 3D printed model.</i>	64
<i>Table 3.9: Summary table for outcomes of making segmented gels in the elevated reservoir model.</i>	66
<i>Table 3.10: A checkpoint to see which specifications had been solved and which were still unmet after the results of the elevated reservoir model, green specifications are ones that have been achieved.</i>	67
<i>Table 3.11: Summary table for outcomes making segmented gels with the insertable moulds method</i>	69
<hr/>	



## List of abbreviations

μl	Micro-litre
ANOVA	Analysis of variance
ATP	Adenosine triphosphate
CAD	Computer aided design
cDNA	Complementary DNA
Col1a1	Collagen1A1
CQAs	Critical quality attributes
DAPC	Dystrophin associated glycoprotein complex
DAPI	4',6-diamidino-2-phenylindole
DGC	Dystrophin associated glycoprotein complex
DM	Differentiation medium
DMCs	Dermis-derived multipotent cells
DMEM	Dulbecco's Modified Eagle Medium
DMSO	Dimethyl Sulfoxide
dNTPS	Deoxynucleoside triphosphates
ECM	Extracellular matrix
EDTA	Ethylenediaminetetraacetic acid
FBS	Foetal bovine serum
FDA	Food and Drug administration
Fgf	Fibroblast growth factor
FPCL	Fibroblast populated collagen lattice
GAGs	Glycosaminoglycans
GM	Growth medium
hDF	Human dermal fibroblasts
HSCs	Haematopoietic stem cells
ICH	International conference for Harmonisation
Ihh	Indian hedgehog
MDCs	Muscle derived cells
MEM	Minimal essential medium
MRF	Myogenic regulatory factors
MSCs	Mesenchymal stem cells
MTJ	Myotendinous junction

MYH	Myosin heavy chain isoform
NaOH	Sodium Hydroxide
NIH/3T3	Mouse fibroblasts cells
NMJ	Neuromuscular junction
OTJ	Osteotendinous junction (enthesis)
PBS	Phosphate buffered saline
PDMS	Polydimethylsiloxane
PLA	Polylactic Acid
PLGA	Polylactic-co-glycolic acid
PTHrP	Para-thyroid hormone-related peptide
PU	Polyurethane
QbD	Quality by design
RT-qPCR	real-time Quantitative Polymerase Chain Reaction
Scx	Scleraxis
TBS	Tris-buffered saline
TGF- $\beta$	Transforming growth factor beta
TNMD	Tenomodulin

## Abstract

Prior to commercialisation, all drugs and medical devices must undergo testing to ensure safety to the end user. Part of this process is the pre-clinical trials stage in which high-throughput testing of the product is performed on cells in monolayer followed by testing in animal models. Monolayer cultures are generally basic, containing one cell type, which leads to minimal testing parameters. The more complex animal tests are often misleading as they do not adequately represent the human physiology and their ethics are also often contested. 3D Tissue engineered models, an evolution of the monolayer model more accurately mimic the structure and biochemistry of specific native tissues. To observe effects on the musculoskeletal system, a model representing these tissues is necessary. This thesis focuses on attempting to create an *in vitro* myotendinous junction (MTJ) for such purposes. Firstly, the most suitable published process for making a 3D tissue engineered skeletal muscle model was identified based on an analysis of requirements. A model using the C<sub>2</sub>C<sub>12</sub> cell line in a collagen hydrogel between two anchor points was chosen and the process was optimised using a Quality-by-Design framework. This was essential to make a system that would lend itself to high-throughput testing in the long run. Following this, a simple process for creating an MTJ, termed 'segmentation' of the gel, was tested and showed a reduction in surface area consistent with cell attachment as previously reported. This involved physically blocking regions of the gel during manufacture. Multiple design iterations were tested to enable reproducibility. Of the tested configurations, a 3D printed PLA mould adhered to a 6-well plate with sliding dividers for segmentation and posts for gel anchor points was found to be optimal. Finally, standardising the use of ice in the gel fabrication process to prevent premature polymerisation of the hydrogel led to the success rate of fabrication to increase to up to 100%. Comparisons with the initial system showed multiple indicators of more consistent gels with reduced failure rates, a reduction in the resources required due to scaling down, and versatility in the design allowing for segmentation and simple adaptation to testing apparatus for future experiments. This system was then tested by only seeding the central region of a gel with C<sub>2</sub>C<sub>12</sub> muscle-precursor cells to create "segmented gels". Compared to homogeneously seeded constructs, the 'muscle' region in segmented gels was found to have no difference in macroscopic behaviour and only a slight decrease in myotube width measurements, still within published parameters. These models exhibited a unique 'bow-tie' shape from the seeding discrepancies in the different regions. During the 14-day culture period, the cells became equally distributed throughout the gel, indicating that they may be migrating over the culture period. These regions also exhibited myotube formation and although less densely populated, a greater incidence of striated myotubes were found in these regions as demonstrated by staining with rhodamine phalloidin. Finally, the end regions were seeded with

human dermal fibroblasts (hDFs) to represent a tendon to create a tendon-muscle-tendon model. Immunostaining showed that the majority of cells in the resulting construct were desmin-positive, a muscle-specific marker. This is in agreement with previous research that shows that dermal fibroblasts can be driven down a myogenic lineage by secreted factors in culture. However, transitional interdigitation between the two morphologically different cell types were observed in some models. This represents the first report of the successful formation of a myotendinous junction in a collagen-based potentially high-throughput system.

## Acknowledgements

Thank you to the Doctoral Training Centre and Loughborough University for giving me this opportunity and my supervisors Mark Lewis, Darren Player and Patrick Wheeler for supporting me throughout this project.

Thank you to everyone in the department, including but not limited to Andrew Capel, Maria Pardo-Figuerez, Nicholas Wragg, Neil Martin, Rowan Rimington, Jacob Fleming, Mark Turner and Luke Baker who tirelessly helped me whenever I was in need and made this project much more achievable. As cliché as it is to say, without you guys, I would not have been able to do what I did.

I would like to also thank my fellow DTC intake, especially Steve Ruck, Carlos Granja, Diogo Mosqueira and Matthew Dunn for listening to my ramblings throughout the course of the project and for providing me with some solid conversation and making it a far more enjoyable process.

Thanks to Max and Philpott for coexisting with me throughout the majority of this process. It was a great period in my life.

Thank you, Georgina, for putting up with me just in general but especially whilst I wrote this.

For anybody else not mentioned, writing a thesis can fry your brain a little and I've very likely forgotten somebody extremely obvious, so even if your name is absent from this page, you still know how much you are appreciated without my saying so.

To my family, thanks for being the driving force to get me here and anywhere else I go. Hopefully you'll be able to finally explain to people what I actually did for my PhD thesis after looking at this big book!

# 1 Literature Review

## 1.1 Embryonic development of the musculoskeletal system

The musculoskeletal system begins to form distinctly during the gastrulation stage of embryonic development, during which the implanted blastocyst forms into three germ layers:

The ectoderm - the foundation for the epidermis and peripheral nervous system; the endoderm - the foundation for the epithelium of the digestive system, digestive organs and lungs; and the mesoderm - the foundation of blood vessels, blood, heart, kidneys, bones, muscles and connective tissues. This mesoderm then further divides into three regions:

The intermediate mesoderm, lateral plate mesoderm and the paraxial mesoderm either side of the neural tube. The latter then segments into cellular agglomerates called somites<sup>1</sup>. The somites then, through the expression of the protein Noggin, become the dermomyotome and the sclerotome which finally develop into the tissues discussed in this thesis.

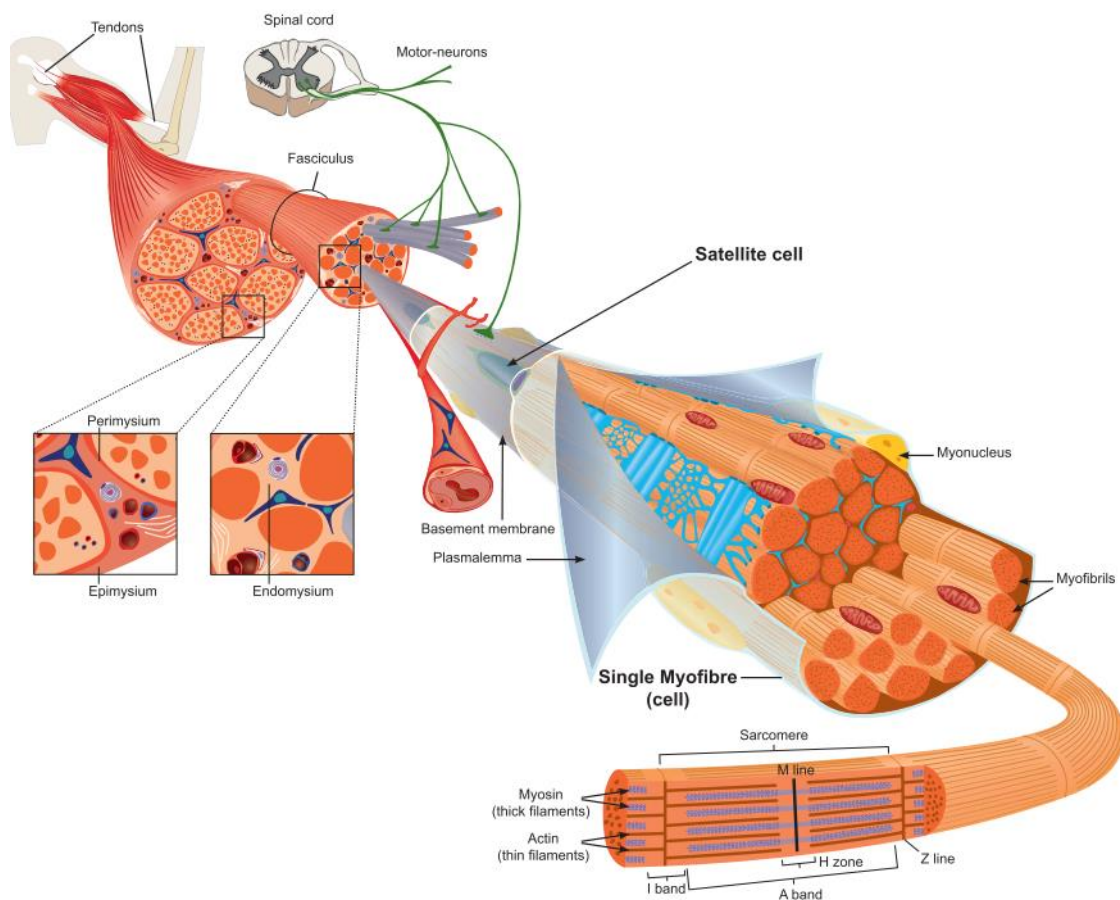
## 1.2 Skeletal muscle

### 1.2.1 Structure of skeletal muscle

Skeletal muscle is highly aligned and organised hierarchically once mature. At the smallest level, it consists of microfilaments of myosin (thick) fibres and actin (thin) fibres as well as titin (elastic) fibres in repeating units called sarcomeres<sup>1</sup>. Myosin and actin are helical compounds consisting of binding sites that lead to contraction. The 'I-band' and 'A-band' created by these filaments are what give muscle a striated appearance<sup>2</sup>. One set of these make up the contractile unit called a sarcomere which are joined end to end in a chain at their z-discs to create myofibrils which are in turn covered in t-tubules to transfer signals from the central nervous system<sup>1</sup>. Bundles of myofibrils make up a single muscle fibre which is aligned parallel to the direction of the muscle action<sup>2</sup>. The muscle fibre is a terminally differentiated, multinucleated cell covered in a sarcolemma and divided from other muscle fibres by the endomysium. The nuclei, mitochondria and other cellular components are pushed to the periphery of the cell<sup>1</sup>. Muscle fibres are grouped together into fascicles, and a single muscle is made out of a collection of fascicles covered in an epimysium. All of the structures in a skeletal muscle are aligned in along a single axis for to work concurrently against tension<sup>3</sup>.

The endomysium, perimysium and epimysium make up the extracellular matrix (ECM)<sup>4</sup>. There is some uncertainty as to how clear the boundaries are between these three types of ECM, but it is clear that they exist and are responsible for bearing much of the passive force in muscle. The main structural

protein in the ECM is collagen and accounts for 1-10% of the weight of muscle in bovine models<sup>5,6</sup> of which the most prominent types are collagen I and III in mature adult muscle<sup>3,7</sup>.



*Figure 1.1: Schematic of the structure of skeletal muscle. Skeletal muscle is a hierarchical tissue where sarcomeres, made up of filaments, are organised into myofibrils. Groups of myofibrils make a single myofiber. Bundles of myofibers make a fascicle, which together make a muscle belly. Adapted with permission from Tajbakhsh et al. 2009.*

## 1.2.2 Formation of skeletal muscle

Most skeletal muscle in the body is derived from the paraxial mesoderm when it begins to clump to create embryonic somite either side of the neural tube<sup>8</sup>. The somite in the limb buds can be divided into the epaxial dermomyotome – which develops into the deep back muscles - and the hypaxial dermomyotome – which is responsible for the development for the other skeletal muscles in the body and limbs. The dermomyotome then divides into the dermatome and the myotome, the latter retaining the hypaxial and epaxial components. Opposite the limb buds, the progenitor cells for skeletal muscle then delaminate from the myotome and migrate where the muscle is to form, these mesenchymal cells are considered to be the origin of positional cues for migrating cells<sup>9</sup>.

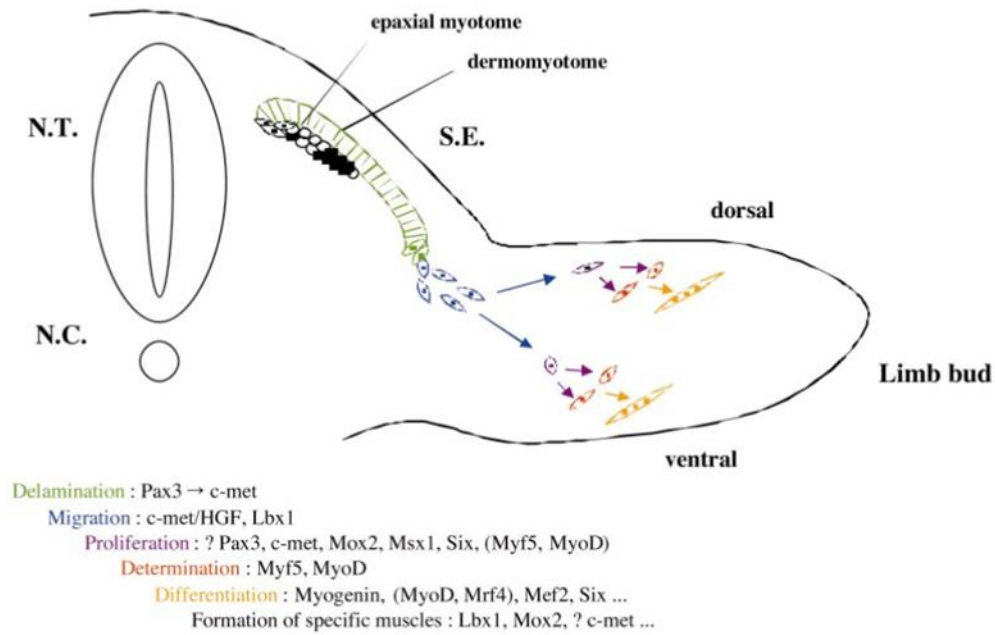


Figure 1.2: Embryonic development of skeletal muscle. Adapted with permissions from Buckingham et al. 2003.

It is well established myogenic regulatory factors (Mrfs) including myoD and Myf5 are important in the formation of skeletal muscle from the precursor cells into a myogenic lineage<sup>4,10-12</sup>, as well as pax3 upstream. Cells only begin to express MyoD and Myf5 once they have migrated to the limb, indicating that they are yet to have been committed to myogenic lineage until then<sup>13</sup>. Somitic cells that do not express these factors are committed to other lineages<sup>14</sup>. After the activation of these two factors, the cells proliferate until expression of crucial differentiation factors, especially Myogenin, as well as Mef2, Mrf4 and MyoD. Here the cells begin to differentiate through the signalling of Pax3. While Myogenin is thought to be the primary driver of differentiation *in vivo*, *in vitro*, Myogenin null myoblasts have been found to also differentiate. The proposed mechanism is through the function of MyoD and Mrf4.

### 1.2.3 Function of skeletal muscle

The primary function of skeletal muscle is to contract, thereby inducing movement in the body through the skeleton. According to the sliding filament theory, the aforementioned contractile unit (sarcomere) is instrumental in skeletal muscle contraction; when the muscle is relaxed, tropomyosin covers the binding sites on the myosin that could otherwise be bound onto by the actin filament<sup>15,16</sup>. The sarcoplasmic reticulum is the store of Ca<sup>2+</sup> ions inside the muscle which releases and reabsorbs the Ca<sup>2+</sup> ions to cause contraction and T-tubules are for transmitting the signal into the depths of the muscle fibres. Contraction is initiated by signalling from a nerve through the neuromuscular junction



(NMJ) that, through a cascade, causes a rise in the level of  $\text{Ca}^{2+}$  ions through the transverse (T)- tubules found surrounding the muscle fibres, supplying each myofibril with simultaneous contraction signals<sup>1</sup>. These  $\text{Ca}^{2+}$  ions cause the troponin complex to translocate the tropomyosin, thereby allowing the binding sites to become available to the myosin on the actin protein chain<sup>17</sup>. An influx of ATP into the system then attracts the myosin to bind to the newly available sites in a cyclical fashion and move down the chain to bring the two z-discs together, shortening the sarcomere and ultimately causing the entire muscle to contract. ATP is then required to reduce the concentration of  $\text{Ca}^{2+}$  ions to allow for the relaxation of the sarcomeres.

## 1.3 Tendon

### 1.3.1 Structure and function of tendon tissue

Tendons can be vastly structurally different depending on the location of the body; tendons connecting large and powerful muscles such as the quadriceps are much shorter and broader than tendons for the fingers for example (see Kannus et al. for review)<sup>18</sup>. Orientation is also generally adapted to the required uses depending on the direction of the potential forces. Tendons can be rounded chord, strap-like bands or ribbons<sup>19</sup>. Nonetheless, most structural properties beyond the baseline are different in different tendons. Tendons and ligaments have multiple times less oxygen consumption than skeletal muscle due to the low cell density in the tissue and are composed therefore predominantly of ECM<sup>19</sup>. Tendon fibres that are in good health are composed of (70% water) parallel type I collagen fibres constituting 65-80% of the dry mass, with elastin making up 1-2% of dry mass. The extracellular matrix around these fibres is composed of proteoglycan at 1-5% and water<sup>19-21</sup>. Similarly to muscle, tendon is also hierarchically arranged.

The basic structure in the tendon is the tropocollagen molecule that crosslinks into a triple helix<sup>18</sup>. These make up microfibrils which in turn make up the fibrils that are gathered together to make a single collagen fibre. Each fibre is then covered in the endotenon. The “primary fibre unit” is the name for a collection of fibres<sup>18</sup>. A group of primary fibres is a secondary fibre unit called a fascicle, which contains tendon fibroblast cells as well as the matrix, these are able to move over each other<sup>22</sup>. These then group to make a tertiary fibre, and finally a bundle of tertiary fibres are a tendon which is covered in the epitenon. The fibrils are orientated in multiple directions within each individual fibre to form spirals that allow it to have strength in multiple directions<sup>18</sup>. Fascicles and tertiary bundles form in a spiral across the tendon<sup>18</sup>. In many regions of the body, above this is the epitenon which exists to prevent the mechanical stress from damaging the surrounding tissues. This is a loose sheath that contains the vascular, lymphatic and nerve supply to the tendon<sup>19</sup>. Additionally, in some tendons there is a paratenon, which is a layer of collagen fibres covering the tissue as a whole<sup>19</sup>. The epitenon is

connected to both the paratenon and the endotenon, these are all collagenous and fibril-based envelopings. It is key to note that there is a lack of consistent, specific nomenclature for tendon subdivisions across the field of research.

Tendon ECM is mostly composed of collagen and elastin fibres. Additionally, ground substance - a collection of molecules outside the fibres such as proteoglycans, glycosaminoglycans (GAGs) and glycoproteins which are also synthesised by the cells, facilitating rapid diffusion of water-soluble molecules and form a matrix into which the cells embed - and anorganic compounds also exist in very small quantities, totalling 0.2 % of the dry mass<sup>19,23,24</sup>. The collagen fibres have a crimped or 'wavy' shape when in the resting state (no tension) and once under tension, these disappear by stretching the fibres in their specifically oriented directions. The elasticity of the fibres allow them to recover their wavy shape once no longer stretched<sup>25</sup>. However, this property is not often found in human tendon fibres<sup>18</sup>. The ability for these fibres to recover their crimping upon relaxation is limited to an elongation of 4% and an 8% elongation is likely to cause rupture in the tissue<sup>26-28</sup>. Both intra- and inter fascicular crimping can be observed albeit irregularly<sup>27</sup>.

The only known function of the tendon in physiology is to transfer force between the skeleton and skeletal muscles, facilitating movement. Due to their relatively acellular and avascular constitution, they are more of a passive tissue mostly consisting of ECM which provides the majority of the mechanical properties through the structure of the collagen fibres.

### 1.3.2 Development of tissue tendon

During embryogenesis, the tendons of the trunk and the limbs develop differently, this is due to the cellular and tissue interactions and behaviours in the differing regions<sup>29,30</sup>.

#### 1.3.2.1 *Tendon tissue development in the trunk*

The trunk tendons develop from Mesenchymal Stem Cells (MSCs) in the dorsal sclerotome adjacent to the myotome<sup>31</sup>. The region they develop into is not morphologically discernible from the sclerotome and differs only in the expression of the scleraxis (*Scx*) gene<sup>32</sup>. This region becomes known as the syndetome. The syndetome relies on signalling from other somites to regulate its growth and development; FGF upregulation through the ERK/MAP kinase pathway from the myotome induces the expression of *Scx* in mice and chicks and allows for the syndetome to come into existence<sup>32</sup>. In order to prevent the undesirable expansion of *Scx* into the sclerotome, Shh proteins synthesise SoxD group proteins in order to limit the transcription of *Scx* in regions other than the anteroposterior sclerotome<sup>32</sup>. Separating the tendon and cartilage progenitors is the role of *Pax1*, the overexpression of which inhibits *Scx*<sup>31</sup>. Brent et al. also postulated that this suggest the possibility of progenitors for both chondrocytes and tenocytes to be of the same origins and the differentiation of the resultant

cells is dependent on levels of Scx expression<sup>30,32</sup>. Therefore, Scx expression is a distinctive marker of tendon progenitors and the cells throughout their development.

TGF $\beta$  has also been found as important in the induction of tendon markers including Scx and tenomodulin (TNMD)<sup>33-35</sup>. In mouse embryos TGF $\beta$  disruption results in absence of all tendon tissue, but only at E12.5 when the progenitors should be aligning between muscle and cartilage tissues<sup>30</sup>. It was also postulated that the connection of these tissue types is orchestrated by TGF signals from the muscle and cartilage progenitors to encourage a second wave of tendon progenitors<sup>33,30</sup>. These tendons will therefore develop to intertwine with the muscle and bones either side of them as the body matures and the tissue types signal to each other.

### *1.3.2.2 Tendon tissue development in the limbs*

As the limb bud begins to develop, the tendon precursors from the lateral plate mesoderm (expressing Scx) migrate to and are intermixed with the migrating myoblasts (muscle progenitors from the ventrolateral lip of the dermomyotome) in the dorsoventral limb regions<sup>36</sup>. At this point, the presence and signalling of other cells is not vital for the tendons to begin developing. The tendon precursors then separate and create the tendon primordia, this restricts muscle growth to prevent it growing directly into the bone<sup>31,37,38</sup>.

Further into development (around E6 in mice), the presence of the muscle becomes more of an important factor. This interdependency for development is reciprocal as the two sets of cells undergo morphogenesis and the tendon contributes to muscle regionalisation while the muscle regulates the tendon progenitor distribution<sup>39</sup>. By E12.5 the tendon progenitors undergo organisation between the differentiating muscle and cartilage and at E13.5 the progenitors differentiate into tendons<sup>30</sup>. Unlike the induction and organisation phases, the later stages of tendon development beginning at the differentiation step require the presence of muscle, resulting in further TGF $\beta$  signalling to induce tendon markers and Fgf signalling such as Fgf4 and Fgf8 which are located in regions close to the tendons<sup>38-40</sup>.

The ECM is deposited from tendon fibroblasts that are given the name tenocytes, they are aligned between the bone and the cartilage that will eventually form the long bones before collagen fibrillogenesis occurs in the tendon region. This is a three stage process involving the assembly of the collagen molecules in close association with the tendon fibroblasts to create fibrils which then organise themselves end to end to fuse into longer fibrils and then associate laterally to create thicker fibres<sup>22,41</sup>. Therefore, the tenocytes dictate the arrangement of the ECM.

## 1.4 Bone

Bone has a number of functions in physiology:

Firstly, it is there to provide mechanical support to the body, thereby allowing movement through providing levers for muscle, it is therefore as strong as possible whilst remaining light<sup>42</sup>. These mechanical properties also allow it to protect vital organs and the central nervous system through physical shielding<sup>43</sup>.

Secondly, bone acts as an ionic reservoir to maintain homeostasis in the blood; due to its high mineral content such as calcium, sodium and phosphate, it can freely exchange ions to prevent drastic fluctuations of blood mineral levels<sup>44</sup>.

Finally, bone is vital in haematopoiesis; it is a store of haematopoietic stem cells (HSCs) which are blood precursors, eventually differentiating into cells such as red blood cells and lymphocytes which are key to a functioning immune system<sup>45</sup>.

Co-cultures of 3D tissue-engineered bone and muscle have been detailed elsewhere and are out of the scope of this thesis<sup>46</sup>. This thesis focuses on modelling the muscle-tendon region, which could then potentially be combined with the aforementioned studies as a step to creating a more complete model of the musculoskeletal system.

## 1.5 Connective tissues

Between the three main tissue types described above are transitional areas where one distinct tissue type is attached to the next. Either side of the tendon is the myotendinous junction (MTJ, muscle-tendon interface) and the osteotendinous junction (OTJ, otherwise known as enthesis, bone-tendon interface). This thesis will focus primarily on the MTJ, although knowledge of the OTJ is useful to pave the way for future experiments. Separate tissue engineered OTJ models have been attempted elsewhere<sup>46</sup>.

### 1.5.1 Myotendinous junction

#### 1.5.1.1 *Structure of the myotendinous junction*

The myotendinous junction (MTJ) is a specialised region of connection between the muscle and the tendon and is the primary region of force transfer between the two tissue types (See Charvet et al. for review<sup>47</sup>).

In the early stages of development, the large nuclei in the myotube fibres and the fibroblasts from the tendon are located near the junction, and therefore near each other. The muscle then forms in

corrugated texture to allow for the infiltration of tendon fibres which develop into heavy interdigitations with long extensions into each other and beyond the z-line in the muscle fibres where the sarcomeres terminate, there are also strands that extend into the subsarcolemmal membrane<sup>48</sup>. Actin filaments extend beyond the final z-line of the contractile unit of muscle and are bundled together by actin binding proteins to form protrusions out of the end of the repeating muscle chains (interdigitations). These are then linked to the sarcolemma by intracellular proteins and transmembrane protein complexes link the basement membrane components to the cytoskeletal elements. The basement membrane is then connected to the collagen-based ECM outside of itself by proteins, thereby connecting the final actin filaments to the ECM of the tendon. This interdigitation is a key feature of the MTJ. The ends of the myofibers are tapered to fit into the ECM of the tendon to form this. These increase the contact area between the two by more than tenfold<sup>49,50</sup>.

The MTJ has protein complexes of the subsarcolemmal, transmembraneous and extracellular types<sup>47</sup>. Two linkage systems exist in connecting the actin and ECM proteins, both work through laminin 211; dystrophin associated glycoprotein complex (DGC) otherwise known as (DAPC) and the  $\alpha7\beta1$  integrin. The key proteins on the tendon side of the junction are tenascin- care and collagen I<sup>51</sup>. And on muscle side – laminins and collagen IV<sup>47</sup>. Data on what is found in the MTJ is scarce<sup>52</sup>, although paxillin, vinculin and talin are expressed in the region<sup>53,54</sup>. These ECM proteins are localised in focal adhesions and are mechanically linked by integrins to actin filaments, creating a system for the longitudinal transmission of force<sup>54</sup>.

With age, the structure of the myotendinous junction changes; in the neonatal stage of life, the junction has a dovetailing shape and towards adolescence it transitions into long extensions into the opposing tissues. Later stages of life lead to the MTJ exhibiting a more jagged structure where the tendon transitions further into the surface of the myofibres<sup>48</sup>.

### *1.5.1.2 Function of the myotendinous junction*

Due to the location of the MTJ, it is the first region outside of muscle that needs to transfer the forces generated in muscular contraction further down the chain. Therefore, it is the primary site of force transmission as well as the first region where significant losses in force can be conceded<sup>47</sup>.

## **1.5.2 Osteotendinous Junction (Enthesis)**

### *1.5.2.1 Development of the enthesis*

Enthesis is the region where the bone attaches to either a tendon, ligament or joint capsule<sup>55</sup>. It is in fact a collection of different tissues that reduce the stress concentration where hard and soft tissues interface<sup>56</sup>. As every muscle/tendon connection is different according to the specific requirements of the joint, selectively focussing on individual junctions allows to see similarities between different

instances, as well as giving an example to model. The achilles tendon is said to be archetypal for this type of model and is generally used to understand the enthesis better<sup>55</sup>.

The order of development of the enthesis in humans is not yet fully understood. However, in rats it has been shown that the periosteal and sesamoid fibrocartilages develop after birth and similarly to tendon, lack of muscle activity leads to an inhibition of development of the enthesis<sup>57</sup>. Indian hedgehog (Ihh) has been linked to being critical in the fibrocartilage development of the enthesis. It is likely that this is related to the development to tendon as the enthesis develops from Sox9 and Scx expressive cells but are not tendon fibroblasts. Again, the TGF- $\beta$  family influence these cells through regulation of the differentiation of these progenitors and specifically regulates the formation of the bone eminence<sup>58</sup> and tendon<sup>33</sup>. Developing tendons then insert themselves into bone eminences during the formation of the bone and tendon, this interface usually inserts itself into a bone eminence, however the literature on the specific mechanisms of this is scarce as it has only recently become studied in depth<sup>59</sup>. The combination of both BMP4 and Scx pathways play an important role the initial formation of the bone eminence and the development of the tendon-bone unit, alongside a number of other BMPs and FGFs that are currently being researched<sup>58,59</sup>.

During the development of the limb skeleton, chondroprogenitors develop into cartilaginous templates for bone. In murine models, bone eminences develop afterwards and do not exist in the original template, suggesting that they develop separately, exhibiting both Sox9 and Scx individually, either side of the interface<sup>58,60</sup>. However, this separately developing module has been recently inspected and requires further research<sup>59</sup>. This new model of modularity has provided an updated outlook on the formation on the enthesis and has evolved the theory of the 'segregation model' where the tissues of the entire unit all stem from the same pool of progenitor cells. This theory is backed by the requirement of Scx – positive cells expressing Sox9 in order for an enthesis to exist and the gradual decrease of progenitors expressing both over the course of the development of the murine embryo<sup>58,60</sup>. There is much more research to be done, however on the specific mechanism.

As for the mineralisation stage, in murine rotator cuffs mineralisation of the enthesis region occurs concurrently with the secondary ossification in the humeral head<sup>61</sup>. The mineral gradient moves into the tissue that is to become the enthesis as endochondral ossification occurs in the epiphyseal bone. Ihh and para-thyroid hormone-related peptide (PTHrP) are key in the chondrocyte differentiation as covered previously. PTHrP plays a role in regulating maturation and mineralisation of the enthesis<sup>62</sup>.

The development of the enthesis is controlled by a combination of biological signalling and physical signals, which continues after birth. After formation, the growth of muscle eminences is closely related to the contraction force of the muscle<sup>63</sup>. This signalling from muscle is essential for tendon formation

and these tendons can be visible in models in the shoulder at E15.5, however the mineralised fibrocartilage in the enthesis cannot be seen until the neonatal stages<sup>61,64</sup>. Paralysis of the muscle leads to no discernible fibrocartilage after 8 weeks and results in the collagen fibres showing less alignment, indicating that musculoskeletal activity beyond birth is important for the development of the enthesis<sup>65,66</sup>.

Due to the lack of research looking at the interactions between all tissue types in joints simultaneously, there is a lack of information on the development of the enthesis. There is a requirement for a deeper understanding of these mechanisms through further studies.

### *1.5.2.2 Structure of the enthesis*

Over the last two decades, research into the enthesis categorises it into two types; either fibrous (otherwise termed periosteal-diaphyseal or indirect) or as found most commonly in the human body, fibrocartilaginous (otherwise termed chondroapophyseal or direct)<sup>56</sup>. Fibrous entheses attach directly onto either the bone or the periosteum via a fibrous tissue, whereas fibrocartilaginous entheses attach through a layer of fibrocartilage as an additional layer to make the transition between uncalcified tendon to calcified bone. It does this by grading between four distinct zones where the properties transition from one into another, making the transition much less abrupt and allowing for transmission of force while being able to withstand the stress concentrated in the interfaces<sup>56,67,68</sup>.

Fibrous tissue (otherwise termed periosteal-diaphyseal or indirect tissue) in fibrous entheses is dense and frequently can be found in the diaphysis of long bones<sup>68</sup>. It is characterised by collagen fibres that are mineralised and break through<sup>67</sup>. The tendon can either attach to the bone in a 'bony' fibrous enthesis or it can attach to the periosteum to make a 'periosteal' enthesis. Little material on them as injuries generally occur in fibrocartilaginous entheses.

Fibrocartilaginous entheses are the standard enthesis in epiphyses and apophyses of bone and are so named because of the fibrocartilage at the interface. It is generally divided into four different zones that slowly transition one into another:

The first is of dense and fibrous connective tissue, very much like the main body of the tendon. The second region of uncalcified fibrocartilage is a region of cartilage without mineral that is avascular and consisting of aggrecan and collagen types I-III as well as fibrochondrocytes<sup>56,67-72</sup>. This region is generally found in tendons that have an insertion point on the diaphyses or metaphyses of bones. This is usually followed by a very straight mechanical boundary known as the tidemark, which is a basophilic line separating the soft tissue of the uncalcified fibrocartilage with the calcified fibrocartilage. The third zone is another region of avascular fibrocartilage but it is in a mineralised

state consisting mostly of type II collagen, so the collagen transitions from being mostly type I to type II in this region<sup>56,67,69,70,72-74</sup>. It is of an irregular geometry which contributes to the mechanical strength of the enthesis, likely due to the increase of surface area in contact between transitional tissues.

The Achilles specifically also has a 'sesamoid fibrocartilage and a 'periosteal fibrocartilage' which form a wall next to the retrocalcaneal bursa which has an adipose protrusion to aid in the movement of the tendon on the bone.

These regions, altogether make up one 'enthesis organ'<sup>55</sup>. Although what exactly constitutes this particular organ is up for debate as there are other anatomical regions in the vicinity that allow for stress dissipation such as the plantar fascia<sup>75,76</sup>. The final zone that follows is bone. As explained earlier in this Section, bone is a matrix of type I collagen with appetite mineral consisting of osteoclasts, osteoblasts and osteocytes. The full extent of the reason behind the existence of the enthesis organ including why there are barriers to vascularisation and direct cell-to-cell signalling is poorly understood<sup>55,68</sup>. However, it is postulated that this region allows for the efficient transfer of force whilst reducing the stress concentration and increasing force dissipation at the interface between hard and soft tissue<sup>55</sup>.

## 1.6 Co-culture models

Many of the tissues developing *in utero* require interactions with nearby cells to fully develop. This is also the case with regards to muscle and tendon. During development, the interactions of muscle and tendon lead to the development of the MTJ, with the force transduction between the two tissues being the main driver for the adult phenotype<sup>24</sup>. Another key point to note is that no muscular development can occur without the tendon's existence, *in utero* no muscle would be able to generate force and develop without an attachment to another tissue as twitching is a key aspect of early muscular development. This highlights the importance of this specific tissue interface, however the development of this junction is poorly understood which has led to the development of *in vitro* models<sup>50</sup>. In long term monolayer cultures, the ability of tenocytes to deposit collagen I and differentiate is decreased<sup>77</sup>, indicating that the conditions may not be sustainably maintain the phenotype. Changing the conditions to more closely represent physiology may create a more sustained tenocytic characteristics.

### 1.6.1 Types of models

Co-cultures involve multiple different cell types being cultured in a single or connected system. They have been developed to emulate native tissues and the interfaces between those tissues more closely. In the musculoskeletal system for example, the interfaces between tissues (the MTJ and enthesis) are



important to allow for transfer of force resulting in locomotion. Due to this, these regions between the three tissue types are where the mechanical strain is concentrated and the enthesis is where the majority of injuries occur requiring orthopaedic surgeries for tendon repair, whilst the MTJ is a common point of damage for a variety of factors including non-direct trauma, wear and aging resulting in degenerative conditions under the umbrella term “tendinopathies” which can in the long term also lead to rupture<sup>19,78,79</sup>. These types of injuries occur most often in fibrocartilaginous tendons and research for treatments is mostly focussed on rotator cuff, achilles tendon and less commonly patellar tendon in accordance with the frequency at which these injuries arise<sup>23</sup>. Due to low vascularity and cellular activity in these regions, regenerative capability of the body without intervention is extremely limited<sup>21</sup>. Therefore, once these ruptures occur, surgical repairs are routinely undertaken and may yield reasonable repair. However, surgical repair in these instances often has the drawback of the new tissue that replaces the damaged being weaker in mechanical strength whilst also not replicating the biological properties which can often lead to repeat failure amongst other problems<sup>64,80–82</sup>.

In order to overcome this and attempt to encourage a more complete repair through regeneration of the tissue, experimental surgical procedures have begun implementing materials in the form of scaffolds in animal models<sup>23,24,78,83</sup>. However, before materials are deemed safe, they are required to go through a standard clinical trial process usually involving a simple monolayer toxicology analysis<sup>84</sup>. While these pre-clinical steps reduce the number of toxic, or non-viable materials that make it through to the next stages of the trials, there are still a large number of products that are found out to be unusable in later stages, wasting the industry time and money<sup>85</sup>. Therefore, improving the relevance and effectiveness of this stage of the process will improve the efficiency of the entire process of developing a device or treatment for medical use by reducing the time wasted on options that are to be deemed unacceptable at later stages.

One of the largest drawbacks of the pre-clinical stage is that the monolayer assessment is too simple to be able to assess the complexities of the body, introducing more complexity to the model can therefore lead to a more relevant result. One way of doing this is to increase the number of cell types in a monolayer culture to make it a co-culture system. This would allow the effects of inputs to be tested on multiple cell types whilst also considering how having different cell types within the system will have an impact on each other, as *in vivo* tissues will almost always involve multiple cell populations. The second option is to alter the monolayer setup to a 3D tissue-engineered cellular model. These 3D models introduce an ECM for the cells to interact with, as well as more directions to migrate, proliferate and signal towards and allow the cells an extra dimension of intra-cellular interactions. Relevant examples of such models include but are not limited to:

### 1.6.1.1 Bone engineered models

Bose et al. review a variety of 3D printing methods have been used to create bone scaffolds from a large range of materials (see full review for details)<sup>86</sup>. It is identified that the pore size and interconnectedness of the pores in the printed material is key for the formation of bone to allow for mineralisation and the movement of nutrients and allow for vascularisation. Bone tissue engineering is rarely published in a 3D pre-clinical model, the majority of these models can be seen with some level of implantation either into a patient or an animal model to allow for the physiological adaptations required to develop bone in the scaffold. In fact, bone is extensively covered in the literature for regenerative medicine purposes, with a wide range of methods<sup>86</sup>. This is presumably due to the model requiring three different cell types (osteoblasts, osteoclasts and osteocytes) to work in coordination to constantly model the bone according to chemical and mechanical cues on the tissue, which would be very difficult to replicate *in vitro*.

### 1.6.1.2 Skeletal Muscle engineered models

A large variety of different models have been made (see review by Christ et al.<sup>87</sup> for more detail). In summary, skeletal muscle tissue-engineered models can be divided into those with synthetic scaffolds and hydrogel models.

Synthetic models include electrospun fibres, films, fibre meshes, sponges, microspheres<sup>88-96</sup>. The cells used in all these models are generally C<sub>2</sub>C<sub>12</sub> murine myoblasts or primary MDCs (rat human and/or mouse muscle derived cells). However, these scaffolds are commonly beyond the ideal stiffness conditions for optimal fibre fusion and maturation which would be that of native muscle tissue<sup>97</sup>. These scaffolds are also not truly 3D and are therefore not biomimetic in that aspect. The final negative is that the architectural integrity of the model is dependent on the scaffold material, so if it degrades over time, it will have negative implications on the structure of the whole model<sup>98</sup>.

Hydrogels try to better replicate the 3D architecture and have been used in 3D skeletal muscle models since they were first mentioned by Vandenberg et al.<sup>99</sup>. They allow for longer cultures that result in better muscle maturity as identified through the myosin heavy chain quantification and imaging of architecture. Following this, based on the mechanics of fibroblast populated collagen lattices (FPCLs), Cheema et al. seeded C<sub>2</sub>C<sub>12</sub> in a system that was in a collagen gel between two fixed points before testing seeding densities to discover that cell-cell contact was essential for the induction of differentiation<sup>100,101</sup>. These constructs structurally look much like *in vivo* muscle as well as having IGF-1, myosin heavy chain, calcium transients and contractile properties in common<sup>102</sup>.

An alternative to collagen is the fibrin model. This can also be cast between two points<sup>103-106</sup> as demonstrated by Strohmman et al.<sup>107</sup> and developed by Dennis and Kosnik<sup>108</sup> by seeding precursor cells

onto a fibrin layer with two suture points. The system “self assembles” into a cylindrical construct between the two sutures with a highly aligned architecture of myotubes with similar mechanical and biological properties with promising results although lacking the tensile strength of native tissue as of yet<sup>89</sup>.

Finally, much research has been done recently with composite gels, combining Matrigel®, a protein mixture from BD secreted from mouse sarcoma cells consisting of mostly collagen IV and laminin, with collagen or fibrin<sup>109</sup>. The factors in the Matrigel have shown potential for better differentiation, higher maturity and improved contractile properties.

Skeletal muscle is currently less frequently researched with the goal of being directly implanted, although that is of interest for more serious injuries with a variety of methods (see Qazi et. Al for review)<sup>110</sup>. For smaller injuries, skeletal muscle has an inherent ability to regenerate itself to a certain extent through the action of satellite cells and therefore, these injuries are left to repair<sup>110</sup>. *In vitro* skeletal muscle models are also used to test tissue behaviour under stimuli such as overload<sup>111</sup> and diseased states such as sarcopenia<sup>112</sup>. Recently, co-culture models with neurons to create a neuromuscular junction (NMJ)<sup>113</sup> and with bone to create an MTJ<sup>46</sup> have been attempted to make these models more relevant by including multiple tissue types to represent the musculoskeletal system more accurately, including tissue interactions and multiple cell types. For example, creating an NMJ allows for testing of toxins that effect the junction specifically such as neurotoxin-based venoms and botulinum toxin which would have not been detected in a simple skeletal muscle gel model<sup>114</sup>. Increasing the number of tissues represented allows for more powerful analysis by enhancing statistical significance. This thesis takes a step into attempting a new method for creating a simple method to create a multi-regional tissue engineered constructs for such purposes.

## 1.6.2 Current skeletal muscle hydrogel designs

The development from 2D cell culture to 3D *In vitro* models of skeletal muscle was a necessary step to overcome the limitations of the simple monolayer model attempting to mimic complex living systems. Tissue engineered models have therefore been developed to recapitulate *in vivo* environments and have been covered in the literature over the past couple of decades using a number of different methods all attempting to create architecture similar to that found in physiological functional skeletal muscle. These 3D models have superior contraction and sarcomeric development compared to 2D models, presumably due to increased number of cell-cell contact in 3D conditions and mechanical stimulus on the model<sup>115</sup>. Fibrin and collagen I matrices are the most commonly matrices used in skeletal muscle models throughout the literature<sup>104</sup>. As described in the literature review Section, no current models exist that fully tissue engineer both the tendon and the bone together

using a simple, cheap setup. So, the focus of this thesis is to take a skeletal muscle model that meets these criteria as a starting point and then to begin to develop it into a muscle-tendon model.

A summary of the main existing methods at the beginning of this project with their key components can be seen in Table 1.1, few of these methods are based solely on collagen, which is the most physiologically relevant and is also cheaper than other matrices like Matrigel® but none have attempted to create two tissue models in a single collagen construct.

Amongst these methods are a number of iterations that differ slightly depending on the group conducting the study. The fundamental goals of all these systems are maturation, structure, survival in culture, contractile ability and regenerative properties<sup>115</sup>. Bian et al.<sup>116</sup> highlighted that the systems need to therefore consider cell seeding densities, have cell attachment sites, allow for compaction and migration thereby allowing for alignment and finally have the required mechanical properties to allow contraction which is why many of these models share fundamental common themes matrices and attachment points. These then allow for unilateral alignment of the cells, which is a vital step in creating fused fibres replicating those of physiological skeletal muscle.

*Table 1.1: Table of systems currently used to 3D tissue engineered skeletal muscle*

Publication	Matrix	Cell type	Containment system	Gel attachment points	Volume
Vandenburgh et al., 1996 <sup>117</sup>	Collagen + Matrigel®	C <sub>2</sub> C <sub>12</sub> murine myoblast	Silicone rubber tubing (4mm)	Velcro tabs or stainless-steel screening	400 µl
Okano and Matsuda, 1998	Collagen	C <sub>2</sub> C <sub>12</sub> murine myoblast	Custom capillary tubing (0.9mm)	Fixed points	Not specified
Vandenburgh et al., 2008 <sup>118</sup>	Collagen + Matrigel®+ Fibrin	Primary murine myoblasts	Custom built wells	Silicone posts	100 µl
Bian et al., 2009 <sup>116</sup>	Fibrinogen + Collagen	C <sub>2</sub> C <sub>12</sub> murine myoblast	PDMS cast against lithography/rapid photopatterning master moulds (1.8 x 1.3 mm)	PDMS (sub-millimetre lithography)	100-600 µl
Chiron et al., 2012 <sup>103</sup>	Fibrin	Primary HDMCs	Suspended between two pins	Silicone pins	150 µl
Smith et al., 2012 <sup>119</sup>	Collagen	Primary rat DMCs	Commercially available single well chamber slide	Polyethylene meshwork	3200 µl
Martin et al., 2015 <sup>113</sup>	Fibrin/Thrombin	C <sub>2</sub> C <sub>12</sub> murine myoblast/ HDMCs	Custom built wells with pins	Stainless steel pins	700 µl
Wragg et al., 2016	Collagen	C <sub>2</sub> C <sub>12</sub> murine myoblast	Commercially available 8-well plates	Polyethylene meshwork	1500 µl

### 1.6.2.1 Tendon engineered models

Tendon tissue engineering is also being researched but with more focus on repairing damage. Due to the high incidence of injuries that occur in the tendon and associated interfaces and the low cell density and vascularity of the tissue compared to muscle, bone and the majority of tissue types in the body, the regenerative capabilities are much more limited to where even small injuries may result in scar tissue formation. This usually leads to a weaker tissue with diminished capabilities compared to the initial tendon<sup>79,80</sup>.

Much like tissue engineered skeletal muscle, tissue engineered tendons also need mechanical tensile cues in order to develop properly<sup>120</sup>. Most models are based on either Achilles tendon, hand flexors and extensors or rotator cuff tendons, as these are the tendons most often requiring repair clinically. With this basis, many tendon models are based on a system very similar to that of skeletal muscle where cells are seeded in collagen between two anchor points<sup>120,121</sup>, alternatively these gels could set in a mould without anchor points<sup>122</sup>. These are then implanted into animal models and have been seen to have positive results. Also like skeletal muscle, there is the possibility of using synthetic scaffolds, polylactic acid (PLA) and chitin/polycaprolactone (PCL) composites have been found to be good candidates<sup>123,124</sup>.

As for the cell types used, a truly specific tenocyte marker is yet to be found<sup>120</sup>, although tenomodulin (TNMD), scleraxis (Scx) and collagen1-A1 (Col1A1)<sup>58</sup> are found specifically in tendon fibroblasts and often used as markers. Cell types used in such models include epitenon tenocytes, tendon sheath fibroblasts, dermal fibroblasts, bone marrow or adipose derived mesenchymal stem cells (MSCs) and muscle derived cells (MDCs)<sup>120,122</sup>. However, MSCs have been found to cause spontaneous ectopic bone formation when healing *in vitro* once implanted at high concentrations<sup>69</sup>. As tendon cells are often referred to as fibroblasts, and are morphologically similar to most other fibroblast populations, dermal fibroblasts are also used in tissue engineered tendon models as well as MDCs and primary tenocytes<sup>122</sup>.

Other examples of single-cell population tissue engineered models include tumors<sup>125-127</sup> and liver<sup>128</sup> for disease modelling.

As can be seen, many models that exist currently are produced with the intention of clinical application. Pre-clinical models as a final goal, while still researched, are not as commonly sought after but are seen as a means to achieving clinical applications. This thesis will focus on matching a suitable tendon model with a tissue engineered muscle model to be incorporated together for *in vitro* pre-clinical modelling.

### 1.6.2.2 *Rationale for combining skeletal muscle and tendon tissue engineered models*

During musculoskeletal development, skeletal muscle develops through twitching, it requires attachments to bone in order for this twitching to be productive to development, it also requires this throughout life in order to maintain stimulus and therefore adapt<sup>129</sup>. Lack of stimuli for skeletal muscle leads to degeneration and morbidity<sup>19</sup>. Tendon also requires the presence and the mechanical stimulus created by muscle to develop properly<sup>33,66</sup>. The two cell types require cross-talk to become fully developed<sup>47</sup>. Having a model of both together then gives the opportunity for two things; firstly, create a system with the correct cellular interactions as they would exist *in vivo*, which is essential for a system to accurately represent physiology; as mentioned above, certain outcomes are undetectable in models until more tissue or cell types are introduced. Secondly, it may allow for better maturation and development of the individual models<sup>66</sup>.

### 1.6.3 **Types of Monolayer Co-cultures**

The majority of cell-based research over the last four decades have been based in monolayer cell culture. The reason for this is the ability to isolate cellular responses and better understood for the specific cell populations of choice. Monolayer cell cultures are generally used to find the best conditions for optimisation of desired cellular behaviours such as proliferation, differentiation, fusion or cell-cell interactions, secreted factors, interactions with a substrate by either geometry or otherwise<sup>130</sup> of specific markers through chemical or mechanical stimuli as well as understanding the mechanisms of these behaviours. A number of co-culture methods for monolayer systems have been identified. They can be divided into those that involve cell-cell contact between the different cell types and those that do not have this contact. The types are summarised in Table 1.2:

Table 1.2: Summary of types of co-culture in monolayer systems adapted from Bogdanowicz et al.<sup>130</sup>

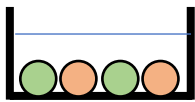

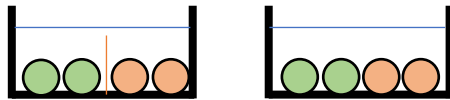
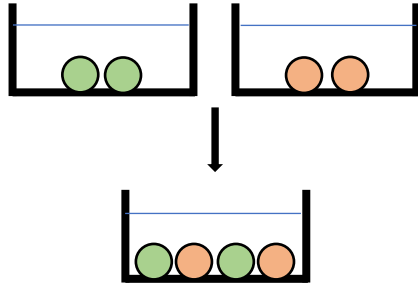
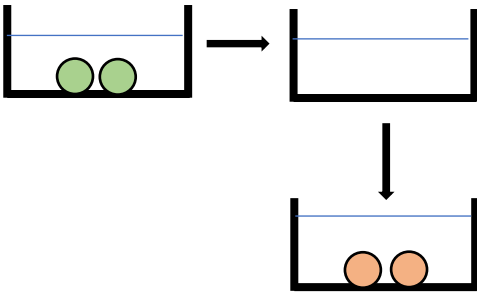
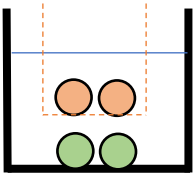
Type of coculture	Name	Method	Schematic	Positives	Negatives
Cell-cell	Mixed culture <sup>131,132</sup>	Two cell types are seeded and cultured in one vessel.		Very simple to set up and use.	Difficult to discern which results belong to which cells.
	Micropatterned <sup>133</sup>	Cell types are seeded into one vessel that has had the surface changed to meet certain criteria, thereby separating cell types by encouraging attachment in certain regions.		Allows for precise placement and proliferation of specific cell populations. Thereby controlling the cell interaction levels.	Need cell types that respond to different patterns. Takes much longer to prepare the vessel.
	Temporary divider <sup>132</sup>	An impermeable divider is placed between the two cell types until a determined time where it is removed and the cell types are cultured together.		Allows control between heterotypic and homotypic cell interactions.	Seal needs to be impermeable and the properties of the divider have a large influence on the system.

Table 1.2 Continued.

Type of coculture	Name	Method	Schematic	Positives	Negatives
No cell-cell contact	Separated co-culture	The cell populations are cultured individually until a certain point where they are combined in a single vessel for the remainder of the culture period.		Allows for the individual reactions of the cells.	The process is in two distinct, large steps meaning that the entire process can be quite arduous and time-consuming.
	Conditioned media <sup>134</sup>	Cell populations are cultured separately, the media from one is then transferred into the other cell population.		Allows to isolate the secreted factors of one cell population and measure the effects on the other cell population.	
	Porous membrane <sup>135</sup>	Seed one cell population in the vessel and the other in a porous membrane.		Effects on each cell population can be measured individually.	Soluble factors can only diffuse in one direction and some cells can block the pores in the membrane when proliferating or migrating.



These models evaluate the functions of a single cell population in a single matrix combined to make a model of a single tissue to understand its behaviour under certain stimuli. This is only limited to understanding how a single cell type can react within a system with no signalling or cross-talk with other cell types. This could include responses to cues such as temperature, gas concentrations, biochemical responses to certain compounds/factors and physical cues such as stretch or compression. However, as described earlier, musculoskeletal tissues are all part of systems and do not exist isolated *in vivo*. Therefore, to more accurately mimic and model these behaviours, it is important to move on from modelling tissues to modelling systems once the former has been established. As mentioned above, 3D tissue-engineered models allow for a more biomimetic system by introducing an ECM and new architecture allowing for seeding, growth, proliferation and signalling in an extra dimension. This has an impact on how the cells interact with each other and with the ECM, changing the outcomes and increased similarity to native tissue. The table above (Table 1.2) describes monolayer coculture types. These can all be implemented in 3D systems with similar outcomes, albeit with an additional element of difficulty in having to include a 3D ECM.

#### 1.6.4 Musculoskeletal co-cultures

##### 1.6.4.1 Monolayer systems

Monolayer co-culture systems have been previously used to model skeletal muscle<sup>109</sup>. While the majority of myoblast experiments have been done in single cell populations, the cells' interactions with many other cell types such as neurons<sup>136,137</sup>, bone marrow stem cells using the porous membrane method<sup>138</sup>, adipocytes using the porous membrane method<sup>139</sup> and conditioned media method<sup>140</sup>, fibroblasts<sup>141</sup> using surface patterning and a low barrier<sup>142</sup> have all been used with good levels of success. However, these are mostly focussed on one specific interface or interaction between tissue types and are rarely focussed on a larger scale of model such as an entire tissue or system.

##### 1.6.4.2 3D systems

As described in earlier sections, the tissues of the musculoskeletal system have individual, unique properties that work in unison to allow for optimum function. Therefore, it is important for all tissues to be involved to maximally understand the behaviour of the system. 3D co-cultures have the same methods available to them as the monolayer methods in Table 1.2, including both cell-cell contact systems and those where different cell populations are separated, although some of the behaviours are likely vary compared to 2D systems due to the introduction of a fabricated ECM.

##### 1.6.4.3 Myotendinous junction tissue engineered models

While the stages in the development of the MTJ are not yet completely understood, a number of attempts have been made to replicate the morphology by groups who have identified the importance

of the region. Larkin et al. investigated a method of pinning self-organised tendon constructs or adult/foetal rat tail segments into a monolayer of C<sub>2</sub>C<sub>12</sub> cells with results indicating morphological similarities to tissue found *in vivo*<sup>24,50</sup>. These constructs were also found to have mechanical properties to match the morphological similarities. The results also showed some level of neonatal MTJ marker paxillin<sup>50</sup>. However, the preparation time for the equipment was minimum three weeks, which is considerably longer than many other 3D systems and presents difficulties when considering that these systems may find use in high-throughput testing.

On the other hand, Merceron et al. went for a different approach, 3D printing polyurethane (PU) and PCL alongside C<sub>2</sub>C<sub>12</sub> and NIH/3T3 cells respectively<sup>143</sup>. The more elastic material was used on the muscle side to provide the best conditions for myoblasts development and equally, a stiff material on the tendon side did the same for the tenocytes. This resulted in a very well controlled architecture, showing a clear interface between two areas of different cell populations in 3D. There was again an increase in MTJ markers such as paxillin. However, the culture period was shorter than many standard periods for skeletal muscle and therefore the full extent of the development of tissues could not be determined. This study was also conducted using materials that are not physiologically representative as the scaffold materials and not the ECM composed the majority of the non-cellular construct. Notably, although these models were mechanically tested, tendon *in vivo* is a less cellularly dense tissue, relying mostly on the strength of the ECM for tensile properties, however, in this study the tissue consisted of mostly tendon cells. Despite these approaches, no material has been published on constructs that have been created with both tissue types made simultaneously and allowed to develop together, as would occur *in vivo* solidifying the adult phenotype for the region as mentioned earlier. Additionally, what also has not been assessed is whether in these 3D models there is an effect on the individual tissues and their development.

#### **1.6.4.4 Enthesis (Osteotendinous junction) tissue engineered models**

There are four stages in the transition between tendon and bone and the two tissue types have vastly different properties; bone is more adapted for compressive strength and stiffness while tendon is solely reliant on tensile strength and elasticity. In research and clinical settings, the interface between these two tissues is generally categorised together with the bone/ligament interfaces due to the structural similarities between the two tissue gradients<sup>144</sup>.

There has been a wealth of research on entheses tissue engineering looking at the clinical applications in tissue repair. This is in contrast to the lack of pre-clinical models due to clinical research being directly applicable and the high incidence of injuries that occur in this region<sup>145</sup>. Nevertheless, clinical applications often still require preparation in *in vitro* stages and could therefore provide useful

information in research. The OTJ requires the engineering of four stages: unmineralized tissue, unmineralized cartilage, mineralised cartilage, mineralised tissue, without having clear boundaries that would lead to stress concentrations between the tendon/ligament and the bone<sup>144</sup>. In monolayer, it was found that when fibroblasts and osteoblasts were separated with a temporary divider there was some evidence for interactions between the cell populations, stimulating the production of cartilage specific factors<sup>132</sup>. Spalazzi et al. studied at this in a 3D model using a triphasic scaffold graded into three regions with three cell populations seeded (fibroblasts, chondrocytes and osteoblasts) for reconstruction of the anterior cruciate ligament (ACL)<sup>146</sup>. This process may be viable for tissue repair, but as a pre-clinical method, the setup requires too much investment to be utilised in high throughput screening. Following this, Ma et al.<sup>147</sup> attempted to do the same, but to simplify extraction of three cell types from a donor, MSCs were taken and cultured into cells similar to the three cell types, and folded them into three sheets on top of each other with two anchor points were created by pinning a single divided bone construct either end of the, no fibrocartilaginous region was observed, potentially due to incorrect mechanics of the system through lack of mechanical load during development<sup>144</sup>. Something to note is that there is speculation that the fibroblasts transdifferentiate in the region due to mechanical factors<sup>148</sup> chondrocytic differentiation seems to be driven by compression while tenogenic differentiation seems to require tension. Finally, Paxton et al. developed a method involving a similar setup to Ma et al. where a fibrin ligament construct was anchored between hydroxyapatite-incorporated polyethylene<sup>149</sup> and brushite cement<sup>150</sup> anchors, using the minerals that are commonly found in bone as anchors to allow for room to develop into a multi-tissue engineered model.

## 1.7 Rationale for developing high-throughput, 3D tissue engineered systems for tissue interfaces

Tissue-engineered 3D models of skeletal muscle have been researched for decades as models of basic biology of muscle tissue to understand differences between muscle types and states, understand factors determining health of the tissue and responses to stimuli or drugs. With respects to drug testing, 2D cellular models are widely used in the pre-clinical stages, but these do not replicate the natural cell environment and are generally concerned with looking at responses within single cell types. As animal models are then used in the following stage, it is important to note that that these are not accurate when determining outcomes in future clinical stages, with the overwhelming majority of drugs ruled as safe in animal models failing human trials<sup>151</sup>. Therefore, 3D tissue engineered models have been developed with a goal of reducing the disparity from the pre-clinical stage, with less intensive resource requirements. However, whilst in some fields these models have been used, such as in burn wound treatments, in other fields such as skeletal muscle research, they have mostly been

used in experimentation in the laboratory, with small experiments to determine specific responses to specific stimuli. Whilst larger scale assays are often limited to 2D models due to the increased simplicity with which they can be used, there has been a recent drive towards introducing higher-throughput 3D testing systems to fulfil these requirements.

Due to the architecturally complex regions that are seen in the interfaces between the three tissue types in the musculoskeletal system, the mechanical properties and therefore the functionality of the system are highly dependent on the maintenance of these interfacial structures. However, injuries to these regions are extremely common, resulting in these tissues recovering with less optimal properties, thereby risking repeat failures. Currently, many models are being used to attempt to repair the damaged interfaces with tissue-engineered constructs. However, the basic biological understanding of these regions is still lacking, as is their specific responses to stimuli leading to a need in representative models of the muscle-tendon-bone interfaces. These models would allow to gather additional understanding of the cellular constituents and mechanisms in the transitional regions as well as the stimuli required to maintain or regenerate healthy tissue.

As both of the above needs are relevant within tissue engineering of the musculoskeletal system, there is a requirement for a model that can fulfil these requirements in order to overcome the current drawbacks of researched test systems.

## 1.8 Conclusions

Many of the systems above have received positive results, especially in regenerative medicine for the purposes they were designed for. A great deal can be learned from all the data gathered in all of these models. Many co-culture systems have shown to have potential in the sphere of musculoskeletal tissue engineering, showing that there are multiple ways to approach these issues. Monolayer systems have paved the way by allowing for testing of mixing of cells types and being the foundation for development of tissue engineered models.

3D models are the current state of the art in terms of models, as they provide a more representative scenario for the cells to behave as they would *in vivo*. This is ideal for pre-clinical testing as it mimics the environment that toxicology test samples will end up in.

Whilst there has been much research into developing the different tissues, with some looking into interfacial tissues, there is no model that is a complete muscle-tendon-bone model, including all the interactions between the multiple tissue and cell types and there is yet room for a method to create such a model. Also, as identified by Wragg et al.<sup>46</sup>, none of these current systems are optimal for high

throughput clinical testing due to either expensive setups or hard to acquire cell types. Based on the existing literature and the above observations, there are still steps remaining to developing a high-throughput, 3D tissue-engineered model containing multiple tissues including the interface.

## 1.9 Thesis Aims

The aim of this thesis is to develop a simple 3D tissue engineered simulated system with the potential to be expanded for high throughput screening that represents two interconnected tissues. In this thesis, skeletal muscle, tendon and bone are the desired tissues as well as all of the associated interfacial regions/tissues between them. Such a model would help reduce wasted resources in pre-clinical testing, by identifying unsuitable materials/ compounds and understanding more accurately the effects on cells and tissues before the need for testing in animal models and/or clinical trials, thereby reducing overall cost of developing treatments, as well as reducing the associated ethical burden of running such trials.

This thesis has two main components:

1. Develop a single existing tissue-engineered skeletal muscle process to be able to output large numbers of samples.
2. Develop the same system to be able to create a single, simple, fully tissue-engineered model, consisting of multiple tissues containing individual cell types. Current models are unable to do this in a simple manner, without preparing substrates or having to create separate tissue engineered models that are then fused. To overcome this, the current process of fabricating gels needs to be developed to adapt to these new requirements.

The specific issues involved with this will be expanded on in Chapter 3.

## 2 General materials and methods

### 2.1 Mammalian cell culture

All cell culture work was carried out under sterile conditions within a class II Heraeus biological safety cabinet. All cell types were incubated at 37 °C and 5% CO<sub>2</sub> in air in a Heracell 150i (Thermo Fisher) incubator when not being used. A master cell bank was created for the work described in this thesis and placed into liquid nitrogen for long term storage (as detailed in Section 2.7). Vials were thawed rapidly in a water bath set to 37°C as needed.

### 2.2 C<sub>2</sub>C<sub>12</sub> skeletal muscle cell line

C<sub>2</sub>C<sub>12</sub> murine myoblasts are a cell skeletal muscle line derived from satellite cells often used for 3D tissue engineered models due to their availability and ability to differentiate into myotubes upon decrease in serum<sup>112</sup>. C<sub>2</sub>C<sub>12</sub> Murine skeletal myoblasts (ECACC), between passage numbers 6-10 relative to the passage obtained, were cultured in a growth medium (GM) consisting of 20% foetal bovine serum (FBS, PAA Laboratory) and 1% (v/v) penicillin/streptomycin (Penstrep, Gibco) in a 4.5 g/L glucose Dulbecco's Modified Eagle's Medium (HG-DMEM) solution (Gibco). Cells were seeded immediately after thawing into T75 flasks for the first 48 hours before being transferred to larger T175 flasks. Every 24 hours, the medium was renewed.

After 4 days, GM was changed to differentiation media (DM) consisting of 2% horse serum (HS, Sigma), 1% penstrep (Gibco) in HG-DMEM (Gibco). 3D skeletal muscle constructs were cultured for 10 days thereafter.

### 2.3 hDF human dermal fibroblasts cells

Dermal fibroblasts are used in tendon models due to their similarity in morphology and genetic expression to tendon fibroblasts<sup>122</sup>. Human dermal fibroblasts were received (CBE, Loughborough University) at passages 3-5 relative to received passage. These were then cultured in growth medium (GM) consisting of 10 % foetal bovine serum (FBS, PAA Laboratory) and 1 % (v/v) penicillin/streptomycin (Penstrep, Gibco) in an HG-DMEM solution (Gibco).

### 2.4 Cell passage

Cells were routinely passaged at 80% confluence. The GM was aspirated and the flask was washed by pipetting PBS and ensuring all areas that contained media were thoroughly coated before removing. This was done twice. Enough trypsin-EDTA (0.05 %) solution (Fisher Scientific) was then pipetted to

cover the surface of the flask with cells attached and the flask was incubated for 5 minutes, allowing for the complete detachment of cells. This was confirmed by visual examination through a light microscope. To prevent potential damage to the cells by the trypsin, its further action was inhibited with the addition of GM (double of the original volume of trypsin added).

## 2.5 Centrifuging

All contents of the flask were transferred with a pipette to a centrifuge tube and centrifuged at 2000 RPM for 5 minutes, the supernatant was then pipetted to leave a cell pellet in the tube. This was resuspended in 1ml of GM before the cells were counted.

## 2.6 Cell counting

20 $\mu$ l of the cell suspension was mixed thoroughly with 180 $\mu$ l trypan blue solution (Sigma) in a 1 ml Eppendorf tube (1 in 10 solution). A single drop of this mix was deposited at the entrance to the counting chamber of a Neubauer haemocytometer beneath the cover slip and allowed to be drawn in through capillary action. Under a light microscope, the number of cells within each outer square of both half-chambers were summated. These were totalled up before being divided by 8 to give the average number in each quadrant. The 1 in 10 dilution with trypan blue meant that this number of cells needed to be multiplied by 10 (the dilution factor) to give an estimate of the number of cells in the cell suspension. The distance in between the chamber and the cover slide is 0.1 mm, so to convert this to the number of cells in 1 ml of suspension, it needed to be multiplied by  $1 \times 10^4$ . This was then multiplied by total volume of GM used in the suspension (1 ml as described earlier).

## 2.7 Cryopreservation

Once counting was completed, cells could be frozen for long term preservation. The cell suspension was centrifuged once again to get a pellet of cells. The cells were then resuspended to accommodate 1 million cells per 900  $\mu$ l (90%) of growth media, this was then mixed with 100  $\mu$ l (10%) of dimethyl sulfoxide (DMSO) (Fisher Scientific). This was all thoroughly mixed before being pipetted into 1.5 ml cryovials (Corning) in 1 ml volumes and all vials were then placed in a 'Mr. Frosty' (Fisher Scientific) in a freezer at -80°C overnight. This allowed for a slow freezing cycle, as is required to preserve maximal numbers of cells, at -1 °C/minute. The next day, all vials were transferred to liquid nitrogen for long term storage.

## 2.8 Tissue engineering of cell seeded 3D constructs

In skeletal muscle, where structure of the tissue influences dictates the function, tissue engineered models give more relevance through better representation of tissue architecture compared to monolayer models. The method used for fabricating cell seeded constructs was adapted from a previously published method<sup>112,152</sup>.

### 2.8.1 Preparation of reagents and equipment

All materials were washed with 70% ethanol, and subject to UV sterilisation for 20 minutes prior to experimentation.

### 2.8.2 Fabrication of PDMS

PDMS silicone elastomer (Sylgard 184, Dow Corning, UK) was provided as a two-part elastomer and curing agent. PDMS for experiments was fabricated by aspirating the elastomer into a container alongside (10% weight of elastomer) of curing agent, the mixture was then emptied into the mould of whichever vessel it was to be used in. These were then left at room temperature for 24 hours to complete curing. PDMS that need to be adjusted in shape was cut with a scalpel.

### 2.8.3 Fabrication of constructs

For collagen constructs of any size to be made, the ratios were as follows (10% of total volume) 10x MEM (GIBCO) was added to (85% of total volume) type-1 rat tail collagen (First Link) in a 50 ml centrifuge tube to give a yellow colour indicating the low pH of the solution. Sodium hydroxide (Fisher) was added in both 5 M and 1 M concentrations sequentially in a dropwise manner, with the tube being agitated after each drop until the colour noticeably changed to pink for the observer. This indicated a change in pH, allowing for both the addition of cells and the polymerisation of the collagen. Cells were then counted in the earlier described method and 12 million cells (4 million/ total ml of gel) were suspended in (5% of total gel volume) of GM and mixed quickly with the collagen mixture before being pipetted into the prepared chambers. Care was taken to pipette as quickly as possible because the collagen began polymerisation as soon as the neutralisation stage was complete and could end up setting in the centrifuge tube or pipette.

## 2.9 Construct culture

The gels were then incubated in standard culture conditions until they had fully set, requiring approximately 10 minutes. A needle was then used to gently detach the gel from the edges and bottom of the chamber. Constructs were thereafter cultured under the standard cell culture conditions mentioned above for the full 14 day period.



### 2.9.1 Calculation of gel success rates

Gel success rate was calculated as the percentage of gels that were successfully fabricated out of those that were attempted, i.e. no tears or breaks in the gel, attached to both anchor points.

### 2.9.2 Calculation of gel survival rates

Gel survival rate was calculated as a percentage of total gels fabricated that are considered evaluable at the end of the 14-day culture period. i.e. those that have no tears or breaks in the gel and are attached to both anchor points.

## 2.10 Macroscopic imaging during culture

The width decrease of the gel is a non-destructive method of identifying if a gel is likely to have fused myotubes at the end of culture. All gels were scanned from below in a desktop scanner (Epson) at regular time points (0, 1, 4, 7, 14 days) to allow for tracking of gel width and surface area as a function of time. Using a scanner ensured that the image was taken from the same distance and vantage point at every time point and therefore would yield a more accurate measurement. Images were analysed on ImageJ.

## 2.11 Immunocytochemistry and microscopy

### 2.11.1 Fixation, permeabilization and blocking

Samples were fixed a 50% methanol/ 50% acetone fixative at -3°C to dehydrate the samples, whilst maintaining the cellular structure. Samples were first PBS washed and were then given a 50% PBS/ 50% fixative solution for 15 minutes to prevent shock to the cells, afterwards samples were left in pure fixative for a further 15 minutes. The fixative was then removed and replaced with PBS, the samples could then be refrigerated until required for analysis.

If further permeabilization of the cell membrane was deemed necessary, triton X-100 was used in the blocking step at a concentration of 0.2% in 1 x PBS for 15 minutes.

### 2.11.2 Immunostaining

Immunostaining can be performed with either monoclonal or polyclonal antibodies. The antibodies are extracted from animals as a response to antigens. Monoclonal are more specific due to the animal's response only produced from a single isolated B-lymphocyte, producing only one antibody. These are then conjugates with a fluorophore and can be bound directly to the protein of interest (direct fluorescence) or bound to a primary antibody that is bound to the protein of interest (indirect fluorescence). Alternatively, conjugated dyes can be used which are incubated directly with the

samples without antibodies. In this thesis, both indirect fluorescence and conjugated dyes were used types were used.

Blocking of the samples was done with goat serum (Sigma Aldrich) which was the same as species as the secondary antibody at 5% in PBS with 0.2% triton X-100 for one hour.

A primary antibody solution of mouse monoclonal anti-desmin antibodies (Dako) (1:200) was made up in the aforementioned blocking solution and incubated overnight at room temperature. This was then followed by the secondary antibody of goat anti-mouse Alexa Fluor (Invitrogen) (1:500) in blocking solution for two hours at room temperature. Cell nuclei were counterstained with DAPI (Invitrogen) (1:1000) in PBS. Phalloidin (Invitrogen) (1:500) was used to stain cell cytoskeletons for 2 hours at room temperature and was added to the secondary antibody.

Between antibody stages, cells were washed 3 times for 2 minutes with PBS. After the final incubation, they were washed 5 times and then mounted on glass slides with fluorescent mounting medium (Dako) and covered with glass cover slips.

Samples were imaged in a Leica DM2500 M fluorescent microscope to look at the surface or a Zeiss LSM880 confocal to image individual planes in the gel.

## 2.12 Image analysis

Both macroscopic and microscopic images were analysed with ImageJ. Gel centre width, gel surface area, myotubes per frame, myotube thickness, myotube length, number of nuclei per myotube and myotube angles were all recorded in myoblast containing models. The scale for these measurements was set according to the known frame dimensions.

## 2.13 Gene expression

### 2.13.1 RNA extraction

After the culture period, gels were removed from their chambers and placed into 1.5 ml RNase free tube (Fisher) with 500  $\mu$ l of TRI-Reagent (Fisher). A stainless-steel bead was then inserted into the tube, and the gels were homogenised using a TissueLyser II (Qiagen). 100  $\mu$ l of chloroform was then added into the tubes, and the tubes were agitated by hand for 20 seconds before being left to incubate for 5 minutes at room temperature. The tubes were then centrifuged at 12000 g for 15 minutes. Only the clear aqueous phase that had risen to the top of the solution was then transferred into a new 1.5 ml RNase free tube and 250  $\mu$ l of isopropyl alcohol (Fisher) was pipetted onto it and left to incubate for 10 minutes at room temperature. The tubes were then centrifuged at 12000 x g for 10 minutes. A small pellet could then be visible at the bottom of the tube. The supernatant was removed, and the

pellet was vortexed with 500 µl of 75% ethanol (Fisher) and centrifuged at 7500 x g for 5 minutes. The ethanol was then removed as much as possible without disturbing the pellet, and the remainder was allowed to air dry for 20 minutes at room temperature. This pellet was then suspended in 50 µl of RNA storage solution (Sigma) and then stored at -80°C until required for PCR.

For all samples, absorbance at 260 nm and the ratio of 260/280 nm (purity) were tested using the Nanodrop 3000 spectrophotometer (Fisher) prior to PCR.

### 2.13.2 RT-PCR

Real time quantitative polymerase chain reaction (RT-qPCR or qPCR) was used to measure expression of genes of interest through messenger RNA (mRNA). It is built on the principles of polymerase chain reaction (PCR) where the mRNA target sequences in the sample are reverse transcribed into complementary DNA (cDNA) which is then amplified for measurement of each. The PCR process works in the following steps for one cycle (Figure 2.1):

Denaturation: The double strands of DNA separate at 90 °C

Annealing: The temperature is decreased to allow for the primer to bind to the DNA target sequence

Extension: A further increase in temperature allows for the DNA polymerase (enzymes that polymerise new DNA sequences) to work most efficiently, adding deoxynucleoside triphosphates (dNTPs) to the chain, completing the DNA reverse transcription.

Cycles are then repeated 30-40 times to amplify enough DNA, this is detected through fluorescence of SYBR® green by measuring it once above background fluorescence known as the threshold cycle ( $C_T$ ). The higher the threshold cycle, the lower the quantity of target gene.

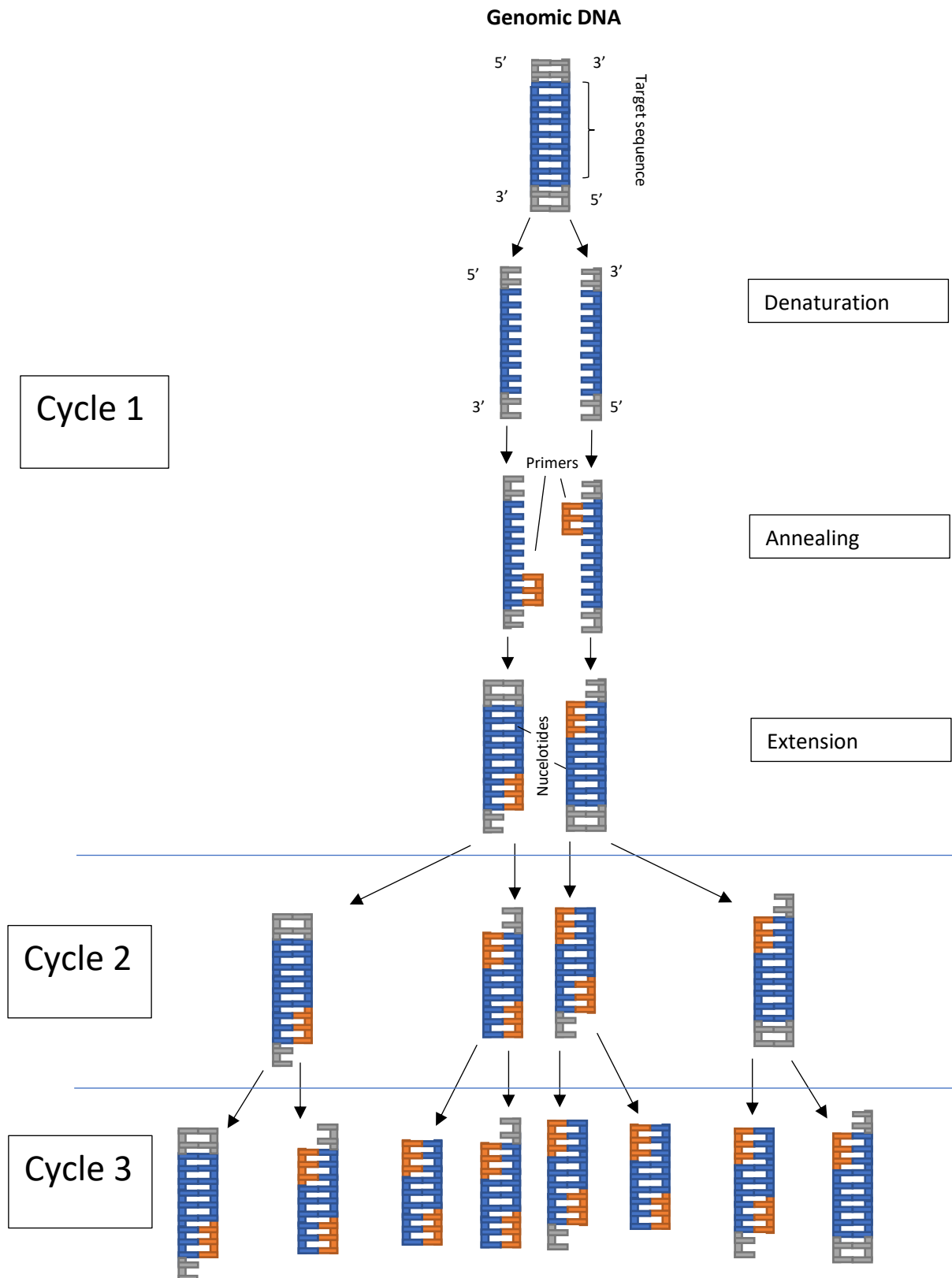


Figure 2.1: Schematic of quantitative polymerase chain reaction showing the three steps per cycle: (A) Denaturation, where the DNA strands are separated, (B) Annealing, where the primer attaches to the target sequence and (C) extension, where the remainder of the DNA strand is synthesised using nucleotides.

### 2.13.3 Primers

Primers were acquired that had been previously designed or used for the C<sub>2</sub>C<sub>12</sub> cell line using melt curve analysis<sup>153</sup>. The two primers used were Myosin heavy chain isoforms MYH1 (fast IIX) and MYH3 (embryonic).

### 2.13.4 Analysis

PCR was performed in a 7300 Real Time PCR System (Applied Biosystems) and ViiA™ 7 RUO software. Quantifast® SYBR® Green one step kits (Qiagen) were used.

For each reaction, 4.7 µl of SYBR® Green was mixed with 0.1 µl forward and 0.1 µl of reverse primer alongside 0.1 µl of quantifast reverse transcriptase kit to create 5 µl of master mix. This was then combined with 5 µl (1:1 ratio) of de-ionised, purified water. Based on standard curves of known RNA concentrations, each primer was validated to ensure a reaction efficiency of 90-110% which found that each reaction required 20 ng of RNA. This dilution meant that each reaction contained 20 ng of RNA and was deposited into a 384-well plate (Applied biosystems).

The reaction cycle was as follows:

<b>Temperature and time</b>	<b>Number of cycles</b>
50°C for 10 minutes	1
95°C for 5 minutes	1
95°C for 10 seconds, 60°C for 30 seconds	40

After this a melt curve analysis was run to exclude non-specific amplification. Relative gene expression was calculated using the equation by Livak & Schmittgen<sup>154</sup> and given in the form of  $2^{-\Delta\Delta CT}$ .

## 2.14 Statistical methods

Statistical analyses were performed on the GraphPad prism 6.0 software (GraphPad Software Inc). In short, group means were compared to determine whether there were differences between conditions and are denoted with asterisk(s) (\*, \*\*, \*\*\*, \*\*\*\*) representing P values of ( $\leq 0.05$ , 0.01, 0.001, 0.0001) respectively. A student's t-test was used for the comparison of two means, and a one or two-way analysis of variance (ANOVA) was used to compare the means of more than two groups. The specific analyses and tests can be seen in the results of each chapter and in figure legends of data. All data is given in the form of Mean  $\pm$  Standard deviation unless otherwise stated.

### 3 Developing the gel-making process to allow for higher throughput and co-culture of multiple gel regions

3D tissue engineered cellular models have been widely explored in the literature (Section 1.6.1.2). While the vast majority have focussed on single cell types within a single matrix, more recent research has focussed on attempting to advance this to replicate two heterogenous engineered tissues in a single system in an attempt to model multiple tissues as a system (Section 1.6.4.3). So far, these systems have not been adapted to be used in pre-clinical modelling, likely because they have not lent themselves to being able to create large numbers of samples in a single setup like arrays do for pharmaceutical testing. Additionally, the co-culture systems are generally complicated, require expensive specialist equipment and are time-consuming to prepare, sometimes requiring two separate tissue types, or a separate decellularized tissue as part of the model<sup>54,143</sup>. These factors, in turn, can lead to variability within between prepared samples as a result of the complex and labour-intensive fabrication processes. The information in this Chapter focusses on the two thesis aims outlined in Section 1.8:

1. Development of a 3D tissue-engineering method for skeletal muscle in collagen to make it easily reproducible enough for future use in large enough numbers for pre-clinical screening applications.
2. Attempt to develop the above model into one that allows tissue-engineering of a 3D model, with a second, separate acellular/unseeded region in the same gel, whilst maintaining the above goal. This will then create two distinct regions within one single hydrogel. The acellular region could then be populated with a complementary cell type in future experiments. The benefit of this would be to allow a stronger mechanical formation of the interface between the two tissue types as it would be one single matrix, while also allowing the cells to interact between regions as they would in vivo.

#### 3.1 Specific Chapter aims

- Develop methods and apparatus to allow for the creation of hydrogels created from a single ECM material that is separated into differently seeded regions.
- Ensure this method is scalable to produce larger numbers of gels in one setup compared to preceding models.
- Maintain or improve the macroscopic uniformity of the gels.

## 3.2 Introduction

### 3.2.1 Process development methodology

A review by Pisano et al.<sup>155</sup> identified four key metrics for evaluating process performance that can be used to compare companies within the same industry. These are namely: quality, development speed, research productivity and manufacturing productivity. Evaluation of these individual metrics for any given process can identify opportunities for development and facilitate process improvement. This established approach can provide a logical structure for the evaluation of the processes in this thesis. The same review places emphasis for an organisation – specifically in the pharmaceutical industry to implement a ‘learn-before-doing’ approach alongside the normal ‘learn-by-doing’. The former approach involves refining and understanding a method by using research and simulations of different kinds prior to implementing the process, while the latter is more constitutes the refining of a process after it has been implemented onto the production line. Scientific research is mostly a ‘learn-before -doing’ field, as it is the development of processes before they are used on a large scale and implemented in production. However, once a system is created and somewhat refined, it is then exposed to the wider scientific community in the form of publications where other researchers can use it. It can be argued that at this point, it is now treading on the line between the two learning styles as new researchers implement the system and refine it themselves after replicating the process i.e. ‘by-doing’.

It is not a realistic expectation to take a published method and manage a solution to the problems it is being utilised to address on the first attempt, this may be because the requirements of the product change since original publications or the scenarios, operators, equipment that are being used are different compared to those reported and instead, an iterative process is necessary to correct all the unforeseeable issues that arise in the development process. The International Conference on Harmonisation (ICH) guidelines – Q8 for pharmaceutical development also stress this by also emphasising the need for process improvement, validation and verification<sup>156</sup>. This was a guideline released through good manufacturing process (cGMP) when the Food and Drug Administration (FDA) was burdened with the volume of quality regulation required in pharmaceutical development. This was followed by the introduction of Quality by Design (QbD), in a way of progressing to a more holistic approach to developing pharmaceuticals and biotechnology products, adjusting the development using gathered knowledge to build quality into the product instead of testing for it at the end<sup>157</sup>. QbD is a developed form of learning-before-doing where a fully characterised process is built which then relies upon learning-by-doing to support continual process improvement. In QbD, Target Product Profiles (TPPs), and Target Product Quality Profiles (TPQP) are first defined, otherwise known as the

quality characteristics that ideally would be achieved to ensure the quality and efficacy of the product. Thereafter, critical quality attributes (CQAs) are decided and are set as an endpoint to move towards with a developing process. This process is incrementally adjusted by identifying the sources of error and understanding individual components and behaviours of the system, ensuring consistent outputs. A risk assessment is then carried out in order to identify the quality attributes that are most likely to impact TPQP. Then a design space is built through experiments to understand the range that exists within the individual parameters which allows the CQAs to remain within acceptable limits.

Within manufacturing industries, the development is more results-oriented on a tight deadline where the process only matters if it attains what is required whilst meeting requirements for cost, time etc. The approach taken is typically a development of a functional process by conducting the minimal experiments required to gather the results. In academic settings, this is a little more process-oriented, as it usually is to ascertain results based on processes in an attempt to develop knowledge and acquire intellectual property that are then translatable and adopted by industry. Academic experiments are more exploratory in nature. In industries such as pharmaceuticals, a combination of internal and external knowledge is required by firms to develop products.

In accordance with these concepts, a risk assessment approach was adopted for the initiation of this Chapter. The design specification in Table 3.2 is foreseeing the potential problems with this thesis before any 'doing' occurs.

The key elements in this thesis can be separated into two process variables:

1. The components: their production methods and their assembly, their composition, properties and their dimensions. i.e. raw materials.
2. The gel fabrication process: While the ratios of the inputs are going to remain similar, the operating procedures, the method in which the components of the gel are treated including timing, temperature, equipment used in the fabrication can all be adjusted. i.e. the method.

While these are presented as two distinct parts in this thesis, development of both must be carefully co-ordinated to ensure the most successful output. To draw another parallel from industrial process development outlined by Pisano et al.<sup>155</sup>, this thesis will use a type of integrated problem solving. This is a consideration in process development which merges considerations from different specialties, in this case the cellular biology associated with the tissue, the engineering of the apparatus and the process engineering of the entire system. This theory is corroborated by the International Conference on Harmonisation (ICH) Q8 guidelines on pharmaceutical development<sup>156</sup> where it is explained that the critical formulation attributes in commercial production batches need to be considered alongside



the available manufacturing process options to select the required manufacturing process and to then find the most appropriate components. For example, here the chemical process of neutralising the collagen needs to be considered, alongside the mould designs to allow for maximal use of that collagen before it is no longer transferable. The technical choices between the different processes and the operating conditions need to be evaluated in unison to yield the best process. The ICH guidelines also highlight that manufacturing process development requires constant monitoring of the critical parameters to regulate the difference made to the quality of the product. These will be measurable outcomes in this project, including macroscopic outcomes, such as percentage of gels that are successfully fabricated, decrease in gel surface area over culture period and microscopic outcomes such as number of myotubes, width of myotubes, length of myotubes and number of nuclei per myotube per microscopic frame which dictate whether or not the model is showing consistent output.

Although this is not an industrial process at this point, all experiments in this thesis are conducted with the goal of attaining high numbers of reliable models for the final product to facilitate this future translation. Therefore, the experiments conducted to understand the feedback between process and operating variables will allow for accurate feedback to ascertain if the new process is yielding the desirable results; this is not always the case in the industrial process where problems can arise from simple scaling up a system or handing the methodology from an operator to a machine that now needs to be optimised to perform the same function<sup>158</sup>.

Since the conception of these models, the different groups experimenting (some of which can be seen in Table 1.1) have accumulated a lot of unpublished findings and knowledge gathered from experience specific to this model. As Pisano et al. state<sup>155</sup>, these kinds of ‘rules of thumb’ or ‘heuristics’ are an alternative way of narrowing down operating conditions in process development. This then reduces the amount of experimental data that needs to be gathered in future models. However, whilst this makes sense in a manufacturing setting where knowledge is shared by everyone working together for a company, in academic research, much of this can often be lost or never reported.

### 3.2.2 Components and setup

In order to achieve the first aim of this Chapter: *“Develop the 3D tissue-engineering method for skeletal muscle in collagen to make it easily reproducible enough for large enough numbers for pre-clinical screening applications,”* the process needs to meet the aforementioned criteria while also lending themselves to being cost effective, easily reproducible in large numbers and consistent. Of the models listed in Table 1.1, collagen models are preferable as it is the majority matrix constituent in both muscle and tendon while also being present in bone, therefore it is more representative of native tissue. Among the collagen models, the older methods are fabricated inside tubing, resulting in a

cylindrical structure. This has been recently forgone for bespoke chambers which allow for shaping of the model as desired – although an overall rectangular shape is the preferred geometry as the starting point for almost all current models; the increased distance across the axis of unilateral strain between the two anchor points allowing for the optimal passive mechanical forces to regulate the development of the model. In order to achieve the required dimensions of these moulds, they are usually made to specification depending on the specific parameters that are determined or used by the investigator. However, previously, a high cost and long production time was associated with bespoke chambers, especially those made from glass, which impacted the economy of testing large numbers of repeats. These models can also require expensive and time-consuming processes to set up on-site, such as photolithography, or – even for the less expensive methods- need to be produced by a third party off-site, increasing cost and time further.

To achieve the second aim of this Chapter: *“Attempt to develop the above model into one that allows tissue-engineering of a 3D model, with a second, separate acellular region in the same gel, whilst maintaining the above goal.”* The chosen method needs to have potential to be adjusted to allow for multiple cell/tissue types within a single model.

Taking these two considerations into account, the cheapest methods with the simplest setup requirements were identified as those of Smith et al.<sup>152</sup> and Wragg<sup>46</sup>. In fact, the method described by Wragg was an evolution of the Smith setup to begin progressing towards a high-throughput model. The key difference between the two is that Smith et al. used bespoke glass chambers/ chamber slides with specific dimensions, whereas Wragg used commercially available 8-well plates with PDMS boundaries to create the desired dimensions for a validated scaled down model. This led to a trade-off between output and consistency, where the bespoke chambers would have more consistent dimensions whilst the 8-well plates allow for higher numbers of samples due to the availability of the plates and smaller gel sizes. The implications of this on the Chapter aims can be seen below in Table 3.1. These two methods will be the starting point for this Chapter. Based on the above critique of the current relevant systems, a design specification can emerge to create a framework for the most suitable process to achieve both Chapter goals. Based on the models that are currently available for skeletal muscle in Table 1.1, desirable properties or methods can be combined to create a model that meets the needs for this Chapter. For example, smaller volume gels, resulting in less cells required per gel which can increase total number made and reduce the strain resources. Additionally, introducing posts or pins as anchor points to systems that have previously not used them could also be an option<sup>118</sup>. By critiquing all the preceding models, a specification can be produced for the new system. This can be seen in Table 3.2.

Table 3.1: Comparison of fabrication methods of Smith et al. and Wragg et al., benefits in line with the aim of this Chapter are highlighted in green and undesirable properties in red.

	Smith et al. <sup>152</sup>	Wragg et al. <sup>46</sup>
Vessel	Bespoke glass chamber moderately expensive but easily acquired/premade	8-well plate cheap and premade/easily purchased
Anchor points	Anchor points are handmade, each one is different dependent on the skill of the fabricator	Anchor points are handmade, each one is different dependent on the skill of the fabricator
Assembly	Quick to assemble – hook anchor points	Slower to assemble, but still quick and simple – close off required area with PDMS, then hook anchor points
Consistency	Variability between chambers low	High variability between each mould due to difficulties in keeping PDMS dividers/blockers identical
Disinfection pre-culture and infection prevention during culture	Easy to sterilise – ethanol + UV, Lid on larger petri dish	Easy to sterilise - ethanol + UV, lid directly on top
Number of constructs from neutralisation process	One gel – Each gel is neutralised separately. No repeat gels with the same collagen can be made.	Two-Four gels – Maximum four gels could be fabricated using a single neutralisation before requiring new collagen to be neutralised.
Cell number required	3.2 ml gel seeded at 4 million cells/ml. Single gel requires 12.8 million cells	1.5ml or 0.25ml gel seeded at 4 million cells/ml. Single gel requires 6 million cells
Control of different cell populations	No specific control of cell populations during seeding. One homogenous gel is pipetted into the mould, all regions throughout containing the same gel with the same cells with the same distribution.	No specific control of cell populations during seeding. One homogenous gel is pipetted into the mould, all regions throughout containing the same gel with the same cells with the same distribution.
Medium capacity	Can only hold one chamber's worth of media volume (minus volume of gel)	Can hold much more media, as when PDMS is removed, opens another chamber's worth of volume
Visibility during culture	Transparent vessel allows for easy imaging during culture	Transparent vessel allows for easy imaging during culture
Potential for mechanical stimulation	Requires transferral to a longer chamber	Requires transferral to a longer chamber
Reusability – how many times the mould can be used for a full culture period	Reusable	Reusable – although less durable and less consistent

Table 3.2: Table evaluating the design specifications for the new system.

Component	Description
<b>Vessel</b>	Vessel should come either commercially available, cheaply, or be easy and cheap to fabricate. Needs to be able to act as the mould for the gel, but also contain the media after the gel has set. Material needs to be compatible with cell culture.
<b>Anchor points</b>	Anchor points should be either part of the vessel, or come prepared with a fast process and consistent dimensions
<b>Assembly</b>	Assembly should require minimal stages. One or two stages such as gluing and positioning after sterilisation is ideal.
<b>Consistency</b>	Dimensions of vessels, anchor points and assembly need to have minimal variability between them.
<b>Disinfection</b>	Disinfection must be simple, a soak in 70% ethanol followed by a predefined period in UV light would be optimal. This means the materials need to be compatible with this process
<b>Prevention of infection</b>	Infected samples need to be discarded immediately and are therefore costly. Preventing infection in samples is paramount.
<b>Volume of samples that can be made per single neutralisation</b>	Three minimum to simplify repeats. However, up to six, nine, twelve or more would allow for more accurate results from testing and experimentation.
<b>Cell number required</b>	4 million cells/ml established standard. So decreased size of construct to 500 ul or smaller to maximise how many samples can be made within a single passage of cells.
<b>Control of different seeding populations</b>	Ability to be able to choose where to seed cells within the gel is necessary for multiple cell populations and tissue types.
<b>Media capacity</b>	Media capacity many times the volume of the gel is ideal, ensuring the cells have all of the nutrients they need to mature.
<b>Visibility during culture</b>	Being able to track the macroscopic changes during culture as well as checking for infection/tears is important to predict the microscopic outcomes of the final gel. A transparent system is therefore optimal.
<b>Reusability/ economy</b>	The system either has to be reusable, or at least produce a very high number of inexpensive repeats with minimal difficulty. It can also alternatively reduce the number of consumables used per experiment.
<b>Potential for adjustments</b>	Design versatile enough to easily be able to introduce new geometries, mechanical stimulation and any other future experiments without significant time delays.

Ideally, if a technique to create the components can be created that is simple and yet highly versatile, a standard manufacturing process can be set up in which multiple different systems can all be fabricated using the same technique allowing for easy comparison between systems and setup using in-house equipment when alternating between them.

### 3.2.3 Fabrication method breakdown

Once the apparatus specification had been defined, the corresponding method in which the raw materials are used needed to be analysed. Based on preliminary trials with the equipment, a number of key areas were identified which impact the whole fabrication process heavily in terms of time and success rate:

It is important to note that the below table (Table 3.3) considers only a single homogenous gel population, i.e. a C<sub>2</sub>C<sub>12</sub> only construct. Introducing more cell types increases the length of the process exponentially and also introduces the difficulty of needing to ensure they are formed together without individual Sections solidifying in isolation. It is clear from the above table that the biggest impact would be made if there was a way to be able to prepare one single batch of gel to make more samples required without having to rush the pipetting into the mould before returning back to the beginning of the whole process for every construct.

*Table 3.3: Breakdown of the method for fabricating a gel, the number of \* represents the increase in time requirement of the stage when making multiple gels based on preliminary experiments*

Stage	Explanation	Impact on process	Improvements	Repeat required for multiple gels?
<b>1. Cell count and resuspension</b>	Counting the total number of cells cultured and resuspending them in media.	Minimal impact in time and success rate.	Automated cell counting would decrease the slightly.	N
<b>2. Cell separation into batches*</b>	In order to save time once the collagen has been neutralised, cells are pre-pipetted into individual centrifuge tubes in the volume containing the required cell density so that they can be pipetted straight in without needing to change pipettes	Increases linearly with the number of samples that are being produced.	Being able to pipette more gels in a single batch reduces the need for multiple iterations of this step for each individual gel.	Y
<b>3. Collagen measurement*</b>	Measuring the required amount of rat tail collagen for the gel being made.	Increases linearly with the number of samples that are being produced. Due to 7B.	Being able to only pipette one single larger batch.	Y
<b>4. Addition of MEM*</b>	Combining the collagen with MEM to indicate for the next step.	Increases linearly with the number of samples that are being produced. Due to 7B.	Being able to only pipette one single larger batch.	Y
<b>5. NaOH drop until indicator changes colour **</b>	Neutralisation of the collagen through addition of sodium hydroxide to initiate the polymerisation. This begins a countdown until the polymerisation prevents the gel from being pipetted by becoming too viscous, meaning the following steps need to be done quickly.	The rush to pipette following this step means that large numbers of cannot be neutralised in one single batch as the gel would set after one or two moulds were filled. This step is the largest cause for problems by increasing the time required at all previous steps as well as causing gels to set too soon or incorrectly.	Extending the time until setting of the gels would make the process yield a much higher number of samples in a shorter amount of time.	Y

Stage	Explanation	Impact on process	Improvements	Repeat required for multiple gels?
<b>6. Combine gel and cells</b> <b>7. Pipette into mould**</b>	Combine the prepared cell suspension with the just-neutralised gel suspension.	This needs to be done very quickly to prevent the setting of the gel in the centrifuge tube or pipette instead of the mould.	As above.	Y
<b>7b. Return to cell count stage (move onto stage 2 if cell count already done)**</b>	Once one or two gels were made, return to the beginning to make one or two more until all were made.	The need to return to the start increases the time exponentially for each gel that is required	Being able to make more gels using a single neutralisation.	Y
<b>8. Incubate</b>	For any gels that had not set, incubate at culture conditions until no longer liquid.	Impact can be large as some gels can take tens of minutes to set.	Make all samples from a single gel suspension so they set simultaneously.	N
<b>9. Add growth media and “float” gels</b>	Add culture media to the construct, remove any unnecessary components (such as PDMS mould components that are no longer needed) and ensure the construct is not adhered to the bottom of the vessel.	Can increase linearly with samples if many components need to be removed and if constructs are particularly difficult to detach from bottom of vessel.	Ensure components do not encourage adherence of the constructs to the surface.	Y
<b>10. Culture</b>	Regular media changes, checks, and images.	None – all culture conditions are standardised. Improving this process is outside of the scope of this project.	None.	N

### 3.2.4 Key points moving forward

The process development can be divided into two parts:

1. Apparatus – all of the components required to make the constructs. These should be as simple to produce, set up and use as possible whilst adapting them to a multiple tissue system through development of the individual components.
2. Fabrication method – including the neutralisation and pipetting. The aim of this thesis is to decrease the time required to make gels through developing the current method.

Combining these two aspects, required for the development of the process, this Chapter aims to create a high volume, multiple tissue construct fabrication process.

### 3.3 Materials and methods

#### 3.3.1 Cell culture and gel fabrication

C<sub>2</sub>C<sub>12</sub> murine myoblasts were cultured and seeded into collagen hydrogels as described in the Chapter 2, Section 2.2 unless otherwise specified.

#### 3.3.2 Initial fabrication method – Single glass bath

##### 3.3.2.1 Setup

Glass chambers (45 x 20 x 7mm) were used as a mould for the gel before also being used as the container for the media throughout the entire culture period (Figure 3.1).

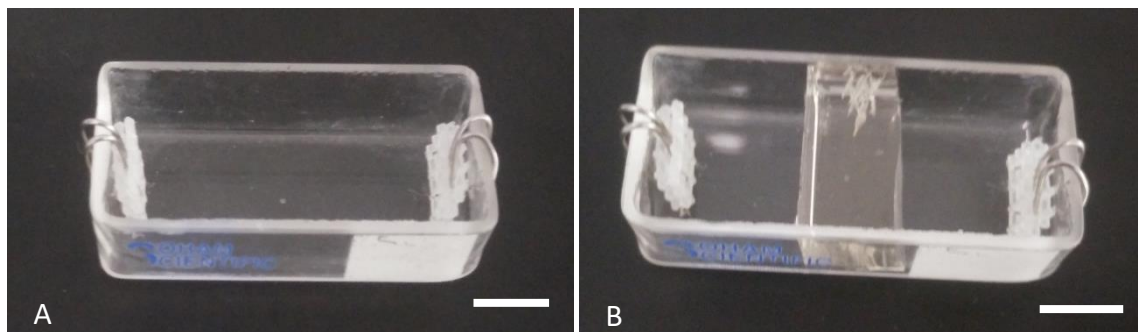


Figure 3.1: A- Glass chamber setup, B- with PDMS blocker. Scale bar = 10mm

Attached to each end of the mould were floatation bars known as “A-frames” These were made from cutting rectangles (15.0 x 6.0 x 1.5 mm) from a sheet of 10 holes inch<sup>-1</sup> polyethylene mesh and then binding three rectangles together with 0.3 mm stainless steel orthodontic wire bent into a shape as can be seen Figure 3.2 before hooking them into the mesh. Before the start of the experiment, all setup equipment was sterilised with 70% IMS, then assembled (Figure 3.1A) and were then left in UV light for 20 minutes.

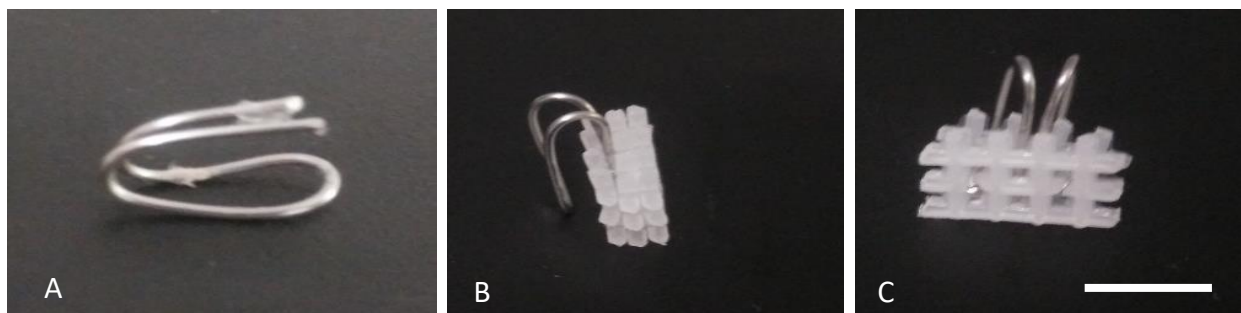


Figure 3.2 (A)- stainless steel orthodontic wire bent to shape a hook. (B) and (C)- hook in the mesh to create an “A-frame” (anchor point), scale bar = 10mm

The first attempts for segmenting gels were run in the original glass chamber arrangement as it was much simpler to fit a divider into the middle of a bespoke chamber than to adapt it to another system that already uses PDMS. A Section of PDMS (15 x 20 x 7mm) was cut using a scalpel and placed directly in the middle of the chamber to keep the two unseeded (acellular) regions in place Figure 3.1B. The idea was to create a cellular C<sub>2</sub>C<sub>12</sub> region flanked by “acellular” regions that would be only collagen on either side that could then be seeded with other cell types (Figure 3.3).

A smaller set of A-frames, one-third of the size were made for a set of miniature gels that were positioned width-ways across the same setup.

### *3.3.2.2 Fabrication of gels and culture method*

Initial stages of gel fabrication followed the method described previously (Smith et al.)<sup>119</sup>, cells were cultured for the total 14 day protocol (Chapter 2, Section 2.9). Separate gels were made for different regions, each requiring a repeat of the gel neutralisation step (Chapter 2, Section 2.8.3). Segmented gels were created by first depositing the peripheral regions, waiting for the collagen to polymerise enough to no longer move when agitated, then the divider was removed and the cell-seeded region was deposited in the newly vacated central region (Figure 3.3). Every bath was put inside a large petri dish and covered with the lid to prevent infection. This process was used for all segmented gels unless stated otherwise.

### *3.3.2.3 Time measurement of fabrication stages*

All time measurements were taken using a stopwatch which was started prior to conducting work in the biological safety cabinet and stopped once the stage in the process was completed.

## **3.3.3 Gel success and survival rates**

Gel success and survival rates were calculated as described in Chapter 2, Section 2.9.



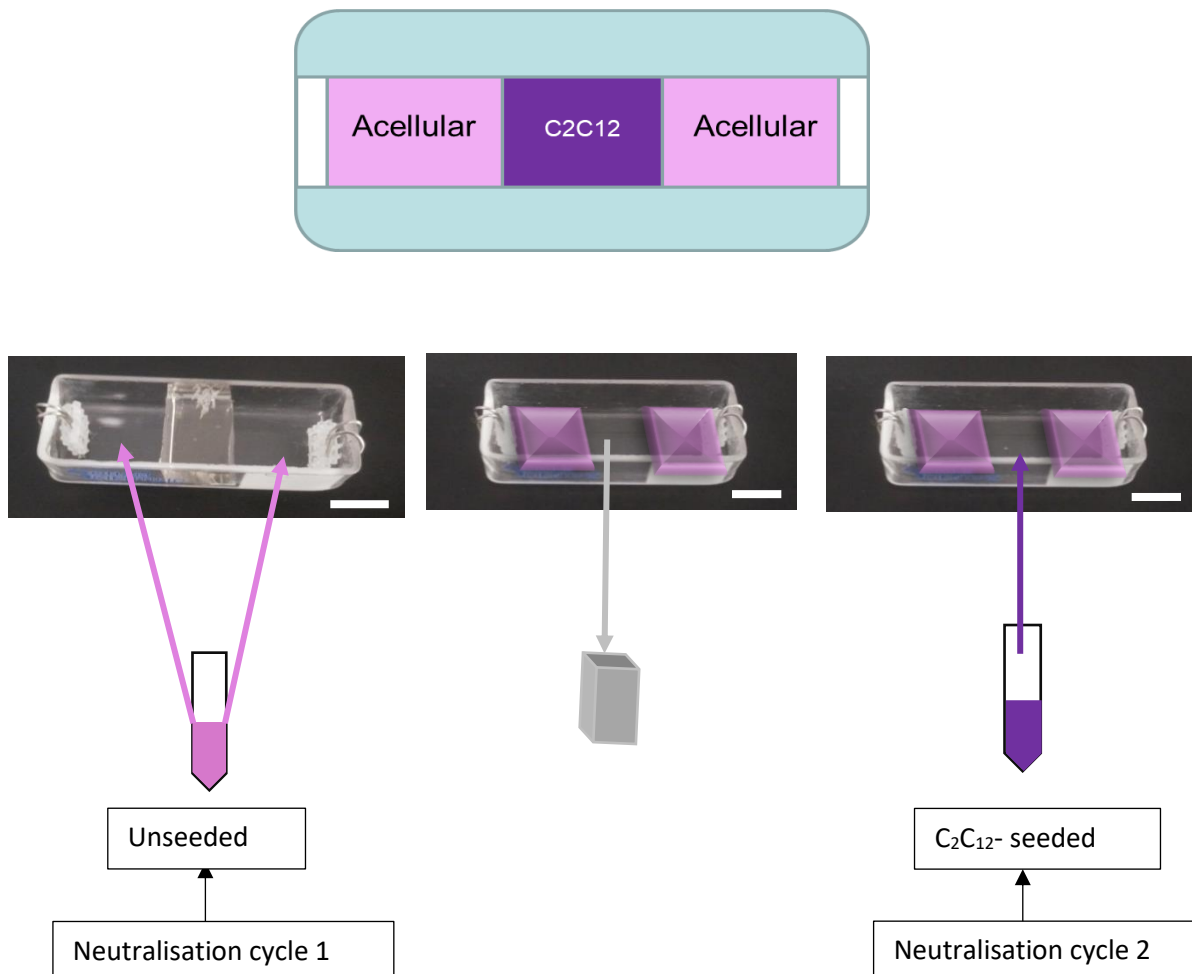
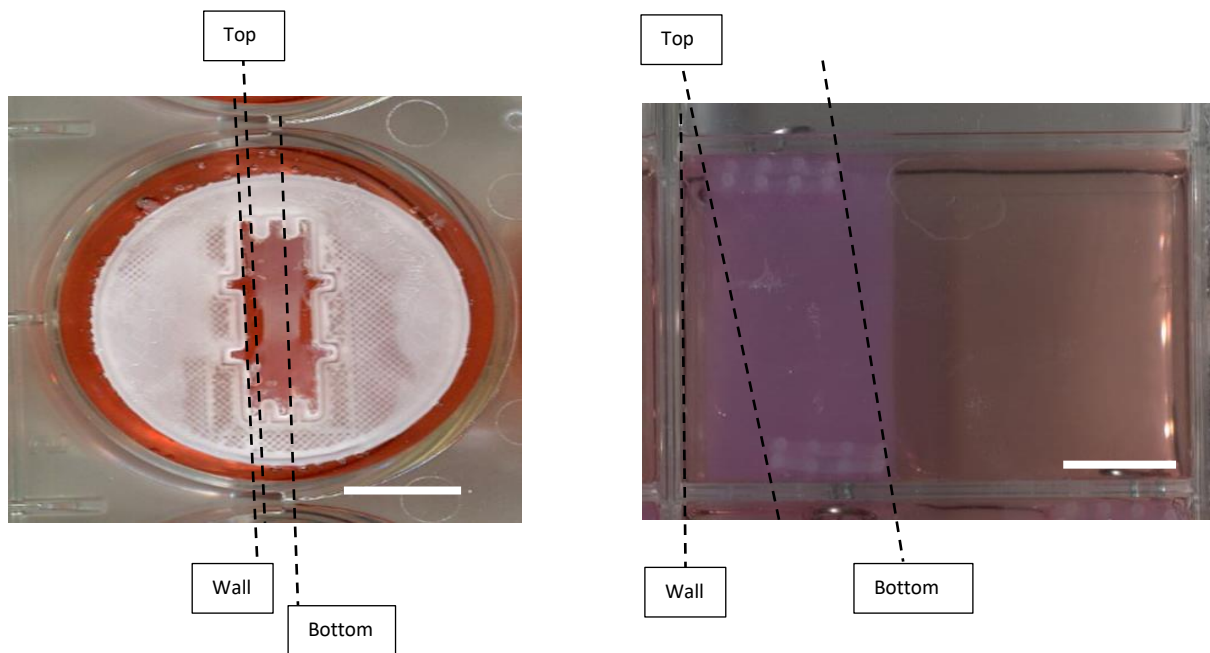


Figure 3.3: Diagram of the steps involved in creating a segmented gel using blockers. The equipment was first set up (A) unseeded (acellular), neutralised collagen was deposited into the available regions and allowed to set before the blocker was removed (B) and C<sub>2</sub>C<sub>12</sub>-seeded collagen was deposited into the central region (C).

### 3.3.4 Angle of components measurements

Using ImageJ, the system was measured for angle differences between the inner wall of the mould, the angle created by the top of both A-frames and the angle created by the bottom two A-frames as shown in Figure 3.4. Angles were measured according to their orientation in the image. The difference between the wall and the tops of the A-frames was termed the “position” of anchor points in the mould, and the difference in angles between the top and bottom of the A-frames was the “A-frame matching”, these were calculated in absolute values as inaccuracies both ways are equally damaging to the system.



*Figure 3.4: Measurement of angles in gel models. Black lines indicate chamber wall, top of A-frames and bottom of A-frames in order. More consistent, straight setups are less likely to change the mechanics of the system and reduce or interfere with the unilateral strain. Scale bar = 10mm*

## 3.4 Results

### 3.4.1 Single bespoke chamber method – segmentation trial

The first step in the project was to determine whether there was a way to adapt this established single tissue method into a multiple tissue method. A simple “blocking” method was used to separate the individual collagen gel parts, otherwise termed “segmentation” of the gel hereon.

#### 3.4.1.1 Segmented gels

The neutralisation step now had to be done twice with two different sets of collagen. One for the cellular region and one for the acellular regions. These were neutralised and set into the mould separately. This presented some new difficulties; the gel had to be set enough to not flow out of the required region once the blocker was removed, but not so polymerised that it would prevent the following gel from merging with it. In these experiments, this did not hinder the successful fabrication, i.e. gels were whole and unbroken, making it through the 14-day culture period without breaking (Figure 3.5). This then led to the conclusion that this method, on the macroscopic scale had the potential to work for incorporating multiple gel populations.

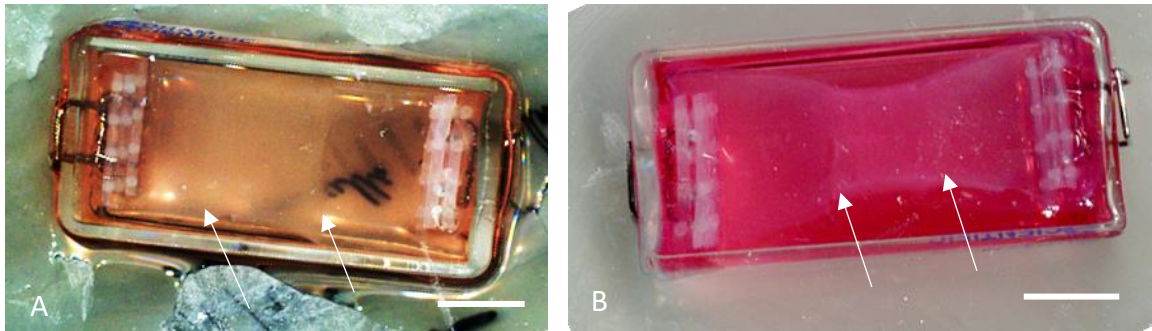


Figure 3.5: Macroscopic scans of bespoke chamber method for segmenting gels at (A) day 1 and (B) day 14. Arrows show interfaces between gel types. Scale bar = 10mm

In terms of the neutralisation stage of the fabrication method, the small volume of collagen used (one third of the usual 1.5ml as it is divided into segments now) meant that a single drop of Sodium hydroxide (NaOH) could make an immediate jump from non-neutralised to over-neutralised, leaving residual liquid and extremely fast polymerisation times. Finding a way to increase the batch of the neutralisation would reduce error.

Table 3.4: Summary table for the original attempt at segmented gels in a glass chamber

<b>Specifications addressed</b>	Control of different seeding populations Assembly
<b>Number of gels attempted</b>	1 gel x 2 repeats
<b>Number of gels successfully fabricated (24 hours)</b>	2
<b>Number of gels successfully cultured for 14 days</b>	2
<b>Brief conclusions</b>	Potentially viable "Bow-tie" shape indicates higher remodelling rates in localised regions.

### 3.4.1.2 Miniature gels

A second experiment was conducted using smaller A-frames across the width of the chamber to determine if the model could be adapted with smaller seeded gels, requiring fewer cells per repeat. However, all gels experienced tearing during the culture period, perhaps because they were too small (which would be in contrast to a number of published examples of small gels), or because the A-frames were too large (Figure 3.6). Alternatively, the setup may not have been uniform enough leading to localised strain in certain regions that were then being exacerbated during movement over the culture period for media changes etc. Therefore, it was concluded that refinement of the system was difficult

at smaller gel sizes due to collagen and material issues, leading to the decision that progression of the system should be maintained with 1.5 ml gels.

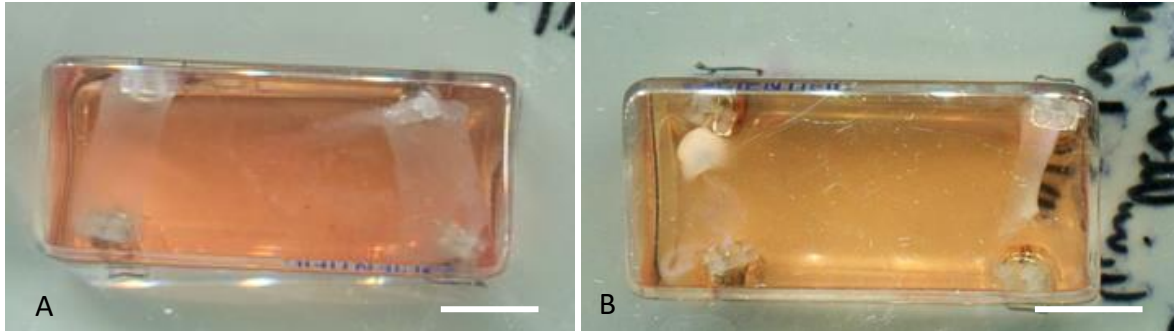


Figure 3.6: The miniature (one-third, 500ul) gels with smaller A-frames at (A) day 1 and (B) day 14. Scale bar = 10mm

Table 3.5: Summary table for miniature (500  $\mu$ l) gels arranged across the glass chambers

<b>Specifications addressed</b>	Cell number required
<b>Number of gels attempted</b>	4 gels x 2 repeats
<b>Number of gels successfully fabricated (24 hours)</b>	3
<b>Number of gels successfully cultured for 14 days</b>	0
<b>Brief conclusions</b>	Not viable

### 3.4.2 8-well plate method

In order to address the volume of constructs that can be made with commonly available equipment, it was decided by Wragg et al. to transition from the bespoke chamber to the 8-well plate, despite the slightly longer setup time required is because 8-well plates are more readily available, produced in large quantities and relatively cheap. Mass produced vessels will be essential for a move to high volume production. This meant that more systems could be set up in a single experiment and will also require less room during fabrication and culture periods. The lid made specifically for the size of the plate also helps prevent infection, without needing to use a second container for sterility, unlike the chamber method which requires housing in a petri dish.

The second reason for this transition was media volume; having enough media is key for development maturity of the cells in a skeletal muscle model. The amount of media that can be put into a glass chamber is severely limited by the construct itself taking up the majority of the room. However, once the PDMS blockers were removed in the 8-well system, more than half the well was now additionally available for media volume.

### 3.4.2.1 Components and setup

Using a modified method from Wragg et al.<sup>46</sup>, a single piece of PDMS was placed in an 8-well plate to create a mould of the same dimensions as a glass chamber (Figure 3.7). A second piece of dimensions 15 x 20 x 7 mm was placed just as previously in the glass chamber method to block the acellular regions. The same method was used to fabricate gels as in Section 3.3.2. Initial fabrication method – Single glass bath

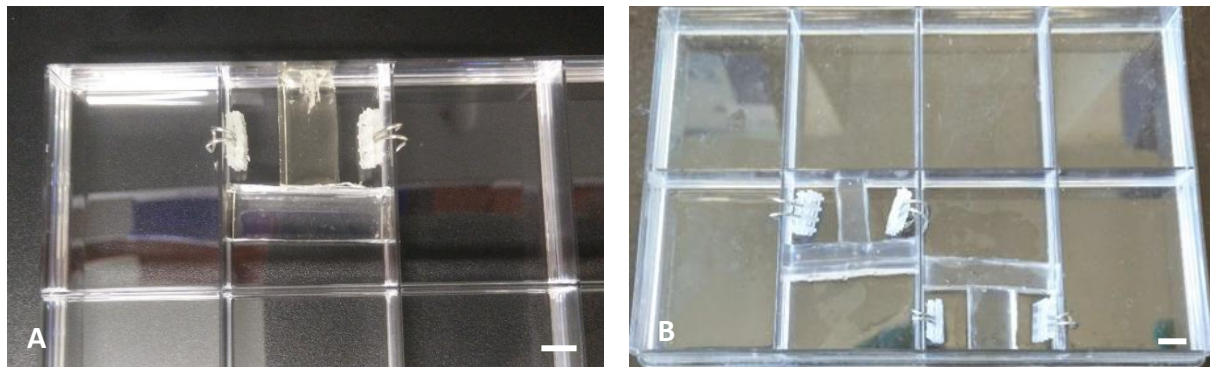


Figure 3.7: Image of the adapted 8-well plate and PDMS setup to attempt segmented gels, (B)- how adjacent wells were set up due to A-frames hanging over edges. Scale bar= 10 mm

The experiment was then repeated to make segmented gels in this system (Figure 3.8).

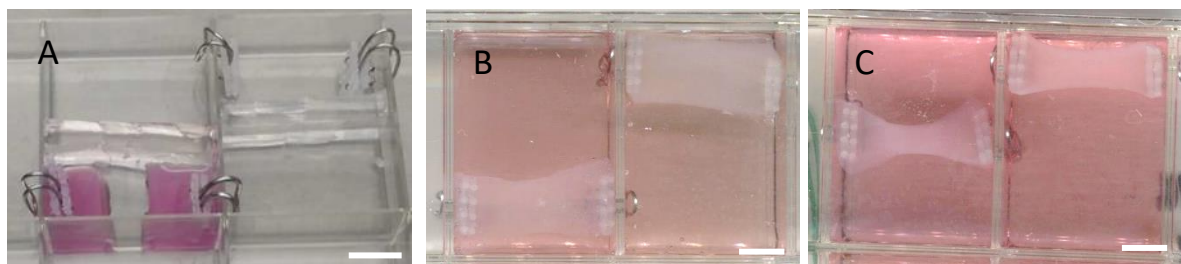


Figure 3.8: Scanned macroscopic examples of the 8-well segmented method (A)- when the acellular regions are set before the cellular gel fills the central space, (B) Day 1 (C) Day 14 with control (right well). Scale bar = 10 mm

### 3.4.2.2 8-well plate outcomes

The higher number of repeats in this experiment demonstrated the issues with this method of segmentation; from a total of 13 gels, 4 were unsuccessful during fabrication due to non-union between the samples (Figure 3.9A). Again, the process of having to quickly pipette the collagen contributed heavily to this, meaning that an entire batch of collagen needed to be neutralised once the peripheral regions had been set, but had to be done quickly to set the middle before risking a separation. After neutralising the gel, the PDMS blocker then had to be removed without damaging the gels which was also difficult, sometimes requiring equipment to go inside the well, risking

infection. The two problems acted together to make this a process that was time sensitive and somewhat unpredictable and therefore, difficult to maintain consistency in.

*Table 3.6: Summary table for outcomes of segmented gels in the 8-well plate*

<b>Key specifications addressed</b>	Vessel Control of different seeding populations Disinfection and infection prevention Media volume
<b>Number of gels attempted</b>	2 gels x 6 repeats + 1 gel
<b>Number of gels successfully fabricated (24 hours)</b>	9 – 4 not attached at interfaces
<b>Number of gels successfully cultured for 14 days</b>	9
<b>Brief conclusions</b>	Potentially viable Same behaviour as glass chamber Blocking with PDMS prevented interfaces forming and resulted in separated gels. A blocking method that does not prevent seeding of the next gel should be the next development.

A new variable was observed in this system which was not seen in the glass chamber method; sliding of A-frames (Figure 3.9B). The width of the glass chambers allowed very little room for movement of the A-frames, however in an 8-well plate, the A-frame has the width of an entire well to move. Reasons for this generally arise from the variability in the A-frames, causing them to sometimes sit at a slight angle on the wall of the well. When the lid is then put on, it presses on the protruding end causing the A-frame to rise up on one side, and then slide. Some A-frames are also not as tightly pressed against the wall, also leading to sliding, highlighting the need for refinement of anchor points.

The final observation was seeping of gel in between blockers, this meant that certain regions were not truly isolated as unwanted mixing could occur beyond the area designated as the interface. Making sure the blockers were more precise would prevent this by creating them more uniformly.

### 3.4.2.3 Premade PDMS

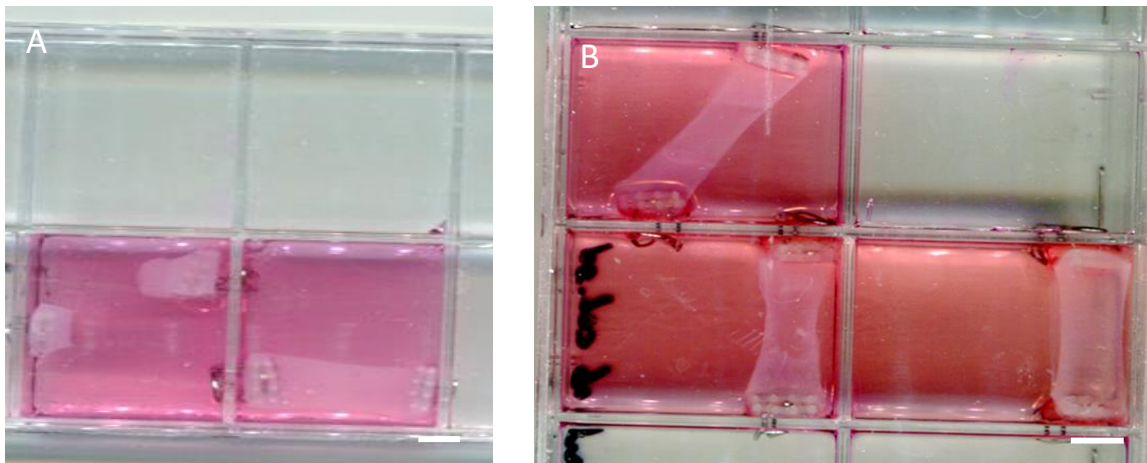


Figure 3.9: Images illustrating issues with the method which included separated gels (A) and sliding of A-frames over the culture period (B). Scale bar = 10 mm

To overcome the seeping that was observed in the 8-well plate experiments, a new set of blockers were made with PDMS, cut with a scalpel and paired together with the PDMS they were cut from, with a number labelled on the front (Figure 3.10). This allowed to ensure that required areas were sealed as they fit flush against each other, being cut from the same piece of PDMS to prevent any leaking of collagen, and made setting faster for the operator as everything was premeasured and only required slotting into place. Although this had no discernible impact on the success of the gels, it did save time during the setup and made an observable difference to the ease of the method (data not shown).

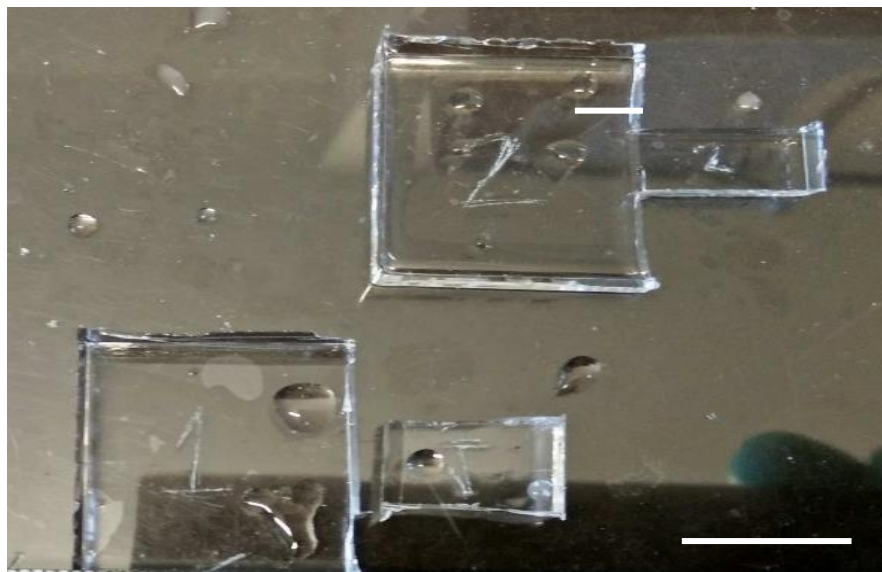


Figure 3.10: Image of premade PDMS blockers which were paired together to provide a more precise seal between segments. Scale bar = 10mm

### 3.4.3 PDMS mould from 3D printed negative with steel dividers

#### 3.4.3.1 Setup and components

It was established that a method dividing a collagen hydrogel into separately seeded regions yielded macroscopically visible results. To overcome all of the variability with the geometries of the constructs from previous experiments; sliding of A-frames and the disparity between polymerisation of regions, it was decided to attempt to make a fully PDMS mould floor with stainless steel dividers, in a similar style to Shansky et al.<sup>117</sup> who used a combination of silicone rubber moulds and aluminium brackets. The mould was made from a 3D printed negative made from PLA with a commercially available 3D printer (Ultimaker 2+, Ultimaker, Netherlands). The 3D printing would allow for precise geometries of the dividers and gels moulds. PDMS was then set against it to create a mould with grooves specifically to allow for stainless steel metal dividers to fit precisely into them. Stainless steel dividers were then laser cut to specification, with an interlocking design so that the walls of the mould were inserted first, beneath the segment dividers, allowing for the mould to remain intact once the dividers were removed to allow the gel segments to form. Each segment was designed to be the same dimensions as the previous experiments in this Chapter. Additionally, this system was designed to be able to be retrofitted with mechanical stimulation apparatus, hence the space at the back of the mould (Figure 3.11). More grooves were also included along the floor of the mould so that a variety of sized gels could be created using a single mould, making it beyond the capabilities of previous models. This mould was placed inside a polymer container and the lid of an 8-well plate was used to attempt to prevent infection.

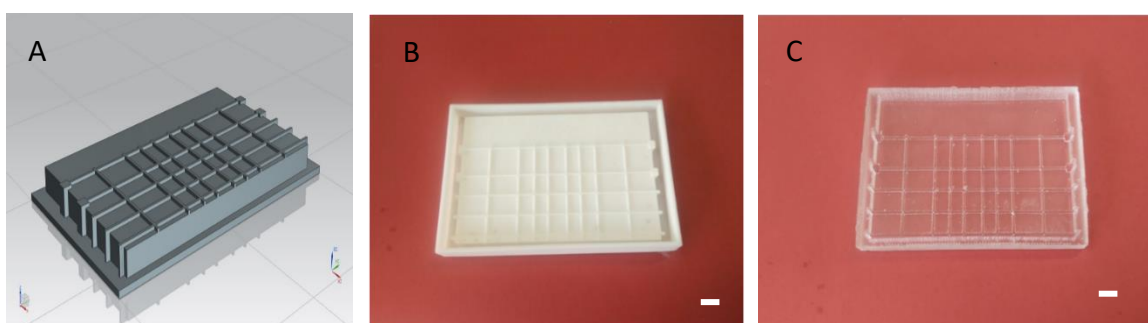


Figure 3.11: Image showing the development of the PDMS mould system: (A) the CAD design of the negative (B) AM (3D printed) PLA negative (C) mould after removal from negative. Scale bar = 10 mm

Gels were then fabricated in the usual method used for systems with dividers (Figure 3.12).



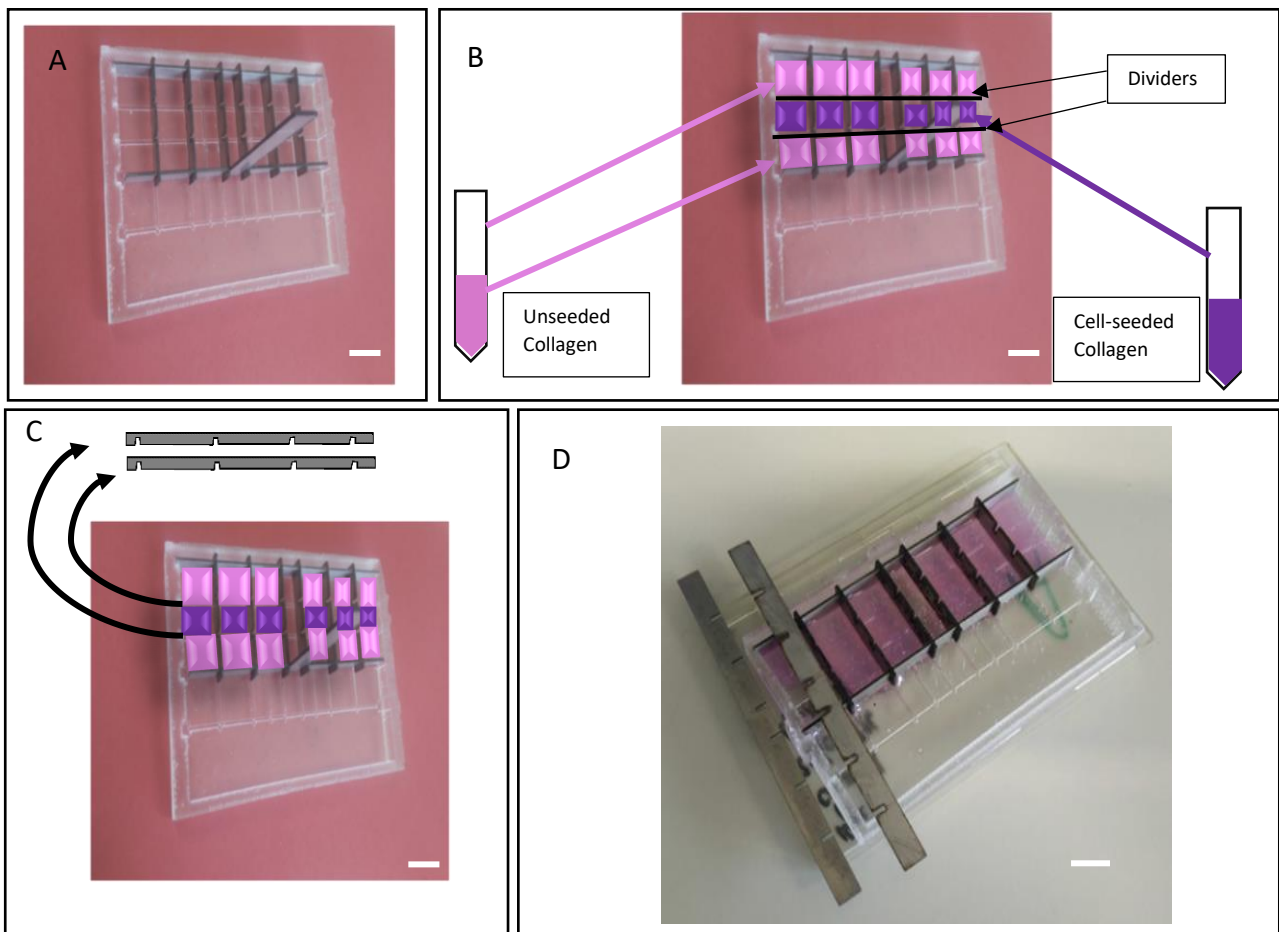


Figure 3.12: Image showing the process cycle for creating segmented gels using the PDMS mould. (A) stainless steel dividers could be used to create a mould for gels of varying sizes, (B) once dividers were in place, unseeded and seeded gels could be added into the required regions, (C) the dividers were then immediately removed to create a multiple segmented gels (D). Scale bar = 10 mm

### 3.4.3.2 PDMS mould outcome

Using the removable walls between segments reduced the number of interfacial separations between gel regions - only 2 of 15 failed at this stage, and simplified the process by removing the need to wait for a precise level of polymerisation.

Two of the three repeats of this method resulted in severe infections in the container. The size of the surface area of the system, with the volume of media in it, no specific lid and the need to use the operator's hand in the model to remove the dividers all may have contributed to this. If this were to be transferred to high-throughput testing systems, this would present a considerable drawback, a severe infection could cost a large number of experiments and could require Sections of the facility to be out of use for an extended period. Of the remaining repeat, contrary to previous experiments and to other groups who have used PDMS, there was very strong adhesion of the constructs to the mould, which prevented the contraction of the mould through remodelling of the matrix (Figure 3.13).



*Figure 3.13: Image showing PDMS mould method with segmented gels (unseeded- $C_2C_{12}$  – unseeded) at day 4. Gels showed little contraction with regions of adhesion between the gels and the mould. Scale bar = 10 mm*

However, remodelling is a key indicator of the success of a gel as it is strongly related to the maturity of the cells at the end of the culture period. This may have occurred due to the large surface areas of the gels in contact with the PDMS, or the amount of time they are in contact with no media while the gel sets. Normal, homogeneous gels would be resilient enough to allow for the physical separation of the two using a hypodermic needle, however the interfaces in the early stages of segmented gels are areas of mechanical weakness, and attempts to do so resulted in separation of gel segments. Finally, the containment unit for this system was not transparent, leading to difficulties imaging and measuring macroscopic results, thereby complicating the process for predicted microscopic outcomes of the model. These are not desirable properties for a high output system, therefore making this system unsuitable for this project. However, the new dividers can be taken forward alongside the

additive manufacturing system for further experiments. They allow for pipetting of both gel types (cellular and acellular) independently without having to wait for one to set before pipetting the other allowing all three segments to be cast within a short space of each other. This saves time in the method cycle, which is ultimately crucial for any system that is to be produced in large numbers, waiting for a gel to set in order to finish the setup would just not be viable.

*Table 3.7: Summary table for outcomes of segmented gels in the PDMS mould method*

<b>Key specifications addressed</b>	Vessel Control of different seeding populations Disinfection and infection prevention# Media capacity Assembly Consistency
<b>Number of gels attempted</b>	5 x 3 repeats
<b>Number of gels successfully fabricated (24 hours)</b>	13 – 2 experienced tearing at interface, marked improvement on previous methods
<b>Number of gels successfully cultured for 14 days</b>	0 – adherence to mould/ lack of contraction/ infection
<b>Brief conclusions</b>	System too unreliable in terms of success and preventing infection Sliding division inserts reduced the amount of tearing at fabrication*

### 3.4.4 3D printed moulds

To develop the model further based on results from the PDMS mould and to address the drawbacks of previous methods it was thought that the use of additive manufacturing to create a mould itself instead of just a negative may be the answer to creating a precise, high volume, versatile model (*Table 1.1*). Moulds were 3D printed and combined with sliding dividers, as previous experiments indicated that these resulted in fewer interfacial inconsistencies.

#### 3.4.4.1 Long model

It was decided to make a segmented gel by attaching three standard sized gels together first to test 3D printed moulds as larger moulds would allow for more room for error before optimisation can take place. Based on the previous iteration, creating a large mould created higher risk of infection. However, this was much smaller than the PDMS mould model and therefore no longer needed to be housed in such a large vessel; it could easily fit into a standard petri dish (Figure 3.14).

### 3.4.4.1.1 Components and setup

A design of three standard 1.5 ml gels in a line end to end (90 x 20 x 10 mm) with two slots for thin, sliding dividers was made with CAD and printed using the Ultimaker 2+ as can be seen in Figure 3.14. Gel fabrication continued to be the same as before.

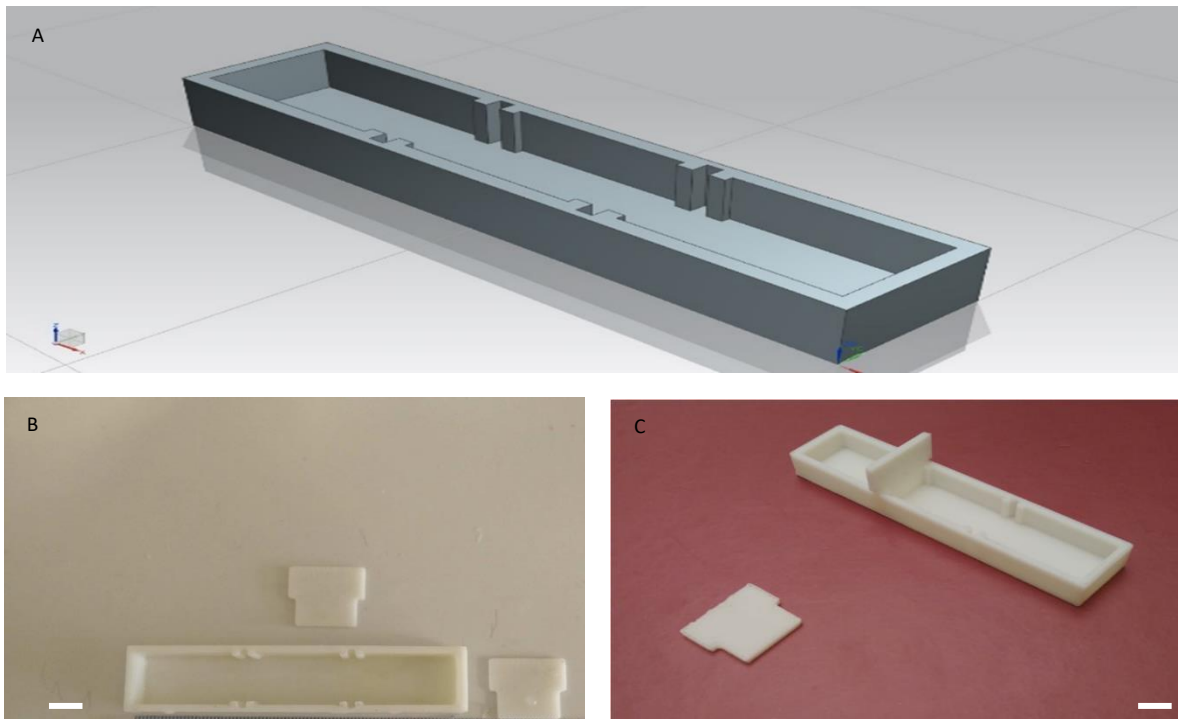


Figure 3.14 : Images showing the long 3D printed model (A) CAD design (B) printed and (C) one sliding divider inserted. Scale bar = 10 mm

The dividers were also 3D printed. Anchor points were hooked over the ends of each side and the segmented gel was fabricated in the usual manner, with the dividers removed as soon as all three segments were pipetted (Figure 3.15A).

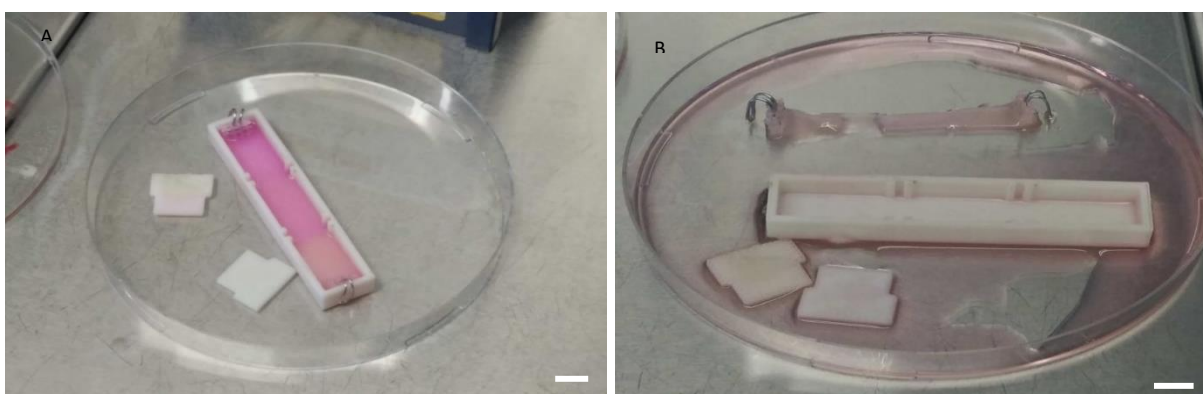


Figure 3.15: Images after 24 hr of culture of the 3D printed long mould method (A) after fabrication of the gel (B) after 24 hours was unable to contain the media but showed that 3D printed structures are effective moulds and sliding dividers can make strong interfaces. Scale bar = 10 mm

### 3.4.4.1.2 Long model outcomes

Two large gels were attempted using this method. Of these, all interfaces were successfully fabricated. However, both moulds had lost all media within 24 hours of culture (Figure 3.15B). The way in which the moulds are printed are layer by layer in lines the width of the nozzle. However, that means that there may be spaces between the lines of polymer, and it is postulated that these are the gaps that allow for the media to escape the mould. Increasing either the print resolution or the density of the material could overcome these. Additionally, this method was not in following with the previous methods which permitted larger media containment volumes outside of the original gel mould. This model was a step backwards in terms of media containment volume as it was a trial method, with the plan to adapt future models as required. This model did not meet the requirement for imaging due to the lack of transparency of the mould.

Again, the thin sliding dividers proved their efficacy, no separation was discovered in the four interfaces that were made. Tearing occurred at these interfaces afterwards when being manipulated for pictures as in Figure 3.15, but maintained integrity through regular culture. Contraction over the very short time period was observed, some evidence of it can also be seen in Figure 3.15, meaning that there was no inhibition to the contraction of the gel, even with the loss of media in the system. The rate at which media was leaving the system or at which point the system had lost all media are unknown. Due to the nature of these failures, no further repeats were performed.

*Table 3.8: Summary table for outcomes making segmented gels in the long 3D printed model.*

<b>Key specifications addressed</b>	Vessel Assembly Disinfection and prevention of infection Media capacity Reusability/ economy Potential for adjustments/ versatility
<b>Number of gels attempted</b>	1 x 2 repeats
<b>Number of gels successfully fabricated (24 hours)</b>	2
<b>Number of gels successfully cultured for 14 days</b>	0 No media was held in the system
<b>Brief conclusions</b>	3D printed PLA structures act as good moulds for constructs* System does not hold media Sliding dividers work very well*

#### 3.4.4.2 Elevated reservoir model

Whilst experiments evaluating the long PLA model indicated that 3D-printed PLA moulds could be used to overcome certain drawbacks of previous systems, the previous model was unable to contain media, as well as having relatively little for media to begin with. A second experiment was conducted to separate the mould and media-containing areas of the system by height in the design, thereby allowing media many times the volume of the gel to be held within the model. This was to be done with maximum print quality to prevent media loss. The depressed region was made with the dimensions of the usual 1.5 ml gel, and the elevated region was made to triple the additional volume of media.

##### 3.4.4.2.1 Components and setup

The dimensions were for a single gel (30 x 20 x 10 mm) with divider slots at every third (10 mm) along the length. The reservoir was then raised (10 mm) above with surface dimensions of 30 x 60 x 10 mm (Figure 3.16). Like with the previous experiment, A-frames were placed at either end of the gel mould region. As for previous models, gels were cast, dividers removed as soon as possible and the whole mould was filled with media.

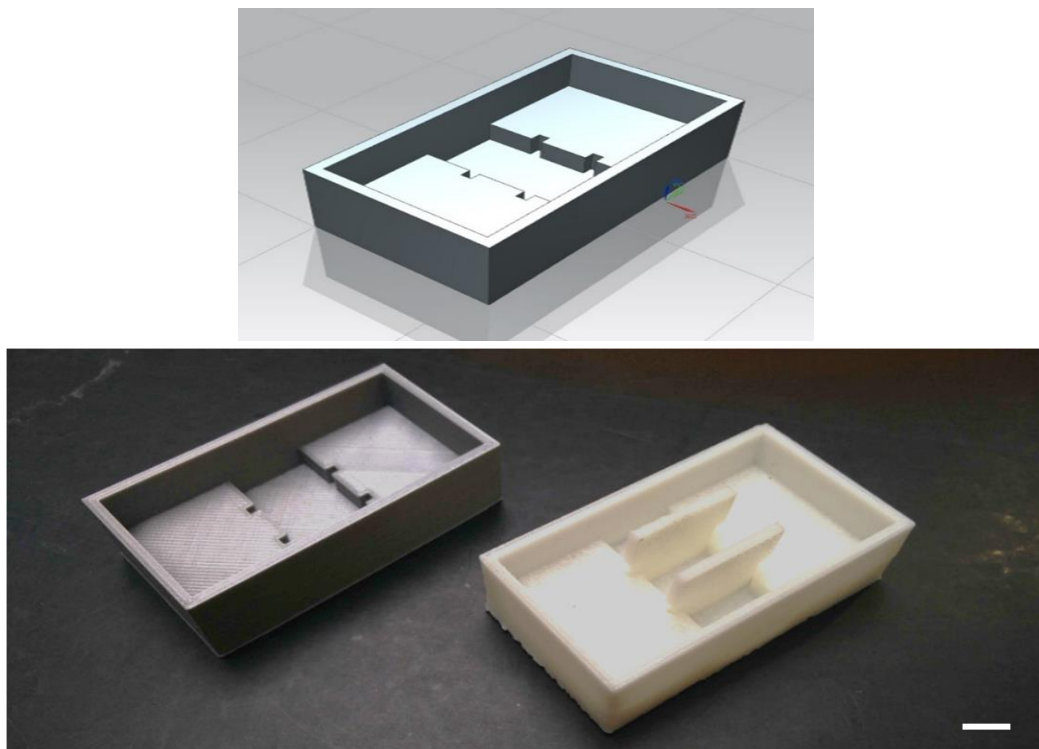


Figure 3.16: Images showing design and finished product of the elevated reservoir model. The gels were to be seeded in the indented region and to be able to contain higher volumes of media in the elevated region. Scale bar =10mm.

### 3.4.4.2.2 Elevated reservoir model outcomes

Table 3.9: Summary table for outcomes of making segmented gels in the elevated reservoir model.

<b>Key specifications addressed</b>	Vessel Assembly Disinfection and prevention of infection Media capacity Reusability/ economy Potential for adjustments/ versatility
<b>Number of gels attempted</b>	1 x 2 repeats
<b>Number of gels successfully fabricated (24 hours)</b>	2
<b>Number of gels successfully cultured for 14 days</b>	0 No media was held in the system
<b>Brief conclusions</b>	3D printed PLA structures act as good moulds for constructs* System does not hold media Sliding dividers work very well*

As with previous 3D-printed models, gels in this experiment were well formed, but no media was contained by the system. Sliding dividers continued to allow for interface formation at a higher rate than observed with blockers. Again, due to the nature of the failures, no further repeats were conducted.

### 3.4.5 Evaluation of design specifications met

After multiple experiments were conducted to develop an understanding of implementation of specific model elements to achieve segmentation, the compiled results were evaluated against the design specifications outlined in *Table 3.2*.

Based on the evaluation of the specifications in *Table 3.10*, the requirements were as follows:

1. A model that maintains a 3D printed manufacturing method as the mould for the gel, within a media containment vessel that is elevated above the mould. This vessel needs to have some sort of readily available lid that fits well onto it. The mould itself needs a transparent bottom and will preferable be smaller than the current standard gel. The most obvious vessel with a transparent bottom, and a lid would be a well plate. Perhaps printing a mould without a bottom and adhering it to a well plate so that the bottom of the plate becomes the bottom of the mould while the inside of the 3D printed mould shapes the sides of the gel would meet this requirement.
2. Based on other models available (*Table 1.1*), the mould can now include posts instead of needed additional A-frames, reducing the amount of variability and the time required to make

separate components. As discussed earlier, other systems use a variety of anchor points including pins and posts. Posts could be printed as part of the mould.

Essentially, what was needed was a smaller bottomless elevated reservoir model with posts attached.

*Table 3.10: A checkpoint to see which specifications had been solved and which were still unmet after the results of the elevated reservoir model, green specifications are ones that have been achieved.*

<b>Component</b>	<b>Description</b>
Vessel	A suitable vessel had not been found.
Anchor points	Anchor points were still variable and handmade. 3D printed anchor points were unsuccessful at making good constructs. Perhaps a post system similar to those published previously would be suitable.
Assembly	The level of assembly was minimal and simple.
Consistency	All moulds are now consistently made in a 3D printer. Anchor point dimensions and positioning were not yet consistent between constructs.
Disinfection	Disinfection with 3D printed moulds required a simple soak in 70% ethanol followed by UV radiation for 20 minutes.
Prevention of infection	Prevention of infection was best seen in well-plate systems.
Volume of samples that can be made per single neutralisation	Currently, only segments from two gels could be made with a single neutralisation – this is identified as a methodological issue rather than an apparatus issue.
Cell number required	4 million cells/ml established standard. 1.5ml gels, but can be decreased simply by shrinking the design before printing.
Control of different seeding populations	Seeding cells in specific regions has become easy with sliding dividers and printed moulds.
Media capacity	Although the media was not held, media capacity by separating the mould and reservoir regions is multiple times the gel's volume.
Visibility during culture	The bottom of the mould is blocked, meaning that scanning the constructs is difficult. A transparent bottom is still preferred.
Reusability/ economy	The moulds can be both reused after sterilisation, or can be cycled due to the extremely low cost of manufacture.
Potential for adjustments	Changing the system is as simple as changing the CAD and printing it, requires no new equipment.

### 3.4.6 Insertable moulds method

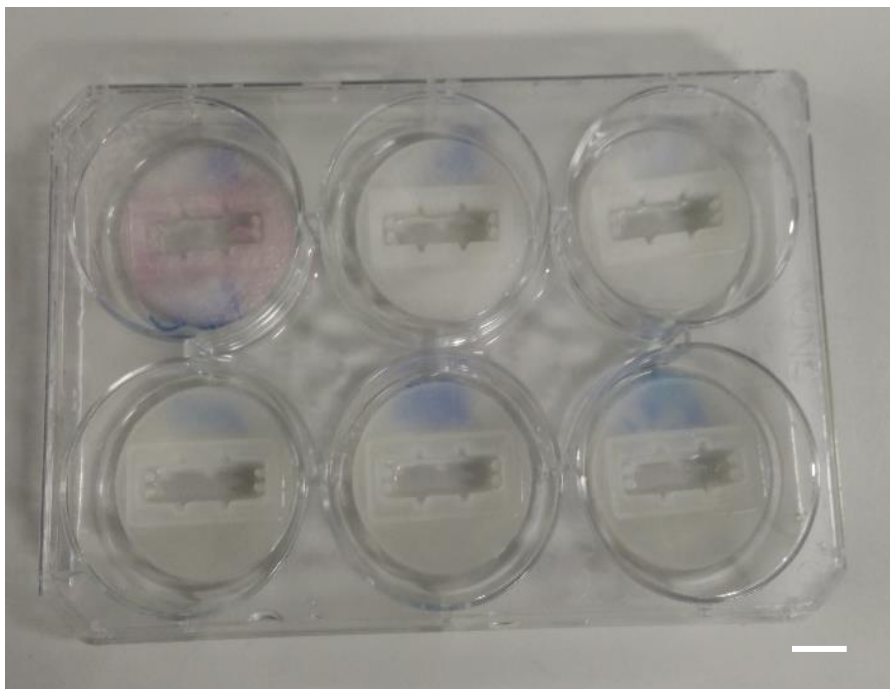
During this evaluation, another system was found to have the required parameters. This was a commercially available PEEK mould that was being used for another skeletal muscle project with similar requirements to those in this thesis. This would later be published in a paper by Jones et al.



using a design donated by Dr. James Phillips (University College London) comparing it to the 8-well method in standard homogeneous 3D skeletal muscle models<sup>159</sup>. This PEEK chamber was precision machined with a 500  $\mu$ l volume and finished with etching for precise chamber dimensions, but was significantly more expensive - £99.60 versus the £4.37 for the 8-well plate method. However, the design was a suitable template for the progression of the elevated reservoir model.

#### 3.4.6.1 Components and setup

The PEEK mould design was altered to allow for sliding dividers, and this was again 3D-printed as with previous models, alongside the dividers. Due to the requirement of a versatile system, the reservoir models were able to be adapted to mimic this system within a single day and were evaluated in the following experiment. These moulds were disinfected using the usual method and then glued one per well in a 6-well plate with aquarium glue (Figure 3.17). These could also be trimmed to fit into an 8-well plate, or whichever commercially-bought culture vessel was available. They were then left under UV for 20 minutes.



*Figure 3.17: Image of six well-plate with all 3D printed moulds adhered using silicon. This was used to fabricate gels and for the entire following culture period. Scale bar = 10 mm*

#### 3.4.6.2 Insertable moulds outcomes

The insertable moulds addressed all but one of the outstanding parameters from the specifications. They allowed for a segmented collagen hydrogen with discrete heterogeneous regions to be fabricated. They allowed for simple and quick production, fast assembly, easy disinfection, they used

a commercially available vessel that has space for many times the volume of the gel in media and a lid to prevent airborne infection, they were one-third the size, thereby using less cells per construct, they were both reusable and economical enough to discard and are versatile enough to be able to adapt the system without any difficulty depending on the needs (Figure 3.18). The three gels that failed were due to the neutralisation and pipetting process, which will be addressed in Chapter 3, Section 3.4.8.

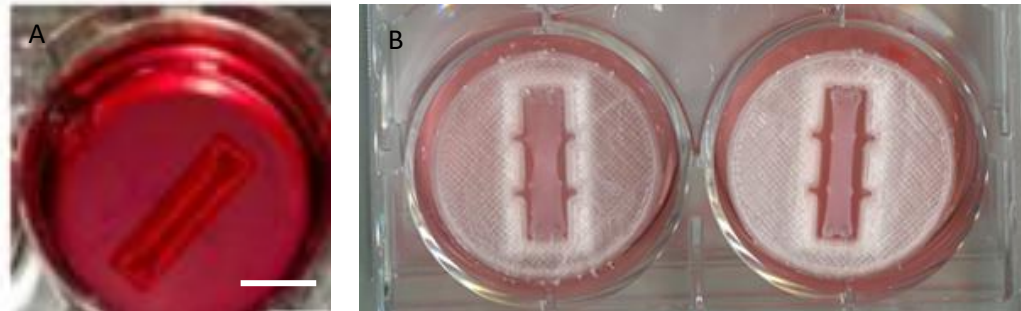


Figure 3.18 (A) The original PEEK mould, image taken from Jones et al. (B) 3D printed PLA mould adapted for segmented gels showing the “bowtie” shape (left) with a control (right). Scale bar = 10mm.

Table 3.11: Summary table for outcomes making segmented gels with the insertable moulds method

<b>Key specifications addressed</b>	<ul style="list-style-type: none"> <li>Vessel</li> <li>Anchor points</li> <li>Assembly</li> <li>Consistency</li> <li>Disinfection</li> <li>Prevention of infection</li> <li>Cell number required</li> <li>Control of different seeding populations</li> <li>Media capacity</li> <li>Visibility during culture</li> <li>Reusability/ economy</li> <li>Potential for adjustments</li> <li>Potential for adjustments/ versatility</li> </ul>
<b>Number of gels attempted</b>	3 gels x 4 repeats
<b>Number of gels successfully fabricated (24 hours)</b>	9 – 3 gels failed due to fast polymerisation after neutralisation
<b>Number of gels successfully cultured for 14 days</b>	9
<b>Brief conclusions</b>	All equipment-based specifications have been met

### 3.4.7 Comparison of models' success and survival rates

In order for a construct to be useful, they need to firstly be made to specification and then make it through the entirety of the culture period without tearing, getting infected or becoming otherwise void. This is termed as the gel success (fabricating successfully) and survival rate (making it to a certain point in time, e.g. 14 days). The previous experiments focussed on finding a system that fulfils the design specification for the thesis, the insertable printed moulds being the forerunners as almost completely matching what was required of the components. It was then important to analyse the survival rates (summarised in the method summary tables at the beginning of each method) to understand if this new system matches with the established one (Figure 3.19).

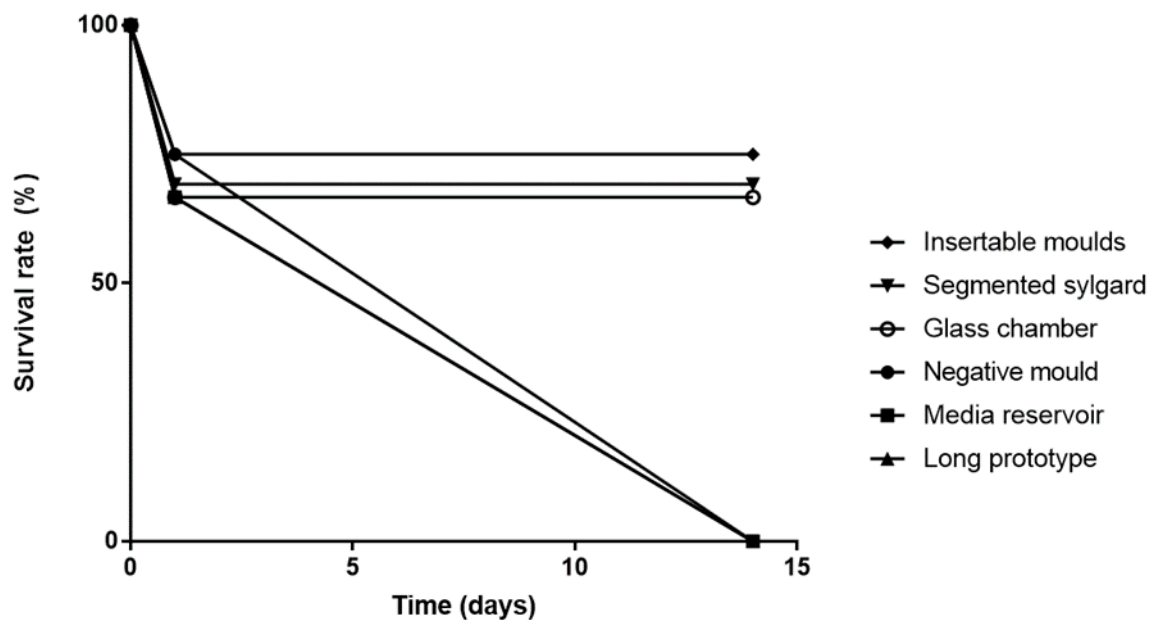


Figure 3.19: The percentage of total gels made using each method that survive to 24hr and then to 14 days without becoming void. All numbers were taken as percentage of total gels made across all repeats.

### 3.4.8 Gel neutralisation and associated polymerisation times

To establish the inherent variability within this method, the time taken for neutralised collagen gels to fully polymerise was measured. Figure 3.20 shows the differences in time that the same process of gel neutralisation can take on different repeats. The time can range from  $6 \pm 2$  minutes to  $20 \pm 6$  minutes for repeats, making this an unreliable part of the process for time. This is also the part that requires the judgement of an operator, meaning this part of the process needs to be utilised as well as possible to save the maximum amount of time on more repeatable processes.

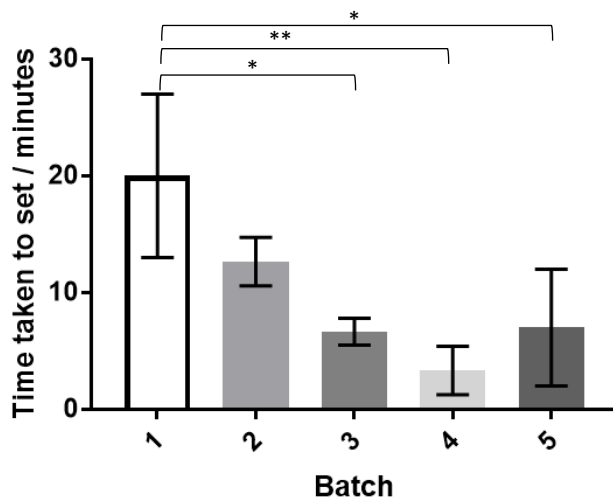


Figure 3.20: Times required for a neutralised collagen gel to set on five different occasions, showing the variability of the neutralisation step. Significant differences were seen between batch 1 and 3 ( $p^*=0.0171$ ), 1 and 4 ( $p^{**}=0.0039$ ), 1 and 5 ( $p^*=0.0199$ ), one-way ANOVA to evaluate the single variable of time to set. Variability in a single batch can be  $\pm 6$  minutes. Taken from  $n= 3 \times 3$  repeats. Error bars =  $\pm$  Standard deviation.

### 3.4.9 Use of ice to slow polymerisation

Ice was included in the methodology for creating gels as it was seen elsewhere to increase the time it took for neutralised collagen to polymerise (Julia Jones, personal communication, November, 2016). Once ice was introduced into the fabrication method in this project, the gel could be pipetted for minutes at a time and kept on ice for tens of minutes meaning that many gels could be pipetted in one batch. This in turn meant that one single gel of a specific type (acellular etc.) needed to be neutralised only once per repeat. This had a number of implications:

1. Everything could be neutralised at the start of the experiment
2. One entire batch of acellular gel could be neutralised and then aliquoted and mixed with cells where needed
3. The loop was no longer necessary where a new neutralisation step was necessary after every 2 constructs made. Allowing for far larger quantities of gels to be made quickly (Figure 3.21).

From a high-throughput perspective, this means one very large batch of collagen can be neutralised and then kept at cold temperatures once mixed with cells to create as many gels as necessary,

minimising the requirement for a skilled operator to just one stage of the experiment, allowing the rest to be automated.

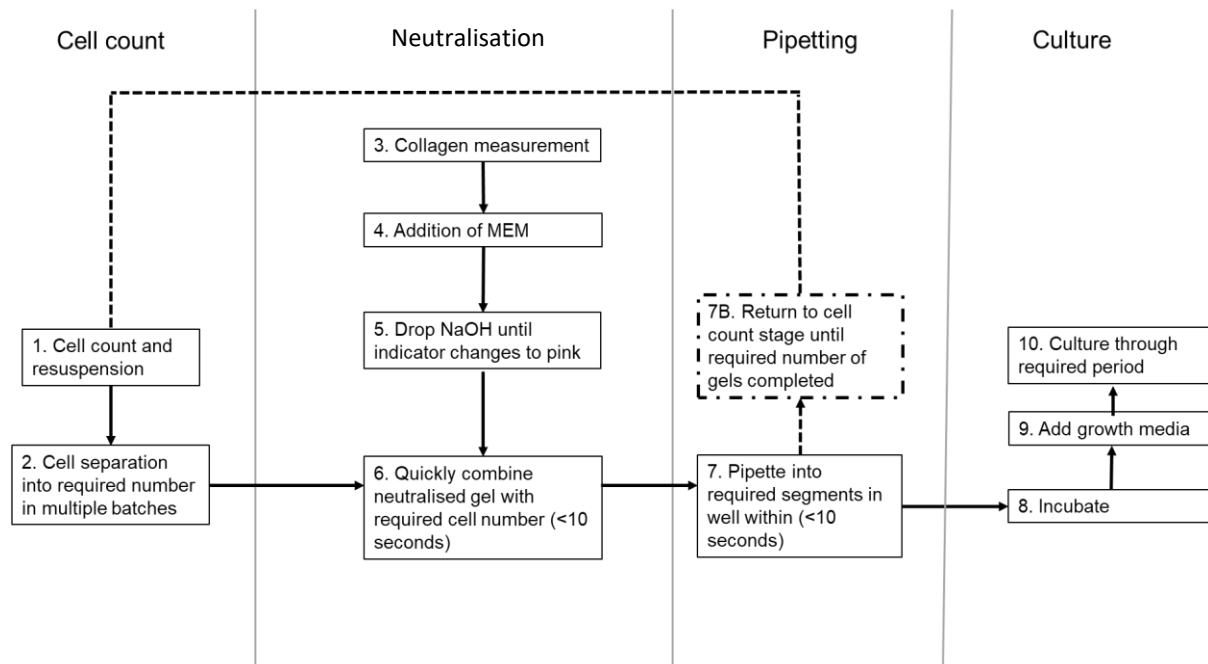


Figure 3.21: Flowchart of the standard for fabricating a gel, using ice to slow the polymerisation of neutralised collagen gels removed the need for step 7B.

### 3.4.9.1 Impact of the inclusion of ice on gel success rates

The use of ice increased the number of successfully fabricated gels from 70% to 100% in 6 gels x 2 repeats. Slowing down the polymerisation removed the majority of the remaining issues associated with the fabrication and maintenance of the model from an operational perspective. This likely occurred due to allowing the aqueous gel to form completely in the mould.

### 3.4.10 Insertable moulds with ice compared to the standard methods

With a new process adopted, it was important to compare it with the previous standards to firstly ensure that the system still produces constructs with the desired properties that were originally being made and secondly, to see whether it has made any improvements on the previous standard.

#### 3.4.10.1 Time required to fabricate

Figure 3.22 Shows how the time required for the entire fabrication of a gel varies with gel number. A single gel requires  $149 \pm 2$  seconds for the 8-well method and  $97 \pm 3$  seconds for the inserts by 4 gels, the difference is  $592 \pm 12$  vs  $123 \pm 2$  seconds (Figure 3.22A) giving a time saved of 7.6 minutes by 4 gels when using the inserts instead (Figure 3.22B). The majority of this time is saved in not having to repeat neutralisation steps as that comprises ~80% of the entire fabrication method (Figure 3.23). Reducing

time for fabricating will allow for more output in higher throughput systems, reducing a bottleneck effect that could be created from waiting times for fabrication.

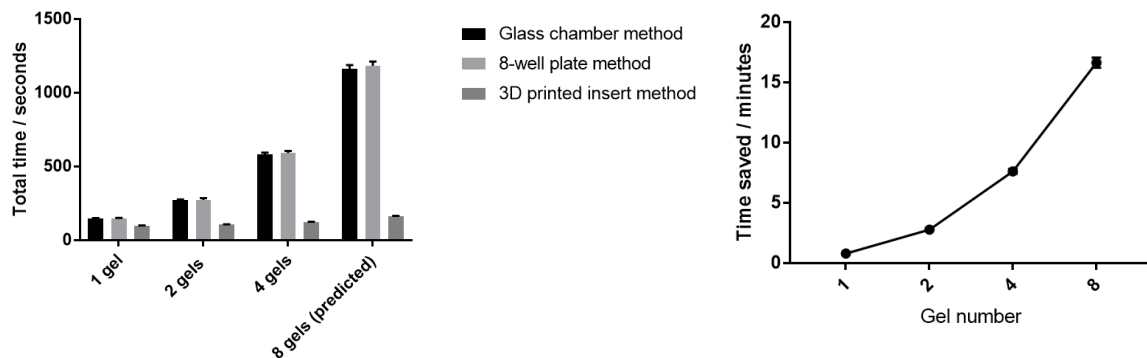


Figure 3.22: The times required to make constructs vs. number of constructs made after cell count stage (left) and the time saved using the insertable moulds method instead of the 8-well method (right). Taken from  $n = 3 \times 2$  repeats. Error bars = Standard deviation

As can be seen in Figure 3.23, the neutralisation time with each gel made has the largest impact on time, while the pipette time (the time to pipette one extra gel into a well) only increases slightly, therefore neutralisation time linearly increases the time required with each gel fabricated. The insertable moulds are one-third the size, needing correspondingly reduced pipette times, but the majority of the time saved was through only needing to neutralise once for all gels in a batch. Comparitively, there was a very small difference when increasing gel number in the times required for pipetting, meaning the time increase was simply due to having to pipette more. This meant that for every extra gel made, even more time was saved with the new system, giving greater return. This, combined with the threefold decrease in model size led to the opportunity to make many more gels than before in a single experiment without risking large differences in cell conditions (for example, the first gels made being without media for longer than the last ones) or gel polymerisation.

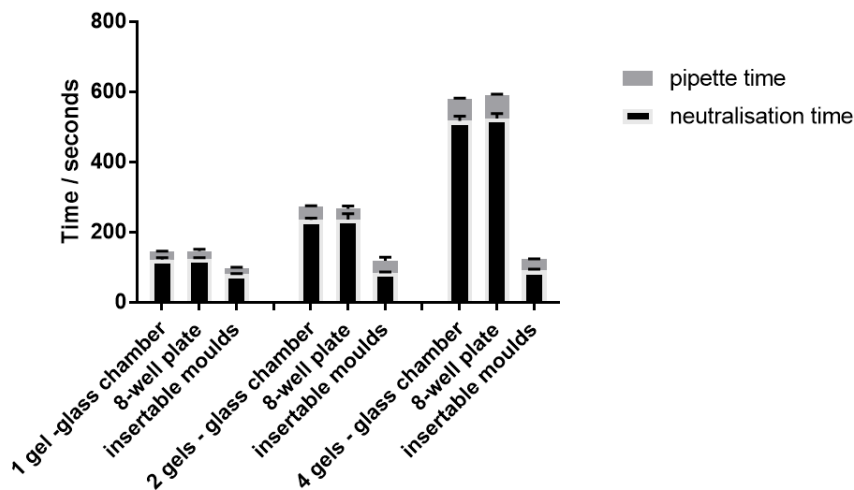


Figure 3.23: A breakdown of the times to prepare and neutralise collagen and seed it with cells and the time to pipette the suspension into moulds for 1,2 and 4 gels total; a comparison of the main methods. Taken from  $n=3 \times 3$  repeats. Error bars =  $\pm$  Standard deviation.

### 3.4.10.2 Contraction comparison

Gel contraction was compared to the established system for validation. Contraction of the gel during the culture period has been found to be a good indicator of the microscopic quality of the gels. It is mediated by the initial attachment and remodelling of the surrounding matrix by the cells and it is theorised that greater contraction of the gel decreases the distances between individual cells, increasing the chance of cell-cell contact which is a driver for fusion into myotubes. Width reduction has been correlated with myotube width in earlier projects<sup>46</sup>. While neither of these systems found their way to 50% of original width benchmark that is correlated with a “good” gel, the point of this experiment was to quantify the difference between the systems (Figure 3.24). Both reduced at the end of the 14-day period to  $62 \pm 4 \%$  and  $63 \pm 1\%$  for the 8-well plate and insertable moulds respectively. No statistical difference ( $P=0.7486$ , t-test, two tailed) was found between the two methods at 14 days indicating that they are similar for gel contraction results.

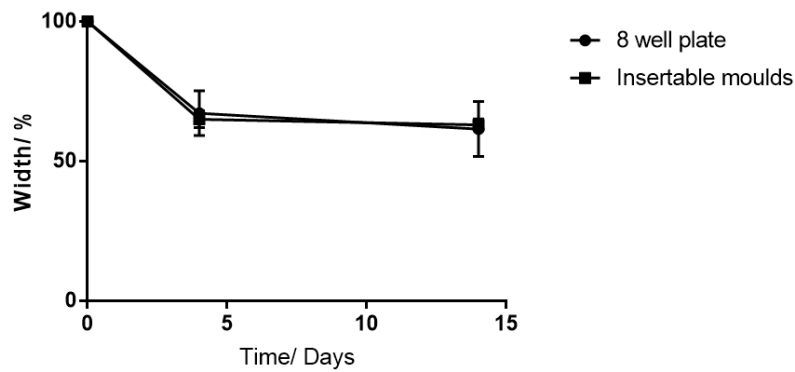


Figure 3.24: Width reduction comparison between 8-well plate method and insertable 3D printed moulds. No statistical difference ( $p=0.7486$ ) (unpaired t-test) between the two sets indicated that the two methods are similar in cell-mediated remodelling outcomes. Taken from  $n=3 \times 3$  repeats. Error bars =  $\pm$  Standard deviation.

### 3.4.10.3 Angle of components comparison

Skeletal muscle systems like this one rely entirely on the passive unilateral force that is created around the anchor points to illicit strain within the system. Once the system is initially set up, the system is left alone to culture over the predefined period, highlighting that the setup is most important for giving the system the best conditions to allow for myotube fusion. Combining these two points, the system needs to be set up in a manner which will allow for unilateral strain through the entire system in a uniform way, meaning every component needs to remain as straight as possible to prevent changing the mechanics of the system.

#### 3.4.10.3.1 Position of the anchor points relative to the wall of the mould

The difference between the angle of the chamber wall and the line created across the top of both anchor points was analysed across 9 samples (3 repeats of 3) for each method (Figure 3.25). This was to investigate how the mould was positioned in the chamber, as strain will be unevenly distributed, resulting in an angled gel. This also means that all of the cells come under different mechanical conditions in different gels. Figure 3.25 shows that the insertable moulds have a much smaller angle made by the mould and the wall at  $0.4 \pm 0.1$  vs. the 8-well plate model at  $6.5 \pm 1.3$  and a considerably smaller variability of angles also. A high throughput testing system needs reproducibility, so the



decreased difference in angle and variance in overall angles of the insertable mould method indicated that it is better suited to applications that require models to be as similar to each other as possible.

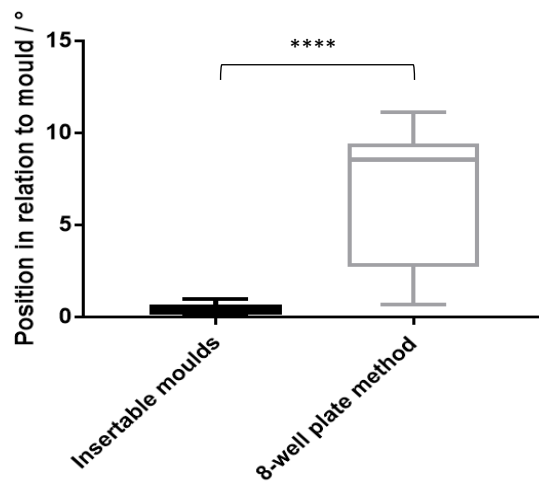


Figure 3.25 : Comparison of angle created by the two anchor points and the wall of the chamber compared in both systems. A smaller difference in angle indicates that the components in the system are more aligned, allowing for a more direct unilateral strain with equal distribution throughout the entire model. A smaller range of angles indicates a more consistent system setup. Insertable moulds were significantly ( $p^{****}<0.0001$ ) (unpaired t-test, one-tail) less variable and less misaligned than the standard system. Taken from  $n=3 \times 3$  repeats. Error bars =  $\pm$  Standard deviation.

#### 3.4.10.3.2 “Matching” of the anchor points

The matching of the anchor points is dictated by the top and bottom angles and whether there is a disparity between the two. This would interfere with making a rectangular sample and with particularly large angle discrepancies, more of a trapezium is formed which can influence the mechanics of the system, having a tighter, smaller matrix on one side and a larger one with more room for cells in the other.

The 3D printed moulds had an angle difference of  $0.3 \pm 0.1^\circ$  while the 8-well plate had an angle difference of  $1.4 \pm 0.4^\circ$ . Again, the insertable moulds showed a more consistent setup with a smaller deviation for creating reproducible gels (Figure 3.26).

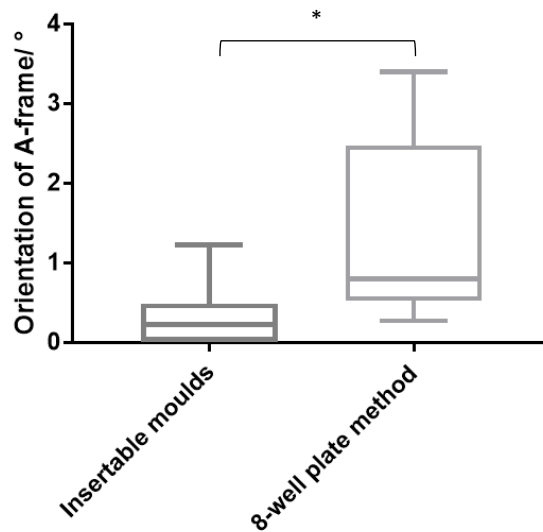


Figure 3.26: Comparison of angle created between the two anchor points at both ends between insertable moulds and 8-well plate method. Less angle variation means a more aligned system with consistent A-frames. Insertable moulds were significantly ( $p^*=0.0116$ ) (unpaired t-test, one-tail) more consistent and aligned. Taken from  $n= 3 \times 3$  repeats. Error bars =  $\pm$  Standard deviation.

#### 3.4.10.3.3 Anchor point “drift”

The distance of an A-frame was measured from the inner wall of the mould at three time points to understand the way it can vary over a culture period. This was then compared to the insertable moulds system, which should have no drift as the posts are constructed as part of it (Figure 3.27). The models’ distance from walls were: Day 1  $0.9 \pm 0.1$  mm (insertable),  $5 \pm 0.7$  mm (8-well), Day 4  $1.0 \pm 0.0$  mm (insertable),  $6.7 \pm 1.6$  mm (8-well), day 7  $0.9 \pm 0.0$  mm (insertable),  $7.9 \pm 1.7$  mm (8-well), day 14  $1.0 \pm 0.1$  mm (insertable)  $8.4 \pm 1.8$  mm (8-well). Whilst the means are significantly less for insertable moulds, that is not as important as the variance between repeated measures. It is key here to note that the error is considerably smaller also due to the decreased variance in the distances of the insertable method.

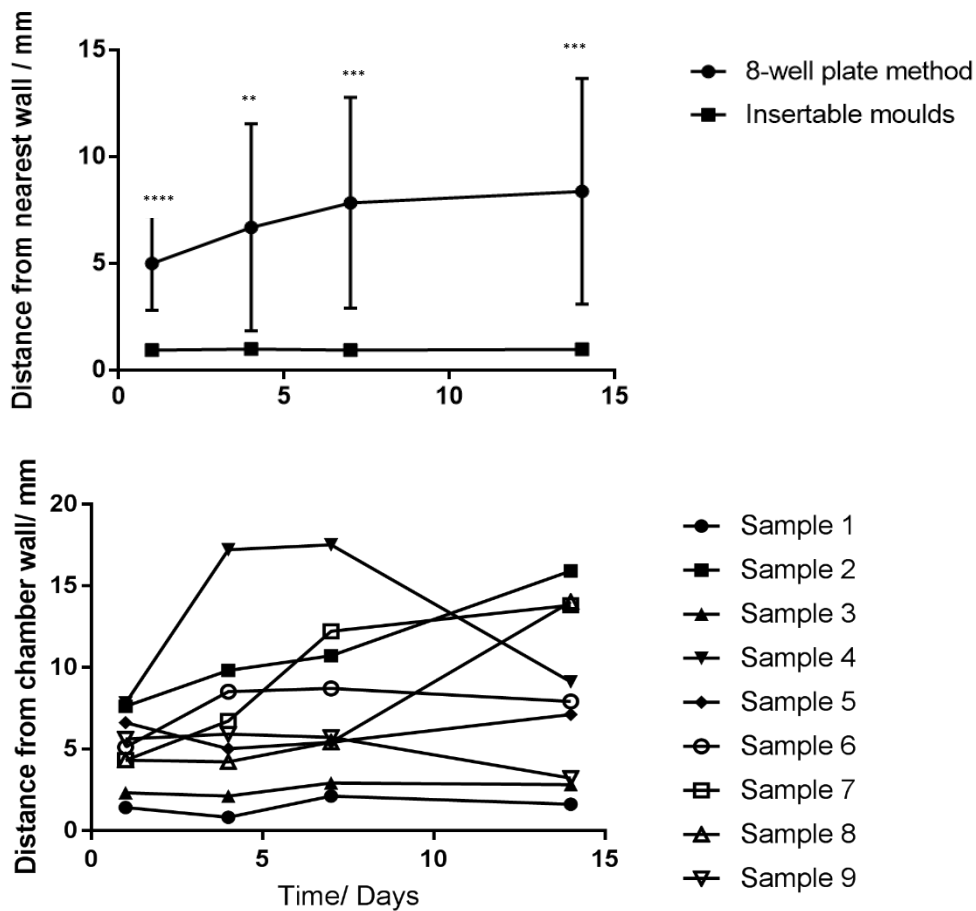


Figure 3.27: Comparison of how anchor points moved throughout the culture period between the 8-well plate method and the insertable moulds Taken from  $n=3 \times 3$  repeats. Error bars =  $\pm$  Standard deviation. (Top) Day 1 ( $P^{***}=0.0028$ ), 7 ( $P^{***}=0.0007$ ) and 9 ( $P^{***}=0.0007$ ) were all significantly different (t-tests). The insertable moulds were significantly less variable. And the individual anchor points from the same experiment in the 8-well plate method and their distance from the chamber wall during the culture period (Bottom) each line represents a repeat. Taken from  $n=3 \times 3$  repeats. Error bars =  $\pm$  Standard deviation.

#### 3.4.10.3.4 Comparison of inconsistencies in size of construct

The size of the mould and therefore the initial gels created was compared by measuring the surface area of the gels at  $t=0$  (Figure 3.28). These were measured in absolute differences, as being smaller and larger is a deviation from what is necessary and the point is not try and average it at 0%, but to instead get the figure as close to 0 for all moulds to ensure it is true to the intended design and reproducible.

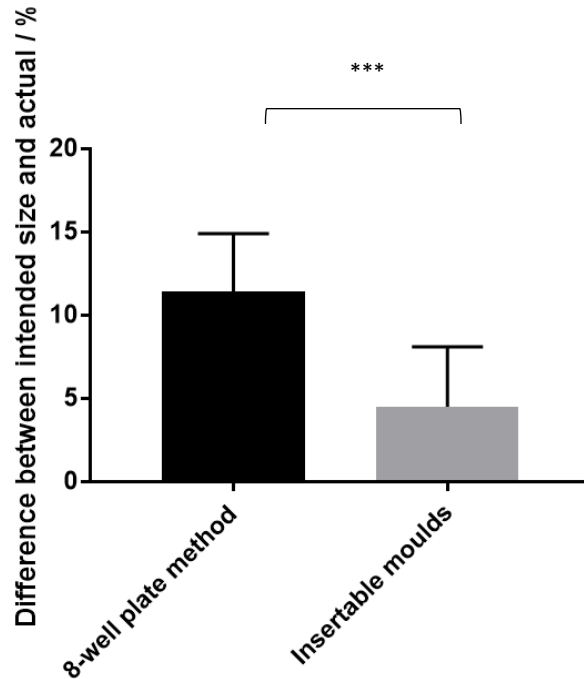


Figure 3.28: Comparison of the imprecision in both methods for creating a mould. Percentage difference between the design and the actual mould was measured for both methods. The two methods were significantly different ( $P^{***}=0.0004$ ) (t-test, one-tail). Taken from  $n=3 \times 3$  repeats. Error bars =  $\pm$  Standard deviation.

The mean numbers for the deviation from required size of the models were  $11 \pm 1$  % and  $5 \pm 1$  % for the 8-well plate and insertable moulds respectively. The moulds were 2.5 times more accurate, although with a very similar error margin.

#### 3.4.10.4 Microstructural comparisons

Brief comparisons were made between the two types of model to determine whether both produced aligned multinucleated myotubes. Experiments have previously determined that the system was scalable, and others have been since done to ensure that this system worked in the same way elsewhere. Based on the stained images (Figure 3.29) the insert moulds produced myotubes in the same way as were expected from the standard system, creating aligned, multinucleated myotubes. The system succeeded in producing the tissue engineered structure for which the original system was developed.

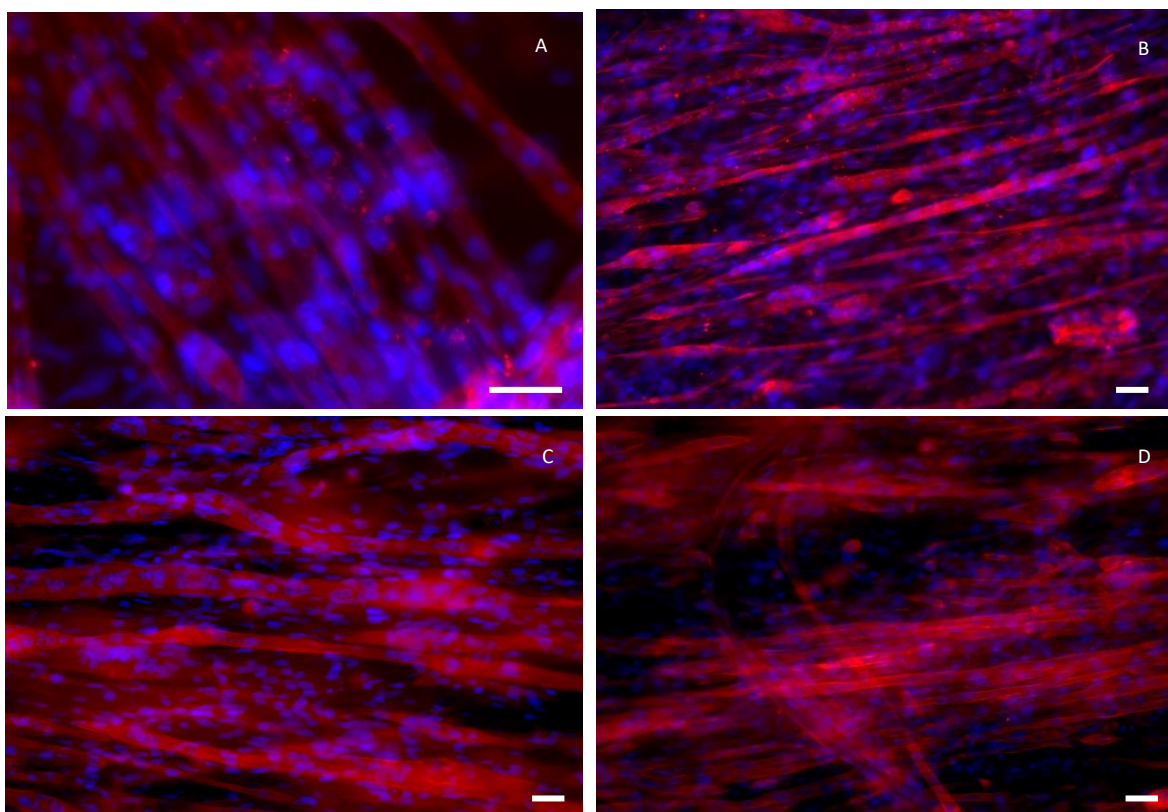


Figure 3.29: Comparisons of stained micrographs of the 3D printed inserts (A,B) to the 8-well model (C,D) showing very similar architectures; well organised, fused, aligned, multinucleated myotubes. DAPI (blue) - nuclei, desmin (Red) - myotubes. Scale bars = 20  $\mu\text{m}$

### 3.5 Discussion

This Chapter describes the development of a small-scale system for creating skeletal muscle models in collagen gels by increasing the number of gels that can be created and introducing a new versatility in the setup of the system, primarily allowing for segments in the gel. This was an example of the “learning-before-doing” that can be found in the pharmaceutical process development field<sup>158</sup>. This can be seen where the profile of the system was first developed based on preliminary experiments, which led to a definition of the key attributes of the system, highlighting the need for process development surrounding collagen neutralisation and product development surrounding the moulds used. Each of these facets was then developed individually and brought together in order to generate an improved system in terms of the desirable parameters. new product or process is released into the commercial setting, by considering the pre-commercial development that allows for the release of the system for it to be tested through doing. In industry, the transition between the two learning methods presents problems as R & D pass a new system on manufacturing. Too early results in not enough knowledge and optimisation of the system which can lead to disastrous consequences on the production floor if a system has a glaring issue that was overlooked. On the other hand, too late of an introduction to manufacturing can lead to overrunning on both time and cost as the adaptation

occurs<sup>155,158</sup>. Although both types of learning are generally covered by science as it treads the line frequently blue sky research and industry as a new method is researched tentatively (simulations and analyses), then brought into preliminary experiments (prototypes), before becoming accepted as standard practice or as a standard model to be used and tested by everyone (learn-by-doing) and experiences unique problems through this<sup>155</sup>.

### 3.5.1 Sharing of knowledge for model development

Science is very much at the stage of process development where the process design and product functionality are highly interlinked, a trait that is also seen in the pharmaceutical industry<sup>158</sup>. Scientific systems are generally not on a profit deadline although they are dependent on funding. They require no rush to be mass produced, allowing for more time for learning-before-doing to ensure that a new process is optimised and ready. Although not every individual experiment is geared towards creating a new product, funding is given out with hope for something in return which is usually a product that can eventually sell, or have a positive impact on society to reduce costs elsewhere. In this case, what can happen is that two different stages of learn-before doing can occur concurrently, where one group is optimising a system and another group takes it on and begins to use it as an early prototype test bed, if not taking it on as an actual test bed and begin 'learn-by-doing'. Inevitably, as the group improving the system moves forward, the latter group's test bed will be an older version but has had a lot of time invested in it with results that are relative to each other so overhauling or updating the system may require a complete shift.

Something akin to this can be seen in the 3D models used in this thesis. While one group moves on to develop a more complete model with a more representative microstructure, or experiments with varying different parts of the process, another picks one that fulfils its requirements to do the job it needs to do and uses it; a type of "doing". This is where it is important to consider that innovation requires the collaboration of different departments within a single firm and external cooperation with other firms and knowledge providers to according Kaufmann et al.<sup>160</sup>, this is highly relevant to this Chapter as the collaboration with an external group involved in similar experiments allowed for the optimisation of the process with the knowledge that they had accumulated from their experiences. The combination of these knowledge bases created a regional innovation system where knowledge was transferred through individual face-to-face interactions as is in the theory behind innovation interactions<sup>160</sup>. This is critical in transferring information regarding processes that are deemed not novel enough to be published in academia.

### 3.5.2 Gel fabrication parameters

Neither success, nor survival rates are often published in the literature when models are created, an observation shared by Wragg et al.<sup>46</sup>. Presumably, this has never been a point of interest for individual models that are being used for proof of concept, small experiments or regenerative purposes which may not require high volumes of experimental repeats. On the other hand, high-throughput systems rely heavily on efficiency with resources and high reproducibility numbers. Figure 3.19 shows the three systems that make it through the 14-day culture period. It is important to note that for some of the above systems, from a process development standpoint, seeing that a method is unable to contain media makes it unviable without the need to gather detailed numbers on it. If the failure is a fundamental part of the model, then the model is not viable in its current version. Additionally, a system that will fail two out of three times is not consistent enough to be in line with the aims of this thesis, even if the fundamentals of the system show some positive results; high throughput screening needs the rare few exceptions failing instead of the rare few exceptions succeeding, this needs to be a reliable, high volume segmentation system. Figure 3.19 is an illustration of which systems can work, and those ones that did have larger sample sizes in order to compare the effectiveness between them more accurately. As expected, the three systems that survive through the entire 14-day period were the chamber system (Smith et al.<sup>152</sup>) the 8-well plate system (Wragg et al.<sup>46</sup>) and the system developed in this thesis- 3D printed insertable moulds. Statistically, there was no significant difference between these three systems and their success rate, indicating that the insertable mould model is at least as reliable as the 8-well plate model for reaching 4 days with a majority of the gels able to generate meaningful results. This means that a system has been created that is equal to a standard method at culturing skeletal muscle hydrogels, whilst also fulfilling the specifications required to create high volumes of gels cheaply and also the versatility to also fabricate segmented hydrogels using the same base model; the standard has been built upon. Nevertheless, one point was still not addressed from the design specification: "Volume of samples that can be made per single neutralisation." This was the single biggest hinderance when attempting to create large numbers of samples within a single batch and led to a vast decrease in the consistency of the gels in each repeat as many of the constructs would have been made from different gel suspensions, neutralised slightly differently. Once the equipment was developed, this was the remaining requirement.

### 3.5.3 Development process of the design of the model

In this Chapter, it was identified that the system had been developed sufficiently to allow for scientific data to be gathered for a variety of different experiments and had been a successful model at doing so<sup>111,152,159</sup>. This model had undergone a slow, iterative improvement process to date— a process very similar to the continuous improvement component of Quality by Design (QbD)<sup>157</sup>. However, if the goal of this small-scale model was to eventually allow for high-throughput testing, then it would require a breakdown of the process variables and a refinement of the ones that inhibit reproducibility. If the second goal was to allow multiple gels to be set in a single construct, then the process variables and components would need to be changed to allow for this. This Chapter covered these two main points.

While QbD guidance documents focus almost exclusively on the customer in a pharmaceutical setting<sup>161</sup>, the approach taken here was to focus on the production of a quality model in itself. Many parallels can be seen between the steps taken in this Chapter and standard QbD practices in industry: Firstly, the Target Product Profile (TPP) was defined, after which the critical quality attributes (CQAs) were decided and highlighted in the form of Chapter aims, these were systematically worked towards using a specified process where sources of faults and individual components were identified and changed incrementally<sup>157</sup>. The Chapter followed a process development methodology, employing problem solving to reduce the gap between what the current process technology can achieve and what is required to succeed in the target market through iterative experiments, each one offering something to learn through technical solutions<sup>158</sup>. Each stage accumulated knowledge and allowed a construction of a process design space, showing the acceptable parameters in the process variables in which the quality of the final model was assured<sup>157</sup>. The aim of these stages was to reduce the “artisan”<sup>46</sup> nature of the gel-making process as much as possible, to be able to represent something that is made on a large scale without the need for the judgement skilled, experienced operators. A system that is reliable based on the process and not on the testing of it. The technology developments in recent times with additive manufacturing allowed for developments that were not available in previous iterations of this model in the past<sup>159</sup>. Now, multiple moulds could be made with a single press of a button on a commercially available printer in significantly less time than it used to take to order custom made ones and for a small fraction of the price at 2.25p per construct compared to other methods.

Firstly, a number of different prototypes were explored and the data on their ability to make a gel and take it through culture was gathered to pick the best systems for the goals of the thesis (Figure 3.19). The two previous standard systems<sup>46,119</sup> and the insertable moulds system presented in this thesis had the highest success rates. The insertable moulds allowed for the easiest separation of the cell types in a single gel, which involved a much simpler method that was less invasive with the 3D printed sliding



dividers. They were also specifically designed for this purpose, easily made in the laboratory on-demand and could be changed to any standard required. A design was thereby chosen.

#### 3.5.4 Collagen gel polymerisation times

To increase the volume that can be made for use in high-throughput screening applications, the time taken to make multiple gels needs to be decreased. Time is a resource and resource efficiency is the second requirement of high-throughput systems alongside reproducibility. Like failure rates, no information has been published on the time required to make a single gel or any number of gels, likely due to the lack of relevance in that aspect when creating small numbers of models. Researchers would take however long they needed to make a construct and complete an experiment in order to gather the relevant data that they were interested in. In large-scale testing, this approach would not be viable; not calculating the time for a process would be a very large and potentially costly oversight for a process.

Developing a process such as this with aims of high throughput is difficult due to the amount of variability inherent within the system. Apparatus variability can be overcome through redesign, as has been done with the insertable moulds system. Time taken for the gel to neutralise is an example of variability in the method. The same volume of rat tail collagen will take different amounts of NaOH to neutralise in any given attempt, so this part of the method cannot be standardised, making this a very time-consuming part of the process, especially when multiple repeats are needed. This may be because of inadequate mixing of the components before being used. However, mixing collagen uniformly is difficult due to the viscosity. Again, no mention of this aspect of engineering 3D hydrogel models is published in the literature, usually it is left up to the experimenter to acquire enough skill to fulfil this stage competently, hence the 'artisan' nature of the process<sup>46</sup>. As very little can be done with automating a stage that needs the judgment of the operator, the number of times this is performed needs to be minimised to streamline the process. Preferably, a single neutralisation stage for each cell population used (or acellular gel) would resolve this. Alternatively, many groups utilise commercially available products where the solutions come in specific volumes and neutralise reliably.

Following on from this, it was highlighted that the gel polymerisation time was variable for each batch, the relevance of this is the unpredictability of the time and therefore an inability to standardise it especially when operating with multiple gels, as every gel, no matter how carefully measured will take a different time to neutralise. The reasons for this are not well understood, although unequal distribution of certain factors in either the collagen or the NaOH might lead to different outcomes as well as environmental factors such as the temperature of the room. Introducing ice based on recommendation from Jones et al.<sup>159</sup> changed the dynamic of the process completely, giving a single

neutralisation stage enough time so that all the required gels could be made in one attempt before leaving them all to polymerise, allowing for extremely simple, yet effective scale-up for the process, a generally difficult thing to achieve with many systems<sup>158</sup>. This was an example of how one group adopts a method to use and standardises it for all experiments, whilst other continue optimising for longer period of time or for other purposes, as is paralleled in industry when firms have different levels of ability/knowledge that they develop through their own learning processes<sup>155</sup>. This is where innovation systems play a role in development<sup>160</sup>. The use of ice had not been discussed with this particular version of the collagen model in any publication until it was compared to the PEEK system<sup>159</sup> where a different institution had incorporated the use of it, which was then adopted as standard. However, a new scientific publication before that would not have been accepted written simply on the alteration of one process variable, and changing a method without a peer-reviewed article is risky, especially in biotechnological fields<sup>158</sup> as it could have negative effects on the system that nobody could predict. In industry, this would usually be kept as a competitive edge as it is in the interest of the company to keep specifics as quiet as possible<sup>155</sup>. This is not always the case in scientific research, as disclosing a new method allows one to be accredited for it by others using it, which saved a great deal of development in this Chapter. However, much like in process development in industry, where a process accumulates 'rules-of-thumb' or 'heuristics', this information being passed on to this project was through the gathering of a body of knowledge from those working on the model.

The second benefit of keeping the neutralised solution cold with larger collagen volumes is that increasing the volume of collagen allows for more room for error when neutralising as the drops of MEM remain the same volume, therefore allowing for a more precisely controllable neutralisation stage. Thereafter, the new method of inserts with ice proceeded to show that the success rates of gel were increased by minimising the stage at which most problems occurred (Figure 3.23), the decrease in failure rates with 3D printed moulds of this shape is supported by Jones et al.<sup>159</sup>

The number of gels producible in a short amount of time had not been a pressing concern before this project, hence the absence of published material looking at how to maximise the output of collagen skeletal muscle models by making the process as efficient as possible<sup>46</sup>. It has been more of interest to use what was a working model to find out the cellular behaviours, genetic expression and the impact certain stimuli have on the two. Compared to the time taken to produce multiple gels in one attempt, the new method was faster by many times (Figure 3.22). Much of this came down to the step that was previously changed and not having to neutralise a new volume of collagen for every gel or two, the other main source of time saved comes from scaling the constructs down to a third of their size.

### 3.5.5 Comparison of 3D-printed inserts to the 8-well plate model

This new faster method was then compared to the standard 8-well plate method in contraction – a phenomenon characteristic of these models<sup>152</sup>. Matrix contraction is mediated by cell activity as they attach to the matrix and begin to pull in the surrounding matrix. In a free floating system the entire gel contracts, but anchor points prevent the gel from detaching to contract equally, therefore a bowing is observed in the middle of the gel<sup>152</sup>. The contraction level is generally considered to be indicative of the strength of the mechanical signal transferred to the cells, leading to reorganisation and alignment unidirectionally<sup>162</sup>. This requirement may differ between cell types. Here, both systems failed to reach 50% reduction in width over a 14-day culture period whereas later experiments in this thesis far exceed that with the same seeding densities and setups, showing some of the inherent variability that can exist in the system, possibly due to cell or collagen batches. Failure to reach 50% reduction in surface area was observed in the 8-well method by Jones et al.<sup>159</sup> However, Jones et al. showed that the “50% rule” was not necessarily indicative of good myotube formation and genetic expression, as both systems had different contraction levels but exhibited no significant difference in these important characteristics. Taking this into account and looking specifically at the similarity in contraction in Figure 3.24, it can be concluded that the lack of significant difference shows that the two methods are interchangeable in this regard.

Additional results that have not been analysed elsewhere are those generated from the positioning and consistency of the custom A-frames in the 8-well plate method. Although mentioned elsewhere briefly as a potential source of inconsistency in the system and therefore its output<sup>46,159</sup>, here it was measured and showed as postulated earlier that the A-frame placement was a source of much inconsistency (Figure 3.25), beginning from the positions they were in when the construct was set and the way they varied throughout the culture period, moving and potentially stimulating the model in ways that were not intended nor reproducible (Figure 3.27). Furthermore, difference in surface area of the mould compared to the design was found to have significantly improved with the 3D printed insert system (Figure 3.28).

Brief qualitative comparisons of stained images of the two methods also showed similarity in the architecture of the construct, with aligned, fused, multinucleated myotubes visible in both (Figure 3.29), concurring with the notion that the two models yield similar results<sup>159</sup>. Unbranched myotube formation is specific to 3D models and physiologically more similar to muscle tissue *in vivo*. These occur as cues are only given in one direction with fewer attachment points between cells than in 2D culture on a flat surface<sup>152</sup>.

As an additional point to consider, the system is supposed to be a fixed constant under which cellular mechanisms will dictate the results. The original system was not designed to exert any active stimuli on the constructs, although some designs have been adjusted to specifically test the effects of active tension on the system<sup>111</sup>. A-frames are sometimes subject to their undesired movement down the side of the well they are hooked over, leading to an uncontrolled, unquantified active strain on the system. As explained by Player et al.<sup>111</sup>, static loading can lead to upregulations of hypertrophic genes which may indeed be desirable for skeletal muscle models in general but require a model that does not add unmeasurable strain to reduce the reliability of results. The 3D-printed inserts showed difference in placement of the two methods and how the 3D moulds eliminate the variability in the drift of the A-frames.

### 3.5.6 Segmentation of the model to create co-culture gels

Alongside the development of the reliability of the system, a simple segmentation method with removable sliding dividers (Figure 3.17) was created which gave the gels a “bowtie” shape in gels that were acellular-C<sub>2</sub>C<sub>12</sub>-acellular setup due to the strong contraction in the middle (Figure 3.18), cell seeded region compared to the peripheral regions that were acellular. Macroscopically, this suggested that the cells were indeed kept within the seeded region, or were at least remodelling mostly in that region and very little in the peripheral regions. The proceeding Chapters will inspect the specific cellular behaviours more closely.

## 3.6 Conclusions

A Quality-By-Design (QbD) process was used in order to develop a collagen hydrogel fabrication system into one that was more consistent while also being adaptable to changes in design depending on testing requirements. Changing the mould from an 8-well plate/PDMS setup to a 6-well plate/3D printed PLA moulds allowed for a larger volume of experiments to be conducted whilst also increased consistency between individual repeats. Following this, borrowing from other methods involving collagen gels, ice was included into the system to allow for an even greater, large-scale version of the process with even greater consistency, as demonstrated by the decrease in variability of size of the constructs, decreased anchor point drift, increased anchor point matching and the same width reductions.

Once developed to allow for larger-scale fabrication and greater consistency, the 3D-printed insert modification to include dividers from preliminary experiments led to the successful segmentation of the gels, with seeded regions separated from unseeded (acellular) regions within a single gel. Further experiments to understand the mechanics of these new gels would now be required.

## 4 Evaluating the new segmented hydrogel system by incorporating a skeletal muscle model between two unseeded regions

As a new apparatus and methodology for the creation of hydrogels had been established, the cells in the segmented gels needed to be seen to behave and respond to the model in the same way as had occurred in the completely seeded hydrogels. This would indicate that the 'muscle' region was behaving in the same way as standard muscle models and would pave the way for the introduction of secondary tissue types into the model.

### 4.1 Introduction

In the previous Chapter, it was reported how a leading standardised method for creating 3D-tissue-engineered skeletal muscle was developed to allow higher volumes of models with greater control of seeding regions through the introduction of physical dividers, in this case muscle and tendon. The segmented models with C<sub>2</sub>C<sub>12</sub> cells seeded only in the central third of the gel were briefly found to work on a macroscopic scale and to form a "bowtie" shape from the difference in contraction created by the middle/seeded Section contracting to a greater extent than the acellular peripheral regions. It was also found that 3D printed inserts were equal in terms of gel contraction and visible myotube formation as the standard 8-well plate method, indicating that 3D-printed inserts could yield similar results to the currently published standard models. In order to further progress this model, it is important to compare 3D printed skeletal muscle models against segmented models to ascertain whether the segmentation process affects the cell-seeded region of the gel. Negative macroscopic and microscopic effects would indicate that the model requires a trade-off in quality of the model in the skeletal muscle region in terms of myotube parameters in order to allow for a multi-tissue model. If no depreciation in the quality of the model in the muscle region is observed, then the segmented model would be a direct development of the skeletal muscle model.

A number of models have been developed for engineering of both tendon and skeletal muscle *in vivo* in both 2D and 3D as discussed in Chapter 2. However, in order to create a muscle-tendon model, a form of 3D co-culture will most likely be required. As discussed in Chapter 2, 3D tissue co-culture either comes in the form of a degradable hydrogel allowing cell-cell contact, or a permeable hydrogel divider<sup>130</sup>. In this Chapter, a hybrid of the two methods is proposed where a removable divider is used to initially separate the gel types before allowing them to fuse and culture together as a single gel. The justification for such a method is because it is vastly simpler in terms of resources and preparation and lower cost than current tissue engineered models for the muscle-tendon interface. Current

models can be divided into those engineered *in vitro* initially, then requiring implantation to complete the model using physiological cues and those that are independently tissue-engineered completely *in vitro*. Models requiring implantation have less uncertainty due to the availability of autologous tissues and cells, as well as the advantage of the physiological cues once implanted driving the tissue to achieve tissue repair and have been used with success in animal models<sup>163</sup>. These usually involve a scaffold that is cultured with a single population of autologous cells *in vivo* before being implanted as a replacement tissue, the scaffold then slowly degrades as the tissue grows using cues from the surrounding tissues with support from the scaffold<sup>145</sup>.

Current tissue-engineered *in vitro* models trying to replicate these cues generally take one of two approaches; separation through materials and adhesion of two individually cultured tissues. Separation through the use of materials is usually achieved through manipulating material properties such as using different electrospun scaffolds<sup>164</sup> or it can be done by patterning or printing a material with desired properties in specific regions as Merceron et al. had great success with<sup>143</sup> where materials of different stiffnesses were co-printed with corresponding cell types using a 3D organ printing system.

Adhesion of two tissues will involve fully tissue-engineering a single tissue and then bonding it to either another tissue engineered construct of a different type, this could be another fully engineered construct or a non-engineered, isolated tissue. Both examples were used by Larkin et al.<sup>54</sup> where rat tails or tendon constructs were pinned onto self-assembling muscle constructs then co-cultured. Whilst this method yields positive results, it requires the use of physiological sections from animals that are already developed, reducing the control over the size and geometry of the model and increasing the requirements for preparation of the model. Additionally, if these were to be used to model human muscle-tendon interfaces, there would be a requirement to use human tendon tissue which is associated with high donor-site morbidity and not feasible on large scales.

All the above processes, while acquiring various levels of success in trying to replicate an interface, have the drawback of not quite being simple or cheap enough to be able to set up for high-throughput systems. The method proposed by Larkin et al.<sup>54</sup> requires an entire culture period for the tendon constructs first. Merceron et al.<sup>143</sup> required a complicated 3D organ bioprinting system for each gel made. Electrospun scaffolds have an impact on tissue mechanics in *in vitro* systems, these are extremely useful when implanted and they can degrade, but if the system is exclusively *in vitro* then this is sub-optimal. A single model using one matrix representative of the tissues would be more representative and simpler to fabricate, in this case, using collagen for the entire model. Therefore, there is a requirement for a simple, mass producible method that requires minimal setup with a single matrix throughout. In this Chapter, it is reported how segmented hydrogels were evaluated as a

potential method to meet these requirements. Firstly, the method was to be tested against the control hydrogels to better understand the mechanisms in the myoblast cell population to the variation in the method.

#### 4.1.1 Chapter aims

- Compare the change in gel surface area, gel width, myotube length, myotube width, myotube alignment, in central regions of fully-seeded gels to centrally-seeded segmented gels to understand whether the myoblasts in both systems result in
- Ascertain whether the unseeded (peripheral) regions remain absent of cells throughout the culture period.

## 4.2 Materials and Methods

### 4.2.1 Cell culture

C<sub>2</sub>C<sub>12</sub> murine myoblasts were cultured as described in Chapter 2, Section 2.1 unless otherwise specified.

### 4.2.2 Tissue engineering of 3D constructs

Collagen hydrogels were fabricated using the method developed in the previous Chapter as follows: 3D printed moulds and dividers were printed using PLA with an Ultimaker 2+ printer (Ultimaker, Netherlands), disinfected in 70% ethanol and left to dry in UV light. They were then bonded to the bottom of a 6-well plate using silicon sealant (King British, UK). Dividers were inserted into the slots for three of the moulds that will be segmented and left out of the three control gels. Cells were passaged and counted. A 3 ml volume of rat-tail collagen was neutralised and then divided into two centrifuge tubes (1ml and 2ml) and kept on ice. The 2ml gel was then mixed with the counted cell population, seeded at the standard 4 million cells/ml whilst the other remained acellular. Segmented, centrally seeded gels had 167 µl cellular gel pipetted into the middle segment and 167 µl acellular gel in each of the peripheral segments while controls had 500 µl of cellular gel pipetted into the mould. Dividers were then quickly removed whilst Sections had not reached a high enough temperature to polymerise to allow Sections to create a single gel. This left a gel as shown in the schematic below (Figure 4.1). These were then cultured under the normal conditions outlined in Chapter 2, Section 2.2 for 14 days.

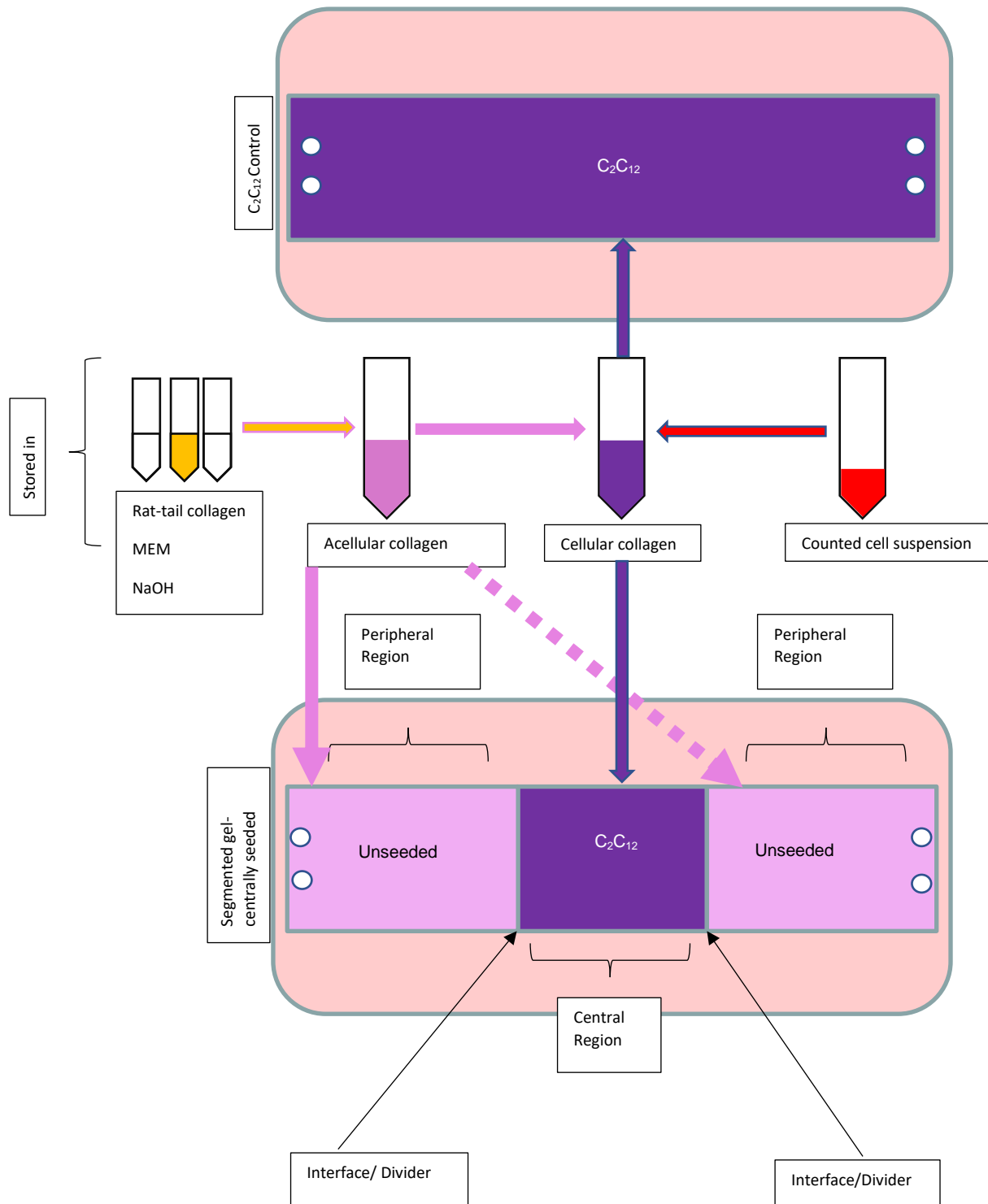


Figure 4.1: Schematic for the fabrication and layout of the segmented gels and controls with key areas labelled that will maintain nomenclature for the remainder of the Chapter.

#### 4.2.3 Macroscopic imaging

Macroscopic imaging during culture was conducted as described in Chapter 2, Section 2.10.



#### 4.2.4 Macroscopic image analysis

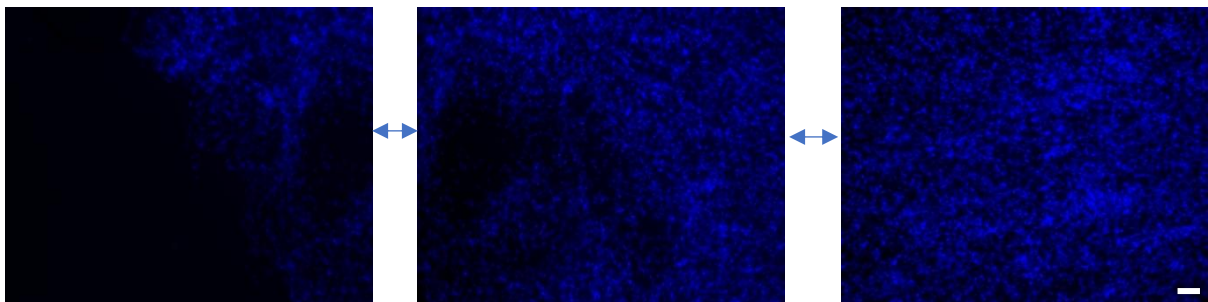
Gel width and surface area were measured using ImageJ as described in Chapter 2, Section 2.12.

#### 4.2.5 Immunofluorescence imaging

Immunohistochemistry was used to assess cell morphologies. Samples to be analysed were fixed, stained and imaged as described in Chapter 2, Section 2.11.

#### 4.2.6 Image stitching

Images of DAPI stained nuclei were taken by individual frames and the platform of the microscope was then moved along the length of the gel. These individual frames were then stitched together using the “stitching” plugin in ImageJ based on a publication from Preibisch et al.<sup>165</sup> (Figure 4.2). These were stitched together end-to-end with the same nuclei on the edge of each image being overlapped to create an end-to-end image of one single strip along the surface of the gel. This is similar to a method used by Wragg et al. previously to construct larger immunostained microscopic images of skeletal muscle constructs from smaller individual images.



*Figure 4.2: Example of how the stitch function was used on ImageJ to combine microscopic images. Using the stitch function on ImageJ to combine individual frames together to create a tiled image of the entire length of the gel for DAPI (nuclei) staining. Scale bar = 100  $\mu$ m*

#### 4.2.7 Microscopic analysis of myotube measurements

Numerical analysis of the microscopic images involved measuring individual features of the microscopic images in ImageJ as in Figure 4.3 of both segmented and control gels.

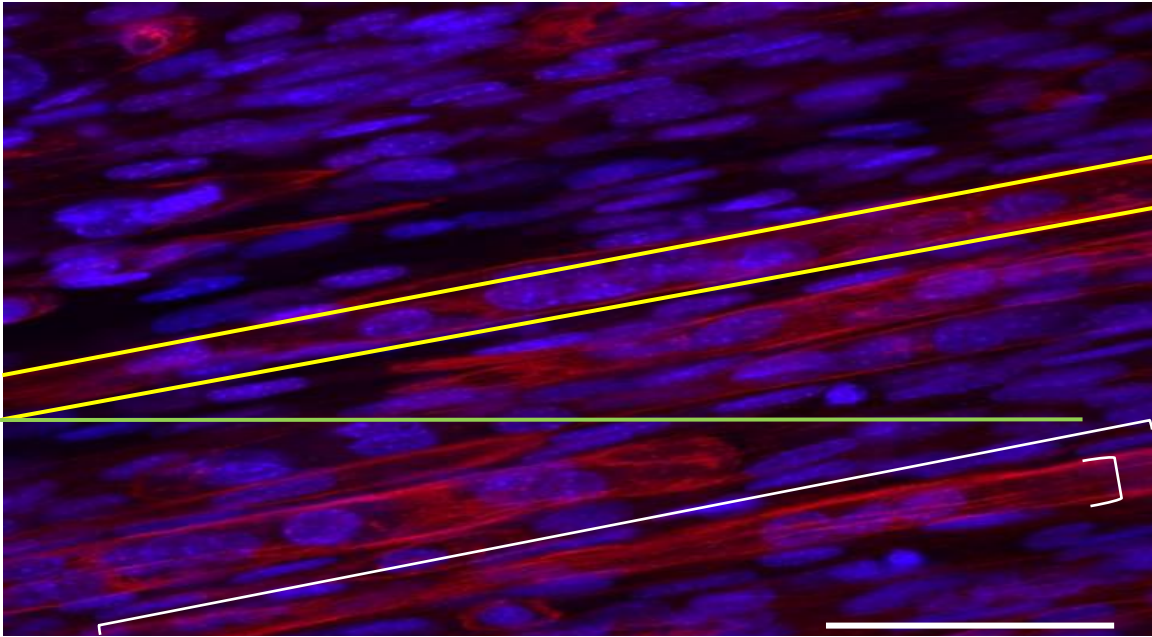


Figure 4.3: Example of how myotube lengths and widths were measured (white lines) and how myotube angles were measured (average of yellow lines against horizontal green line). Actin filaments were stained with rhodamine phalloidin (Red) whilst nuclei were stained with DAPI (blue). Scale bar = 50  $\mu\text{m}$ .

These images were analysed using the previously published method for parameters that are standardly compared in publications including myotube length, width, number of nuclei per tube and number of tubes per frame<sup>46,159</sup>. These have in previous publications been limited to a single frame and are therefore not always true representations of these measurements, therefore certain parameters are usually given arbitrary units as published by Jones et al.<sup>159</sup>. Frame size is also dependent on the equipment being used to take images so is not standardised to a threshold between different studies.

Myotube alignment was also measured. This was conducted by measuring the individual angles created by every myotube to the horizontal of the frame and evaluating the difference between them and the total frame average as has been shown in previous publications<sup>46</sup>. Angles were measured from the line created by the top of the tube at intersections to the frame, and by the bottom and averaged for each myotube. Alignment is a relative measure and myotube alignment is a comparison of the angle of one myotube compared to the rest within an image. Comparing them frame by frame would not allow for a sufficient relative measure as each sample is likely to be mounted at a slightly different angle and the myotubes may also be aligned slightly differently, leading to an inconsistency between images. Therefore, an average was taken of each frame, this would represent how an ideally aligned myotube in this system would be orientated. Each individual angle had the average then subtracted from it to compute a 'deviation from alignment' value. This would show how far each individual

myotube across each frame was away from being aligned perfectly. The closer to zero, the more aligned each cell can be considered to be compared to the others.

#### 4.2.8 RT-PCR measurements

RNA extraction and quantification, and RT-qPCR were conducted as described in Chapter 2, Section 2.13.

#### 4.2.9 Gel success and survival rates

Gel success and survival rates were calculated as described in Chapter 2, Section 2.9.

### 4.3 Results

#### 4.3.1 Gel contraction

In order to ascertain whether there were macroscopic differences in the behaviours of segmented gels compared to the standard model over the 14-day culture period, the gels were imaged at 0 hr, 24 hr, 7, 14 days. Figure 4.4 shows an example of these scans and the differences observed in the gels over the culture period, showing n=3 of both segmented and control gels in a single repeat.

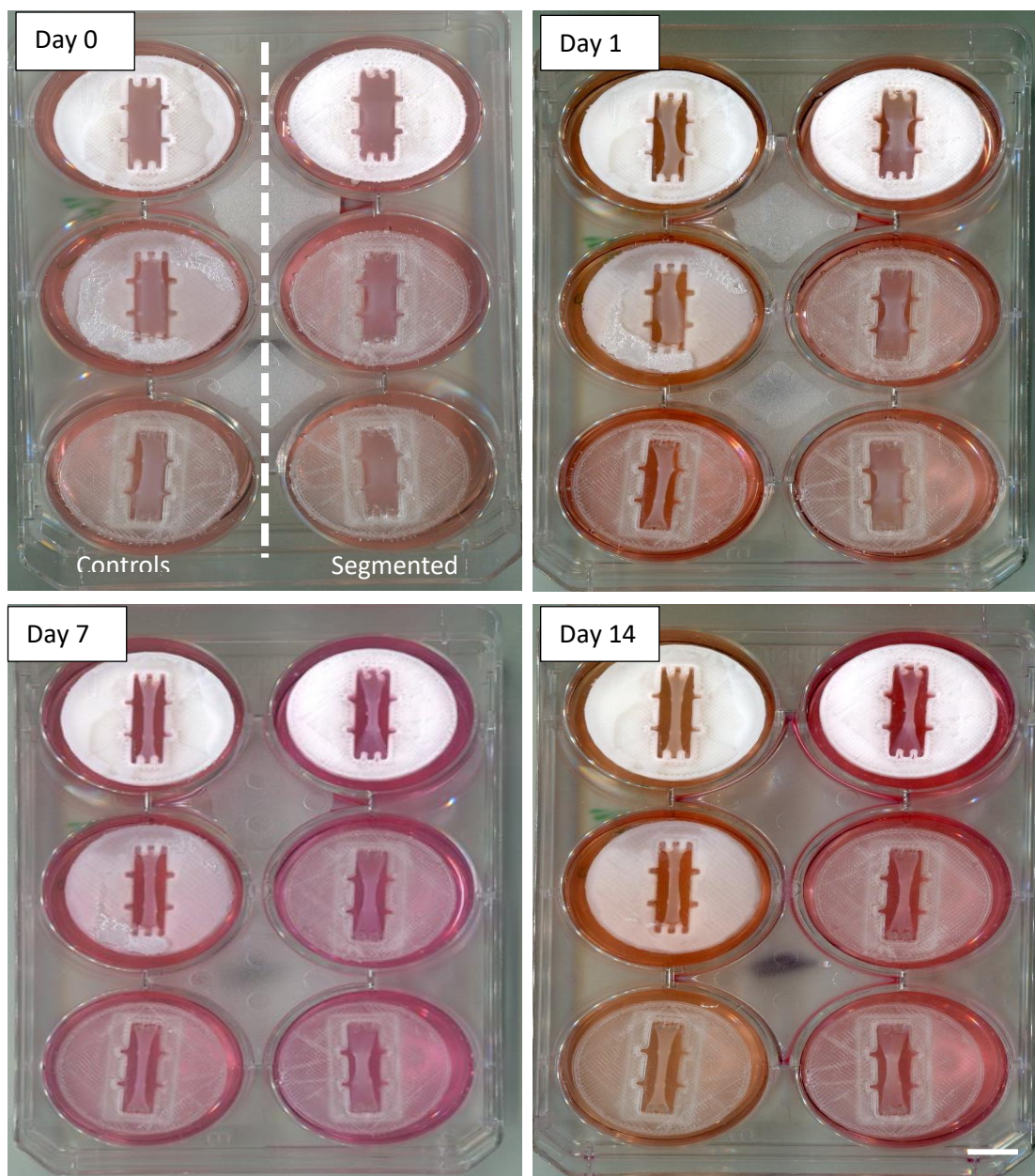


Figure 4.4: Contraction of control gels (left of each well) and segmented gels (right of each well) at key time points over the 14-day culture period. This figure represents  $n=3$  (3 controls seeded throughout and 3 segmented, seeded centrally only). All moulds were printed using the same method and equipment. Scale bar = 10 mm.

#### 4.3.1.1 Macroscopic imaging of gel size over 14-day culture period

To determine whether the segmented gels behaved in a similar fashion to the standard system, measurements from scans of each plate were taken at key time points; 0 h, 24 h, 4 days and 14 days and the results were compared (Figure 4.5).

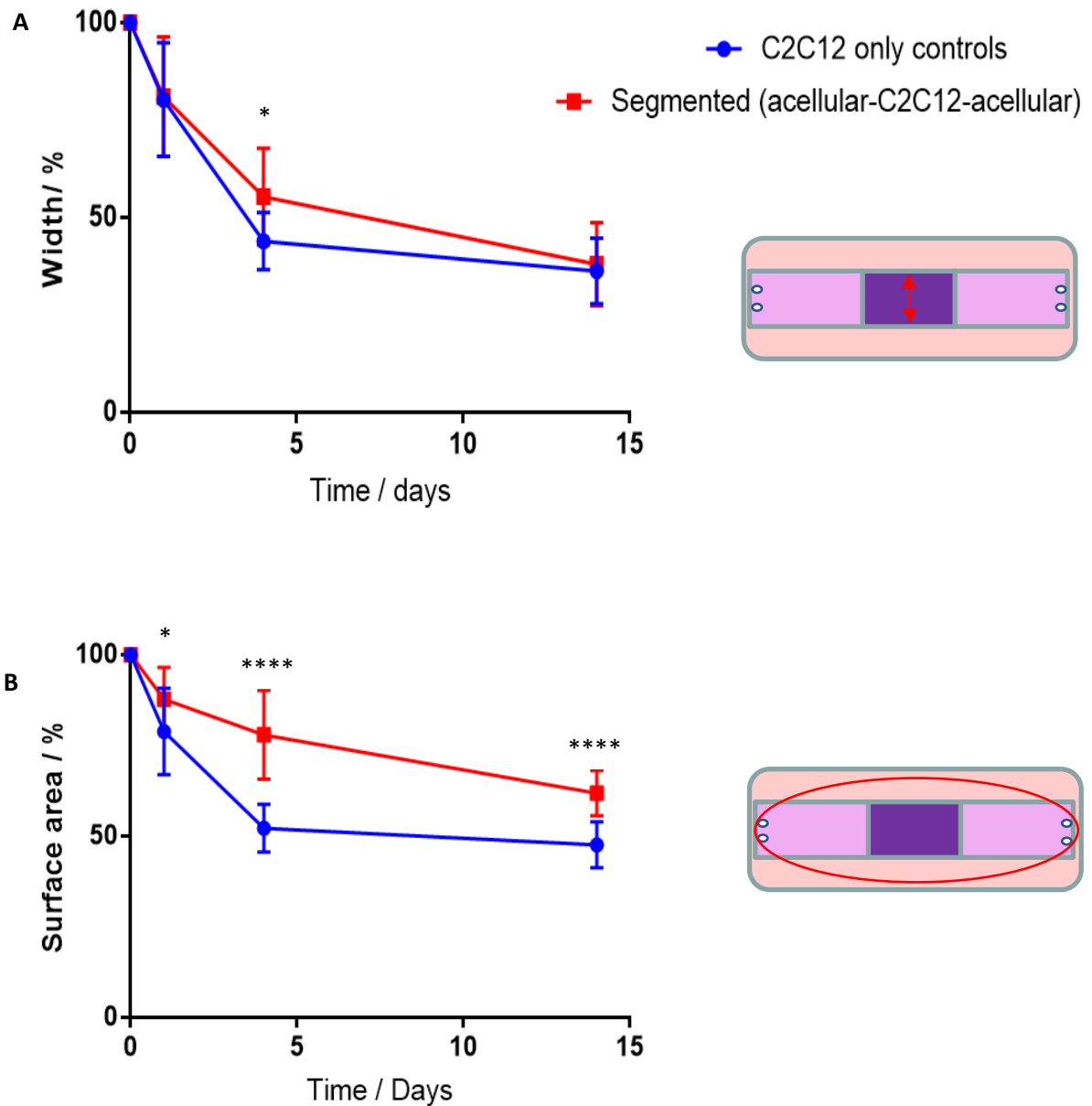


Figure 4.5: Contraction of the segmented gels compared to the contraction of skeletal muscle contracts based on width of central region (A) and total surface area of gel measured using imageJ (B). Taken from  $n=9 \times 3$  repeats (excluding 2 gel failures in  $C_2C_{12}$ ). The width of the gels were only significantly less on the segmented gels on day 4 ( $p=0.0031$ ) (t-test) while the surface areas were significantly less for the segmented gels over all three time points after the initial, day 1 ( $p=0.0161$ ), day 4 ( $p<0.0001$ ) and day 14 ( $p<0.0001$ ).

#### 4.3.1.2 Gel contraction comparisons

Gel contraction was measured in the same way as the previous Chapter to determine the extent of cellular remodelling of the construct. All gels contracted over the 14-day culture period. In terms of width, the only significant difference seen was at day 4 where the controls had  $44 \pm 7$  % while the segmented gels were  $55 \pm 12$  % of their original width in the centre of the gel (mean  $\pm$  deviation)

(Figure 4.5A). Day 0 and 14 had no significant difference. At the end of the culture period, segmented gels and controls had a width of  $38 \pm 10\%$  and  $36 \pm 8\%$  respectively.

As anticipated, a larger difference was seen in the overall surface area of the gel where all four time points saw significant differences (Figure 4.5B). At 24 hours,  $78 \pm 12\%$  was seen in controls and a significantly larger ( $p^*=0.0161$ )  $87.8 \pm 9\%$  in segmented gels (t-test). At 4 days, these figures were at  $52 \pm 6\%$  and  $78 \pm 1\%$  ( $p^{****}<0.0001$ ) at 14 days  $48 \pm 6\%$  and  $62 \pm 6\%$  ( $p^{****}<0.0001$ ) where control gels were significant smaller in surface area.

As no difference in central gel width was observed, to better understand the difference in overall gel surface areas between control gels and segmented gels, the surface area of peripheral regions were also measured and compared (Figure 4.6). The peripheral regions in the control gels were found to be  $39 \pm 1\%$  of their original surface area, whilst the segmented gels were less reduced at  $59 \pm 4\%$  of original surface area.

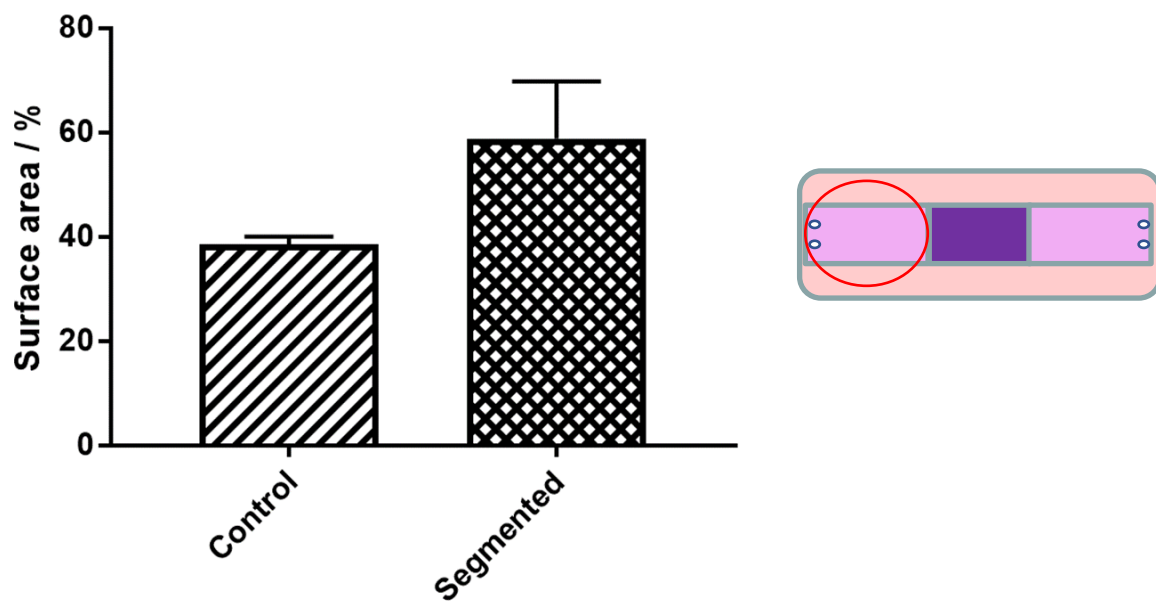
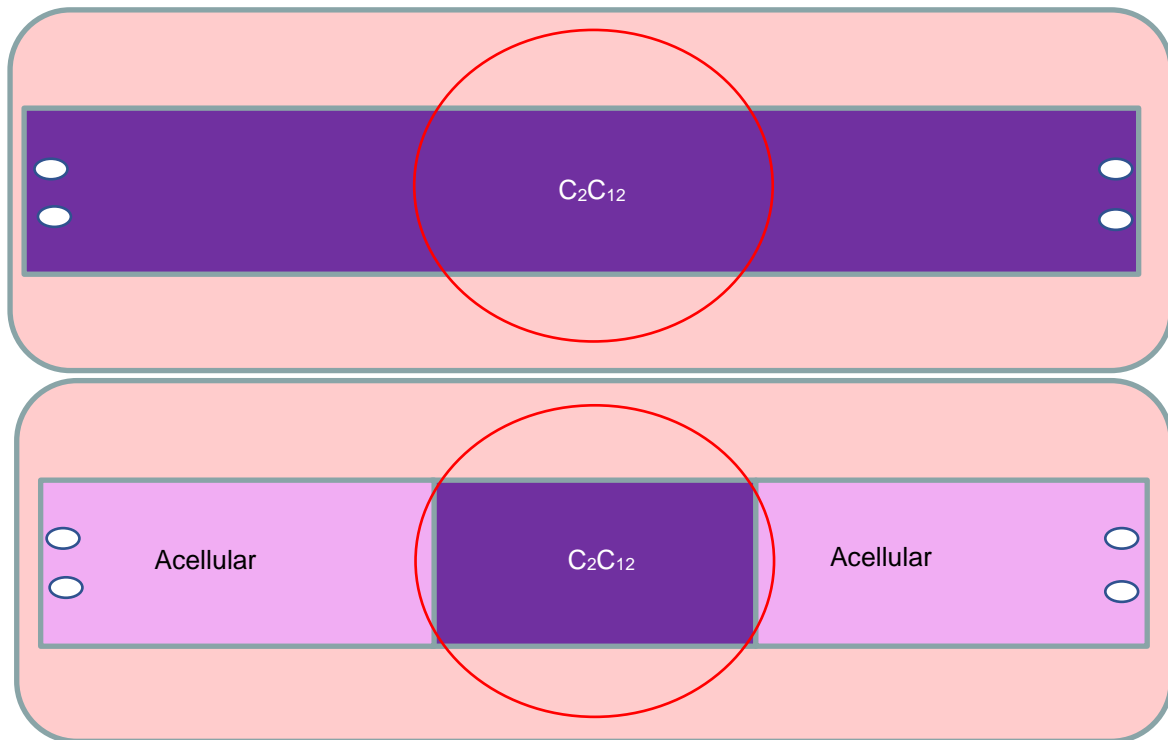


Figure 4.6: Comparison of the percentage of the original surface area in the peripheral regions of both the control and segmented gels. Taken from  $n=3 \times 2$  repeats. Error bars show standard deviation.

#### 4.3.2 Microscopic analysis of cellular regions in segmented gels and controls

Based on the contraction comparisons, the observable cellular remodelling results were seen to be similar in both models despite the change in methodology. As macroscopic contraction analysis is used as a non-destructive method to predict if the microscopic architecture will attain fused and aligned

myotubes once immunostained and imaged, it was important to next analyse the microscopic structure of both gels in their central regions (Figure 4.7).



*Figure 4.7: The central (cell-seeded for seg) regions were analysed and compared between the two gel types initially for microscopic and macroscopic measurements.*

#### 4.3.2.1 Immunostained image comparisons

The central regions of both gel types showed aligned, multinucleated myotubes in both with even some highly mature, sarcomeric organisation also visible (Figure 4.8). Few nuclei can be seen to not be sharing a cell body with another nucleus, indicating high fusion efficiency. The central portion of the segmented were found to show similar cellular architecture and development the  $C_2C_{12}$  skeletal muscle models, but to determine to what extent these results were comparable, more precise measurements of these features were required.

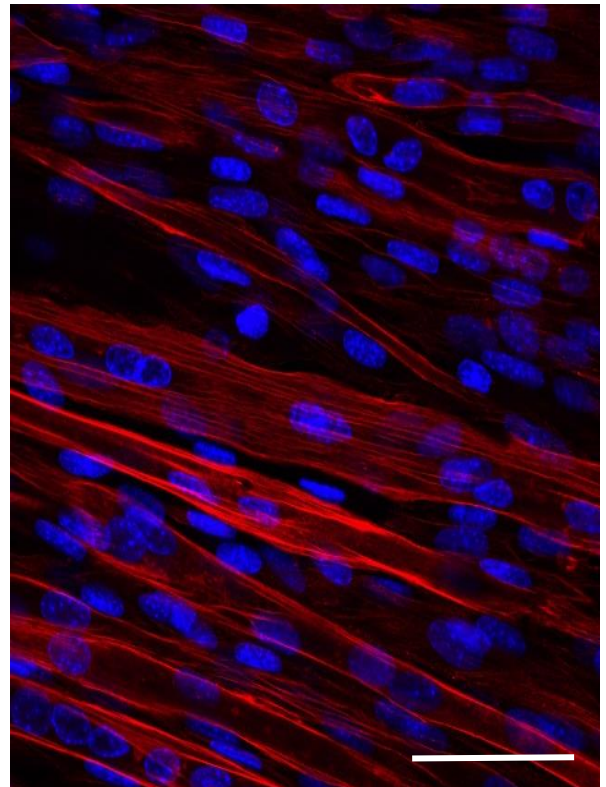
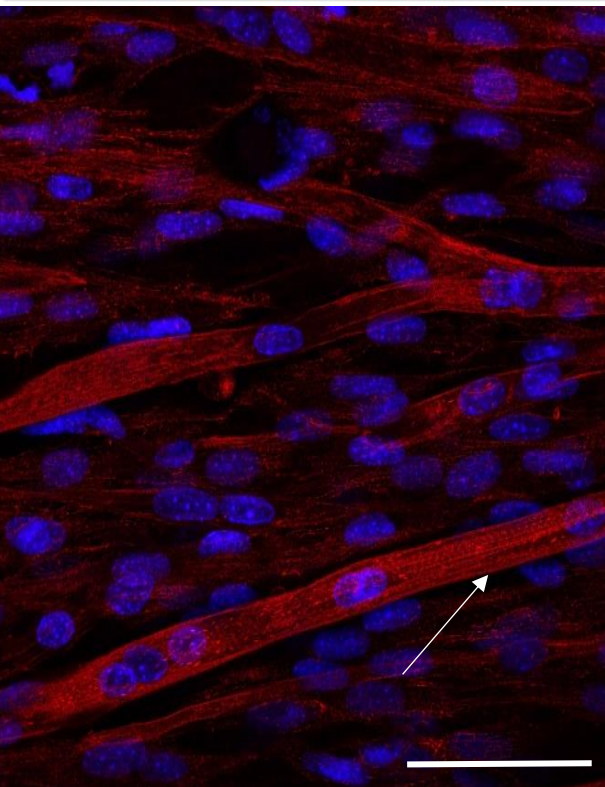
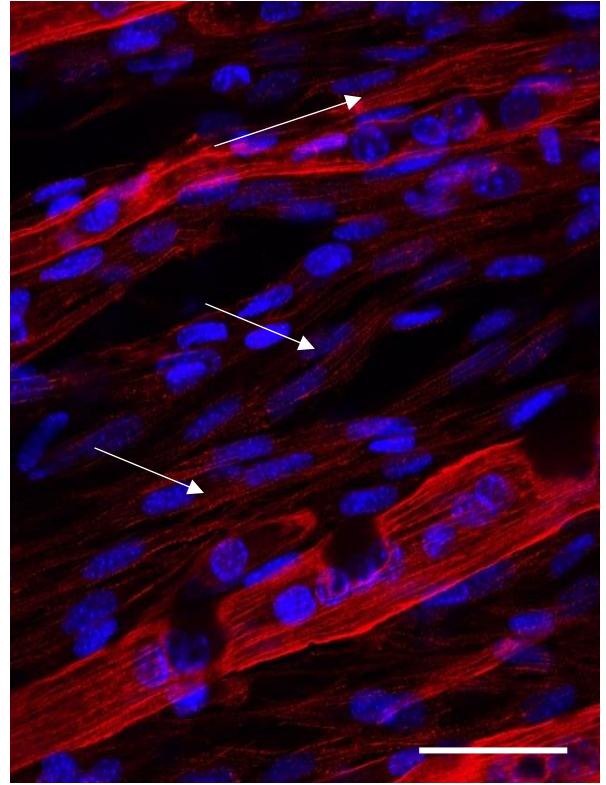
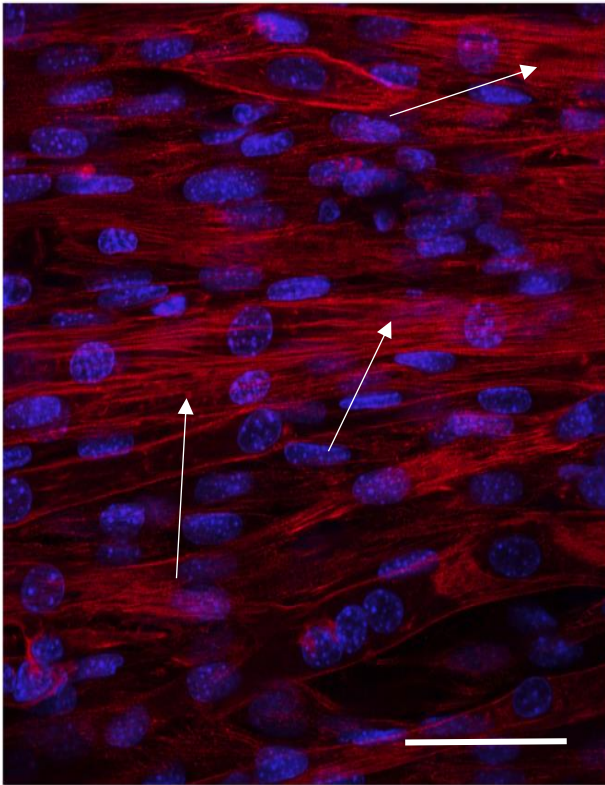


Figure 4.8: Immunostained images for  $C_2C_{12}$  control gels (Left) and segmented gels (Right) with rhodamine phalloidin for actin filaments (red) and DAPI for nuclei (blue). Both conditions showed high levels of fusion and alignment based on these images. Scale bar = 50  $\mu\text{m}$ . White arrows indicate areas with organised sarcomeric structures (striations).



#### 4.3.2.2 *Myotube measurement comparisons*

To make the models studied in this experiment comparable to published models in musculoskeletal tissue engineering, a number of standard parameters for microscopic quantification were used, measuring myotube length, width, number of nuclei per tube and number of tubes per frame as well as myotube alignment. However, the information provided by these measurements can be limited in their usefulness, this is commonly due to the length of myotubes being longer than the length of the frame they are being measured in, thereby limiting the results to measurable within the frame or simply larger than the frame with no accurate quantification. Nonetheless, these have been often used as indicators of whether a model is succeeding in forming multinucleated myotubes and can be found for this experiment in Figure 4.9 and Figure 4.10.

Figure 4.9 shows comparisons of the quantified myotubes per frame,  $11.2 \pm 1$  for segmented gels and  $10.3 \pm 1$  for controls with no observable difference. No difference was also seen in myotube length  $166.7 \pm 4 \mu\text{m}$  (segmented) and  $171.9 \pm 4 \mu\text{m}$  (controls) and nuclei per myotube per frame  $6.5 \pm 0.3$  (segmented) and  $6.9 \pm 0.3$  (controls) (Figure 4.10A). Likewise, no observable disparity between the setups was seen in myotube width (Figure 4.10B)  $12.6 \pm 0.5 \mu\text{m}$  for segmented gels and  $14.2 \pm 0.4 \mu\text{m}$  of the controls.

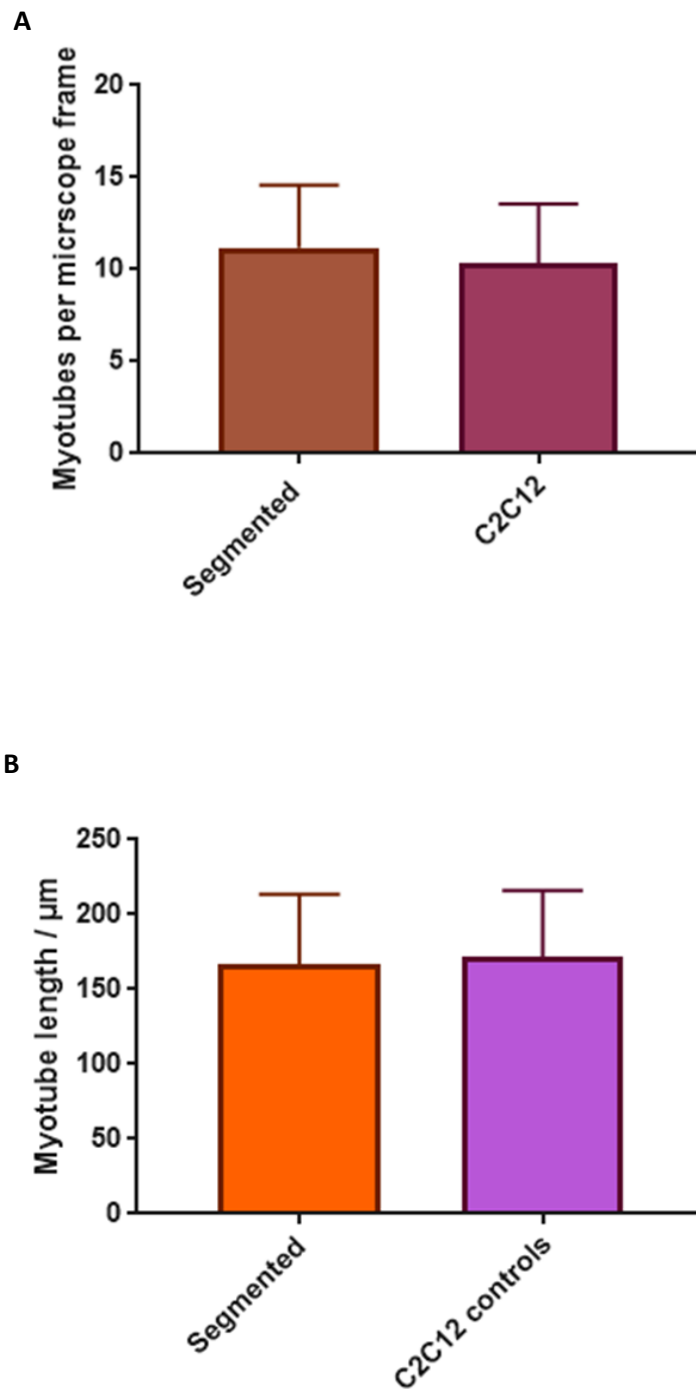


Figure 4.9: Comparison of data gathered from immunostained images between  $C_2C_{12}$  control gels and segmented gels for myotubes per microscope frame visible (A) and length of myotubes in each frame (B). Note that myotube length is limited to length of the frame as many go from one edge to the other, and is therefore not a true indicator of the length of each tube. No difference could be observed between the two systems. Error bars = standard deviation. Taken from  $n=2 \times 2$  repeats.

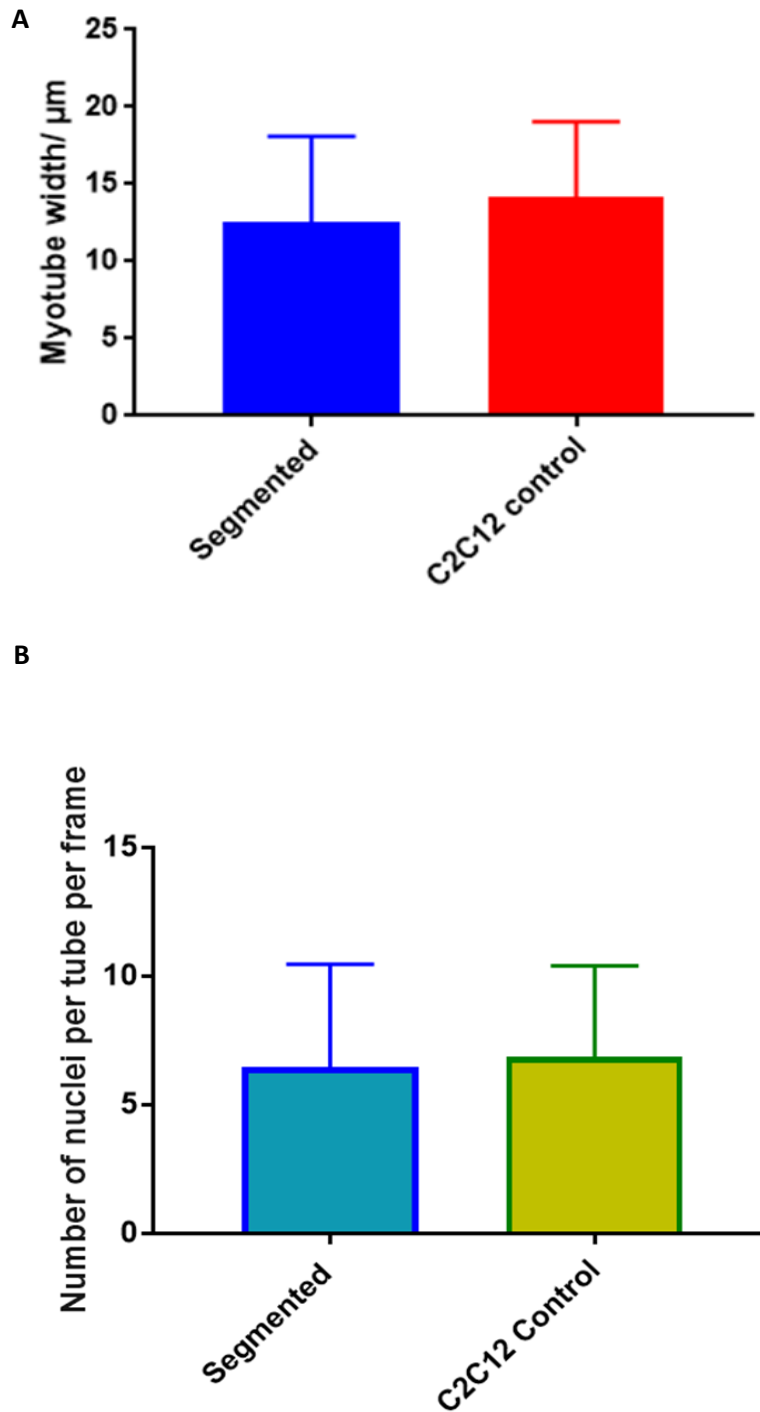


Figure 4.10: Comparison of data gathered from immunostained images between  $C_2C_{12}$  control gels and segmented gels for myotubes width (A) and number of nuclei per myotube (B). No observable difference could be seen between the two setups. Error bars = standard deviation. Taken from  $n=2 \times 2$  repeats.

### 4.3.2.3 Myotube alignment

Figure 4.11 shows the deviations of the myotubes from the average of each frame. What can be seen is that the majority of tubes are within 10° of being in alignment with the average alignment from the frame. As these are deviations from an average in the positive and negative range, calculating a mean of all the values would equate to zero. Therefore, to understand the average magnitude of the deviation, a mean of the absolute figures can be taken for both the controls and segmented gels and compared (Figure 4.12). No observable difference was seen in the alignment of the myotubes in either setup with the means equating to  $4.3 \pm 0.4$  and  $4.4 \pm 0.4$  for the cellular and acellular regions respectively.

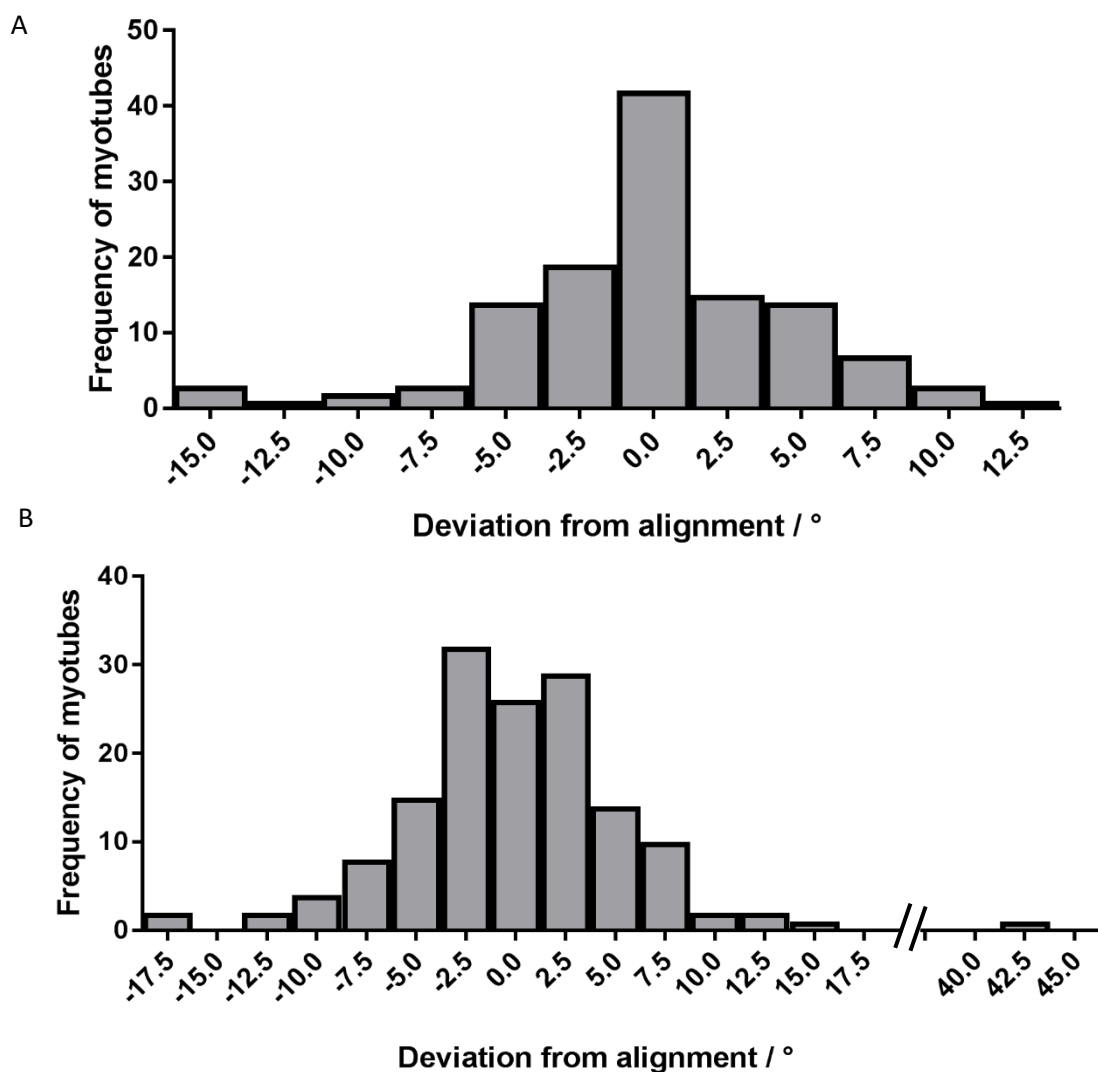


Figure 4.11: The difference between the measured myotube angles and the average for the frame it is in for the control gels (A) and the segmented gels (B), indicating how far the tubes are from perfect alignment with each other. Taken from  $n=3 \times 3$  repeats.

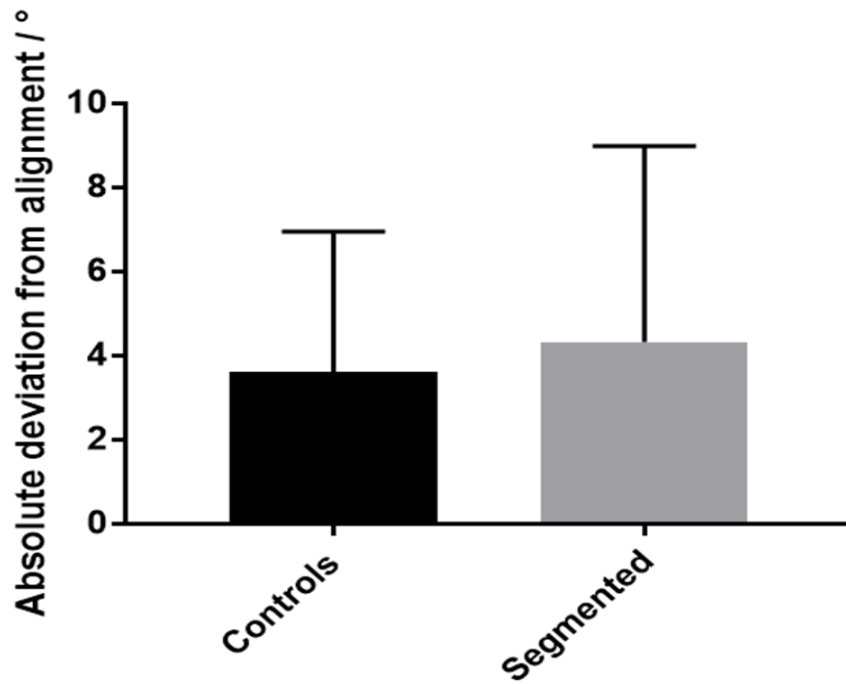


Figure 4.12 Difference in the deviation from alignment between the segmented gels and the controls. No observable difference could be found. Taken from  $n = 2 \times 2$  repeats. Error bars =  $\pm$  Standard deviation.

#### 4.3.2.4 Genetic expression of skeletal muscle markers

In addition to the microscopic measurements taken, RT-QPCR was conducted to ascertain the expression of two myosin heavy chain isoforms; MYH1 and MYH3. MYH3 is a marker for contractile, adult cells, whilst MYH1 is a marker for neonatal cells. MYH1 is downregulated in physiology and is replaced by MYH3 as the body matures into adulthood. Figure 4.13 Shows the differences in expression of these markers between the two systems.

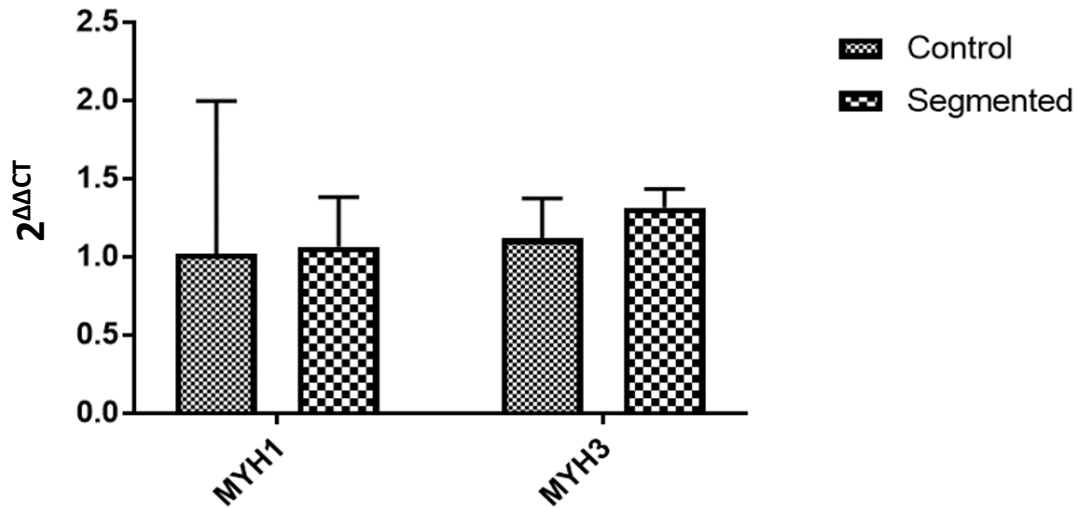


Figure 4.13: Genetic markers for muscle maturity comparisons between the control and segmented gels. Taken from  $n = 2 \times 2$ . Error bars = standard deviation.

#### 4.3.3 Peripheral region observations

Despite no cells being seeded in the peripheral regions of the gels, it was noticed that there were phalloidin and DAPI positive regions (Figure 4.14), including multinucleated cells (Figure 4.15) beyond the initial interfaces created by the dividers during the fabrication stage leaving a macroscopic line visible with the naked eye (Figure 4.16). This indicated myoblasts and myotubes potentially several millimetres from the central, seeded region.

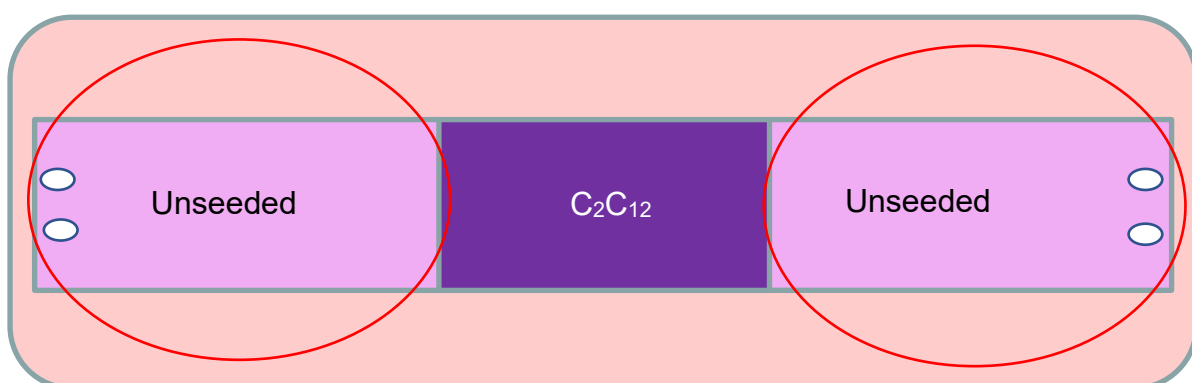
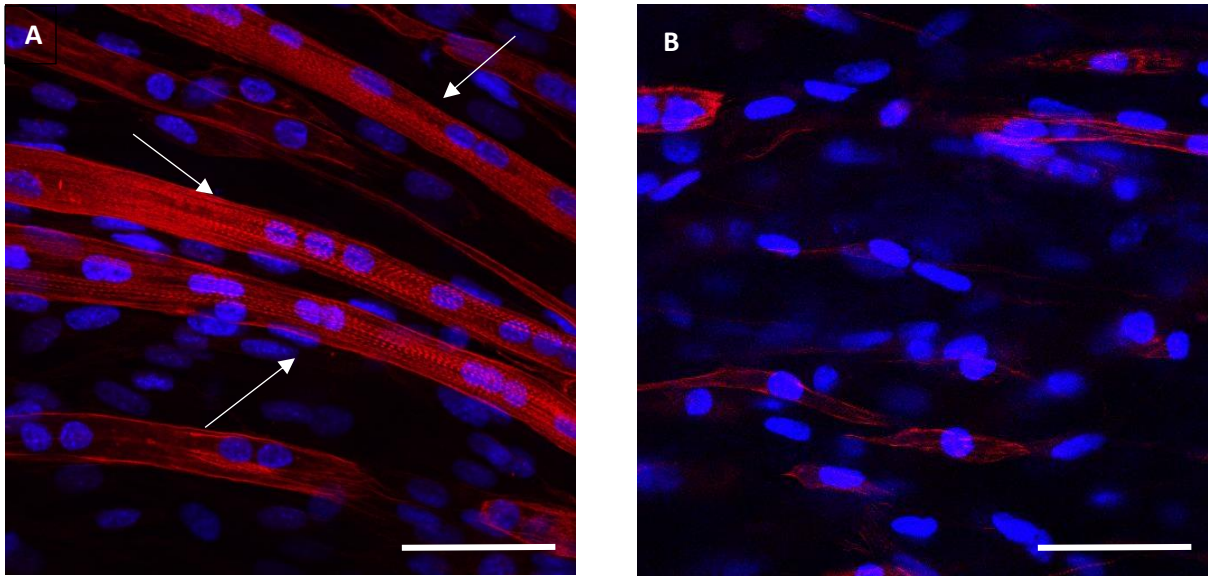


Figure 4.14: Schematic demonstrating the regions that were analysed in this Section. The unseeded regions were analysed next to understand the behaviour of the cells that were seeded only in the centre of segmented gels.



*Figure 4.15: Immunostained images of the acellular regions which were observed to show areas of highly striated, aligned myotubes (A) within large areas of sparse, undifferentiated myoblasts(B). Actin filaments were stained with rhodamine phalloidin (red) whilst nuclei were stained with DAPI (blue). Scale bar = 50  $\mu$ m*

Based on the previous macroscopic analyses either the cells were migrating across the interface, the cell number was not constant throughout the gel or the cell number was not directly related to contraction. Further to this, it was observed in the immunostained samples that there were myotubes located in the peripheral (acellular) regions of the gels (Figure 4.15). It was observed that the acellular regions that had a higher incidence of highly developed, fused myotubes alongside visible striations (Figure 4.15A). These were found intermittently amongst mostly unfused and low-density cells (Figure 4.15B).

The unexpected observation of the acellular regions led to another experiment to understand the behaviour and positioning of gels over the culture period.

#### **4.3.3.1 Migration of cells experiment**

To better understand whether the cells were moved into the peripheral regions through mechanical means when the dividers were removed, or if this was caused by cell migration into an acellular space, or if there was a sudden increase in nuclei in certain areas, an experiment was conducted where cells were seeded in the central region only and then fixed and stained at 24 hr, 4 days and 14 days (Figure 4.16). This would allow for an understanding of the cellular positioning in the gel over the different time periods. A 14-day control was set up to compare the density of the cells visible at the end of the culture period.

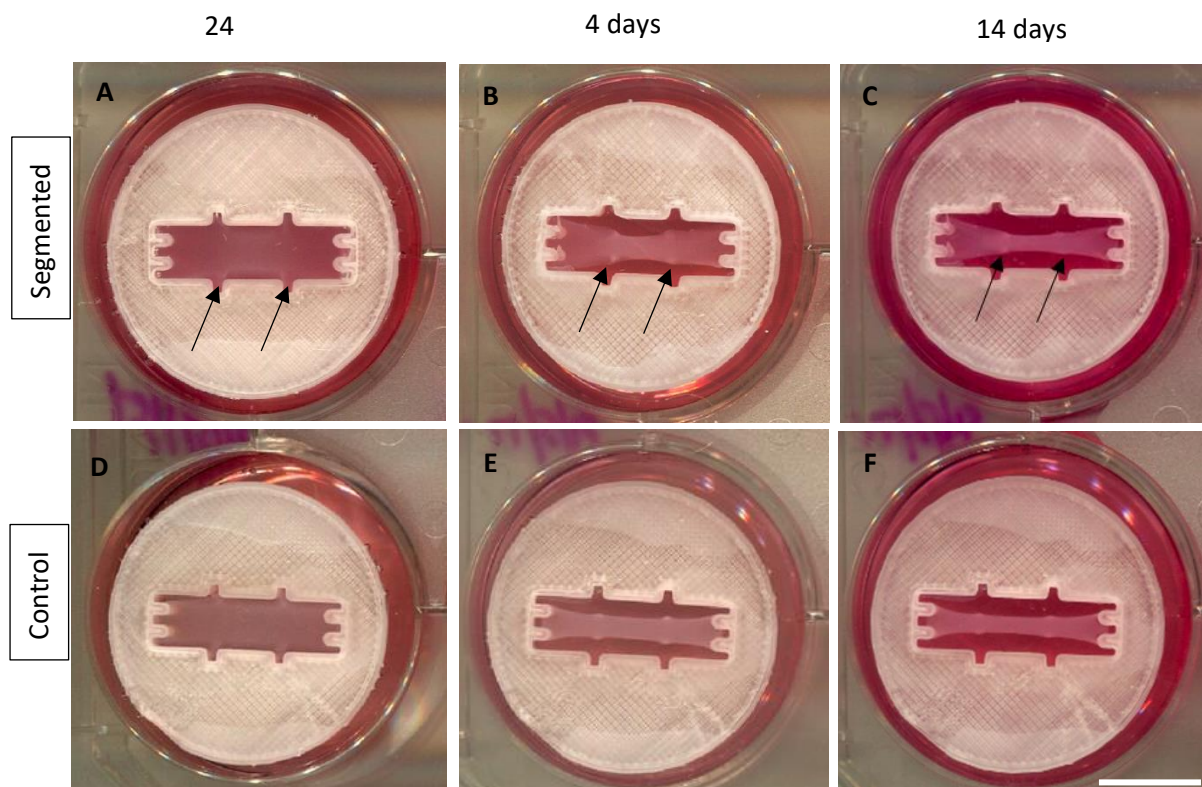


Figure 4.16: Comparison of segmented gels with C2C12 gels and how the interfaces look at different time points. A clear difference can be seen in the coloration of the regions in the segmented gels (A, B, C) when compared to the uniform coloration of the C2C12 gels (D, E, F). The notches in the mould are where the dividers are placed and therefore are the points at which interfaces should initially be formed in the segmented gels. The black arrows show these regions. Scale bar = 10 mm. Image represents  $n=1$ .

#### 4.3.3.1.1 Nuclei placement in segmented gels

Gels at each time point were imaged across their length and the images were stitched end-to-end. As can be seen in Figure 4.17, cells are observed to be more densely concentrated in the central regions at 24 h, but by 14 days they are more evenly distributed throughout with what is assumed to be an increase in the number in the peripheral regions and a decrease in the centre. The microscopic interface, therefore was no longer matched to the macroscopically visible interface (Figure 4.16, black arrows).

The decrease in the central region may indicate that the cells are moving out into the matrix available to them and not that they are simply proliferating into the acellular regions. However, it is important to note that these images are taken in a single plane and do not necessarily represent nuclei density throughout the gel.





Figure 4.17: Stitched images of the length of the centre of the gel displaying the nuclei distribution at three points in the culture period and the control at 14 days. Black arrow indicates difference in focus between individual images that are stitched together due to gel surface variability.

#### 4.3.3.1.2 Comparisons of microscopic cellular parameters between segmented gel regions

Based on the presence of cells in the unseeded regions at the end of the culture period, it was then of interest to compare the peripheral regions of both gels. The aim of this thesis was to create discrete regions within a collagen gel with different cell populations. Therefore, the next analysis was to ascertain if the cells in the peripheral (unseeded) regions were responding to their environment differently to those in the central (seeded) regions within segmented gels. The same, standardly published parameters of the immunostained images were compared in Figure 4.18.. The smallest difference was seen in myotube length per frame  $166.7 \pm 4.3$  (cellular) which was less than  $189.2 \pm 6.0$  (acellular). These measurements are, as explained earlier, limited by the microscope frame. A further discussion of the drawbacks of these measurements can be found in Section 4.4.3.

Observable differences were seen in the other measurements where acellular gels were wider on average  $31.8 \pm 6.5 \mu\text{m}$  compared to the cellular gels  $12.56 \pm 0.5 \mu\text{m}$ . However, the error for the acellular gels were also over twelve times larger.

Similarly, the average number of nuclei per myotube per frame was greater for acellular regions  $12.02 \pm 1$  nuclei compared to  $6.5 \pm 0.3$  nuclei in the cell-seeded regions whilst the average number of myotubes per frame was higher in the cellular region  $11.2 \pm 1$  tubes than the  $4.3 \pm 0.7$  tubes acellular.

Interestingly, alignment of myotubes was not found to differ in the two regions. The average absolute deviation from alignment was found to be  $4.3 \pm 0.4^\circ$  cellular region,  $4.4 \pm 0.4^\circ$  in the acellular region (Figure 4.19).

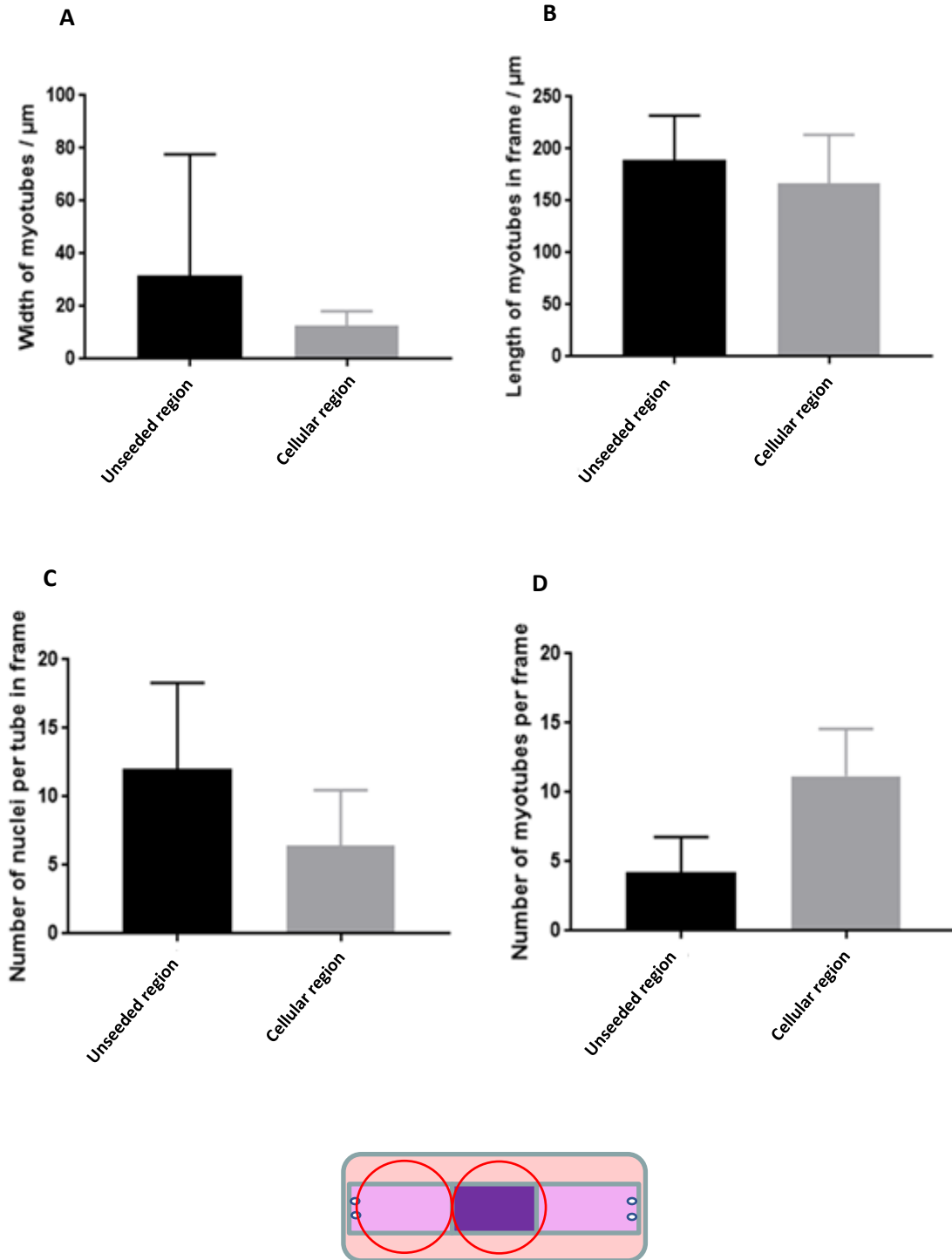


Figure 4.18: Comparison of the acellular region to the cell seeded region in segmented gels. Width of myotubes (A) (C) the number of nuclei per tube (B) the length of myotubes ( $p^{**}=0.0040$ ) while the (D) number of myotubes per frame were significantly. Taken from  $n = 2 \times 2$  repeats. Error bars =  $\pm$  Standard deviation

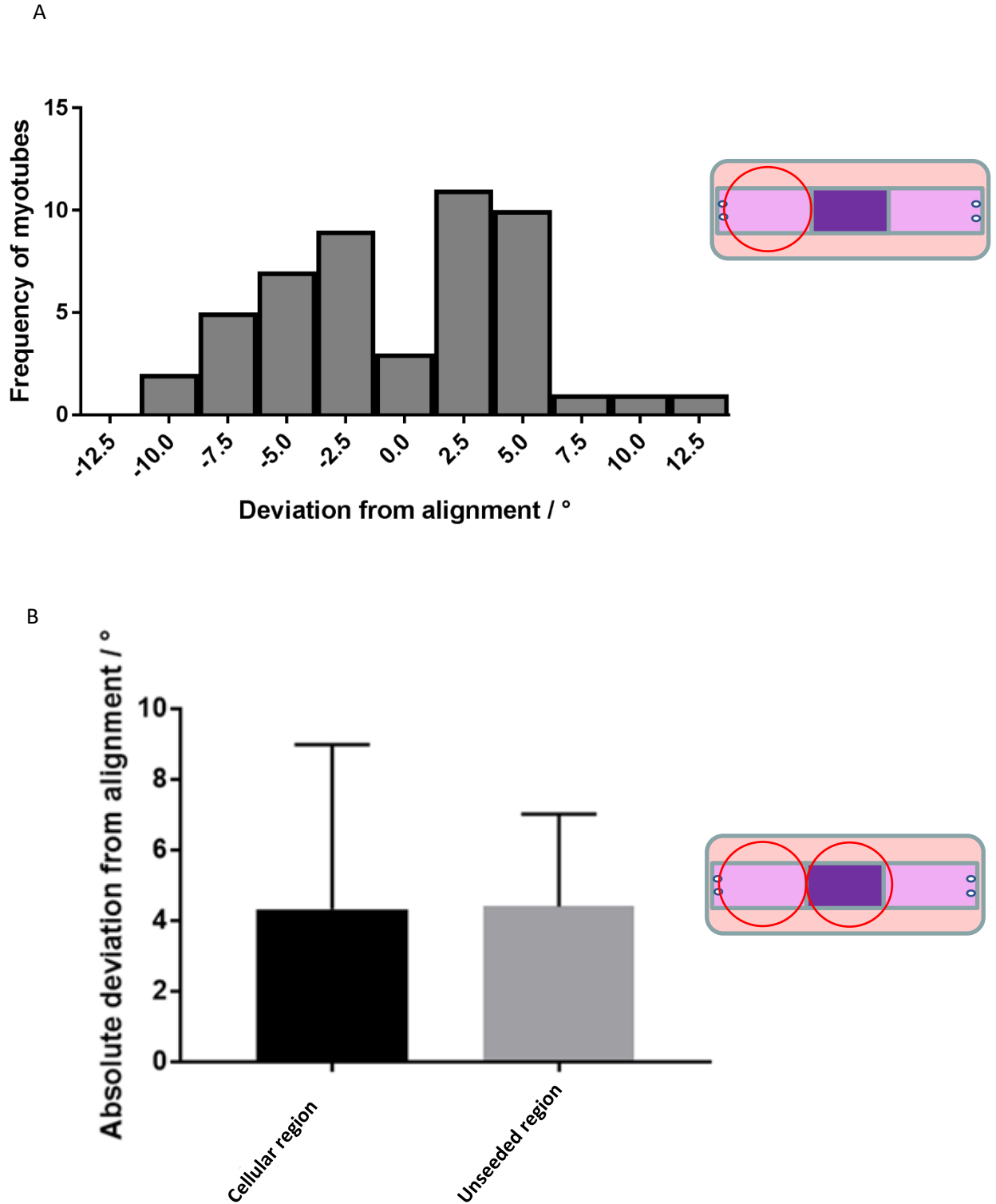


Figure 4.19: Myotube deviation from average frame alignment in the acellular regions of the segmented gels (A), and the comparison of the average deviation in absolute terms to the cellular regions (B). No significant difference was found in deviation from alignment ( $p=0.9102$ )(t-test). Taken from  $n=3 \times 3$  repeats. Error bars =  $\pm$  standard deviation.

Finally, as there were many limitations seen with measure cellular parameters in single-frame images, this measurement method was compared to tile-scans of control gels. Significant differences were seen in myotube length and nuclei per tube even when measuring the same myotubes.

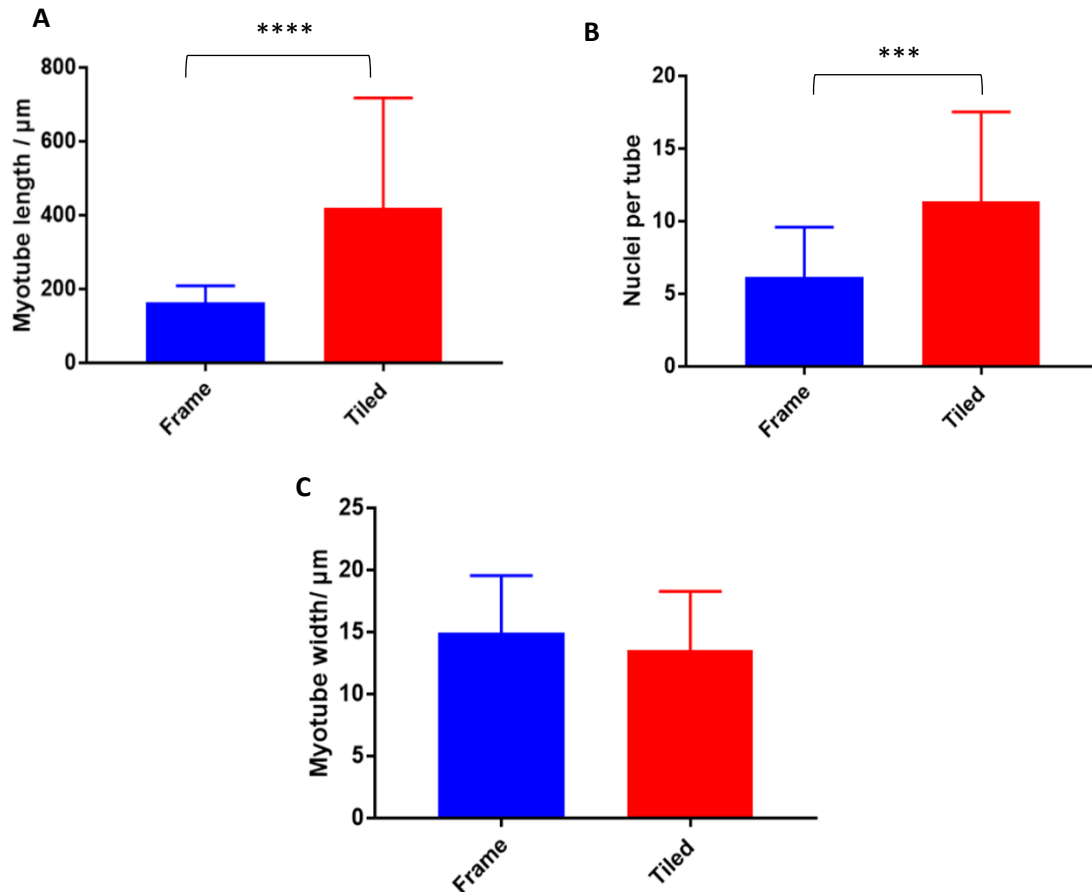


Figure 4.20: Comparison of the standard frame-by-frame analysis of stained images to the tile scan analysis. Tile scans allow for a more meaningful measurement of myotube length(A) ( $p^{****}<0.0001$ ), and therefore number of nuclei per myotube(B) ( $p^{***}=0.0002$ ) (t-test). No difference was seen in myotube width (C). Taken from  $n=3 \times 3$ . Error bars =  $\pm$  Standard deviation

## 4.4 Discussion

### 4.4.1 Gel comparisons

In the previous Chapter, a method was developed through a QbD framework where a gel could be seen to be partitioned into individual Sections. The aim of this Chapter was to ascertain if segmenting a gel would have an impact on the development and success of the cellular components of the model. Therefore, it was paramount to compare the two gel types and assess their differences macroscopically and microscopically.

#### 4.4.1.1 Comparison of the size reduction in gels

As explained in the previous Chapter, contraction of the gel is the primary non-destructive method used to approximately predict whether it is to be successful in producing a fused cellular architecture. The reduction in gel size is a product of the cell-matrix interactions as the cells attach and remodel the matrix, a process the cells undergo before they begin to fuse<sup>112,152,166</sup>. Generally, it is noticed that the centre contracts more than the peripheral regions of a uniformly-seeded gel in standard rectangular configurations and the smaller gels or gel regions become over the culture period, the higher the density of cells and therefore the higher the likelihood larger or more densely distributed myotubes<sup>46</sup>.

Both segmented and control gels were seen to contract more in the first four days compared to the rest of their culture period, this agrees with results previously published<sup>46,152</sup>. The faster size reduction in early culture is likely linked to two factors: Firstly, in order to induce fusion at day 4, the serum content of media is reduced to begin the cell fusion phase in the myoblasts. Secondly, once the cell volume is reduced to a certain extent, the cells are more likely to fuse. This is because cell-cell contact is essential for fusion and the reduction in the size of a gel increases the probability for cells to come in contact with each other. However, the control gels had a much larger decrease in contraction after the initial four days (Figure 4.5). The smaller decrease in volume reduction rate in the segmented gels indicated that there were differences in these parameters between the two gel types. Both sets of gels had equal seeding densities in their cell-seeded regions. Controls were seeded throughout the gel whilst segmented gels were seeded in only the central third of the total gel volume. As seeding densities in seeded regions were equal, cell-cell contact and differentiation should begin simultaneously for both gel types, meaning contraction of the gel should reduce at the same rate. The higher rate of continued volume reduction of the segmented gels indicated that the centrally-seeded cells possibly did not remain localised in that region of the gel. If that were the case, it would suggest that cells were migrating in the gel. As cells were only seeded centrally in the segmented gels, cells distributing themselves across the sample would equate to an evenly-seeded control sample with one-third the seeding density of the controls, which would have a strong reduction on the amount of cell-mediated remodelling as a whole<sup>167</sup>.

To analyse this more closely, the measurements of gel dimensions were studied. As the central regions of both gels were seeded with the same cell density, it was not unexpected that the widths of both gel types were not different. However, it was assumed that then there would be a corresponding difference in total surface area between the two models; if the central regions contracted the same amount in both gels due to the same seeding density, then the overall contraction of the whole segmented gel, it follows, should be diminished as the model contains fewer total cells. The control

gels were found to have a final surface area of  $48 \pm 6$  % of the original, which was a reduction of 52%. As the segmented gels had a third of the number of cells, a linear relationship would anticipate a reduction of 18 %, leading to a total surface area of 82 % at day 14. However, the reduction seen was  $62 \pm 6$  %, a 38 % reduction and over double what would be expected under a linear relationship. Incidentally, this level of reduction is comparable to those seen in standard gels seeded uniformly with primary cells, which generally yield better results than cell lines<sup>119</sup>. Mudera et al. have previously also demonstrated that seeding densities may not have linear relationship with the contraction of a gel and that “optimal” densities exist for specific gel volumes<sup>168</sup>. However, it is key to note that the mechanics of the segmented model is likely to be different if cells migrate across the gel, as there would initially be a greater cell volume in the central region that would then decrease as the cells migrated outwards. Comparisons of equal total gel seeding densities of segmented gels and control gels are an area that could be further studied and may yield new understanding of the mechanics of these systems.

To further investigate this, separate analysis of the peripheral regions alone showed that the reduction in the segmented gels (unseeded regions) was approximately two-thirds of the controls. Considering no gels at all were seeded in these regions, two-thirds of the cell-mediated contractions could be considered high for just the peripheral regions being “pulled in” with the central region contracting. This again suggested that the cells were not remaining in their seeded region in the segmented gels.

In normal, uniformly-seeded gels, the contraction is caused by the cellular interaction with the matrix as they reposition themselves, and *in vivo* muscle regeneration occurs through the migration of satellite cells, it is not then unreasonable to think that the cells in the central region of a gel can migrate across into other regions within a 14-day period. This is likely the reason for why multiple approaches have been taken to make certain regions preferable or viable for a specific single cell type in other experiments attempting a muscle-tendon interface in an effort to keep the cells localised<sup>143</sup>.

No models identical to the segmented model have been published before so it is difficult to compare how far C<sub>2</sub>C<sub>12</sub> myoblasts can migrate from a cellular gel into an acellular gel, although it is known that migration is not unusual in primary cell cultures that may contain more than one cell type<sup>169</sup>.

#### 4.4.1.2 Myotube comparisons

The interest of this experiment was to discover whether the centrally-seeded (muscle) region of the segmented gels performed as the entire gel is expected to in a standard, uniformly-seeded 3D tissue-engineered skeletal muscle collagen model. Therefore, comparisons were made between the seeded central region in a segmented gel and the central region of a standard model (control gel).

As stated by Smith et al.<sup>119</sup>, “function follows form” when relating to skeletal muscle constructs; aligned myotubes allow for the unidirectional functional contraction of the whole muscle construct when tested, recreating the main feature of skeletal muscle<sup>102</sup>. Aligned myotubes are formed as a result of tension in the system, but have also been found to be influenced by the cell density and original surface area of the matrix<sup>46,166</sup>. Alignment is generally seen to be highest in the centre of the construct where the gel contraction is highest<sup>46,119,162</sup>. This pattern was also seen in this experiment. However, as only the centres of these constructs were being compared, it stands to reason that potentially these results may be slightly skewed when compared to those analysing an entire gel, especially as the regions immediately adjacent to anchor points tend to have poor alignment due to stress-shielding “delta-zones”<sup>167</sup>.

The function of *in vivo* muscle is directly related to the size of the fibres and their density within the tissue. Larger myotubes are generally seen *in vivo* than those modelled *in vitro*. Therefore, microscopic measurements are indicative of the potential functionality of the final model and are used as an analogue in tissue engineered models. Both groups of gels had no significant difference in myotube number per frame, length per frame, and number of nuclei per tube per frame. There was a difference observed in the myotube width between the two models, where the control gels were found to be wider. However, the measurement taken for segmented gels of  $13 \pm 1 \mu\text{m}$  was within previously published error margins for tube width. This may potentially have been caused by overall cell density of the gel being lower at the end of the 14-day period if cell migration was occurring. This indicated that there were no observable differences in the central, seeded region of segmented gels and the central region of control gels.

There was, however, an observable difference in the cellular measurements in the peripheral (unseeded) region of the segmented models compared to the central (seeded) regions of the same model and the entirety of control models. Previously published models have shown little variation in cellular architecture within single gels, other than stress-shielded “delta-zones” near anchor points<sup>167</sup>. In contrast to this, the peripheral (unseeded) regions in this experiment showed varied architecture in between samples, varying from regions of very low or no visible cells or fusion to certain highly mature, organised regions. Potentially, this is caused by the fact that the central region has uniform seeding, but the peripheral regions are not in any way controlled in the distribution of cells, causing the distribution to be facilitated completely by where the cells migrate to and fuse. This was the first microscopic evidence that there were cells located in the unseeded regions at the end of the culture period, if they arrived there through migration, this could have showed that the cells that migrate the furthest were either completely unable to fuse-either due to low levels of cell-cell contact, or were highly myogenic. However, no clear correlation of their myogenicity and distance migrated could be



established as there was no way of discerning if the remaining cells had not fused because of low cell-cell contact or low myogenicity.

The final observation from this experiment was that the macroscopic interface created by the dividers and difference in gel seeding in segmented gels was not able to be matched with any microscopic interfaces. Many of the results in both macroscopic and microscopic measurements indicated cell migration, therefore an experiment was conducted to deduce if this was occurring.

#### *4.4.1.3 Cell distribution across the samples during the culture period*

The distribution of cells within the sample throughout the culture period is likely to play a key role in the outcomes of segmented gels. Based on previous studies, it would seem that the seeding density plays the largest role in terms of the outcome of the construct in relation to cell number and any proliferation that may or may not occur does not have a noticeable impact on the system<sup>167,168</sup>. Any variations to this parameter through repositioning of the cells into less densely populated areas is likely to affect the mechanics of the system.

Microscopic analysis of the surface of the gels illustrated that the C<sub>2</sub>C<sub>12</sub> cells begin at a high concentration in the seeded, central region in segmented gels, before being more evenly distributed throughout the model by the end of the culture period. As the earliest time point was 24 hr, it is not determined whether the small number of nuclei visible in the peripheral regions are there from the fabrication stage, where very miniscule differences in the volumes of the gels pipetted into the regions may have led to one region flowing over the top, or whether the removal of the dividers agitated the system enough to cause some mixing. Nevertheless, this experiment demonstrated that the cell distribution over the 14-day culture period changed within samples and provided evidence that cells may be migrating large distances throughout the gel. These results present opportunities for further studying the mechanisms of cell locomotion through collagen hydrogels using this model.

Additionally, these results corroborate with the observations made that the myotubes in the acellular regions were more sporadic and less consistent, but seemed to have been formed through the fusion of more cells and were larger on average than those in the cellular region. Perhaps those cells that are able to migrate further have greater potential to fuse into larger myotubes, this would also be a line of research that could be undertaken using this model.

Whether or not proliferation also played a part in this alteration of the cell distribution, or was the main driver, could not be determined based on these results. Metabolic testing or proliferation assays of the systems would shed some light on this topic.

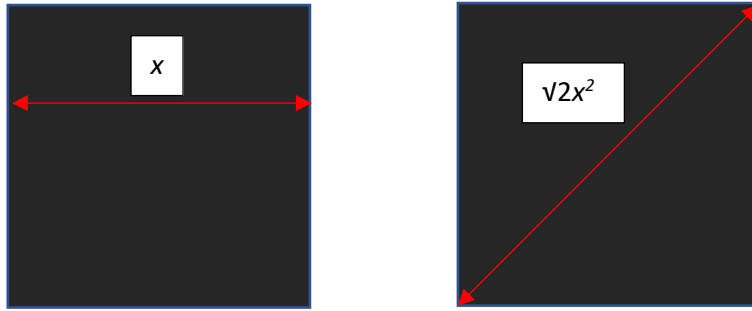
#### 4.4.2 Gene expression

The gene expression at different stages of skeletal muscle constructs have been well documented in the literature previously<sup>119,153,167</sup>. Many genes of interest are routinely analysed for 2D and 3D skeletal muscle models such as myogenin, MyoD and MYH isoforms. When deciding which genes are relevant, it is important to remember the aim of this Chapter. This Chapter was not an evaluation on whether or not the 3D tissue engineered model is a viable model for recapitulation of skeletal muscle, that has been done multiple times elsewhere and those publication analysed whether the genetic expression was found to be representative<sup>111,119,159,167</sup>. The aim here was to take that established and studied model, and try to replicate it in the central region of a segmented gel consistently, allowing space for development into a co-culture system.

No significant difference was observed in the expression of myosin heavy isoforms in either the immature (MYH3) or the mature (MYH1) isoforms between gels, indicating that the segmented gels were not observably different in stages of development. The established model and the segmented gels performed similarly. It is important to note that the entire gels were taken to assess these genetic markers, meaning that it is not exclusively the central regions that were being analysed. It could be the case that the peripheral regions were influencing the outcomes here with either higher or lower of expression of certain markers which could have skewed the results. This may be compounded by the aforementioned distribution of contraction and cell migration. For a better understanding, experiments could be conducted to separate each segment in both gel types to draw more accurate comparisons of genetic expression in gel regions.

#### 4.4.3 Evaluation of current measuring techniques

Current published measuring techniques for these models usually involve measuring what is visible in a single microscope frame. These have been very useful for determining things such as whether long myotubes are formed, how many nuclei they contain, the myotube density visible, and the width of myotubes. Many of these measurements are referred to in arbitrary units<sup>159</sup> due to the limitations of extrapolating data for a whole gel from a single microscope frame. This constrains the results for a number of reasons. Firstly, the orientation of the cells in the frame can then have an impact on the measurements. For example, in Figure 4.21A, in a perfectly square frame, tubes that are aligned parallel to the top and bottom edges will be measured as shorter than those that are orientated at a closer to 45° angle due to Pythagoras' theorem, even if this is not representative of the reality.



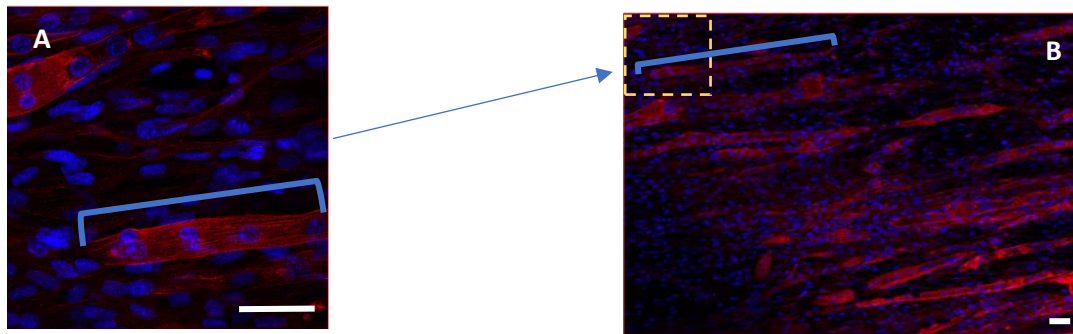
*Figure 4.21: Measuring different orientations of myotubes in a limited frame size can have an impact on measurements even if they are the same length. Myotubes aligned with the edges of the frame are more limited in their measurement than those at an angle.*

Secondly, on a similar note, as the tubes cannot fit into the frame, the amount of each tube that is measured is completely undetermined, meaning that the 200  $\mu\text{m}$  measurement that does not fit into the frame could be from a myotube of any greater length, therefore not discriminating between myotubes being only slightly larger than the frame, or double the size. An example of this can be seen in Figure 4.22. Due to advances in technology and its accessibility, it is perhaps better to take tiled scans of as large of an area of the gel as possible on confocal microscopes (Figure 4.22B) to get more accurate representations of cellular architecture and therefore put definitive units on these measurements. Comparison of the two methods, showed that a more accurate measure of the architecture can be found through the measurement using a tiled scan. This is because the entire length of a myotube is visible, giving the measurement and removing the chance of it being counted twice. Additionally, alignment is likely to be better measured this way as the error is removed from having to average the angles of myotubes in each frame. The alignment can be looked at as an average of the whole system, or entire areas can be chosen for analysis. An example of the impact this can have can be seen in the comparative results of the two measuring methods.

For comparative purposes to published literature, single frame analysis gives enough information by analysing whether myotubes are fusing, their width and if they are long enough to span across a large part of the frame. But now that the capabilities are there, more accurate analysis of the entire model can be conducted instead of taking small representative measurement samples in future projects.

Confocal microscopy would also allow overcoming the other current limitation of microscopic techniques; all measurements are done in a single focal plane. Due to the nature of a 3D tissue, much of the light required for imaging through the gel is blocked by the matrix, this is an important reason for using confocal microscopes to take images in 3D samples. Additionally, they can be used to create a 3-dimensional stack, termed a 'z-stack' to create a virtual model of the entire gel. For large gels this is time consuming but as the model decreases in size to become more resource-efficient, it will be

more manageable to create z-stacks for all gels in their entirety and get a complete picture of their structure for analysis.



*Figure 4.22: Comparison of the standard measurement in a single frame (A) and the measurement of a fused myotube in a tile scan (B). The former would give a 162  $\mu\text{m}$  measurement while the tile scan would give a more accurate measurement of 530  $\mu\text{m}$ .*

## 4.5 Conclusions

In this Chapter, the experiments comparing fully seeded collagen gels with centrally-seeded (segmented) gels indicate that the cellular part of the new segmented gels result in morphologically and genetically similar system to that of the central part of the standard collagen skeletal muscle model. This suggests that the central “muscle” region is unaffected in terms of cellular mechanics by being fabricated in between two unseeded (acellular) segments. This in turn, indicates that the segmented model can lend itself to being a skeletal muscle model with other cell types in the periphery, giving opportunity for a co-culture interface model.

The experiments in this Chapter also suggest that the cells seeded in the centre of segmented gels are able to migrate across the interfaces with a range of many millimetres to then continue culture in the unseeded regions. Analysis of peripheral regions suggest that these migrating cells result in either very highly developed myotubes, or completely unfused cells, presumably because of the inconsistency of the cell-cell contact in the peripheral regions. If this is the case, in essence, by day 14 the model effectively becomes a less dense standard gel with a very well-developed centre and undeveloped peripheral regions with some sparse mature myotubes. This does not detract from the central region, but does present an issue for modelling interfaces using this method, as this could mean that interfaces created through segmentation do not keep cell populations localised. Further experiments of interest would involve introducing cells into the peripheral regions to see whether both cell types remain within their regions.

Finally, it was noted that the current standard “per frame” measure immunostained hydrogels shows unrepresentative quantifications, and suggested that expanding to tile scans of gels may overcome this drawback.

## 5 Developing the segmented system by incorporating a “tendon” region to create a tendon-muscle-tendon construct

As the muscle regions in segmented gels were found to have similar outcomes to those in standard skeletal muscle constructs, it was key to attempt to seed the peripheral regions with different cell types with the intention of creating a muscle-tendon interface and thereby a model of the tissue interface. The different cell types could then be analysed to understand their interaction and whether or not they are physiologically representative.

### 5.1 Introduction

In the previous Chapter, the newly adapted segmented method for creating multiple gel types in a single model was compared to the standard, published method of creating a 3D tissue engineered skeletal muscle collagen model. The results concluded that all microscopic parameters pertaining to myotubes were the same in both models, except for myotube width which was still within published ranges. This led to the conclusion that including a central “muscle” region in a segmented gel does not change the desired properties for which these models are generally made. The next step in the development to meet the aims of this thesis was to take this central muscle region and attempt to combine it with an adjacent cellular region by seeding cells into the peripheral regions that were previously unseeded. The previously discovered myoblast migration may then be limited by another cell population occupying the space through greater numbers of cell-cell contact through saturation of the matrix.

In order to achieve this, a model of tendon would be needed to combine to the aforementioned skeletal muscle model. Tendon tissue models are widely researched due to the prevalence of injuries in both athletes and the general population and their notoriously limited regenerative ability due to low cell number and vascularity of the tissue<sup>145</sup>. Most injuries that occur in the tendon tissues are in the interfaces due to stress concentration in these regions from a transition in tissue dimensions and mechanical properties between tissue types. The natural regenerative process usually replaces the injured tendon with less functional scar tissue meaning that surgical suturing or grafts are often required for more adequate repair or more severe injuries, leading to a less functional repaired tissue and donor site morbidity<sup>144,170</sup>. For this reason, the majority of tendon research has been done with the intent to repair damaged tendon as part of the entire tissue system within physiological conditions<sup>120,163</sup>. This is in slight contrast to skeletal muscle, which has a good blood supply, is densely cellular as a tissue and is a very rare site for serious injury to occur, with excellent regenerative

capabilities for non-severe injuries, therefore the research is more focussed on *in vitro* models due to the less pressing demand in clinical applications<sup>87,94,115</sup>.

Many animal models are used for tissue-engineered tendon repair<sup>78,124,144</sup>. Much like skeletal muscle, this is generally achieved using a scaffold or a matrix with a cell type seeded onto it. Due to the similarity in structure, tendons and ligaments in tissue engineering are addressed together<sup>83,171</sup>. Primary models using human tendon cells are avoided due to donor site morbidity caused by the aforementioned regenerative limitations of the tissue<sup>172</sup>. The main matrix component of tendon *in vivo* is collagen<sup>145</sup>, much like skeletal muscle and is therefore very suitable for creating a segmented tissue using the same matrix for both tissue types, although as stated before, both tissue types have multiple materials used as the ECM in *in vitro* models. Many other features are shared between the two, including the hierarchical nature of the substructure and 3D models being more representative of the spatial organisation of the system<sup>145</sup> giving further reason for why the two would work concurrently in a model such as the one developed in this thesis. Additionally, it is postulated that muscle and tendon require interactions between the two cell types for correct development for tendon<sup>122</sup> while the reciprocal was also postulated for the development of muscle<sup>46</sup>.

Although predominantly acellular, especially when compared to the other tissues in the system, tendon tissue does have a cellular component. The primary cell type that exists in tendon is not fully characterised, it is thought to be a type of fibroblast named a tenocyte, although the specific markers separating this from other fibroblasts is not commonly agreed upon<sup>145</sup>. Whilst there is a very low number of cells compared to other tissues, the main role of these tendon cells is the maintenance of the ECM<sup>110,173</sup>. Nonetheless the best cell source for engineered tendons has been researched and multiple cell types have been used to model tendons including muscle-derived cells, mesenchymal stem cells and fibroblasts being the most researched due to their similarity to tenocytes<sup>174</sup>. It is important to note that even the sizes and shapes vary between specific tendons<sup>18</sup> and therefore success criteria for each specific tissue-engineered tendon may be different.

Looking at the scope of this thesis, a high-throughput testing system would need easily accessible cell types. From the above cells, fibroblasts have commonly been studied because of the efficiency with which they can be extracted without causing secondary donor site morbidity and the ease with which they can be expanded<sup>122</sup>. This makes them an ideal candidate cell type for this Chapter.

Beyond tissue engineering of single tissue-types, a small number of attempts to make a muscle-tendon unit *in vitro* model from scratch have been made<sup>54,164</sup>. Most recently, Merceron et al.<sup>143</sup> used a 3D integrated organ printing system which laid down a layer of polyurethane coprinted with a layer of C<sub>2</sub>C<sub>12</sub> in one region with poly  $\epsilon$ -caprolactone and 3T3 on the other, with a transition in the middle of

the two. The two materials had different properties, ensuring the model was elastic on the muscle side and stiff on the tendon side to overcome the difficulty in spatially distributing the cell types and keeping them in their specific region for the culture period. This also provided optimal properties for culturing the specific cell type.

Therefore, the aim of this Chapter is to compare uniformly-seeded skeletal muscle constructs and fibroblast tendon constructs to segmented gels with acellular peripheral regions, and also segmented gels with fibroblast-seeded peripheral regions.

## 5.2 Materials and methods

### 5.2.1 Cell culture

C<sub>2</sub>C<sub>12</sub> murine myoblasts and human dermal fibroblasts (hDFs) were cultured and seeded into collagen hydrogels as described in Chapter 2, Section 2.1 and Section 2.3 respectively as described.

### 5.2.2 Gel fabrication

Gels were fabricated set using the method developed previously in Chapter 3 and outlined in Chapter 4, Section 4.2.2. These were adapted to the configurations below (Figure 5.1), both cell types were seeded in the gels at a concentration of  $4 \times 10^6$  cells/ml of gel to maintain consistency in comparisons between samples and experiments. These were then cultured in normal skeletal muscle culture conditions as described in Chapter 2, Section 2.9 with 4 days in GM and 10 days in DM.

In addition to the C<sub>2</sub>C<sub>12</sub> (muscle) controls and the hDF (tendon) controls, the segmented gels were also used as a control for the peripheral regions as the behaviour of cells and therefore the microscopic and macroscopic results in centrally-seeded gels were different to that of uniformly-seeded gels, as demonstrated in the previous Chapter.



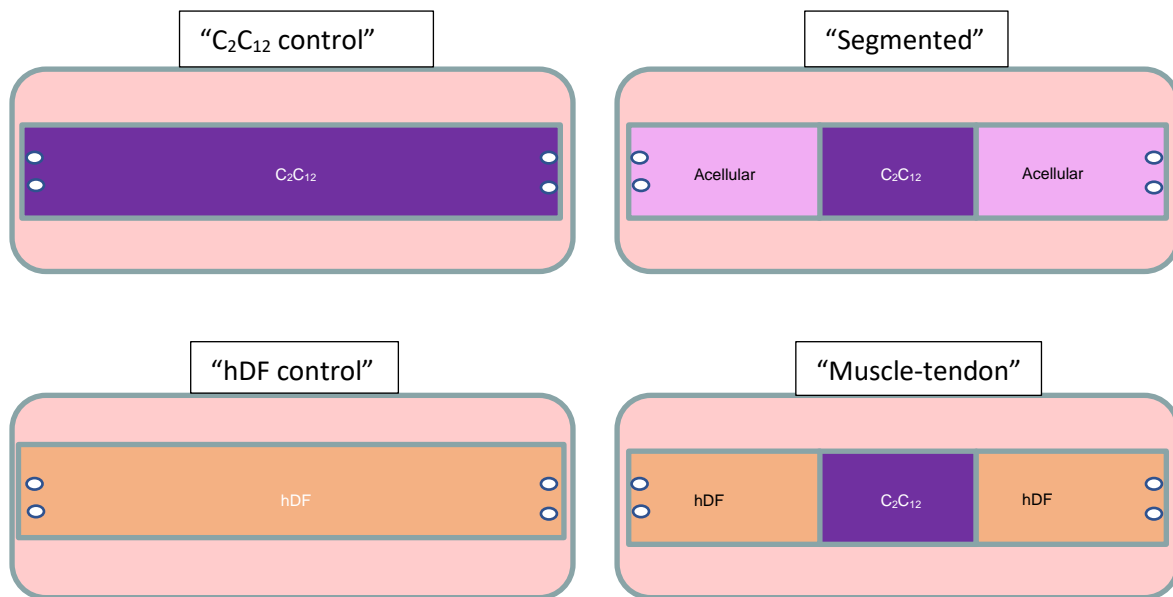


Figure 5.1: Schematics of all the experimental models that were tested in this Chapter in regards to the seeding of each region of the gel.

### 5.2.3 Gel survival rate

Gel survival rate was calculated as described in Chapter 2, Section 2.9.

### 5.2.4 Immunostaining of gels and microscopy

Gels were immunostained as described in Chapter 2, Section 2.11 with the addition of desmin staining with the intention of differentiating between desmin positive (muscle) cells and fibroblasts as described in Chapter 2, Section 2.11.2. Confocal microscopy was conducted as in Section 2.11.

## 5.3 Results

### 5.3.1 Gel survival rate

Of the gels made, the success rate for an unbroken gel that made it through the entire culture period was measured. The survival rate was found to be 87.5% minimum ( $C_2C_{12}$  controls) and higher for all other gels. A large improvement from the initial model and in line with the previous Chapter's results (Figure 5.2).

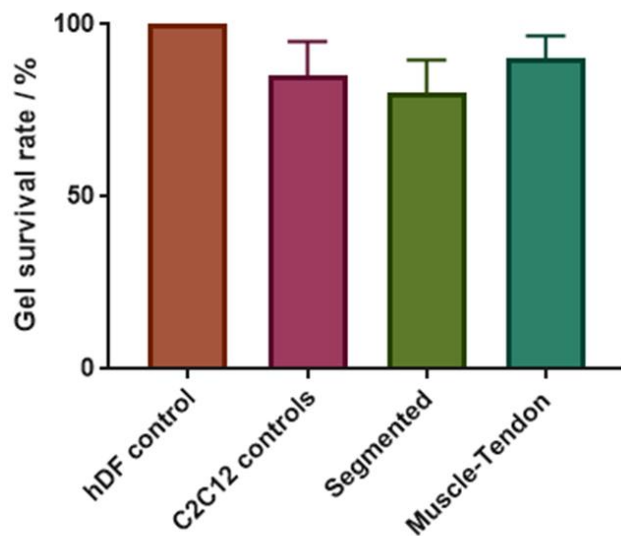


Figure 5.2: Comparison of the number of the percentage of gels attempted that make it through the entire culture period. Taken from  $n=3 \times 3$  repeats. Error bars =  $\pm$  Standard deviation.

### 5.3.2 Gel contraction

#### 5.3.2.1 Macroscopic imaging

The macroscopic decrease in gel size over the culture period was again measured at key intervals to understand the level of cell-mediated remodelling of the gel. The gels all contracted over the 14-day period in a similar fashion to previous experiments as can be seen in Figure 5.3. These gels were measured at each time point to find if there were any differences in the behaviour of the cells depending on cell type and location within the gel.

In the peripheral regions, all gels except for the segmented controls decreased to below 50% of initial surface area with no significant differences between them, this indicated that the muscle-tendon models were macroscopically behaving similarly to the standard C<sub>2</sub>C<sub>12</sub> system, as were the hDF (tendon) controls (Figure 5.4A). The segmented system only decreased to  $70.8 \pm 6\%$  of original surface area which is approximately half of the decrease of the other models.

At 14 days, no observable difference was seen in the contraction of the central region of any of the gels (Figure 5.4). All gels but the segmented controls contracted to below 50% of original total surface area. The segmented controls decreased to  $55.4 \pm 3\%$  which agrees with the previous Chapter while enforcing the previous point further (Figure 5.5A). The width at the centre was found to be below 40% of original width for all gels at day 14 and there were no observable differences between them (Figure 5.5B).

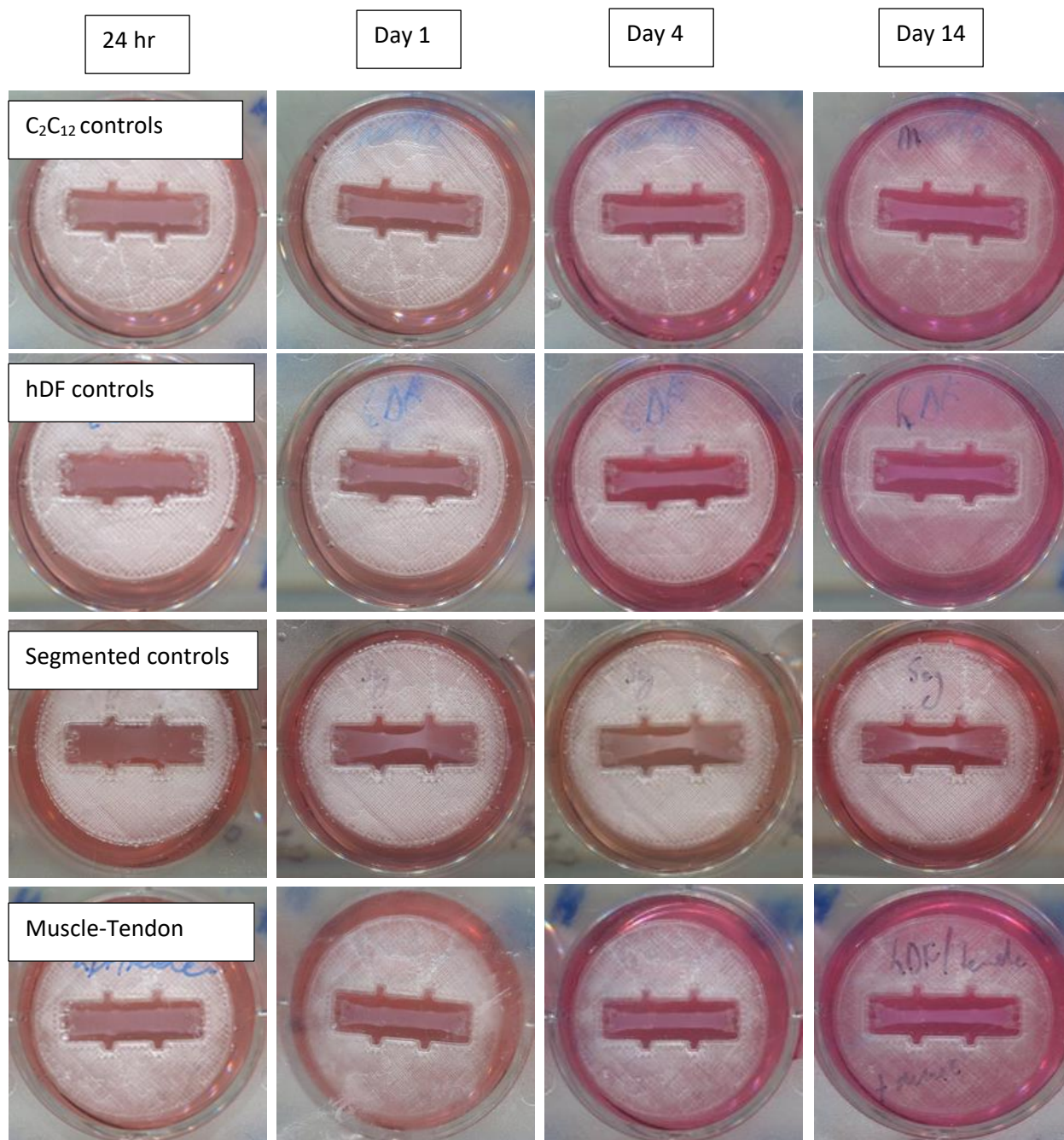


Figure 5.3: Images of gel types at each macroscopic measurement time point. Image shows n=1.

5.3.2.2 Gel contraction comparisons

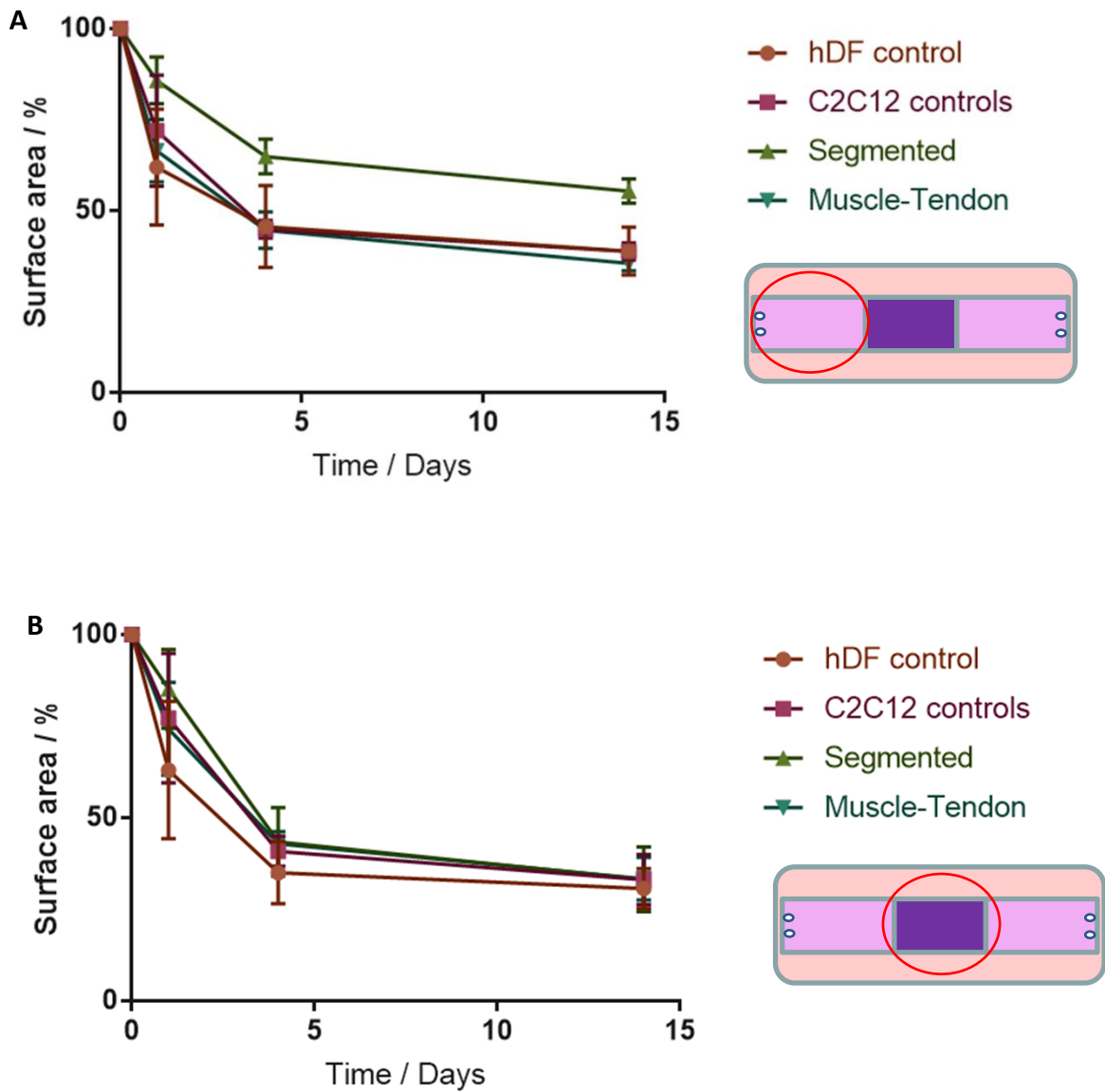


Figure 5.4: Comparisons of contraction in peripheral regions (A) and central regions (B) of the gels. Taken from  $n=2 \times 3$  repeats. Error bars =  $\pm$  Standard deviation

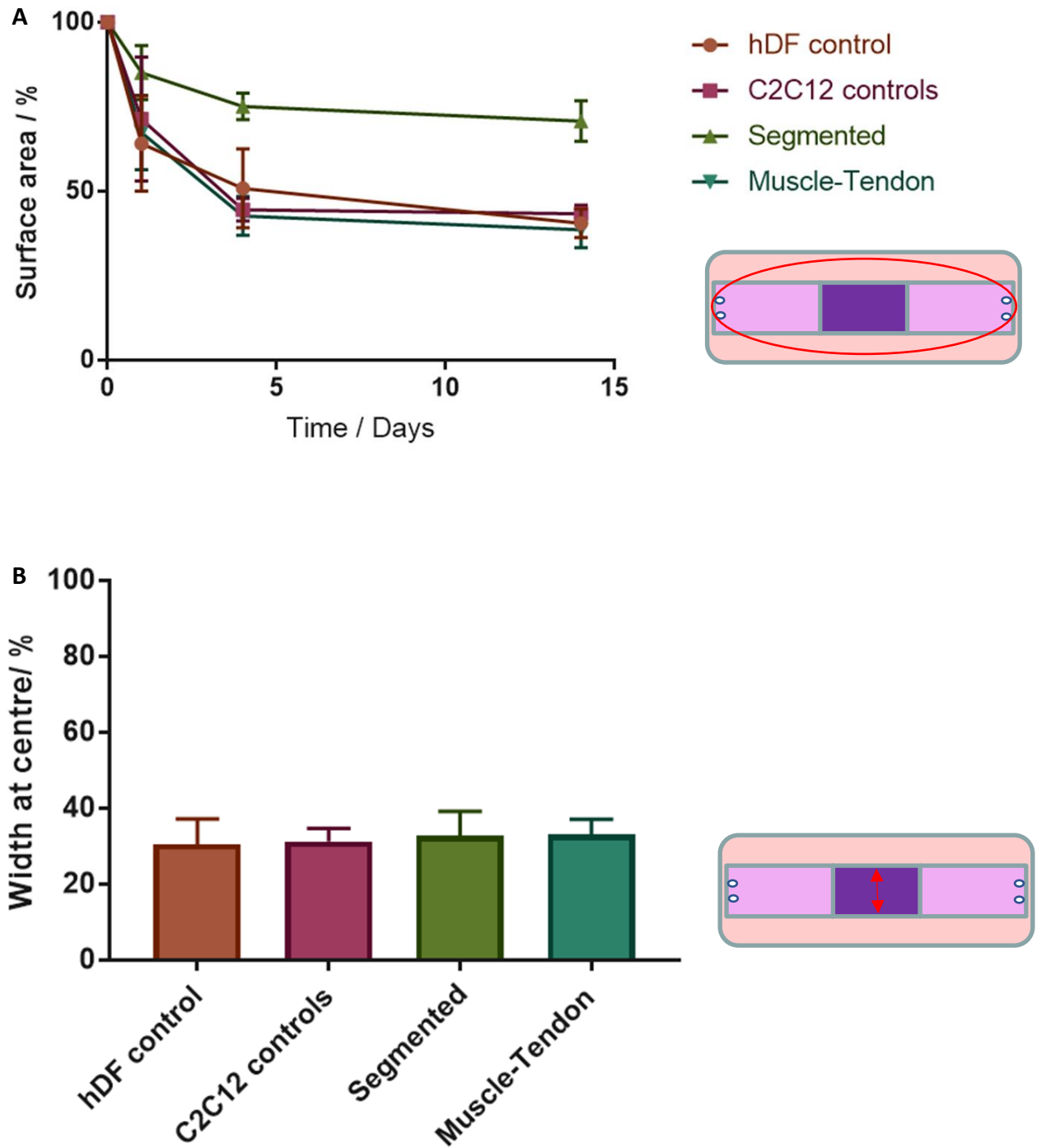


Figure 5.5 Comparisons of total gel surface area reduction (A), and final width in the central region at 14 days (B). Taken from  $n=2 \times 3$  repeats. Error bars =  $\pm$  Standard deviation.

### 5.3.3 Microscopic analysis of cellular regions

#### 5.3.3.1 Comparison of uniformly-seeded control gels

Control gels for both C<sub>2</sub>C<sub>12</sub> and hDFs were first looked at to ascertain the morphologies of the two cell types in these models. Figure 5.6 shows that a clear difference can be seen between the multinucleated, fused myotubes (A) and the spindle shape fibroblasts that are in contact in a 3D network (B). It should be noted that the desmin resulted in non-specific binding as can be seen in the image (B).

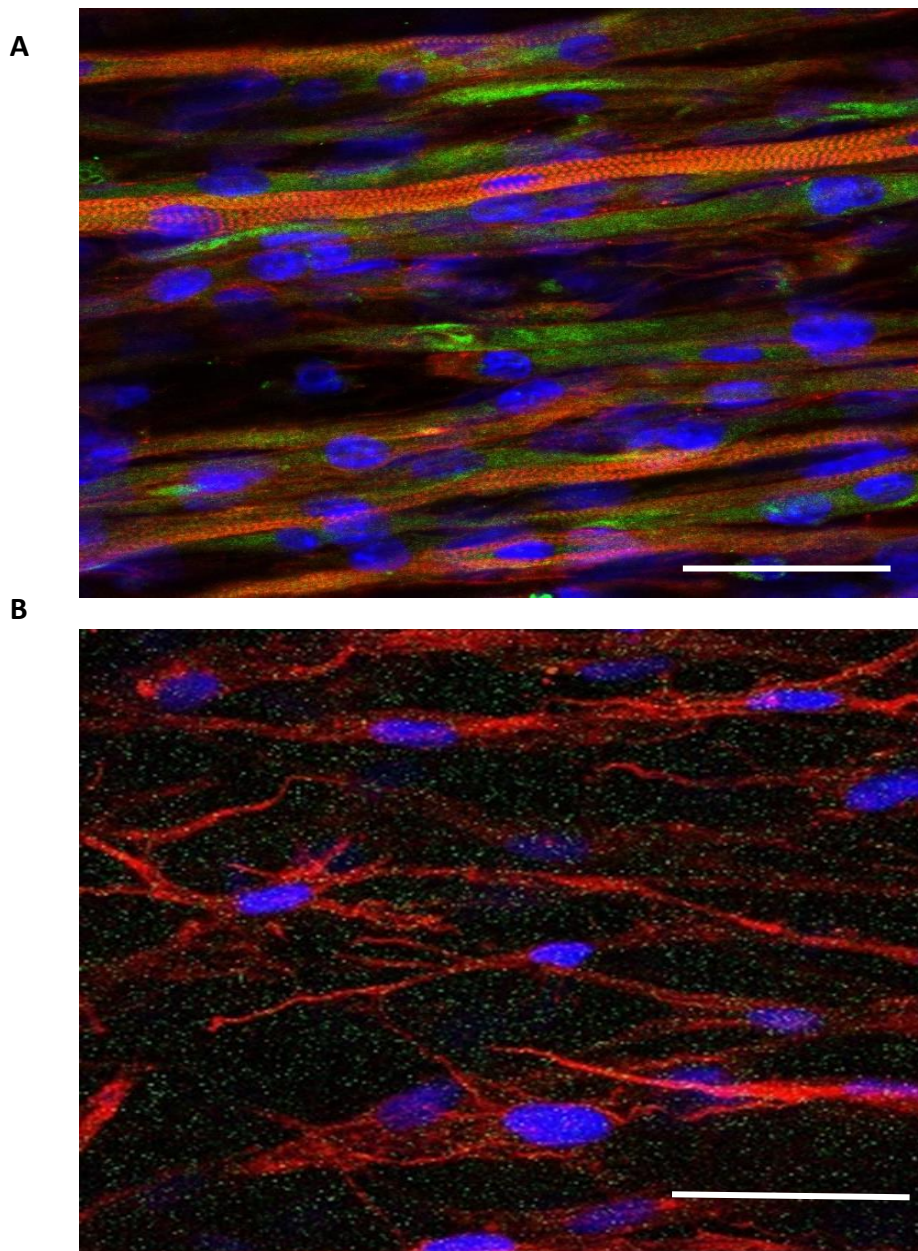


Figure 5.6: Examples of control gels for C<sub>2</sub>C<sub>12</sub> cells (A) and hDF (B). These can be seen to have very different morphologies. Actin filaments were stained with phalloidin (red) for actin filaments, desmin (green) to identify muscle-specific proteins and nuclei were stained with DAPI (blue) Scale bar = 50 μm.

### 5.3.3.2 Analysis of cellular architecture in muscle-tendon gels

The central and peripheral regions in muscle-tendon models were individually examined, showing the difference between the morphologies of the cells. It should be noted that desmin was visible in both types of cells, it was also seen in very few of the hDF controls (Figure 5.7), therefore desmin does not necessarily act as the indicator that it was intended to be used as to identify the location of myoblasts.

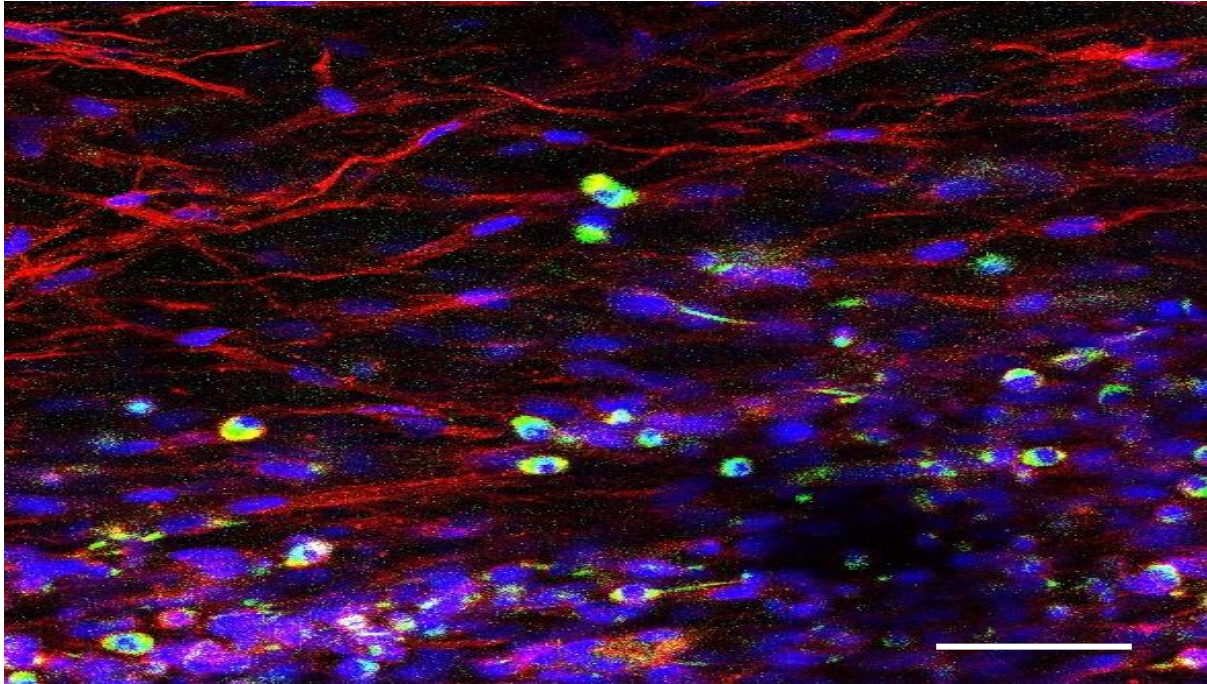


Figure 5.7: Example of hDF-only control demonstrating desmin positivity in some regions. Actin filaments were stained with phalloidin for actin filaments (red), desmin for muscle-specific protein (green) and nuclei were stained with DAPI (blue). Scale bar= 50  $\mu$ m.

Cells in the central region of the gels (Figure 5.8 left) had visibly fused multinucleated, aligned cells whereas the peripheral region (Figure 5.8B), whilst still somewhat aligned, were morphologically different. Where these two cell types transition could be seen in Figure 5.9. Areas of thick myotubes come to a halt where non-fused cells begin to be more commonly seen. These are the interfaces between the two engineered tissue models, but interestingly, they were found to be in a different location to where the visible interfaces were created when the gels were fabricated similarly to the results seen in previous Chapters.

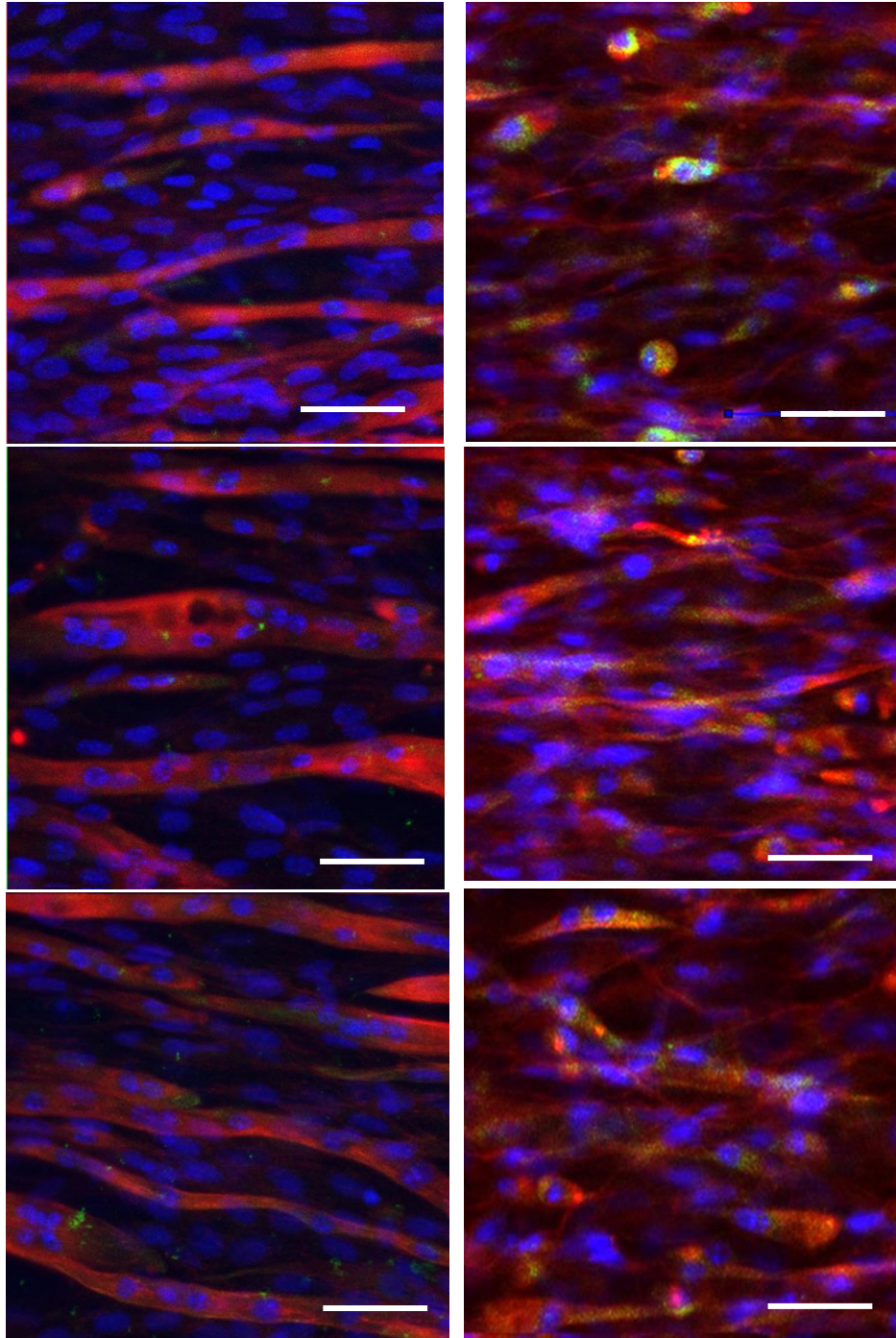
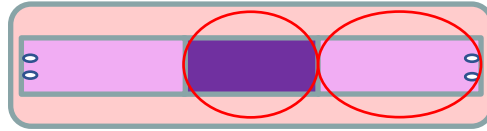


Figure 5.8: Examples of central regions in the Muscle-Tendon model (left) and the peripheral region (right). Myotubes can be seen in the central region and are absent in the peripheral regions, where only unfused cells are visible. Actin filaments were stained with phalloidin for actin filaments (red), desmin for muscle-specific protein (green) and nuclei were stained with DAPI (blue). Scale bar= 50  $\mu\text{m}$ .



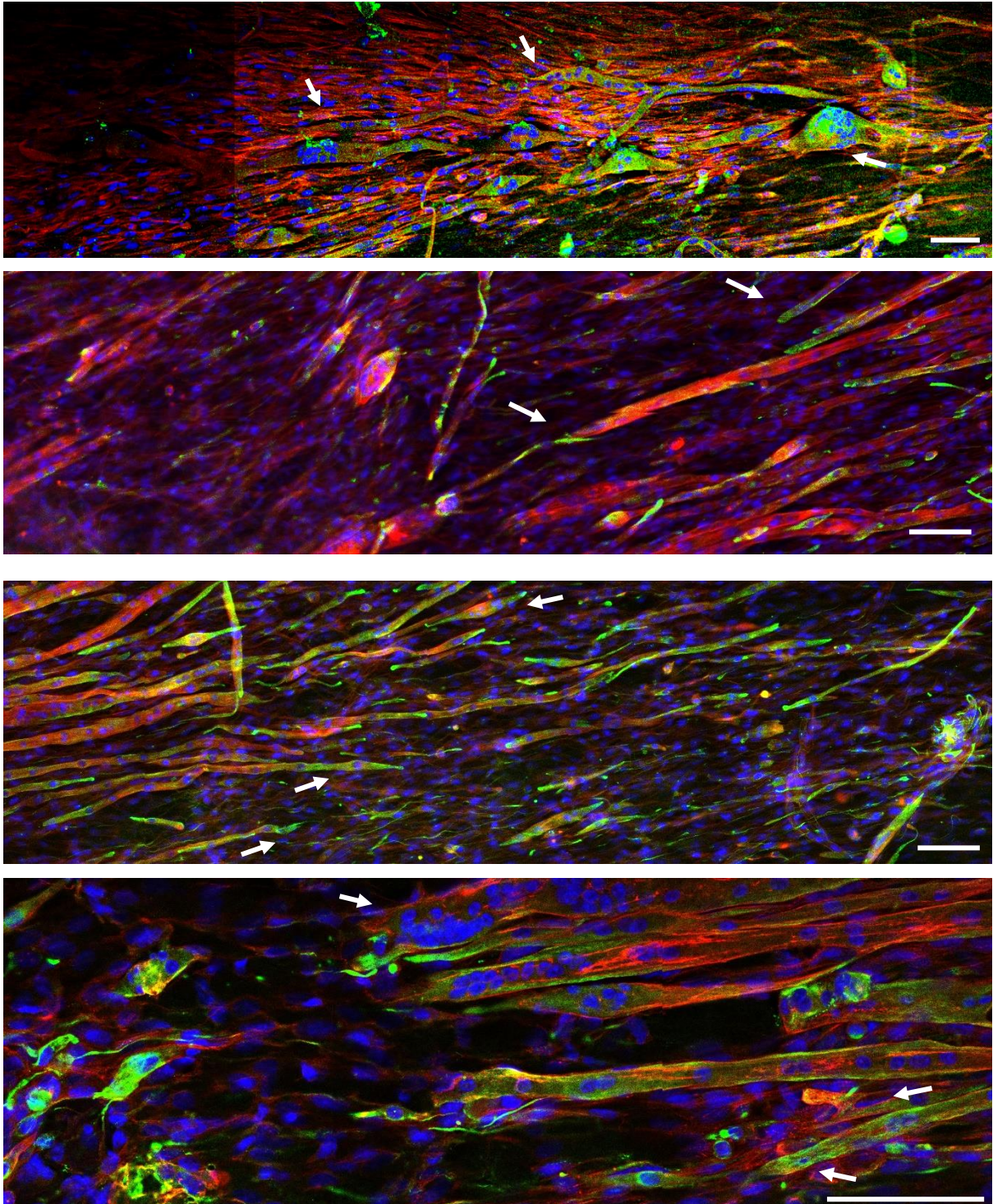
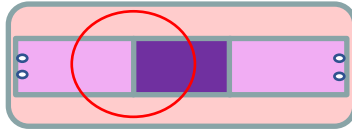
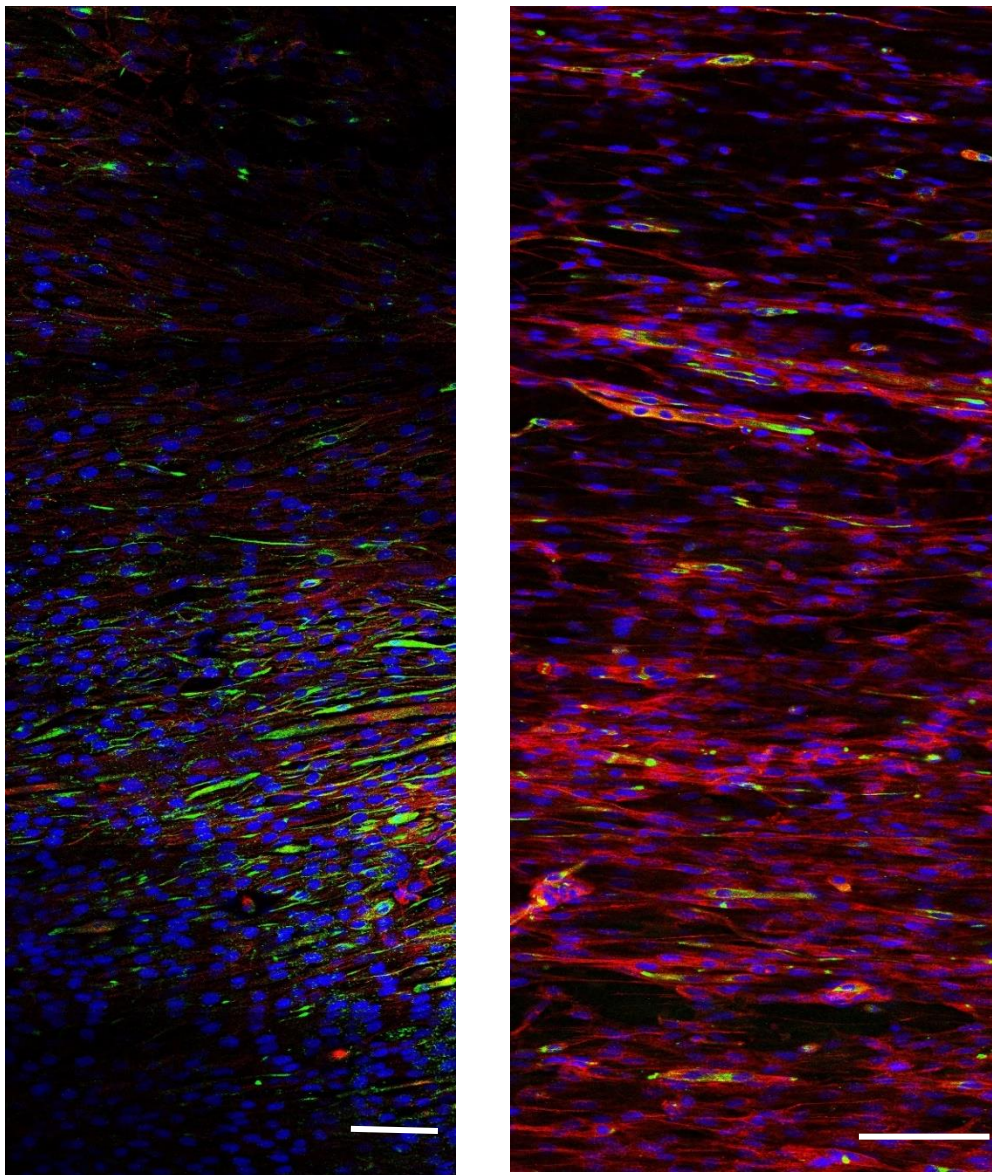


Figure 5.9: Examples of images of cellular interfaces in muscle-tendon gels. These differed from the visible interface that is created in the gel fabrication in terms of position, nonetheless they were seen to be present in a small number of samples. Scale bar = 100  $\mu\text{m}$ . White arrows indicate examples of how myotubes transition into areas of unfused cells. Actin filaments were stained with phalloidin for actin filaments (red), desmin for muscle-specific protein (green) and nuclei were stained with DAPI (blue).

However, not all gels exhibited the clear differences in cell types (Figure 5.10). In fact, the majority of gels showed a mixture of cell types in all regions, where it was not easily discernible which cell type was present. This, in part was due to the presence in desmin detected in regions of the hDF controls, preventing the identification of muscle and fibroblast cells. This could be overcome somewhat with an identification of the morphology of each cell type in these models, however it is a sub-optimal method of identifying the two, especially when cell types are distributed homogeneously throughout the gel by the end of the culture period. Nonetheless, the immunostained confocal images indicated that the segmentation did not work in the majority of the samples.



*Figure 5.10: Many gels showed no clear difference between two cell regions throughout the entirety of the gel. Many looked homogeneously mixed throughout. Actin filaments were stained with phalloidin for actin filaments (red), desmin for muscle-specific protein (green) and nuclei were stained with DAPI (blue). Scale bars = 100  $\mu$ m*

### 5.3.4 Myotube comparisons in central regions

The myotube data between the central regions of the gel types containing C<sub>2</sub>C<sub>12</sub>s were then compared to see if there was any difference caused by the introduction of a second cell type. An observable difference was seen in myotube length (Figure 5.11A), where the muscle-tendon model was  $167.8 \pm 45 \mu\text{m}$  against the  $189.8 \pm 37 \mu\text{m}$  for the C<sub>2</sub>C<sub>12</sub> controls. However, as mentioned in previous Chapters, this was measured per visible frame and therefore not necessarily indicative of an effect of construct type. No difference was seen in myotube width (Figure 5.11B) where the measurements were  $13.4 \pm 6 \mu\text{m}$ ,  $13 \pm 5 \mu\text{m}$  and  $14.7 \pm 5 \mu\text{m}$  for the muscle-tendon, C<sub>2</sub>C<sub>12</sub> control and segmented control respectively.

Observable differences were seen in number of nuclei per tube per frame between all three of the muscle-tendon, C<sub>2</sub>C<sub>12</sub> controls, segmented controls and the models (Figure 5.12A) the means of which were  $7.14 \pm 3$ ,  $5.57 \pm 2$ ,  $9.9 \pm 4$  nuclei respectively. While myotubes per frame were not affected by gel type at  $6.44 \pm 1$ ,  $6.89 \pm 2$  and  $7.89 \pm 2$  myotubes respectively (Figure 5.12B).

Figure 5.13 and Figure 5.14 show the distribution of the individual myotube angles in relation to the mean of the frame they were measured in. Figure 5.14B summarises these distributions by showing the absolute deviation of the myotubes in each model. Absolute measurements were used as averages of measurements could hide deviations by deviating either side of zero equally. Observable differences could be seen between controls at  $2.6 \pm 3^\circ$  and the other gels, with segmented at  $3.8 \pm 3^\circ$  and muscle-tendon at  $4.4 \pm 3^\circ$ .

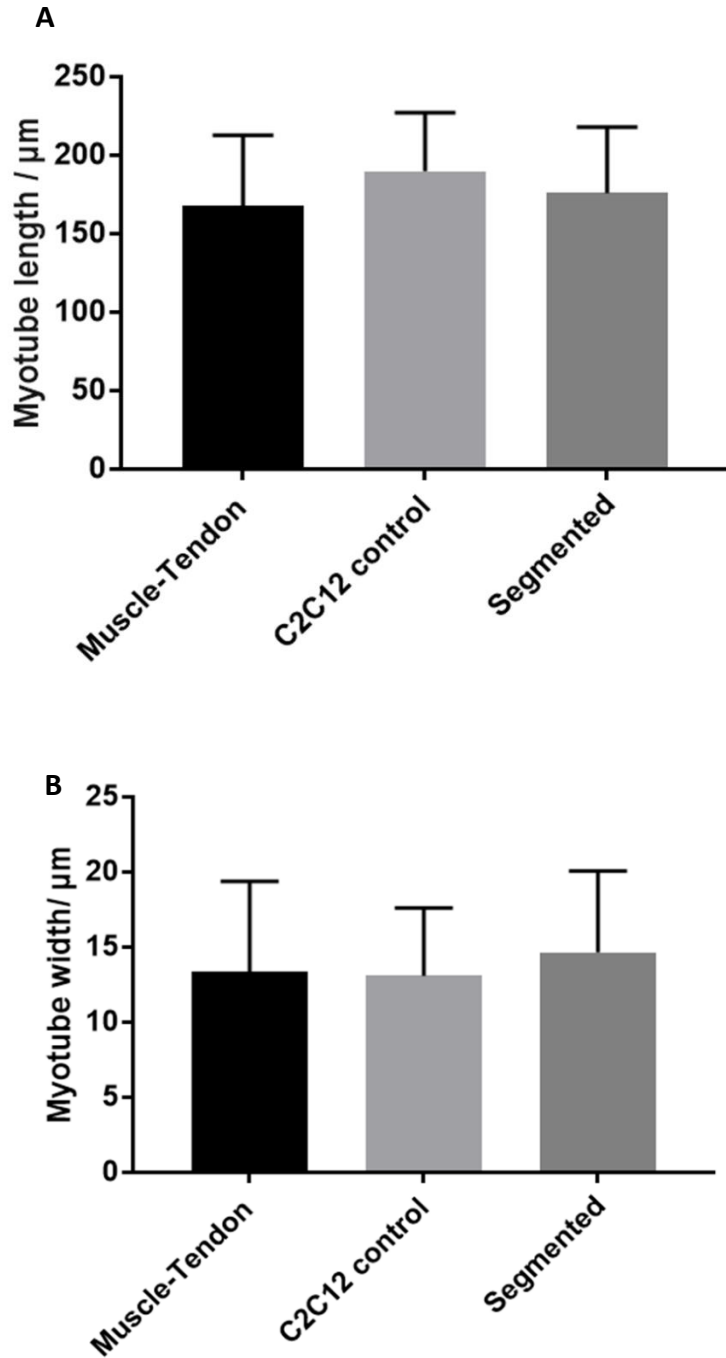


Figure 5.11: Comparison of myotube length and width between the muscle-tendon, C<sub>2</sub>C<sub>12</sub> controls and segmented controls. Muscle-tendon was shorter than C<sub>2</sub>C<sub>12</sub> control. As explained, these measurements are limited by frame size, therefore a slight difference does not necessarily indicate a large difference in the outcomes of these gels. No differences were seen in the myotube width between all models. Taken from n=2 x 2 repeats. Error bars =  $\pm$  Standard deviation

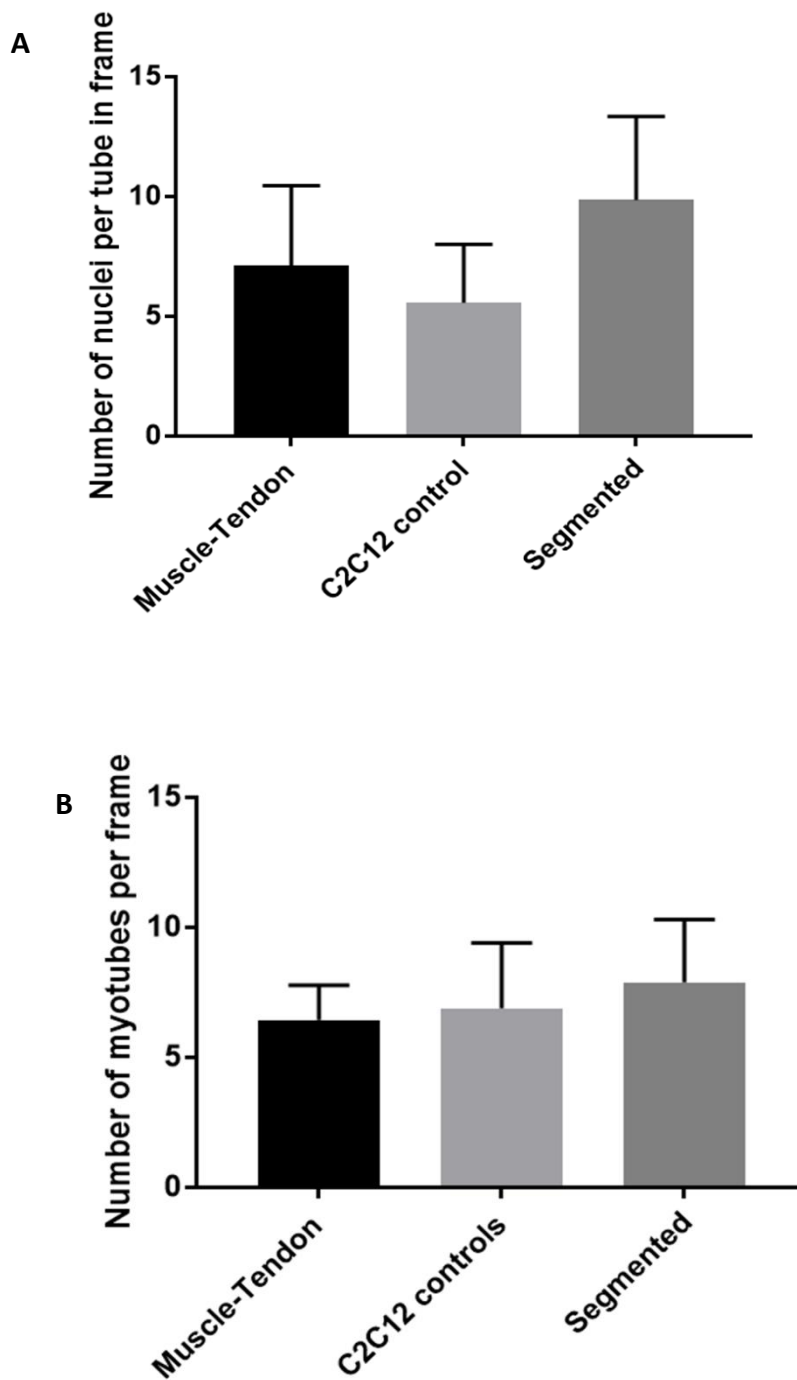
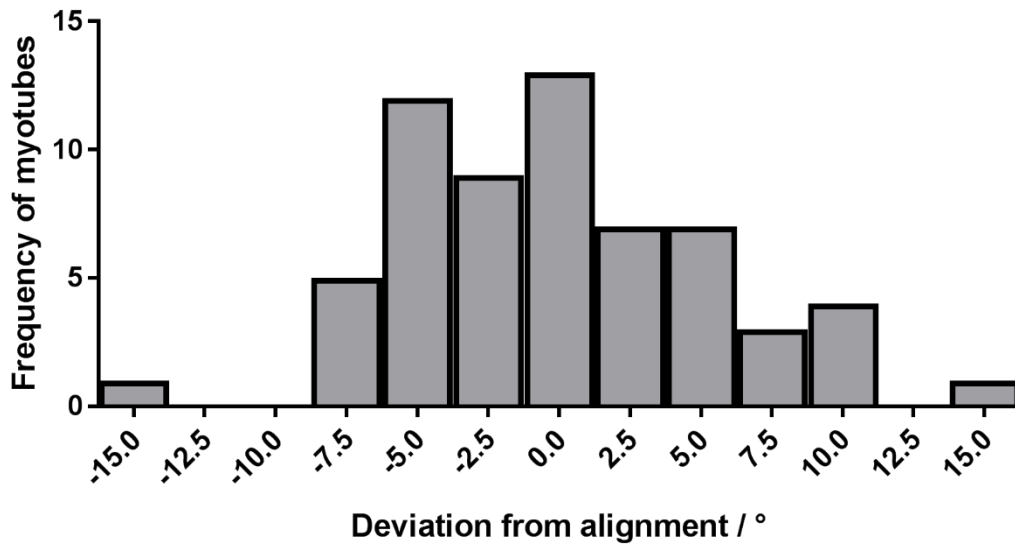


Figure 5.12: Comparison of microscopic parameters between the muscle-tendon, C2C12 controls and segmented controls. (A) Number of nuclei were different between all models. (B) Small observable differences were also seen in number of myotubes per frame. Taken from  $n=2 \times 2$  repeats. Error bars  $\pm$  Standard deviation

A



B

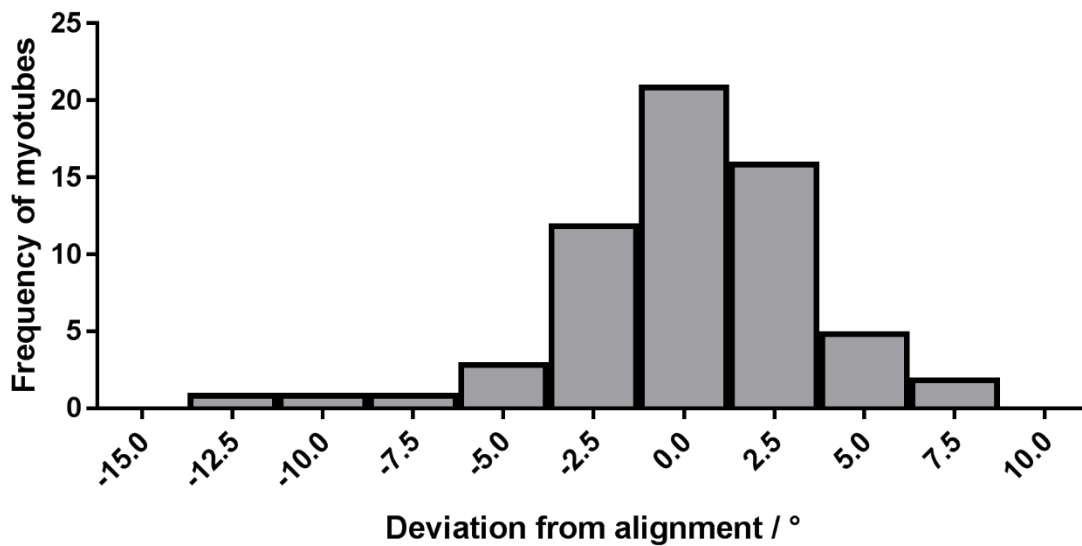


Figure 5.13: The difference between the measured myotube angles and the average for the containing frame in (A) the muscle-tendon gels and (B) the muscle control gels. Taken from  $n=2 \times 2$  repeats. Error bars =  $\pm$  Standard deviation

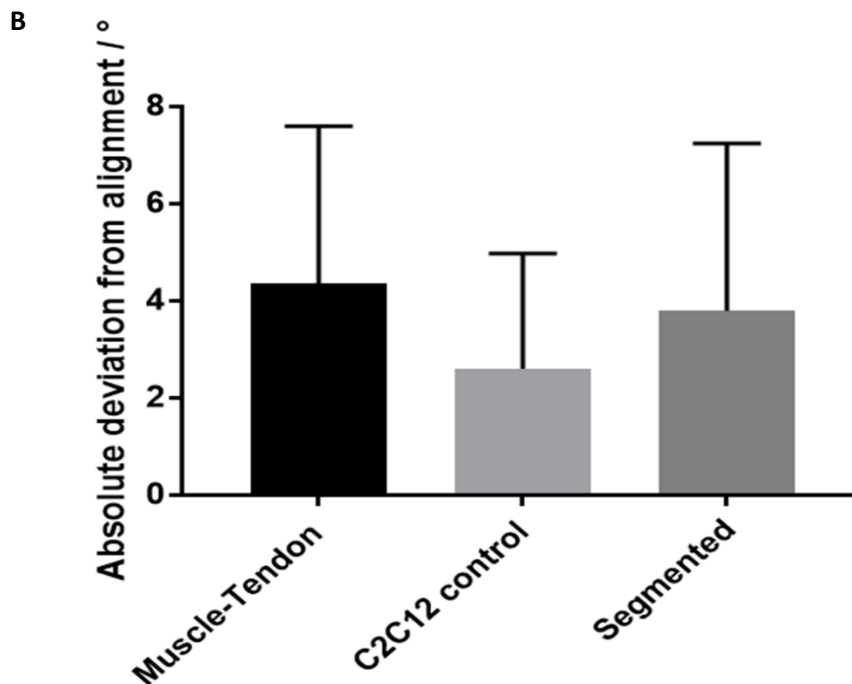
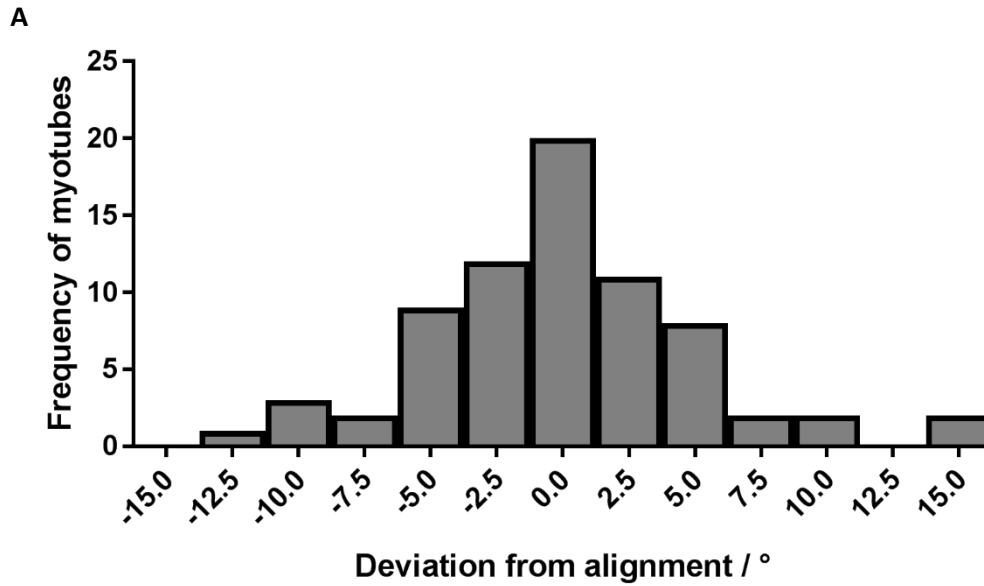


Figure 5.14: (A) The difference between the measured myotube angles and the average for the frame in segmented gels (B) the absolute differences in average alignment for all gels. Absolute values were calculated as any deviation is undesirable so simply averaging at zero is not what is required. Taken from  $n=2 \times 2$  repeats. Error bars show standard deviation. Error bars =  $\pm$  Standard deviation

### 5.3.5 Gene expression

Whilst the majority of the focus of this Chapter was to create a model that was morphologically more similar to native tissues and much can be determined from the morphology of muscle tissue, it was also of interest to analyse whether the addition of a second cell type to the model would impact the genetic expression of the muscle model, whether or not it would impact the maturation or influence the development as other co-culture studies have shown with 3D skeletal muscle. The same genes - MYH1 and MYH3- were looked at as in the previous Chapter using RT-qPCR.

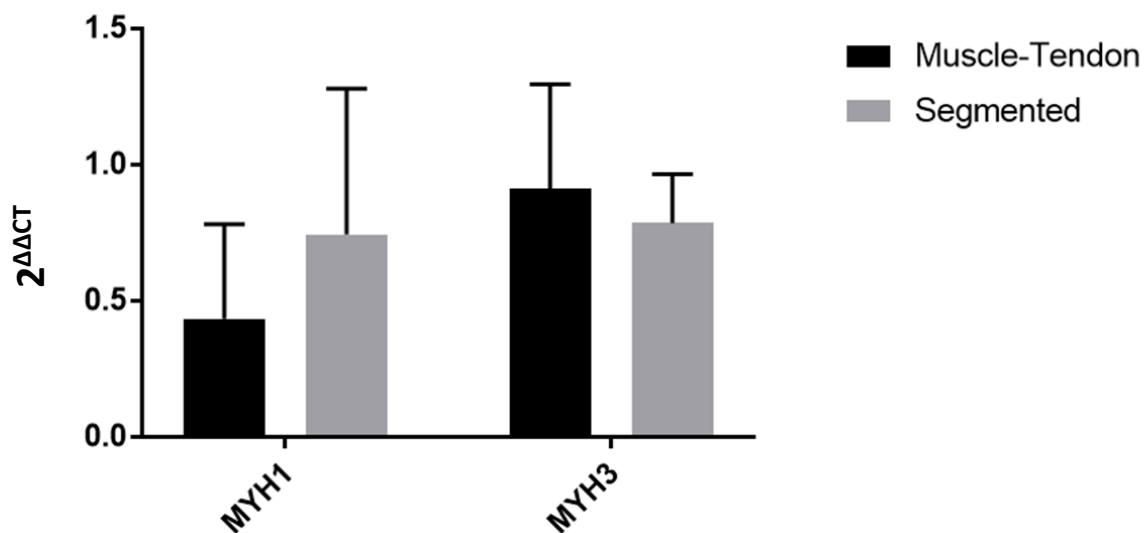


Figure 5.15: RT-qPCR results for the two myosin heavy chain isoforms MYH1 (adult) and MYH3 (embryonic) in segmented and muscle-tendon gels. No significant difference was seen between the two. Values for MYH1 were  $0.4 \pm 0.4$  and  $0.7 \pm 0.5$ , values for MYH3 were  $0.9 \pm 0.4$  and  $0.8 \pm 0.2$  for muscle-tendon models and segmented controls respectively. Taken from  $n=2 \times 2$  repeats. Error bars show standard deviation.

While there was no significant difference between the expression of either isoform, there was a large variability between the models the means of which were MYH1:  $0.4 \pm 0.4$  for muscle-tendon and  $0.7 \pm 0.5$  for segmented controls and MYH3:  $0.9 \pm 0.4$  for muscle-tendon and  $0.8 \pm 0.2$  for segmented controls.

## 5.4 Discussion

The aim of this Chapter was to ascertain whether adding a second cell type allowed for the creation of an interfacial model between a skeletal muscle and tendon model. To achieve this, the cells needed to be kept in the regions that they were seeded in and allowed to be in contact to create a gradual transition from one tissue into another. This had to be done whilst maintaining the integrity and the



function of each of the individual tissues. For this reason, the analysis in this Chapter was twofold: did the muscle region remain the same as a standard skeletal muscle model and were two distinct tissue regions created?

#### 5.4.1 Comparison of macroscopic behaviour

Building on the previous Chapter and the conclusion that seeded regions of segmented gels behaved much in the same way with the same outcomes as the standard gels, it was time to incorporate a second “tissue” in the peripheral regions to attempt to create a muscle-tendon model. The cell type identified in tendon tissues are fibroblast-like cells, called tenocytes<sup>163</sup>. Whilst these are hard to come by in the form of primary cells due to donor site morbidity, other fibroblasts are not, especially dermal fibroblasts which are more readily available<sup>122</sup>. Human dermal fibroblasts were seeded in the peripheral region with C<sub>2</sub>C<sub>12</sub> cells in the central region to create a tendon-muscle-tendon model.

The total survival rate of all gels in these experiments was 87.5% or higher, indicating a high output from the methodology developed in this thesis. The majority of the ones that failed were due to failures at the interface. This, like previous samples in Chapter 1, could have been due to incorrect setting at the interface, perhaps due to a gel setting too quickly or dividers being left in too late. Alternatively, the inherent variability in the collagen neutralisation and the system as a whole may have a percentage of models such as this which do not work. Optimisation of these shortcomings are important for future development towards high throughput systems.

The macroscopic results indicate that C<sub>2</sub>C<sub>12</sub>S and fibroblasts behaved similarly in terms of cell-mediated gel remodelling, as regardless of the combination of the cells in the three regions, as long as there were cells present, the contraction of the collagen had no significant difference. This was highlighted when even the segmented gel, which was the only one to be significantly different in surface area of peripheral regions, had the same width and surface area of the central region, the only place it was seeded with cells. This shows that as long as either cell type was in a particular region of the gel, the outcome in terms of cell-mediated remodelling would likely be the equal.

The contraction of fibroblasts in a model such as this have been previously shown and is therefore unsurprising in this model. The system used in this thesis originates in fibroblast populated collagen lattice (FPCL) (first introduced by Bell et al.)<sup>175</sup> which was later adapted to not be free-floating by introducing anchor points and was then used in skeletal muscle models<sup>162</sup>. FPCLs are most commonly used to model wound healing, therefore contraction is a key element of the model, the specific mechanisms of which are documented elsewhere<sup>176</sup>.

#### 5.4.2 Comparisons of cellular properties

Comparing the skeletal muscle regions of the C<sub>2</sub>C<sub>12</sub> controls, segmented (unseeded-C<sub>2</sub>C<sub>12</sub>-unseeded) controls and the (tendon)-muscle-tendon gels showed many similarities in their cellular architecture. Myotube width and number of tubes per frame were not affected between model types, presumably this is due to the seeding density being the same for the same volume of gel in each of the seeded regions. The myotube length also saw no measured difference between all three model types. The key thing to note is that whilst width is relatively well represented in a frame, the length is severely limited by the size of the frame and the relative angle of the cells as mentioned in the previous Chapter. So, a significant difference, if it is larger than the width of the frame, is not necessarily indicative of a real difference. This can also somewhat apply to the number of nuclei per tube per frame and number of tubes per frame. However, according to previously published measurements, these were representative of current model measurements<sup>46,159</sup> and should be expanded to using larger image scans when possible, however this demonstrates that there is a minimum threshold at which all the myotubes in the samples are fusing.

On the other hand, myotube width and number of tubes per frame were no different between models, indicating that the density of fused cells and their resulting width were the same no matter what the setup. Pairing this with the similarity in lengths and understanding that the number of nuclei in a frame may not be representative, it can be concluded that the resulting myotubes from all the setups are similar in morphology.

As explained in the previous Chapter, myotube alignment is indicative of mature muscle cell development and representative of native tissue. In contrast with what was discovered by Rao et al.<sup>177</sup> the presence of fibroblasts in contact with the a C<sub>2</sub>C<sub>12</sub> model showed no clear improvement of the alignment of the myotubes in the model.

Looking at the gene expression of the myosin heavy chain isoforms MYH1 and MYH3, no difference could be found between the two gel types. However, the errors on these data were very large, indicating that although the gel types seemed no different on average, they were both very variable in their outcomes in terms of gene expression. For segmented control gels, this may be due to what was discovered in the previous Chapter with regards to cell migration and how some myotubes were found to be very mature. Further work with larger repeats are required.

#### 5.4.3 Cellular interaction observations

To find out whether or not the two regions created a distinct interface and were kept in their respective regions, immunostained images were compared. Desmin was used as a muscle-specific

filament stain whilst rhodamine phalloidin was used for actin staining to show the filaments of all cells, DAPI was used for the identification of nuclei. This type of counterstaining, using desmin to stain for specifically for muscle with a different stain for the other cell types such as fibroblasts is a method that can be commonly used to distinguish between cell types<sup>178</sup>. This assumes that non-muscle cell lineages are not myogenic and will therefore not be desmin positive. However, in this Chapter, using this method reduced the distinction between cell types: the muscle-tendon co-cultures had a majority of desmin positive cells within them meaning that almost all cells in the model were stained with both desmin and rhodamine phalloidin.

Fibroblasts themselves are not desmin positive as desmin is a muscle-specific filament protein. However, some experiments have managed to drive them down a myogenic lineage. For example, MyoD1 has been used to induce desmin positivity in dermal fibroblasts through transdifferentiation<sup>179</sup>. More similarly to the experiments in this Chapter is the work of Goldring et al. who introduced dermal fibroblasts into the muscle of the mdx (Duchenne's muscular dystrophy) mouse model and found that the dermal fibroblasts participated in new myotube formation<sup>180</sup>. Building on this, it was discovered that dermal fibroblasts grown in medium conditioned by muscle cells would convert to a myogenic lineage due to the factor Galectin-1 which is secreted in myogenic cultures. Using transfected COS-1 cells to increase secretion of Galectin-1, this conversion can reach 100% of cloned dermal fibroblasts in conditioned media, but this secretion also occurs at a lower level with C<sub>2</sub>C<sub>12</sub> cultures. Therefore, C<sub>2</sub>C<sub>12</sub> secretions of Galectin-1 into media have been shown to cause dermal fibroblasts to become desmin positive when cultured in said media. Further work also found that the same results are mirrored in human cells, stating that human dermal fibroblasts can also become desmin positive when cultured in muscle cell conditioned media<sup>181</sup>. The potential mechanisms postulated for this are either direct transdifferentiation into a different cell type of the fibroblasts, or a sub-population from the dermis with characteristics of stem cells exist in the culture. As these fibroblasts were cultured from primary cells, either mechanism could explain the expression of desmin in these experiments.

In this experiment, the images of the immunostained gels showed desmin positivity throughout the samples, with a few occasional exceptions. This meant that the fibroblasts, if they were still in the gel regions at the end of the culture period, were mostly desmin positive. Desmin positivity was almost completely absent from hDF control gels, apart from a small number of exceptions observed where no more than a few were positive in an entire gel (data not shown). Although further repeats are needed, a small number of desmin-expressing cells could indicate that there is indeed a sub-population of cells within the culture.

As all cells were cultured in the same media within the same models, it could be assumed that the media acted as 'conditioned' in a way by the present C<sub>2</sub>C<sub>12</sub> cells and this could have led to the aforementioned conversion of fibroblast cell type to a myogenic lineage. Interestingly, the literature states that this does not occur in all fibroblast types, for example, myofibroblasts do not convert under these conditions and are also do not express desmin normally. This would explain why some experiments using desmin in co-cultures would be able to distinguish between myogenic and non-myogenic cell types without inducing a change<sup>182</sup>. The scarce research on the mechanisms of change of expression has been focussed on the dermal fibroblast cell population.

Due to the lack of availability on information of similar models, this could be an explanation as to why there were so few non desmin-positive cells visible in the confocal images despite the careful seeding of the different cell types in specific regions. It is important to note that whilst the hDFs were primary cells used in this experiment, after high numbers of passages, they may have potentially lost their original fibroblastic characteristics. Nevertheless, the muscle-specific immunostain was unreliable in the analysis of the images for the purposes of this Chapter, requiring an analysis of the morphology of the cells instead to judge whether the requirements had been met.

#### 5.4.4 Comparison of cellular architecture

In order to answer whether or not two distinct tissue regions were created, the cell morphology needed to be objectively analysed for changes in cellular architecture. The images in Figure 5.9 showed that there were regions where thick myotubes came to a sudden halt and areas with other cell morphologies began. These were often found to not accurately correspond to the interface created between gel regions during fabrication. Therefore, these could be termed as secondary interfaces. This type of architecture is similar to that visible in experiments by Rao et al.<sup>177</sup> in a co-culture of C<sub>2</sub>C<sub>12</sub> and 3T3 fibroblasts, where large, thick tubes suddenly transition into areas of thinner, less aligned cellular networks. This is also somewhat similar to what was observed by Merceron et al.<sup>143</sup> who also used the same cell types. However, in contrast to these publications, this Chapter showed thicker, more developed tubes at the interfaces with a much less defined interface, which is reflective of the focus of each respective study.

The interfaces in this Chapter were often not very defined or uniform and were not visible in all gels, but they could be in a total of 4 interfaces out of a total 18 (9 gels). This again highlights the variability of the gels, echoing results of their genetic expression. The initial system for creating gels before this thesis had inherent variability in and of itself, some models would not yield the same results as others, even within a single repeat and the reasons are generally unexplained. This would commonly occur when there was only a single cell type within a single gel. The variability becomes compounded as the

number of gels and cell types increase, giving rise to higher unpredictability of the model. One likely reason for this variability could come from lack of specific control of removal of the dividers. In other words, they are removed whenever the pipetting is finished, regardless of how long that takes, resulting in some gels being left with the dividers in for a longer period which may lead to certain segments polymerising first, creating more of a semi-barrier between the two cell types, preventing as much movement between the two. Alternatively, it may be related to the migration of the cells and the interactions between the two, for example, Rao et al. demonstrated that myoblasts and fibroblasts that are within short range of each other can lead to a decrease in myoblast differentiation due to cross talk<sup>177</sup>. Similar effects may have limited the development of the myoblasts in the cultures in this Chapter and led to models with a mixture of unfused myoblasts, fibroblasts and myotubes which could only be discerned by the morphology as desmin was detected in most cell filaments, preventing a simple distinction between cell types.

At the time of this thesis, few similar models exist as identified by Rao et al.<sup>177</sup> to be compared to, leading to a lack of good information to use as a benchmark for these models. Out of the current attempts to create such a model, this Chapter found a much simpler model with much more variable results and would require more optimisation and analysis for a clearer outlook on the system.

## 5.5 Conclusions

The experimental results in this Chapter suggested that human dermal fibroblasts and C<sub>2</sub>C<sub>12</sub> myoblasts perform similar extents of matrix remodelling when seeded in the same densities in collagen gels. Using the segmentation method, tendon-muscle gels were fabricated with some evidence of transitions between cell types once immunostained, with regions of multinucleated myotubes adjacent to regions of single-nuclei cells, similar to those seen in other experiments attempting to replicate these interfaces. These indicated that it may be possible to create models with muscle-tendon interfaces using this system. However, the transitions were observed inconsistently suggesting that the parameters in the system were not optimised to allow for uniformity between or even within samples. Additional experiments with regards to times at which dividers are removed, environmental temperature, and seeding densities would allow for better understanding of the creation of interfaces. Additionally, desmin staining for myofilaments was found to not be an effective differentiator between cell types, this may have been due transdifferentiation of dermal fibroblasts in the presence of Galectin-1 from the co-culture of C<sub>2</sub>C<sub>12</sub> cells. Further experiments with different sources of fibroblasts as a tendon model could yield more clear differences between the two cell types, allowing for a clearer understanding of the microstructure of the models.

## 5.6 Key findings

The data gathered in this thesis takes steps towards a potential method for creating a single *in vitro* tissue engineered collagen model consisting of multiple regions of different cell populations using a simple method that could be adapted for high throughput testing. Firstly, current models of *in vitro* 3D skeletal muscle were evaluated and the simplest in regards to preparation and equipment was identified, a collagen model between two anchor points. This was then developed into a method that was more consistent by optimising the individual steps and the use of resources, before it was adapted to being able to allow for multiple gel populations to be made in a single gel; termed segmentation of the gel. Secondly, the standard C<sub>2</sub>C<sub>12</sub> murine myoblast models were tested against segmented gels with unseeded peripheral regions to ascertain if the introduction such regions would change the output of the skeletal muscle regions of the gels, resulting in the muscle regions of the new gels being almost identical to the standard. Finally, the originally unseeded peripheral regions were seeded with a tendon-like cell types (hDFs) in an attempt to create a muscle-tendon model, leading to a model with some evidence of ability to create such an interface, but not yet reliably indicating a need for further research and optimisation

Much of the focus of this thesis has not been previously studied or published due to lack of relevance at the experimental level in academia. For example, no detailed breakdown of the process components and the variability of the chosen collagen system has been published elsewhere. The aim of this system is for testing, simulating conditions to study the reaction of the tissues to certain stimuli, therefore tissue engineered models need to be as uniform as possible between samples with large output numbers. Hence, it is vital to look at the inherent variability in the system and minimise it, as was done in the first experiments of this thesis. Once steps were taken towards creating a more reliable process, the model could be adapted to try and separate regions within the tissue.

Again, very few models exist at the time of writing this thesis which tissue engineer a muscle and tendon region inside a single collagen model without the use of additional biological components such as decellularized tissue making comparable data very limited. Merceron et al.<sup>143</sup> used 3D organ printing to lay down two adjacent substrates layer-by-layer with cell/hydrogel mix in layers in between substrate layers, creating a 'muscle' region conjoined with a 'tendon' and a clear interface where the two merge. The technique found good success and control of regions, but the ECM composed of hyaluronic acid, gelatin and fibrinogen was not necessarily representative of physiological tissue and required specialised equipment in the form of an organ printer, which at this point in time would limit the volume of output of the system. Ladd et al.<sup>164</sup> seeded C<sub>2</sub>C<sub>12</sub> myoblasts and 3T3 fibroblasts on electrospun PLA and PCL scaffolds for a similar effect but with no ECM present. Larkin et al. created

an MTJ with self-organised collagen constructs involving laminin, also with good outcomes<sup>54</sup>. However, the experiments took considerable preparation with sylgard for the wells being left three weeks to cure and the laminin requiring a week before use. Lastly, Rao et al.<sup>177</sup> created a co-culture of tendon and muscle collagen gels, but these were not intended as a muscle-tendon model and were not in unilateral tension to cause alignment. Based on the existing models, no simple, cheap, quick to assemble model exists for the fabrication of a muscle-tendon interface, neither does one exist completely using a tissue-engineered collagen gel. The main constituent of physiological muscle and tendon is collagen, therefore the model optimised and used in this thesis was a collagen model.

In this thesis, the individual components of the entire process of creating a standardised gel were initially analysed, which despite being very widely and successfully used as an experimental model, had specific stages identified that were causing the difficulty in making it a higher output system by making it more of an artisan process<sup>46,159</sup>. Firstly, much of the setup was made by hand, creating differences in every model that was made and limiting the number of samples made to the number of setups that can be handmade by the operator. Secondly, the non-handmade chambers were bespoke and expensive, requiring long periods of waiting times to be made and delivered. Also, the gels required high numbers of cultured cells due to their volumes, there was no accurate way to separate parts of the gel for different cell populations to create multiple tissue systems, there was little versatility in the setup to allow for new prototypes or for easy follow-up experiments such as mechanical stimulation. The fabrication process was held back heavily by having to repeat the entire neutralisation of collagen cycle every one or two gels made as the neutralised collagen would set too quickly to give time to fabricate more gels.

Preliminary attempts to separate gel regions found that, if made quickly enough a single gel can be made out of three smaller collagen regions with their own seeding, this gel would then contract much more in seeded regions than in unseeded regions. However, these were difficult to produce due to the aforementioned limitation with neutralised collagen.

Multiple different additive manufactured well systems were attempted, learning that 3D printed shapes worked well as moulds and that sliding “dividers” with slots in the side of the moulds were the best for separating a single gel. The final prototype resembled one that was published at the time<sup>159</sup> and was then adapted to match the published geometries with the sliding dividers incorporated. Now very large numbers of moulds could be made with the use of a commercially available 3D printer with only hour-long wait times and be used on the very same day once adhered into a standard 6-well plate. Other prototypes were made, altering the geometries of the system to create different test samples and another model was developed where the mould form a moveable miniature joint where

muscle constructs could be cast either side and the tension in their inherent systems could affect each other's development. These pave the way for new experiments that could be conducted to find optimal parameters for such systems. The first experiment in the new system compared how a segmented unseeded (acellular)-C<sub>2</sub>C<sub>12</sub>-unseeded gel would perform against a homogeneously seeded C<sub>2</sub>C<sub>12</sub> gel. Interestingly, the middle 'muscle' regions of both gels were not observably different in terms of macroscopic or microscopic measurements, indicating that there was little effect on the ability of these gels to create the desired architecture when set up in this manner.

The locomotion of cells is a key part in the creation of many collagen-based tissue engineered constructs due to the contraction of the gel it results in. Additionally, to the previous finding, this thesis observed that the C<sub>2</sub>C<sub>12</sub> cell nuclei, whilst concentrated in the region they were seeded initially, were more homogeneously spread throughout the gel by the end of the 14-day culture period. It can be deduced that these cells may have migrated many millimetres. Cell locomotion is a large part of how collagen matrices are contracted in these models and therefore may explain why the difference in contraction between the two gel types were not as large as expected; the cells were migrating further in relative terms and mediating greater contraction. These unseeded regions saw a lower incidence of fused myotubes, but the ones that did fuse were more often thicker, larger in nuclei number and striated.

However, this migration was not optimal in terms of creating multiple gel regions with clear interfaces within a single gel. Ideally, the cells would halt their migration once they made contact with a second cell type. With the goal of creating a muscle-tendon tissue, human dermal fibroblasts- a cell type used in tendon modelling- were introduced into the peripheral regions of the gel to make a tendon-muscle-tendon construct. The macroscopic behaviour of this gel was found to be the same as all other homogenous gel controls, regardless of the cell type seeded, indicating that the fibroblast and myoblast locomotive behaviour is the same within a collagen gel. Immunostained comparisons showed that the majority of cells in the gel were desmin expressive, even those in the tendon regions. Some studies have shown that Galectin-1, a factor released by myoblasts in culture can cause dermal fibroblasts in both humans and mice to become desmin positive, indicating that this may have occurred in the co-culture here<sup>180,181</sup>. However, morphological differences could be seen between the two cell types in some constructs and although only few gels showed it, there were regions with interfaces between the two cell types in an approximation to interdigitation somewhat similar to what Rao et al observed in their experiments<sup>177</sup>.

Whilst the initial muscle-only model that this thesis began on was adapted to be more acceptable for a reliable, high-throughput system and a method was developed for segmenting a gel to make a



muscle-tendon model, the two were not reached in unison. The segmentation model as it stands is not yet consistent enough in creating muscle-tendon models successful, clear interfaces. The current rate of visible microscopic interfaces is at 22% of total interfaces made and therefore is a proof-of-concept that needs further development and optimisation to be used in high-throughput testing.

## 6 Future work

### 6.1 Future work on previous Chapter outcomes

#### 6.1.1 Segmentation improvements

The major drawback of the system investigated is that few interfaces showed a muscle-tendon transition, leaving small repeat numbers for gathering data. The process of segmenting is still variable, leading to some interfaces showing a transition whilst others do not stop the gel from merging into one co-culture. Further experiments can be conducted investigating the neutralisation process and how to standardise it with specific amounts of solvents, the time required before dividers should be removed, ways of designing dividers to cause less of a disturbance during removal. Also new studies should be conducted looking into how seeding densities affect the migration and interfacial behaviours of the system. This will allow for a more robust model with higher statistically successful output. Ultimately, a model where all three regions are deposited simultaneously would prevent discrepancies.

Tendon models can be made from a range of different tenocyte-like fibroblasts. With the desmin positivity of the dermal fibroblasts found in this thesis, a different cell type for the tendon could be used for a clearer understanding of the microscopic structure of the model. Additionally, the cell types used should be single species in order to minimise cross-species models and variability as they will not be representative of final uses.

As mentioned previously<sup>46</sup>, myotube analysis from microscopic data is too time consuming for high-throughput systems and can also be inconsistent due to the sample size limit of a frame. However, most are destructive methods. RT-qPCR could be utilised to measure gene expression, but no specific markers for skeletal muscle maturation currently exist, so myogenin and MyoD1 are often used to measure regulation profiles over time<sup>111,152,166</sup>. Alternatively, collagen markers could be used. With tendon tenomodulin can be used as a specific marker of tendon maturation and Col-1 is also often used although is not specific to tendon<sup>122</sup>. However, collagen marker results will be affected by the matrix of the model and would therefore not be reliably measurable. Wragg<sup>46</sup> also identified the enzyme-linked immunosorbent assay (ELISA) as another potential method due to the increased sensitivity of protein detection. All of these methods require destruction of the model and are also measures that indicate whether a model might be successful, none are primary determinations of a skeletal muscle model's success. Skeletal muscle function is dependent on the structure of the cell, therefore the only measure for whether a model has formed successful, mature myotubes is through the identification of mature myotubes through microscopic assessment. Hence, a method of real-time

measurement of the system would allow for good comparisons of structural formation and final morphology such as live tagging of proteins with in-incubator microscopes<sup>46</sup>. Alternatively, assessment of the function by stimulating contraction would indicate if the structure is functional, usually performed in self-assembling models<sup>89,113</sup>. However, these are more difficult to perform in collagen gels due to the dense matrix that has been further remodelled<sup>46</sup>.

Genetic expression of each individual region could be analysed for certain markers instead of the gel as a whole to understand how the separate tissue regions respond to being in the coculture model, although the fabricated and secondary interface are not located in the same region, making isolations of regions difficult.

Many published models are cultured for longer than two weeks to allow time for the full development of cells and some of the cultures had not fused properly over the given period which is in line with other findings longer culture times can be tested with this co-culture model.

To verify whether this model is useful for the intended purpose, it can be tested with discovered compounds and effects compared to those *in vivo* and current testing methods as well as mechanical stimulation experiments.

Finally, this can be combine with previous muscle-bone 3D co-cultures to create a complete muscle-tendon-bone model.

### 6.1.2 Versatility in geometry of 3D printed moulds

Because 3D printing has opened up so many opportunities, there are a large number of mould designs that can now be attempted to make different kinds of models.

So far, most models have focussed on one small organoid. 3D printed systems can be designed to include multiple organoids into a miniature system. For example, a skeletal muscle construct is a group of myotubes in a matrix, making an analogue of a fascicle. To more accurately represent the full organ, multiple fascicles can be created in a single model, although this requires more complex designing, and can involve making use of all three axis in designs.

Traditionally, models are usually designed in the XY plane and then extended through the Z axis. For example, a rectangle is created as a mould, and then extended upwards in the Z plane to make a cuboid, and that is a standard shaped mould. For the tube-shaped moulds, they are circles that are then extended upwards. But now, new intricate shapes can be created with variances in the Z axis with more complex shaped moulds for different tissue systems. For example, muscle begins with a small cross-sectional area at the MTJ, then increases in size towards the middle of the muscle belly,

this can be recreated in a multifascicular model with certain fascicles angling outwards more than others between the two MTJs.

Finally, moving parts in a model are now easily made with precision on a large scale, leading to consistent models that can involve articulating joints allowing for different types of stimulations with multiple tissue models.

As Bian et al.<sup>116</sup> demonstrated, varying the design of the moulds when making skeletal muscle collagen gels can yield interesting results in the way the cells align and fuse and can influence the architecture of the model by guiding the fibres in certain directions. Some additional prototype moulds were tested during the term of this project but were deemed not in the scope:

### 6.1.3 “Skinny” gels

The leading stimulus of these systems is the mechanical strain created inherently by cellular remodelling in the gel whilst being held by the anchor points. Strain mechanics are changed by the geometry of the sample though, thereby changing the way in which the cells align and fuse.

It was observed that many of the gels that were being fabricated had dense, well-aligned myotubes on the edge of the gel. This may be because it is an area of strain concentration as there is nowhere outside to dissipate to, also cells are not able to migrate out at the edges so may accumulate more there than elsewhere in the gel. The question was, then, what if the entire gel was made as an edge? Would that improve the density of the entire gel? A new design was made with a very thin (2mm) opening for the gel in the middle with the normal sized mould on either end. This shaped the sample like a standard engineering tensile test sample, which concentrates the tension in the thin region.

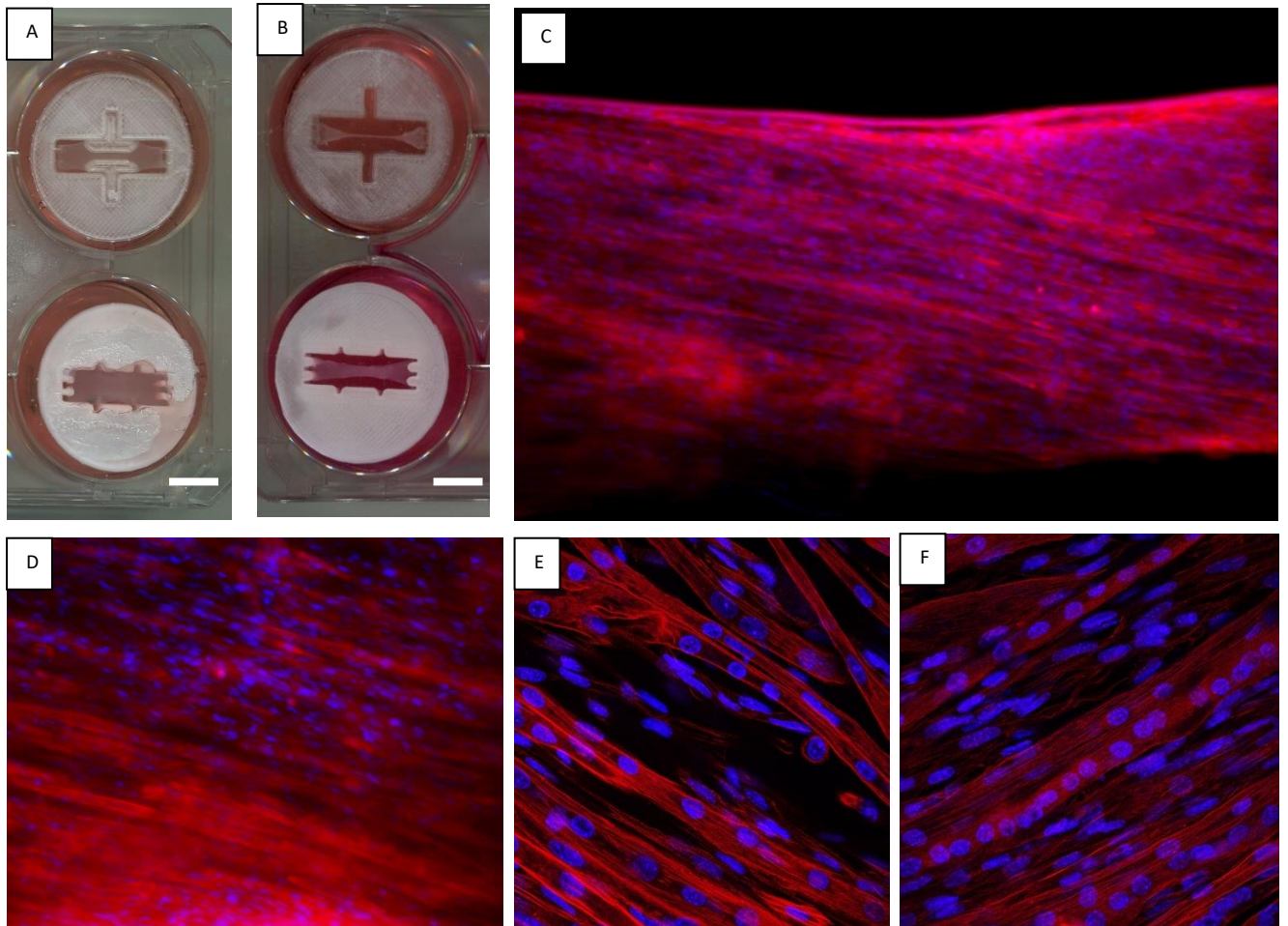
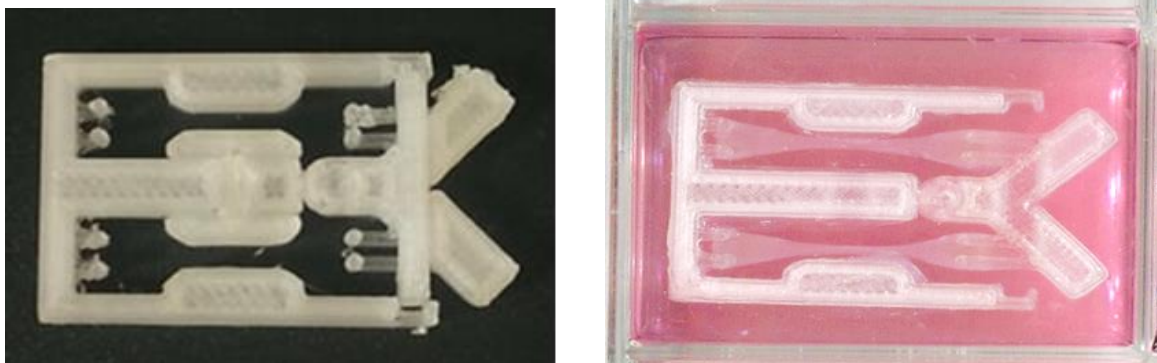


Figure 6.1: Examples of "Skinny" gel geometry, macro images and day 0 (A) and day 14 (B), Phalloidin (Red) and DAPI (blue) stained images at 10x (C), and 20x (D,E,F). From 2 gels over 2 repeats.

The preliminary attempts using a new geometry seemed to have some successful results. At the very least they were successful gels, with highly dense, aligned myotubes. This seems to echo what was discovered by Bian et al.<sup>116</sup> But will require more experimental repeats to determine whether useful. Nonetheless some potential can be seen.

## 6.2 Miniature Joint models



*Figure 6.2: Demonstration of how the mini-joint model could use two constructs in a single mould (A). The resulting (B) gels could exert force on each other during development which may have positive effects as it occurs in vivo.*

Developmentally, skeletal muscles are connected to the skeleton and twitching is an essential part of embryonic musculoskeletal development. Muscles often come in agonist and antagonist pairs, the two alternating between contraction and stretch. Therefore, these models can be developed to work in antagonistic pairs, exhibiting opposing forces on each other. A prototype for this was developed during this project. This had potential to be attached to a motor and stimulate two models at the same time, perhaps one in compression and the other stretched, released factors could then be measured.

## 7 References

1. Alberts, B., Johnson, A., Lewis, J., Raff, M., Robers, K. & Walter, P., *Molecular Biology of the Cell*. (Garland Science, 2007).
2. Bell, G. H., Emslie-Smith, D. & Paterson, C. R. *Textbook of physiology*. (Churchill Livingstone, 1980).
3. Gillies, A.R., Lieber, R. L. Structure and function of the skeletal extacellular matrix. *Muscle Nerve* **44**, 318–331 (2012).
4. Tajbakhsh, S. Skeletal muscle stem cells in developmental versus regenerative myogenesis. *J. Intern. Med.* **266**, 372–389 (2009).
5. Bendall, J. R. The elastin content of various muscles of beef animals. *J. Sci. Food Agric.* **18**, 553–558 (1967).
6. Dransfield, E. Intramuscular composition and texture of beef muscles. *J. Sci. Food Agric.* **28**, 833–842 (1977).
7. Light, N. & Champion, A. E. Characterization of muscle epimysium, perimysium and endomysium collagens. *Biochem. J.* **219**, 1017–1026 (1984).
8. Buckingham, M., Bajard, L., Chang, T., Daubas, P., Hadchouel, J., Meilhac, S., Montarras, D., Rocancourt, D & Relaix, F., The formation of skeletal muscle: From somite to limb. *J. Anat.* **202**, 59–68 (2003).
9. Christ, B. & Ordahl, C. P. Early stages of chick somite development. *Anat. Embryol. (Berl)*. **191**, 381–396 (1995).
10. Tajbakhsh, S., Rocancourt, D., Cossu, G. & Buckingham, M. Redefining the genetic hierarchies controlling skeletal myogenesis: Pax-3 and Myf-5 act upstream of MyoD. *Cell* **89**, 127–138 (1997).
11. Gilbert, S. F. Osteogenesis: The development of bones. *Developmental Biology* (2000). Available at: <http://www.ncbi.nlm.nih.gov/books/NBK10056/>. Accessed 10 October 2018.
12. Rudnicki, M.A., Schnegelsberg, P.N., Stead, R.H., Braun, T., Arnold, H.H & Jaenisch, R., MyoD or Myf-5 is required for the formation of skeletal muscle. *Cell* (1993). doi:10.1016/0092-8674(93)90621-V
13. Tajbakhsh, S., Rocancourt, D. & Buckingham, M. Muscle progenitor cells failing to respond to

- positional cues adopt non- myogenic fates in myf-5 null mice. *Nature* **384**, 266–270 (1996).
14. Kablar, B., Krastel, K., Ying, C., Tapscott, S.J., Goldhamer, D.J. & Rudnicki MA. Myogenic Determination Occurs Independently in Somites and Limb Buds. *Dev. Biol.* **206**, 219–231 (1999).
  15. Huxley, A. F. Muscular contraction. *J Physiol* **243**, 1–43 (1974).
  16. Tregear, R. & Marston, S. The cross-bridge theory. *Physiol. Rev.* **63**, 1049–1113 (1983).
  17. Gomes, A. V, Potter, J. D. & Szczesna-Cordary, D. The role of troponins in muscle contraction. *IUBMB Life* **54**, 323–333 (2002).
  18. Kannus, P. Structure of the tendon connective tissue. *Scand. J. Med. Sci. Sports* **10**, 312–320 (2000).
  19. Sharma, P. & Maffulli, N. Biology of tendon injury: Healing, modeling and remodeling. *J. Musculoskelet. Neuronal Interact.* **6**, 181–190 (2006).
  20. O'Brien, M. Structure and metabolism of tendons. *Scand. J. Med. Sci. Sports* **7**, 55–61 (1997).
  21. Williams, J. G. Achilles tendon lesions in sport. *Sports Med.* **3**, 114–135 (1986).
  22. Zhang, G., Young, B.B., Ezura, Y., Favata, M., Soslowsky, L.J., Chakravarti, S. & Birk D.E. Development of tendon structure and function: Regulation of collagen fibrillogenesis. *Journal of Musculoskeletal Neuronal Interactions* **5**, 5–21 (2005).
  23. Apostolakos, J. Durant, T.J., Dwyer, C.R., Russell, R.P., Weinreb, J.H., Alaei, F., Beitzel, K., McCarthy, M.B., Cote, M.P. & Mazzocca A.D. The enthesis: a review of the tendon-to-bone insertion. *Muscles. Ligaments Tendons J.* **4**, 333–342 (2014).
  24. Zerhouni, E. A. Ultrastructure of myotendinous junctions in tendon-skeletal muscle constructs engineered in vitro Tatiana. *Science (80- )*. **306**, 1895 (2004).
  25. Butler, D. L., Grood, E. S., Noyes, F. R. & Zernicke, R. F. Biomechanics of ligaments and tendons. *Exerc. Sport Sci. Rev.* **6**, 125–181 (1978).
  26. Elliott, D. H. Structure and function of mammalian tendon. *Biol. Rev.* **40**, 392–421 (1965).
  27. Rowe, R. W. The structure of rat tail tendon fascicles. *Connect. Tissue Res.* **14**, 21–30 (1985).
  28. Hess, G. P., Cappiello, W. L., Poole, R. M. & Hunter, S. C. Prevention and treatment of overuse tendon injuries. *Sports Med.* **8**, 371–384 (1989).



29. Tozer, S. & Duprez, D. Tendon and ligament: Development, repair and disease. *Birth Defects Res. Part C - Embryo Today Rev.* **75**, 226–236 (2005).
30. Schweitzer, R., Zelzer, E. & Volk, T. Connecting muscles to tendons: tendons and musculoskeletal development in flies and vertebrates. *Development* **137**, 2807–2817 (2010).
31. Brent, A. E., Schweitzer, R. & Tabin, C. J. A somitic compartment of tendon progenitors. *Cell* **113**, 235–248 (2003).
32. Brent, A. E., Braun, T. & Tabin, C. J. Genetic analysis of interactions between the somitic muscle, cartilage and tendon cell lineages during mouse development. *Development* **132**, 515–528 (2005).
33. Pryce, B. a *et al.* Recruitment and maintenance of tendon progenitors by TGFbeta signaling are essential for tendon formation. *Development* **136**, 1351–1361 (2009).
34. Lorda-Diez, C. I., Montero, J. A., Martinez-Cue, C., Garcia-Porrero, J. A. & Hurle, J. M. Transforming growth factors  $\beta$  coordinate cartilage and tendon differentiation in the developing limb mesenchyme. *J. Biol. Chem.* **284**, 29988–29996 (2009).
35. Pryce, B. A., Brent, A. E., Murchison, N. D., Tabin, C. J. & Schweitzer, R. Generation of transgenic tendon reporters, ScxGFP and ScxAP, using regulatory elements of the scleraxis gene. *Dev. Dyn.* **236**, 1677–1682 (2007).
36. Chevallier, A., Kieny, M. & Mauger, A. Limb-somite relationship: origin of the limb musculature. *J. Embryol. Exp. Morphol.* **41**, 245–258 (1977).
37. Chen, J. W. & Galloway, J. L. The development of zebrafish tendon and ligament progenitors. *Development* **141**, 2035–45 (2014).
38. Schweitzer, R., Chyung, J.H., Murtaugh, L.C., Brent, A.E., Rosen, V., Olson, E.N., Lassar, A. & Tabin CJ. Analysis of the tendon cell fate using Scleraxis, a specific marker for tendons and ligaments. *Development* **128**, 3855–3866 (2001).
39. Kardon, G. Muscle and tendon morphogenesis in the avian hind limb. *Development* **125**, 4019–4032 (1998).
40. Edom-Vovard, F., Schuler, B., Bonnin, M.-A., Teillet, M.-A. & Duprez, D. Fgf4 positively regulates scleraxis and tenascin expression in chick limb tendons. *Dev. Biol.* **247**, 351–366 (2002).
41. Yurchenco, P. D., Mecham, R. P. & Birk, D. E. *Extracellular matrix assembly and structure.*

- General Pharmacology: The Vascular System* **26**, (Elsevier Science, 1995).
42. Rho, J. Y., Kuhn-Spearing, L. & Zioupos, P. Mechanical properties and the hierarchical structure of bone. *Med. Eng. Phys.* **20**, 92–102 (1998).
  43. Rodan, G. A. Bone homeostasis. *Proc. Natl. Acad. Sci. U. S. A.* **95**, 13361–13362 (1998).
  44. Copp, D. H. & Shim, S. S. The homeostatic function of bone as a mineral reservoir. *Oral Surgery, Oral Med. Oral Pathol.* **16**, 738–744 (1963).
  45. Orkin, S. H. & Zon, L. I. Hematopoiesis: An Evolving Paradigm for Stem Cell Biology. *Cell* **132**, 631–644 (2008).
  46. Wragg, N. Development of a 3D Tissue Engineered Skeletal Muscle and Bone Pre-Clinical Co-Culture Platform. *Thesis*, Loughborough University (2016),.
  47. Charvet, B., Ruggiero, F. & Le Guellec, D. The development of the myotendinous junction. A review. *Muscles. Ligaments Tendons J.* **2**, 53–63 (2012).
  48. Ovalle, W. K. Anatomy and Embryology The human muscle-tendon junction A morphological study during normal growth and at maturity. **1**, 281–294 (1987).
  49. Tidball, J. G. & Lin, C. Structural changes at the myogenic cell surface during the formation of myotendinous junctions. *Cell Tissue Res.* **257**, 77–84 (1989).
  50. Larkin, L. M., Calve, S., Kostrominova, T. Y. & Arruda, E. M. Structure and Functional Evaluation of Tendon–Skeletal Muscle Constructs Engineered in Vitro . *Tissue Eng.* **12**, 3149–3158 (2006).
  51. Chiquet, M. & Fambrough, D. M. Chick myotendinous antigen. I. A monoclonal antibody as a marker for tendon and muscle morphogenesis. *J. Cell Biol.* **98**, 1926–1936 (1984).
  52. Koch, M., Schulze, J., Hansen, U., Ashwodt, T., Keene, D.R., Brunken, W.J., Burgeson, R.E., Bruckner, P. & Bruckner-Tuderman L. A Novel Marker of Tissue Junctions, Collagen XXII. *The Journal of biological chemistry* **279**, 22514–22521 (2004).
  53. Katsumi, A., Orr, a W., Tzima, E. & Schwartz, M. A. Integrins in mechanotransduction. *J. Biol. Chem.* **279**, 12001–4 (2004).
  54. Larkin, L. M., Calve, S., Kostrominova, T. Y. & Arruda, E. M. Structure and Functional Evaluation of Tendon–Skeletal Muscle Constructs Engineered in Vitro . *Tissue Eng.* **12**, 3149–3158 (2006).

55. Shaw, H. M., Vázquez, O.T., McGonagle, D., Bydder, G., Santer, R.M. & Benjamin M. Development of the human Achilles tendon enthesis organ. *J. Anat.* **213**, 718–724 (2008).
56. Benjamin, M. & Ralphs, J. R. Entheses--the bony attachments of tendons and ligaments. *Ital. J. Anat. Embryol.* **106**, 151–157 (2001).
57. Rufai, A., Benjamin, M. & Ralphs, J. R. Development and ageing of phenotypically distinct fibrocartilages associated with the rat Achilles tendon. *Anat. Embryol. (Berl)*. **186**, 611–618 (1992).
58. Blitz, E., Sharir, A., Akiyama, H. & Zelzer, E. Tendon-bone attachment unit is formed modularly by a distinct pool of Scx- and Sox9-positive progenitors. *Development* **140**, 2680–90 (2013).
59. Zelzer, E., Blitz, E., Killian, M. L. & Thomopoulos, S. Tendon-to-bone attachment: From development to maturity. *Birth Defects Res. Part C - Embryo Today Rev.* **102**, 101–112 (2014).
60. Sugimoto, Y. Takimoto, A., Akiyama, H., Kist, R., Scherer, G., Nakamura, T., Hiraki, Y. & Shukunami C. Scx+/Sox9+ progenitors contribute to the establishment of the junction between cartilage and tendon/ligament. *Development* **140**, 2280–8 (2013).
61. Schwartz, A. G., Pasteris, J. D., Genin, G. M., Daulton, T. L. & Thomopoulos, S. Mineral Distributions at the Developing Tendon Enthesis. *PLoS One* **7**, (2012).
62. Provot, S. & Schipani, E. Molecular mechanisms of endochondral bone development. *Biochem. Biophys. Res. Commun.* **328**, 658–665 (2005).
63. Kahn, J., Shwartz, Y., Blitz, E., Krief, S., Sharir, A., Breitel, D.A., Rattenbach, R., Relaix, F., Maire, P., Rountree, R.B., Kingsley, D.M. & Zelzer, E. Muscle Contraction Is Necessary to Maintain Joint Progenitor Cell Fate. *Dev. Cell* **16**, 734–743 (2009).
64. Galatz, L. M., Ball, C. M., Teefey, S. A., Middleton, W. D. & Yamaguchi, K. The outcome and repair integrity of completely arthroscopically repaired large and massive rotator cuff tears. *J. Bone Joint Surg. Am.* **86-A**, 219–224 (2004).
65. Thomopoulos, S. Kim, H.M., Rothermich, S.Y., Biederstadt, C., Das, R. & Galatz LM. Decreased muscle loading delays maturation of the tendon enthesis during postnatal development. *J. Orthop. Res.* **25**, 1154–1163 (2007).
66. Schwartz, A. G., Lipner, J. H., Pasteris, J. D., Genin, G. M. & Thomopoulos, S. Muscle loading is necessary for the formation of a functional tendon enthesis. *Bone* **55**, 44–51 (2013).

67. Lu, H. H. & Thomopoulos, S. Functional Attachment of Soft Tissues to Bone: Development, Healing, and Tissue Engineering. *Annual review of biomedical engineering* **15**, 201–226 (2013).
68. Benjamin, M. Kumai, T., Milz, S., Boszczyk, B.M., Boszczyk, A.A. & Ralphs J.R. The skeletal attachment of tendons--tendon 'entheses'. *Comp. Biochem. Physiol. A. Mol. Integr. Physiol.* **133**, 931–945 (2002).
69. Gulotta, L. V & Rodeo, S. A. Growth factors for rotator cuff repair. *Clin. Sports Med.* **28**, 13–23 (2009).
70. Wrana, J. L., Attisano, L., Wieser, R., Ventura, F. & Massague, J. Mechanism of activation of the TGF- $\beta$  receptor. *Nature* **370**, 341–347 (1994).
71. Scott, A. Cook, J.L., Hart, D.A., Walker, D.C., Duronio, V. & Khan, K.M. Tenocyte responses to mechanical loading in vivo: a role for local insulin-like growth factor 1 signaling in early tendinosis in rats. *Arthritis Rheum.* **56**, 871–881 (2007).
72. Juneja, S. C. & Veillette, C. Defects in tendon, ligament, and enthesis in response to genetic alterations in key proteoglycans and glycoproteins: a review. *Arthritis* **2013**, 154812 (2013).
73. Padulo, J., Oliva, F., Frizziero, A., Maffulli, N. & Padulo, J. principles and recommendations in clinical and field science research Corresponding author : **3**, 250–252 (2013).
74. Angeline, M. E. & Rodeo, S. A. Biologics in the Management of Rotator Cuff Surgery. *Clin. Sports Med.* **31**, 645–663 (2012).
75. Snow, S. W., Bohne, W. H., DiCarlo, E. & Chang, V. K. Anatomy of the Achilles tendon and plantar fascia in relation to the calcaneus in various age groups. *Foot ankle Int.* **16**, 418–421 (1995).
76. Milz, S., Rufai, A., Buettner, A., Putz, R., Ralphs, J.R. & Benjamin, M. Three-dimensional reconstructions of the Achilles tendon insertion in man. *J. Anat.* **200**, 145–152 (2002).
77. Eliseev, R., Schwarz, E.M., Zuscik, M.J., O'Keefe, R.J., Drissi, H. & Rosier, R.N. a *et al.* Smad7 mediates inhibition of Saos2 osteosarcoma cell differentiation by NFkappaB. *Exp. Cell Res.* **312**, 40–50 (2006).
78. Novakova, S. S. Mahalingam, V.D., Florida, S.E., Mendias, C.L., Allen, A., Arruda, E.M., Bedi, A. & Larkin L.M. Tissue-engineered tendon constructs for rotator cuff repair in sheep. *J. Orthop. Res.* **36**, 289–299 (2018).

79. Platt, M. A. Tendon Repair and Healing. *Clin. Podiatr. Med. Surg.* **22**, 553–560 (2005).
80. Baldino, L., Cardea, S., Maffulli, N. & Reverchon, E. Regeneration techniques for bone-To-Tendon and muscle-To-Tendon interfaces reconstruction. *Br. Med. Bull.* **117**, 25–37 (2016).
81. Corry, I. S., Webb, J. M., Clingeffer, A. J. & Pinczewski, L. A. Arthroscopic Reconstruction of the Anterior Cruciate Ligament. *Am. J. Sports Med.* **27**, 444–454 (1999).
82. Robertson, D. B., Daniel, D. M. & Biden, E. Soft tissue fixation to bone. *Am. J. Sports Med.* **14**, 398–403 (1986).
83. Dourte, L. A. M., Kuntz, A. F. & Soslowsky, L. J. Twenty-five years of tendon and ligament research. *J. Orthop. Res.* **26**, 1297–1305 (2008).
84. Mak, I. W., Evaniew, N. & Ghert, M. Lost in translation: animal models and clinical trials in cancer treatment. *Am. J. Transl. Res.* **6**, 114–8 (2014).
85. Ledford, B. Y. H. 4 Ways to fix the clinical trial. *Nature* **477**, 7–9 (2011).
86. Bose, S., Roy, M. & Bandyopadhyay, A. Recent advances in bone tissue engineering scaffolds. *Trends Biotechnol.* **30**, 546–554 (2012).
87. Christ, G. J. Soft Tissue Reconstruction : Skeletal Muscle Engineering. *Stem Cell Biol. Tissue Eng. Dent. Sci.* 1–27 (2014).
88. Aviss, K. J., Gough, J. E. & Downes, S. Aligned electrospun polymer fibres for skeletal muscle regeneration. *Eur. Cells Mater.* **19**, 193–204 (2010).
89. Huang, Y.C., Dennis, R. G., Larkin, L. & Baar, K. Rapid formation of functional muscle in vitro using fibrin gels. *J. Appl. Physiol.* **98**, 706–713 (2004).
90. McKeon-Fischer K.D. & Freeman, J.W. Characterization of electrospun poly(L-lactide) and gold nanoparticle composite scaffolds for skeletal muscle tissue engineering. *J. Tissue Eng. Regen. Med.* **5**, 560–568
91. Zatti, S., Zoso, A., Serena, E., Luni, C., Cimetta, E. & Elvassore N. Micropatterning Topology on Soft Substrates Affects Myoblast Proliferation and Differentiation. *Langmuir* **28**, 2718–2726 (2012).
92. Saxena, A. K., Jennifer, M., Benvenuto, M., Willital, G. H. & Vacanti, J. P. Skeletal Muscle Tissue Engineering Using Isolated Myoblasts on Synthetic Biodegradable Polymers: Preliminary Studies. *Tissue Eng.* **5**, 525–531 (1999).

93. Saxena, A. K., Willital, G. H. & Vacanti, J. P. Vascularized three-dimensional skeletal muscle tissue-engineering. *Biomed. Mater. Eng.* **11**, 275–281 (2001).
94. Levenberg, S. Rouwkema, J., Macdonald, M., Garfein, E.S., Kohane, D.S. & Darland D.C. Engineering vascularized skeletal muscle tissue. *Nat. Biotechnol.* **23**, 879–884 (2005).
95. October, R. Thoughts on the microstructure of polycrystalline thin film CuInSe<sub>2</sub> and its impact on material and device performance. **30**, 21–38 (1991).
96. Thorrez, L., Shansky, J., Wang, L., Fast, L., VandenDriessche, T., Chuah, M., Mooney, D. & Vandenburgh H. Growth, differentiation, transplantation and survival of human skeletal myofibers on biodegradable scaffolds. *Biomaterials* **29**, 75–84 (2008).
97. Engler, A. J., Griffin, M.A., Sen, S., Bönnemann, C.G., Sweeney, H.L. & Discher, D.E. Myotubes differentiate optimally on substrates with tissue-like stiffness: Pathological implications for soft or stiff microenvironments. *J. Cell Biol.* **166**, 877–887 (2004).
98. Bian, W., Liau, B., Badie, N. & Bursac, N. Mesoscopic hydrogel molding to control the 3d geometry of bioartificial muscle tissues. *Nat. Protoc.* **4**, 1522–1534 (2009).
99. Vandenburgh, H. H., Karlisch, P. & Farr, L. Maintenance of highly contractile tissue - cultured avian skeletal myotubes in collagen gel. **24**, 166–174 (1988).
100. Eastwood, M., McGrouther, D. A. & Brown, R. A. A culture force monitor for measurement of contraction forces generated in human dermal fibroblast cultures: evidence for cell-matrix mechanical signalling. *Biochim. Biophys. Acta - Gen. Subj.* **1201**, 186–192 (1994).
101. Eastwood, M. Effect of precise mechanical loading on fibroblast populated collagen lattices: morphological changes. *Cell Motil. ...* **40**, 13–21 (1998).
102. Passey, S., Martin, N., Player, D. & Lewis, M. P. Stretching skeletal muscle in vitro: Does it replicate in vivo physiology? *Biotechnol. Lett.* **33**, 1513–1521 (2011).
103. Chiron, S. Complex interactions between human myoblasts and the surrounding 3D fibrin-based matrix. *PLoS One* **7**, 2–9 (2012).
104. Hinds, S., Bian, W., Dennis, R. G. & Bursac, N. The role of extracellular matrix composition in structure and function of bioengineered skeletal muscle. *Biomaterials* **32**, 3575–3583 (2011).
105. Matsumoto, T., Sasaki, J., Alsberg, E., Egusa, H., Yatani, H & Somura, T. Three-dimensional cell and tissue patterning in a strained fibrin gel system. *PLoS One* **2**, 1–6 (2007).

106. Boonen, K. J. M. Langelaan, M.L., Polak, R.B., van der Schaft, D.W., Baaijens, F.P. & Post, M.J. Effects of a combined mechanical stimulation protocol: Value for skeletal muscle tissue engineering. *J. Biomech.* **43**, 1514–1521 (2010).
107. Strohman, R. C., Bayne, E., Spector, D. & Obinata, T. Myogenesis and histogenesis of skeletal muscle on flexible membranes in vitro. 201–208 (2000).
108. Dennis, R. & Kosnik, P. I. Excitability and isometric contractile properties of mammalian skeletal muscle constructs engineered in vitro. *Vitr. Cell. Dev. Biol. ...* 327–335 (2000).
109. Shansky, J., Del Tatto, M., Chromiak, J. & Vandeburgh, H. A simplified method for tissue engineering skeletal muscle organoids in vitro. *In Vitro Cell. Dev. Biol. Anim.* **33**, 659–661 (1997).
110. Qazi, T. H., Mooney, D. J., Pumberger, M., Geißler, S. & Duda, G. N. Biomaterials based strategies for skeletal muscle tissue engineering: Existing technologies and future trends. *Biomaterials* **53**, 502–521 (2015).
111. Player, D. J. Martin, N.R., Passey, S.L., Sharples, A.P., Mudera, V. & Lewis M.P. Acute mechanical overload increases IGF-I and MMP-9 mRNA in 3D tissue-engineered skeletal muscle. *Biotechnol. Lett.* **36**, 1113–1124 (2014).
112. Sharples, A. P. Player, D. J. Martin, Mudera, V., Stewart, C.E. & Lewis M.P. Modelling in vivo skeletal muscle ageing in vitro using three-dimensional bioengineered constructs. *Aging Cell* **11**, 986–995 (2012).
113. Martin, N. R. W., Passey, S.L., Player, D.J., Mudera, V., Baar, K., Greensmith, L. & Lewis M.P. Neuromuscular junction formation in tissue engineered skeletal muscle augments contractile function and improves cytoskeletal organisation. *Tissue Eng. Part A* **21**, (2015).
114. Lewis, R. L. & Gutmann, L. Snake Venoms and the Neuromuscular Junction. *Semin Neurol* **24**, 175–179 (2004).
115. Juhas, M., Ye, J. & Bursac, N. Design, evaluation, and application of engineered skeletal muscle. *Methods* **99**, 81–90 (2016).
116. Bian, W. & Bursac, N. Engineered skeletal muscle tissue networks with controllable architecture. *Biomaterials* **30**, 1401–1412 (2009).
117. Vandeburgh, H., Del Tatto, M., Shansky, J., Lemaire, J., Chang, A., Payumo, F., Lee. P., Goodyear, A. & Raven L. Brief Report Tissue-Engineered Skeletal Muscle Organoids for

- Reversible Gene Therapy Hum. Gene Ther. Nov 10;7(17):2195-200 (1996).
118. Chromiak, J.A., Shansky, J., Perrone, C. & Vandeburgh H.H. Bioreactor perfusion system for the long-term maintenance of tissue-engineered skeletal muscle organoids In Vitro Cell Dev Biol Anim. Oct;34(9):694-703 (1998).
  119. Smith, A. S. T., Passey, S., Greensmith, L., Mudera, V. & Lewis, M. P. Characterization and optimization of a simple, repeatable system for the long term in vitro culture of aligned myotubes in 3D. *J. Cell. Biochem.* **113**, 1044–1053 (2012).
  120. Shearn, J. T., Kinneberg, K.R., Dymont, N.A., Galloway, M.T., Kenter, K., Wylie, C. & Butler, D.L. Tendon tissue engineering: Progress, challenges, and translation to the clinic. *J. Musculoskelet. Neuronal Interact.* **11**, 163–173 (2011).
  121. Juncosa-Melvin, N., Boivin, G.P., Galloway, M.T., Gooch, C., West, J.R., Sklenka, A.M. & Butler, D.L. Effects of Cell-to-Collagen Ratio in Mesenchymal Stem Cell-Seeded Implants on Tendon Repair Biomechanics and Histology. *Tissue Eng.* **11**, 448–457 (2005).
  122. Chen, B., Ding, J., Zhang, W., Zhou, G., Cao, Y., Liu, W. & Wang, B. Tissue Engineering of Tendons: A Comparison of Muscle-Derived Cells, Tenocytes, and Dermal Fibroblasts as Cell Sources. *Plast. Reconstr. Surg.* **137**, 536e-544e (2016).
  123. Ouyang, H., C.H. Goh, J., Thambyah, A., Teoh, H. & Hin Lee, E. Knitted Poly-lactide-co-glycolide Scaffold Loaded with Bone Marrow Stromal Cells in Repair and Regeneration of Rabbit Achilles Tendon. *Tissue Eng.* **9**, 431–439 (2003).
  124. Sato, M., Maeda, M., Kurosawa, H., Inoue, Y., Yamauchi, Y. & Iwase H. Reconstruction of rabbit Achilles tendon with three bioabsorbable materials: histological and biomechanical studies. *J. Orthop. Sci.* **5**, 256–267 (2000).
  125. Fischbach, C., Chen, R., Matsumoto, T., Schmelzle, T., Brugge, J.S., Polverini, P.J. & Mooney DJ. Engineering tumors with 3D scaffolds. *Nat. Methods* **4**, 855–860 (2007).
  126. Hutmacher, D. W., Loessner, D., Rizzi, S., Kaplan, D.L., Mooney, D.J. & Clements J.A. Can tissue engineering concepts advance tumor biology research? *Trends Biotechnol.* **28**, 125–133 (2010).
  127. Villasante, A. & Vunjak-Novakovic, G. Tissue-engineered models of human tumors for cancer research. *Expert Opin. Drug Discov.* **10**, 257–268 (2015).
  128. Lin, C., Ballinger, K. R. & Khetani, S. R. The application of engineered liver tissues for novel



- drug discovery. *Expert Opin. Drug Discov.* **10**, 519–540 (2015).
129. MacIntosh, B. R., Gardiner, P. F. & McComas, A. J. *Skeletal muscle: form and function*. (Human kinetics, 2006).
  130. Bogdanowicz, D. R. & Lu, H. H. Studying cell-cell communication in co-culture. *Biotechnol. J.* **8**, 395–396 (2013).
  131. Proffen, B. L., Haslauer, C. M., Harris, C. E. & Murray, M. M. Mesenchymal Stem Cells from the Retropatellar Fat Pad and Peripheral Blood Stimulate ACL Fibroblast Migration, Proliferation, and Collagen Gene Expression. *Connective tissue research* **54**, (2013).
  132. Wang, I. E., Shan, J., Choi, R., Oh, S., Kepler, C.K., Chen, F.H. & Lu, H.H. Role of osteoblast–fibroblast interactions in the formation of the ligament-to-bone interface. *J. Orthop. Res.* **25**, 1609–1620 (2007).
  133. Khademhosseini, A., Suh, K.Y., Yang, J.M., Eng, G., Yeh, J., Levenberg, S. & Langer R. Layer-by-layer deposition of hyaluronic acid and poly-L-lysine for patterned cell co-cultures. *Biomaterials* **25**, 3583–3592 (2004).
  134. Jiang, J., Leong, N. L., Mung, J. C., Hidaka, C. & Lu, H. H. Interaction between zonal populations of articular chondrocytes suppresses chondrocyte mineralization and this process is mediated by PTHrP. *Osteoarthr. Cartil.* **16**, 70–82 (2008).
  135. Marshall, J. Transwell® Invasion Assays. in *Cell Migration: Developmental Methods and Protocols* (eds. Wells, C. M. & Parsons, M.) 97–110 (Humana Press, 2011). doi:10.1007/978-1-61779-207-6\_8
  136. Guo, X., Gonzalez, M., Stancescu, M., Vandeburgh, H. H. & Hickman, J. J. Neuromuscular junction formation between human stem cell-derived motoneurons and human skeletal muscle in a defined system. *Biomaterials* **32**, 9602–9611 (2011).
  137. Demestre, M. Formation and characterisation of neuromuscular junctions between hiPSC derived motoneurons and myotubes. *Stem Cell Res.* **15**, 328–336 (2015).
  138. Gunetti, M. Tomasi, S., Giammò, A., Boido, M., Rustichelli, D., Mareschi, K., Errichiello, E., Parola, M., Ferrero, I., Fagioli, F., Vercelli, A. & Carone, R. Myogenic Potential of Whole Bone Marrow Mesenchymal Stem Cells In Vitro and In Vivo for Usage in Urinary Incontinence. *PLoS One* **7**, (2012).
  139. Choi, S. H. Chung, K.Y., Johnson, B.J., Go, G.W., Kim, K.H., Choi, C.W. & Smith, S.B. Co-culture

- of bovine muscle satellite cells with preadipocytes increases PPAR $\gamma$  and C/EBP $\beta$  gene expression in differentiated myoblasts and increases GPR43 gene expression in adipocytes. *J. Nutr. Biochem.* **24**, 539–543 (2013).
140. Takegahara, Y., Yamanouchi, K., Nakamura, K., Nakano, S. ichi & Nishihara, M. Myotube formation is affected by adipogenic lineage cells in a cell-to-cell contact-independent manner. *Exp. Cell Res.* **324**, 105–114 (2014).
  141. Hicks, M. R., Cao, T. V. & Standley, P. R. Biomechanical strain vehicles for fibroblast-directed skeletal myoblast differentiation and myotube functionality in a novel coculture. *AJP Cell Physiol.* **307**, C671–C683 (2014).
  142. Goetsch, K. P., Snyman, C., Myburgh, K. H. & Niesler, C. U. Simultaneous isolation of enriched myoblasts and fibroblasts for migration analysis within a novel co-culture assay. *Biotechniques* **58**, 25–32 (2015).
  143. Merceron, T. K., Burt, M., Seol, Y.J., Kang, H.W., Lee, S.J., Yoo, J.J. & Atala A.A. 3D bioprinted complex structure for engineering the muscle-tendon unit. *Biofabrication* **7**, (2015).
  144. Smith, L., Xia, Y., Galatz, L. M., Genin, G. M. & Thomopoulos, S. Tissue-engineering strategies for the tendon/ligament-to-bone insertion. *Connect. Tissue Res.* **53**, 95–105 (2012).
  145. Doroski, D. M., Brink, K. S. & Temenoff, J. S. Techniques for biological characterization of tissue-engineered tendon and ligament. *Biomaterials* **28**, 187–202 (2007).
  146. P. Spalazzi, J., Doty, S., L. Moffat, K., Levine, W. & H. Lu, H. Development of Controlled Matrix Heterogeneity on a Triphasic Scaffold for Orthopedic Interface Tissue Engineering. *Tissue Eng.* **12**(12):3497-508. (2006).
  147. Ma, J., Goble, K., Smietana, M., Kostrominova, T., Larkin, L. & Arruda, E.M. Morphological and Functional Characteristics of Three-Dimensional Engineered Bone-Ligament-Bone Constructs Following Implantation. *J. Biomech. Eng.* **131**, 101017–101019 (2009).
  148. Matyas, J. R., Anton, M. G., Shrive, N. G. & Frank, C. B. Stress governs tissue phenotype at the femoral insertion of the rabbit MCL. *J. Biomech.* **28**, (1995).
  149. Paxton, J. Z., Donnelly, K., Keatch, R. P. & Baar, K. Engineering the Bone–Ligament Interface Using Polyethylene Glycol Diacrylate Incorporated with Hydroxyapatite. *Tissue Eng. Part A* **15**, 1201–1209 (2009).
  150. Paxton, J. Z., Grover, L. M. & Baar, K. Engineering an *In Vitro* Model of a Functional Ligament

- from Bone to Bone. *Tissue Eng. Part A* **16**, 3515–3525 (2010).
151. Gholobova, D., Gerard, M., Decroix, L., Desender, L., Callewaert, N., Annaert, P. & Thorrez, L. Human tissue-engineered skeletal muscle: a novel 3D in vitro model for drug disposition and toxicity after intramuscular injection. *Sci. Rep.* **8**, 1–14 (2018).
  152. Smith, A. S. T., Passey, S., Greensmith, L., Mudera, V. & Lewis, M. P. Characterization and optimization of a simple, repeatable system for the long term in vitro culture of aligned myotubes in 3D. *J. Cell. Biochem.* **113**, 1044–53 (2012).
  153. Martin, N. R. W. Passey, S.L., Player, D.J., Khodabukus, A., Ferguson, R.A., Sharples, A.P., Mudera, V., Baar, K. & Lewis M.P. Factors affecting the structure and maturation of human tissue engineered skeletal muscle. *Biomaterials* **34**, 5759–65 (2013).
  154. Livak, K. J. & Schmittgen, T. D. Analysis of Relative Gene Expression Data Using Real-Time Quantitative PCR and the 2- $\Delta\Delta$ CT Method. *Methods* **25**, 402–408 (2001).
  155. Pisano, G. Learning : An Empirical Analysis of Process. *Strateg. Manag. J.* **15**, 85–100 (1994).
  156. Ich. International Conference on Harmonisation (ICH) of Technical Requirement for Registration of Pharmaceuticals for Human Use, Pharmaceutical Development, Q8 (R2), ICH, August 2009. *ICH Harmon. Tripart. Guidel.* **8**, 1–28 (2009).
  157. Rathore, A. S. & Winkle, H. Quality by design for biopharmaceuticals. *Nat. Biotechnol.* **27**, 26–34 (2009).
  158. Pisano, G. P. Learning-before-doing in the development of new process technology. *Res. Policy* **25**, 1097–1119 (1996).
  159. Jones, J. M. Player, D.J., Martin, N.R.W., Capel, A.J., Lewis, M.P. & Mudera V. An assessment of myotube morphology, matrix deformation, and myogenic mRNA expression in custom-built and commercially available engineered muscle chamber configurations. *Front. Physiol.* **9**, 1–9 (2018).
  160. Kaufmann, A. & Tödtling, F. Science-industry interaction in the process of innovation: The importance of boundary-crossing between systems. *Res. Policy* **30**, 791–804 (2001).
  161. Yu, L. X. Pharmaceutical quality by design: product and process development, understanding, and control. *Pharm. Res.* **25**, 781–91 (2008).
  162. Eastwood, M., Porter, R., Khan, U., McGrouther, G. & Brown, R. Quantitative analysis of collagen gel contractile forces generated by dermal fibroblasts and the relationship to cell

- morphology. *J. Cell. Physiol.* **166**, 33–42 (1996).
163. Liu, W., Chen, B., Deng, D., Xu, F., Cui, L. & Cao Y. Repair of Tendon Defect with Dermal Fibroblast Engineered Tendon in a Porcine Model. *Tissue Eng.* **12**, 775–778 (2006).
  164. Ladd, M. R., Lee, S. J., Stitzel, J. D., Atala, A. & Yoo, J. J. Co-electrospun dual scaffolding system with potential for muscle-tendon junction tissue engineering. *Biomaterials* **32**, 1549–1559 (2011).
  165. Preibisch, S., Saalfeld, S. & Tomancak, P. Globally optimal stitching of tiled 3D microscopic image acquisitions. *Bioinformatics* **25**, 1463–1465 (2009).
  166. Mudera, V., Smith, A. S. T., Brady, M. A. & Lewis, M. P. The effect of cell density on the maturation and contractile ability of muscle derived cells in a 3D tissue-engineered skeletal muscle model and determination of the cellular and mechanical stimuli required for the synthesis of a postural phenotype. *J. Cell. Physiol.* **225**, 646–653 (2010).
  167. Cheema, U., Yang, S. Y., Mudera, V., Goldspink, G. G. & Brown, R. A. 3-D in vitro model of early skeletal muscle development. *Cell Motil. Cytoskeleton* **54**, 226–236 (2003).
  168. Mudera, V., Smith, a S. T., Brady, M. a & Lewis, M. P. The effect of cell density on the maturation and contractile ability of muscle derived cells in a 3D tissue-engineered skeletal muscle model and determination of the cellular and mechanical stimuli required for the synthesis of a postural phenotype. *J. Cell. Physiol.* **225**, 646–53 (2010).
  169. Griffin, C. A., Apponi, L. H., Long, K. K. & Pavlath, G. K. Chemokine expression and control of muscle cell migration during myogenesis. *Journal of Cell Science* **123**, 3052–3060 (2010).
  170. Wang, Z. *et al.* In vitro investigation of a tissue-engineered cell-tendon complex mimicking the transitional architecture at the ligament-bone interface. **29**, 1180–1192 (2015).
  171. Benjamin, M. & Ralphs, J. R. Fibrocartilage in tendons and ligaments — an adaptation to compressive load. *J. Anat.* **193**, 481–494 (1998).
  172. Shah, R., Knowles, J. C., Hunt, N. P. & Lewis, M. P. Development of a novel smart scaffold for human skeletal muscle regeneration. (2013). doi:10.1002/term
  173. Liu, Z. (Cindy) & Geisbrecht, E. R. Moleskin is essential for the formation of the myotendinous junction in *Drosophila*. *Dev Biol.* **359**, 176–189 (2011).
  174. Kryger, G. S., Chong, A.K., Costa, M., Pham, H., Bates, S.J. & Chang J. A Comparison of Tenocytes and Mesenchymal Stem Cells for Use in Flexor Tendon Tissue Engineering. *J. Hand*

- Surg. Am.* **32**, 597–605 (2007).
175. Bell, E., Ivarsson, B. & Merrill, C. Production of a tissue-like structure by contraction of collagen lattices by human fibroblasts of different proliferative potential in vitro. *Proc. Natl. Acad. Sci. U. S. A.* **76**, 1274–8 (1979).
  176. Dallan, J. C. & Ehrlich, H. P. A review of fibroblast-populated collagen lattices. *Wound Repair Regen.* **16**, 472–479 (2008).
  177. Zelis, R., Nussberger, J., Clemson, B., Waeber, B., Grouzmann, E. & Brunner H.R. Neuropeptide Y Infusion Decreases Plasma Renin Activity in Postmyocardial Infarction Rats. *J. Cardiovasc. Pharmacol.* **24**, 896–899 (1994).
  178. Takase, S., Leo, M. A., Nouchi, T. & Lieber, C. S. Desmin distinguishes cultured fat-storing cells from myofibroblasts, smooth muscle cells and fibroblasts in the rat. *J. Hepatol.* **6**, 267–276 (1988).
  179. Boularaoui, S. M., Abdel-Raouf, K.M.A., Alwahab, N.S.A., Kondash, M.E., Truskey, G.A., Teo J.C.M. & Christoforou N. Efficient transdifferentiation of human dermal fibroblasts into skeletal muscle. *J. Tissue Eng. Regen. Med.* **12**, e918–e936 (2018).
  180. Barondes, S. H. & Haywood-Reid, P. L. Externalization of an endogenous chicken muscle lectin with in vivo development. *J. Cell Biol.* **91**, 568–572 (1981).
  181. Goldring, K., Jones, G. E., Sewry, C. A. & Watt, D. J. The muscle-specific marker desmin is expressed in a proportion of human dermal fibroblasts after their exposure to galectin-1. *Neuromuscul. Disord.* **12**, 183–186 (2002).
  182. Isikli, C., Hasirci, V. & Hasirci, N. Co-culture in cartilage tissue engineering. *J. Tissue Eng. Regen. Med.* **6**, 135–143 (2012).